

Evolution of Community Metabolism



The research presented in this thesis was carried out at the Department of Theoretical Biology, Vrije Universiteit Amsterdam, The Netherlands.

Coverpicture: Cosmariums have entered a dead cell to feed on its remains. Cosmariums belong to the green algae, which are typically known as photosynthesizers (autotrophs). This picture, however, shows that they are also capable of consuming organic matter (heterotrophy). The combination of auto- and heterotrophic capabilities implies that cosmariums basically are mixotrophs. The omnipresence of mixotrophy and its important role in aquatic food webs are increasingly recognized. Copyright © S.A.L.M. Kooijman

Coverdesign: T.A. Troost

Movie (pages 1-173): TT-productions

Printed by: Febodruk - www.febodruk.nl

VRIJE UNIVERSITEIT

EVOLUTION OF
COMMUNITY METABOLISM

ACADEMISCH PROEFSCHRIFT

ter verkrijging van de graad Doctor aan
de Vrije Universiteit Amsterdam,
op gezag van de rector magnificus
prof.dr. L.M. Bouter,
in het openbaar te verdedigen
ten overstaan van de promotiecommissie
van de faculteit der Aard- en Levenswetenschappen
op dinsdag 7 november 2006 om 13.45 uur
in de aula van de universiteit,
De Boelelaan 1105

door

Tineke Annemarie Troost

geboren te Assen

promotor: prof.dr. S.A.L.M. Kooijman
copromotor: dr.ir. B.W. Kooi

Contents

1	General Introduction	1
1.1	Combining DEB and AD	1
1.2	Dynamic Energy Budget theory	3
1.2.1	Simplifications	3
1.3	Adaptive Dynamics theory	4
1.3.1	Evolutionary branching points	4
1.3.2	Simplifications	5
1.4	Thesis outline	6
2	When do mixotrophs specialize? Adaptive Dynamics theory applied to a Dynamic Energy Budget model	9
2.1	Introduction	10
2.2	Methods	11
2.2.1	Model description	11
2.2.2	Predicting the evolutionary outcome	17
2.2.3	Levins' graphical approach applied to the mixotroph model	19
2.3	Results	23
2.4	Discussion	25
2.4.1	Intrinsic vs. extrinsic properties	25
2.4.2	Boundaries of the affinities' trait space	27
2.4.3	Cost level	28
2.4.4	Cost function	29
2.4.5	Evolutionary branching	30
2.5	Conclusions	31
3	Bifurcation analysis of ecological and evolutionary processes in ecosystems	37
3.1	Introduction	38
3.2	The ecological model formulation	39
3.2.1	The population model	39
3.2.2	The ecosystem model	42
3.2.3	Numerical bifurcation analysis of the ecosystem	43
3.3	The evolutionary model formulation	44
3.3.1	Invasion of a monomorphic resident population	45

3.3.2	Bifurcation analysis of the evolutionary model	48
3.3.3	Bifurcation diagrams for the monomorphic resident population	49
3.3.4	Invasion of the dimorphic resident population	53
3.3.5	Bifurcation diagrams for the dimorphic population	54
3.4	Discussion and conclusions	57
3.5	Acknowledgments	60
4	Ecological specialization of mixotrophic plankton in a mixed water column	63
4.1	Introduction	64
4.2	Modeling mixotrophs in a water column	65
4.2.1	Assimilation and evolution	66
4.2.2	Spatial structure, light gradient and vertical transport	68
4.2.3	Evolutionary analysis	70
4.3	Results and discussion	71
4.3.1	Vertical profiles and evolutionary outcomes	71
4.3.2	Open and closed systems	74
4.3.3	The role of diffusion and turbulent mixing	76
4.3.4	Effects of the total nutrient content	78
4.4	Conclusions	79
4.4.1	Evolution of specialization	79
4.4.2	Concluding remarks on system structure	80
5	Joint evolution of predator body size and prey-size preference	93
5.1	Introduction	94
5.2	Model description	95
5.2.1	Population dynamics	95
5.2.2	Scaling considerations	96
5.2.3	Incoming prey densities	99
5.2.4	Functional responses	99
5.2.5	Choice of units	102
5.3	Methods	102
5.3.1	Ecological analysis	102
5.3.2	Adaptive Dynamics theory	103
5.3.3	Evolutionary analysis	105
5.4	Results	106
5.4.1	Ecological analysis	106
5.4.2	Evolutionary analysis	108
5.5	Discussion	110
5.5.1	True predators versus parasitic predators	110
5.5.2	Imperfect upper triangularity	111
5.5.3	Evolution under increased levels of ecological realism	112
5.5.4	Evolutionary effects of environmental factors	114
5.5.5	Evolutionary effects of feeding modes	114
5.6	Conclusions	117

6	Seasonality as a driver of body size evolution	127
6.1	Introduction	128
6.2	Methods	130
6.2.1	Model description	130
6.2.2	The periodic environment	133
6.2.3	Evolutionary equilibria	133
6.2.4	Evolutionary trajectories	135
6.3	Results	136
6.3.1	Effects of seasonality	136
6.3.2	Effects of variations in seasonality	138
6.4	Discussion	140
7	General Discussion	149
7.1	Specialization into and within functional groups	149
7.2	System structure	152
7.3	Adaptive traits and trade-offs	153
7.4	Conclusions	154
	Summary	159
	Samenvatting	163
	Dankwoord	167



1

General Introduction

1.1 Combining DEB and AD

A biological community is a group of species that occur together in space and time [1]. The structure of a biological community is described by characteristics such as the number of species of which it consists, the type of the species interactions, their biomass distribution, and their interaction strengths. The structure of a community is closely related to its dynamics and its functioning, involving ecological processes such as biomass production and retention, nutrient cycling and energy dissipation, which, in turn, may affect community stability, persistence and resilience.

Community structure and functioning do not arise at random, but are the result of many different processes. Some of these processes, such as for instance population growth, lead to a quantitative change in the community structure, and may take place on short (ecological) time scales. Other processes, such as the entry of new species and the adaptation or extinction of existing ones, may lead to a qualitative change in community structure, and are typically associated with longer (evolutionary) time scales.

In many modeling studies, these long-term processes are simply ignored, and the number of species, their interactions, and the involved parameter values are assumed to be fixed. Yet, qualitative changes in community structure and functioning are very important, as they allow communities to develop and enable them to adapt to changing environmental conditions. Obviously, long-term changes in community structure and functioning are essential when, for example, predicting the consequences of climate change, designing strategies for environmental management, or studying sustainable exploitation of natural resources.

One way of incorporating qualitative changes in the structure of a model community is by means of an assembly process. In assembly models such as the Web World model [2], new species are selected from an existing pool of species and are incorporated if they add to the community in a stable way [7]. The assembly process may thus correspond to migration of new species from

surrounding areas into the community. A problem with assembly models is that the results largely depend on the specific supply of new species throughout time. Consequently, each simulation run may have a very different outcome, which makes the results difficult to analyze and interpret.

An alternative for the assembly process is evolution. Evolutionary models involve adaptation and speciation through mutation and selection. The phenotypic characteristics, subject to evolution, are referred to as adaptive traits. The values of the adaptive traits of new species are not chosen at random, but are based on those of their (successful) ancestors, from which they deviate by small mutational steps. The size and direction of these mutational steps are stochastic, but when they are small and rare the evolutionary change of the adaptive traits becomes deterministic and predictable (see Section 1.3).

A model that does include evolutionary processes to shape the food web structure is the ‘speciation model’ [20]. This model, however, does not consider any population dynamics, so that speciations and extinctions are again included as random events. An evolutionary community model that includes population dynamics, is the one developed by Ito & Ikegami [11], which uses a diffusion process to describe the mutational process. Like in the Web World model, it considers one adaptive trait for the ability of predation and one for the vulnerability to predation. These traits represent morphological or behavioral characteristics, but they are not assigned particular features, and neither are they linked to physiological processes or traded off with each other. As a consequence, the model results may not always lead to realistic results. For example, the populations may evolve towards ever larger trait values, unless explicit boundaries are defined.

Some models do include concrete adaptive traits that are linked to physiological processes. For example, the size-structured evolutionary food web model developed by Loeuille and Loreau [15] uses body size as the adaptive trait. However, their model incorporates various empirically derived functions and is based on the elegant but not very realistic Lotka-Volterra-dynamics, in which the rate of encounter between consumers and resources is proportional to the product of their masses.

In this thesis, I include more realism in evolutionary community models. For this, two very promising ideas are combined, the Dynamic Energy Budget (DEB) theory on metabolic organization [13, 14, 18] and the Adaptive Dynamics (AD) theory on evolutionary speciation [5, 6, 9, 17], which so far existed separately with hardly any links between them. DEB theory was used to formulate models concerning system dynamics on an ecological time scale, while AD theory was mainly applied to unrealistically simple ‘toy’ models. The aim of this thesis is to apply AD theory to models based on DEB theory, to include multiple adaptive traits, to consider inhomogeneities in space and time, and to formulate AD theory methods in a more general bifurcation theoretical framework.



1.2 Dynamic Energy Budget theory

Dynamic Energy Budget theory [13, 14, 18] is a modeling framework for metabolic organization. It consists of physiological rules that describe the uptake and use of energy and material. It is derived from first principles and provides a quantitative framework for modeling any living organism. These organisms are considered to consist of two state variables, structural biomass and reserves. Assimilates derived from food are added to the reserves, which then fuel all other processes including maintenance, growth and reproduction. As a result, growth and reproduction do not depend directly on the available food resources, but rather on the reserves. These have a broader interpretation than is generally the case for storage material: reserves are not set aside for later use, but consist of all material that is available for metabolic use, now or later. DEB theory does not only take into account the energy fluxes, material fluxes and chemical reactions occurring between the species in a community, but also explicitly formulates the fluxes and chemical reactions occurring between the community and its environment, the total of which is referred to as 'community metabolism'.

1.2.1 Simplifications

To keep the analysis feasible, I use various approximations to simplify the DEB models. In Chapters 2 to 4 this is done by assuming that the organisms' surface-area to volume ratio does not change during their lives. This is a reasonable assumption for small organisms such as algae, that reproduce through growth and division. It eliminates the distinction between the individual and the population, which simplifies the model considerably. Furthermore, the energy reserves of the organisms are not considered, but only their structural biomass.

In Chapter 5, a different simplification is used. Here, the assumption is made that the organisms grow quickly to adult size. As a result, their juvenile stage can be ignored and all individuals in the population are either embryos or adults. Adults do not grow, but only reproduce, which contrasts with reproductive dividers such as mentioned above. Also, all adults are assumed to have the same size, which again leads to a constant surface-area to volume ratio. Although the reserves of these organisms are considered, they are assumed to be in equilibrium with their environment, which means that the scaled reserve density is equal to the scaled functional response. This assumption of an ecological equilibrium is not problematic, because focus lies on the evolutionary dynamics rather than on the ecological ones. These ecological dynamics are assumed to be much faster than the evolutionary dynamics, such that, when regarded on an evolutionary time scale, the system can be considered always to be at its ecological equilibrium. In Chapter 6, such an equilibrium assumption can no longer be made, as a periodically fluctuating environment is considered. In this case the reserves have to be modeled explicitly throughout time.

1.3 Adaptive Dynamics theory

Adaptive Dynamics (AD) theory helps analyze phenotypic evolution under density or frequency-dependent selection [5, 6, 9, 17]. The concept of evolution has been introduced by Darwin and Wallace [4, 22]. According to Darwin, biotic factors in general, and competitive interactions in particular, were the main factors driving natural selection. By putting the emphasis on the direct competition between individuals, the impression was created that the environment was simply a ‘static arena’ for selection. Wallace, in contrast, put more emphasis on the struggle against enemies, predators and the physical environment. These same two views underly two alternative approaches that still exist in the field of ecology, the so-called demographic and autoecology approach [10]. The seeming incompatibility between the two views has led to the ‘competition controversy’ in community ecology [3, 23]. AD theory, however, combines the two views, by assuming a feedback loop between the population and the environment. This feedback loop implies that the environment is affected by the density or frequency distribution of the phenotypes present in the system. As a result, the environment and the fitness landscape are not static, but may change along with the evolution of the species or populations in it. Changes due to such a feedback loop may be small and irrelevant when considering short periods and small regions, but can not be ignored when temporal and spatial scales become larger.

AD theory focuses on adaptive traits that characterize an individual. Other traits are assumed to be constant over time and among all individuals belonging to a (mono-phylogenetic) taxon. The trait values are inherited from parent to offspring, but small changes may arise due to mutations. Whether a mutant may invade the resident population depends on its invasion fitness. This invasion fitness is defined as the mutant’s long-term per capita growth rate in the environment that is ‘set’ by the resident population; this resident population is assumed to be in equilibrium with its environment, and thus has a growth rate of zero. Hence, by definition, the individuals belonging to the resident population always have a zero invasion fitness. Mutants with a negative invasion fitness will die out, but mutants with a positive invasion fitness may replace the resident population. A series of such replacements will lead to a phenotypic change of the population. As long as mutations are small, and sufficiently rare for the resident population always to be close to its population-dynamical equilibrium when probed by a mutant, the direction and endpoint of phenotypic change can be deterministically approximated by means of the so-called canonical equation of Adaptive Dynamics [6].

1.3.1 Evolutionary branching points

An evolutionary equilibrium is reached when the organisms have attained a trait value at which the local fitness gradient is zero. Various types of evolutionary equilibria are possible, but two of the most important to biological



communities are the continuously stable strategy (CSS) and the evolutionary branching point (EBP) [8, 9, 16, 17].

A CSS is an attracting and evolutionarily stable strategy. This means that the population will evolve towards the corresponding trait value, and then remain there, because this value corresponds to a local fitness maximum. Hence, a CSS forms an evolutionary endpoint at which evolution comes to a halt.

The EBP is an attracting but evolutionarily *unstable* strategy. The population will evolve towards it, but along with this process the fitness landscape changes and has formed a local fitness minimum when the corresponding trait value is reached. As a result, selection becomes disruptive, and the population will split into two (coexisting) populations, which process is referred to as ‘evolutionary branching’. Evolutionary branching of asexually reproducing organisms, as are all model organisms in this thesis, may correspond to sympatric speciation in sexual organisms. Evolutionary branching thus provides the system with a mechanism for autonomously increasing its biodiversity.

1.3.2 Simplifications

Various factors in this thesis complicate the AD analysis, for which solutions or simplifications have to be found. In Chapters 2 and 5, two adaptive traits are considered instead of one, so that the standard graphical approach of AD theory, the so-called Pairwise Invasibility Plot (PIP), can not be used. In Chapter 2 this problem is solved by using Levin’s graphical approach adjusted for density-dependent selection [21]. This approach is based on the assumption that first the population will always evolve towards the trade-off curve, and then along it. The curve is formed by a one-dimensional range of trait value combinations, at which the two trait values cannot be increased both at the same time; any increase in one of the trait values necessarily implies a decrease in the other. In Chapters 3 and 4, the two traits are simply combined into one by assuming a direct trade-off between them. In Chapter 5 again two adaptive traits are considered, but here their simultaneous evolution is analyzed through simulations and bifurcation analysis.

Another complicating factor is environmental heterogeneity. In Chapter 4 a one-dimensional water column with a light-intensity gradient is studied. As a result, the specific growth rate of organisms varies with depth and can no longer be used as a direct measure for the invasion fitness. Instead, a fitness measure has to be used that takes into account growth rates at every depth, which is found in the dominant eigenvalue of the linearized system. In Chapter 6 again a heterogeneous environment is assumed. This time, however, the fluctuations occur not in space but in time. To study the corresponding evolutionary dynamics we apply Floquet theory, which transforms periodic systems to traditional linear systems.

1.4 Thesis outline

In Chapters 2 to 4, specialization into two traits representing different trophic functions is studied. Trophic functions are (interactions with) ecosystem processes, such as primary production, nitrification and respiration. For this, a model of a population of mixotrophic organisms is used. Mixotrophs are capable of both autotrophy and heterotrophy, i.e., they can use both inorganic and organic carbon as a material and energy source. Evolution enables these organisms to specialize in autotrophic and heterotrophic assimilation. Their two adaptive traits represent the affinities for the autotrophic and heterotrophic assimilatory pathways. After evolutionary branching (Section 1.3.1), two populations may result, an autotrophic one in which the organisms have lost their abilities for heterotrophy, and an heterotrophic one in which the organisms have lost their abilities for autotrophy. This process may correspond to the autonomous development of a single-species community into a very simple food web.

Chapter 2 studies the consequences of introducing an indirect and physiologically-based trade-off function, instead of a simple and direct one, as is often used in evolutionary models. This trade-off function involves the costs for the autotrophic and heterotrophic machineries. Chapter 3 discusses the application of numerical bifurcation analysis to study the evolutionary dynamics of ecosystem models, and Chapter 4 more closely investigates the role of environmental factors on the evolutionary outcomes. This is done by placing the mixotrophs in a spatially heterogeneous environment, a mixed water column with a light-intensity gradient.

In Chapters 5 and 6 another approach is used in which the focus lays on specialization *within* a trophic function, instead of on specialization *into* trophic functions. In this case, evolution allows the organisms to specialize, not by increasing or decreasing the ability for a certain metabolic pathway, but by increasing the affinity of a given pathway for one or another substrate. Hence, when studying specialization within a trophic function, the substrate, instead of the trophic function, becomes the focus.

For studying specialization within a function, I focus on body size as the main adaptive trait, because it can characterize a range of substrates or prey populations, as well as predator populations. Differences in body size are associated with differences in scale of time and space in which the organisms live, and they reflect differences in physiological processes and life histories. Also, much is known about the relations between body size and physiology [12, 13, 19], which play a central role in DEB theory. From the basic assumptions of DEB theory various body-size scaling relationships can be derived and understood, which makes this modeling framework very suitable for studying body-size related processes.

In Chapters 5 to 6, we use a predator-prey model that considers two life stages for the predator, embryos and adults. In Chapter 5, not one but two adaptive traits were considered, the predator body size and its prey-size preference. Together, these properties determine which predator-prey size com-



binations are established and thus largely define the structure of a community. Though in this study the energy reserves of the organisms are taken into account, they are assumed to be in equilibrium with their (constant) environments. As a result, they form a burden rather than a profit to the organisms, slowing down their reproduction rates. This, of course, does not do justice to the large role of reserves in the real world. Therefore, in Chapter 6 these reserves and their evolutionary advantage in a fluctuating environment are studied.

In the General Discussion (Chapter 7) the results are summarized and the two approaches (specialization into and within trophic functions) are compared. The roles of system structure and parameters are discussed, followed by a discussion on role of adaptive traits and trade-offs in modeling realistic evolutionary communities.

References

- [1] Begon, M., Harper, J. L., and Townsend, C. R. (1990). *Ecology: Individuals, populations and communities*. Blackwell Scientific Publications, 2nd edition.
- [2] Caldarelli, G., Higgs, P. G., and McKane, A. J. (1998). Modelling coevolution in multispecies communities. *Journal of theoretical Biology*, 193:345–358.
- [3] Cooper (1993). The competition controversy in community ecology. *Biology and Philosophy*, 8(4):359–384.
- [4] Darwin, C. R. (1995). *The origin of species by means of natural selection*. Graymercy Books, republication of 1st ed.
- [5] Dieckmann, U. (1997). Can adaptive dynamics invade? *Trends in Ecology and Evolution*, 12:128–131.
- [6] Dieckmann, U. and Law, R. (1996). The dynamical theory of coevolution: a derivation from stochastic ecological processes. *Journal of Mathematical Biology*, 34:579–612.
- [7] Drossel, B. and McKane, A. J. (2002). Modelling food webs. *arXiv.org*, page arXiv:nlin.AO/0202034v1.
- [8] Geritz, S. A. H., Kisdi, É., Meszéna, G. and Metz, J. A. J. (1998). Dynamics of adaptation and evolutionary branching. *Evolutionary Ecology*, 12:35–57.
- [9] Geritz, S. A. H., Metz, J. A. J., Kisdi, É., and Meszéna, G. (1997). Dynamics of adaptation and evolutionary branching. *Physical Review Letters*, 78:2024–2027.
- [10] Hengeveld, R. and Walter, G. H. (1999). The two coexisting ecological paradigms. *Acta Biotheoretica*, 47: 141–170.

-
- [11] Ito, H. C. and Ikegami, T. (2006). Food-web formation with recursive evolutionary branching. *Journal of theoretical Biology*, 238:1–10.
- [12] Kooijman, S. A. L. M. (1986). Energy budgets can explain body size relations. *Journal of Theoretical Biology*, 121:269–282.
- [13] Kooijman, S. A. L. M. (2000). *Dynamic Energy and Mass Budgets in Biological Systems*. Cambridge University Press.
- [14] Kooijman, S. A. L. M. (2001). Quantitative aspects of metabolic organization; a discussion of concepts. *Phil. Trans. R. Soc. B*, 356: 331 - 349.
- [15] Loeuille, N. and Loreau, M. (2005). Evolutionary emergence of size-structured food webs. *PNAS*, 102(16):5761–5766.
- [16] Metz, J. A. J., Nisbet, R. and Geritz, S. A. H (1992). How should we define ‘fitness for general ecological scenarios? *Trends in Ecology and Evolution*, 7:198–202.
- [17] Metz, J. A. J and Geritz, S. A. H. and Meszéna, G. and Jacobs, F. J. A and van Heerwaarden, J. S. Adaptive Dynamics, a geometrical study of the consequences of nearly faithful reproduction. In: van Strien, S. J. and Verduyn Lunel, S. M. (Eds.). *Stochastic and Spatial structures of dynamical systems*. KNAW Verhandeligen, Amsterdam, 1996 pp. 183–231.
- [18] Nisbet, R. M. and Muller, E. B., and Lika, K. and Kooijman, S. A. L. M. (2000). From molecules to ecosystems through dynamic energy budget models. *J. Anim. Ecol*, 69: 913 - 926
- [19] Peters, R. H. (1983). *The Ecological Implications of Body Size*. Cambridge University Press, New York.
- [20] Rossberg, A. G., Matsuda, H., Amemiya, T., and Itoh, K. (2005). An explanatory model for food-web structure and evolution. *Ecological complexity*, 2:312–321.
- [21] C. Rueffler, T. van Dooren, J. A. J. Metz. Adaptive walks on changing landscapes: Levins’ approach extended. *Theor. Pop. Biol.* 65 (2004) 165–178.
- [22] Wallace, A. R. (1858). On the tendency of species to form varieties, and on the perpetuation of varieties and species by natural means of selection. III On the tendency of varieties to depart indefinitely from the original type. *J. Proc. Linn. Soc. London*, 3:53–62.
- [23] Walter, G. H. and Paterson, H. E. H. (1995). Levels of understanding in ecology - interspecific competition and community ecology. *Australian journal of ecology*, 20(3): 463–466



2

When do mixotrophs specialize? Adaptive Dynamics theory applied to a Dynamic Energy Budget model

Tineke A. Troost, Bob W. Kooi, Sebastiaan A.L.M. Kooijman
Published in *Mathematical Biosciences* 163 (2003): 19-32

Abstract

In evolutionary history, several events have occurred at which mixotrophs specialized into pure autotrophs and heterotrophs. We studied the conditions under which such events take place, using the Dynamic Energy Budget (DEB) theory for a physiological modeling basis and Adaptive Dynamics (AD) theory for the evolutionary analysis. We modeled a population of mixotrophs that are capable of both autotrophic and heterotrophic assimilation. The organisms have a certain affinity for both pathways; mutations in these affinities enable the population to evolve. Evolutionary branching points provide an opportunity for the mixotrophic population to split up and specialize into separate autotrophs and heterotrophs. Evolutionary branching points, however, are found only under specific conditions which depend on intrinsic properties such as the cost function, the level of the costs and the boundaries of trait space. Only at intermediate cost levels and when an explicit advantage to pure strategies exists, may branching occur. Due to the constraints on the affinities and their indirect trade-off, only some of the more complicated cost functions give rise to an evolutionary branching point. In contrast to the intrinsic properties, extrinsic properties such as the total nutrient content or light intensity were found to have no effect on the evolutionary outcomes at all.

2.1 Introduction

In recent years, the omnipresence of mixotrophy and its important role in aquatic food webs have been increasingly recognized [1, 16, 17]. Mixotrophy is the nutritional strategy which combines autotrophic and heterotrophic feeding. Heterotrophy depends on outside sources of organic food materials; it includes feeding modes like pinocytosis (uptake of dissolved organic carbon) and phagocytosis (uptake of particulate organic material). In contrast, with autotrophy, organic material can be manufactured from inorganic sources, which may be done by means of chemotrophy (using energy from specific inorganic molecules) or phototrophy (using energy from sunlight). Although many combinations of such heterotrophic and autotrophic types are possible, the term ‘mixotrophy’ is often reserved for the combination of phototrophy and phagotrophy [17]. This type of mixotrophy is often encountered in planktonic protists, which is the kind of organisms that we focus on in this study. Mixotrophy is a common phenomenon among these organisms, and they occur in a variety of freshwater and seawater habitats [6, 14, 16, 18].

In the course of evolution, specialization of phototrophs and heterotrophs from a common mixotrophic ancestor has occurred several times. One of the earliest of such events can be found in the early development of prokaryotes. Probably, life started out with chemolithoautotrophs, as both organic matter and dioxide were rare at the time life emerged on earth [10, 19]. Then, early in evolution, phototrophy arose among prokaryotes [5]. Subsequently, from the phototrophic machinery, the respiratory chain could evolve. This led to phototrophic organisms with a central glucose-based metabolism. Some of these prokaryotes improved their photosynthetic abilities; others, however, lost their ability to photosynthesize, and specialized in heterotrophy.

Evolutionary branching occurred again later in evolution, in the eukaryotes. The first eukaryotes were heterotrophic and some acquired phototrophy by endosymbiosis. This had resulted in mixotrophic eukaryotes. Yet, in the course of evolution the majority of these mixotrophs specialized again in either the autotrophic or the heterotrophic direction [14].

Although evolutionary branching makes up an important part of evolutionary history, it is still not well understood why or under what conditions they take place. Also its relation with the environment is not quite clear, although in some taxa mixotrophy appears to be associated with oligotrophic environments (low nutrient supply). This may be related to the fact that mixotrophs have access to two food sources, which increases their chances of survival during periods when one or both sources are limited [18]. Specialized organisms such as pure autotrophs and heterotrophs would then be thought to occur in *eutrophic* environments (nutrient rich). Yet, mixotrophic protists are known to be very abundant in a range of *eutrophic* to *oligotrophic* waters [17].

Another, more ‘intrinsic’, factor that might regulate the occurrence of evolutionary branching could be the balance between costs and benefits involved in mixotrophy. Benefits include the better chance of survival mentioned above, but access to two food sources might also reduce the nutrient losses that are



due to stoichiometry requirements, increasing the growth efficiency of the organism. In addition, mixotrophs may have the benefit of eating their competitors which will reduce interspecific competition for food, as was suggested by Thingstad et al. [18]. On the other hand, costs are related to building and maintaining the apparatus for both phototrophic and heterotrophic assimilation. In case of phototrophy, complex photosystems have to be build, as well as protection mechanisms against UV damage. For phagotrophy, for instance, it might be necessary to actively regulate the cell volume. Studies show that the apparatus involved in phototrophy can account up to 50% of the energy for cell synthesis, and comprises a corresponding fraction of the total cell biomass, although large differences exist between the various species [14]. Energy and biomass involved in the heterotrophic function seems much smaller, probably less than 10% of the total cell biomass [14].

In this paper we use a modeling approach to study the balance between costs and benefits of mixotrophy and its implications for evolutionary behavior. In order to keep our focus, we study this balance and underlying mechanisms for a very simple model-system with a homogeneous environment. The costs and benefits lead to a certain trade-off between autotrophy and heterotrophy, which is used to study under which conditions evolutionary branching occurs. Furthermore it is studied how the evolutionary behavior is related to the environment or to such system properties as total carbon and nitrogen content.

In order to model the mixotrophy system we use the Dynamic Energy Budget (DEB) theory, which is a modeling framework based on physiological mechanisms for the uptake and use of energy [8]. Then, to study under which conditions the mixotrophs will branch, we apply Adaptive Dynamics (AD) theory [2, 13]. The mixotrophy model differs in several aspects from the simple models used so far to develop AD theory. Inherent difficulties are solved by using an alternative method based on Levin's graphical approach, which was extended for density dependence [15]. This graphical method takes into account both natural selection acting on differences in fitness between phenotypes and constraints on the possible set of phenotypes. A trade-off between two traits is shaped by the boundary of this set of possible phenotypes. Instead of assuming a specific function for the trade-off curve as is often done, we derive the trade-off between autotrophy and heterotrophy on basis of mechanisms defining the costs and benefits of assimilation. In addition to providing an example of how AD theory is applied to a DEB model, this study may also improve our understanding of AD theory, as its predictions can be interpreted by the physiological mechanisms underlying the model.

2.2 Methods

2.2.1 Model description

We model the population of mixotrophs and its abiotic environment by means of DEB theory [8]. This theory is a modeling framework for metabolic pro-

cesses with physiological rules for the uptake and use of resources. It respects the principles of energy and mass conservation, and stoichiometric constraints on the synthesis of biomass. We use a simplified version of the mixotrophy model presented by Kooijman et al. [9] that has only one state variable for the mixotrophic organisms (biomass V) and three state variables for the environment: detritus D , dissolved inorganic carbon DIC and dissolved inorganic nitrogen DIN . The latter two states consist of one chemical element only; biomass and detritus are thought of as generalized compounds containing both carbon and nitrogen and other elements, which have a fixed chemical composition. It is assumed that elements other than carbon and nitrogen are not limiting the growth of the organisms, and that the environment is homogeneous; self-shading is neglected. The system is closed for mass, but open for energy.

The four state variables partake in 5 transformations: assimilation A (autotrophic or heterotrophic, A_A or A_H), growth G , maintenance M and death H ; a diagram of these transformations and the corresponding fluxes is shown in Figure 2.1. A mixotrophic organism assimilates the dissolved inorganic carbon and nitrogen from the environment and turns it into biomass and energy via the autotrophic pathway. When the organism dies, its biomass becomes available in the form of dead biomass (detritus) via the heterotrophic pathway of its conspecifics. Maintenance costs, overhead costs for growth and stoichiometric constraints take care of the conversion of organic carbon and nitrogen back into their inorganic form. The changes in state variables can be summarized as:

$$\frac{d}{dt}X_C = X_V(j_{C,A_A} + j_{C,A_H} + k_M), \quad (2.1a)$$

$$\frac{d}{dt}X_N = X_V(j_{C,A_A} + j_{C,A_H} + k_M) n_{N,V}, \quad (2.1b)$$

$$\frac{d}{dt}X_D = X_V(j_{D,A_H} + h), \quad (2.1c)$$

$$\frac{d}{dt}X_V = X_V(j_{V,G} - h), \quad (2.1d)$$

where X_i is the concentration of state variable i and $j_{i,j}$ is the specific flux of compound i partaking in transformation j ; Both the specific maintenance rate k_M and death rate h are assumed to be constant; $n_{N,V}$ is a chemical coefficient which stands for the amount of nitrogen per carbon atom in biomass. The notation used in these and following equations is introduced in Tables 2.1 and 2.2; default values of the parameters are given in Table 2.3.

Biomass and detritus, which consist of general compounds, are expressed in the amount of carbon. Overhead costs for the transformation of inorganic material into biomass (via the autotrophic route) are paid from photons and not from carbon. Therefore, the uptake flux of dissolved inorganic carbon j_{C,A_A} is equivalent to (minus) the autotrophic assimilation flux j_{V,A_A} . The flux of detritus is calculated from the heterotrophic assimilation flux j_{V,A_H} , which is corrected for overhead costs by means of a yield coefficient, $y_{D,V}$. This

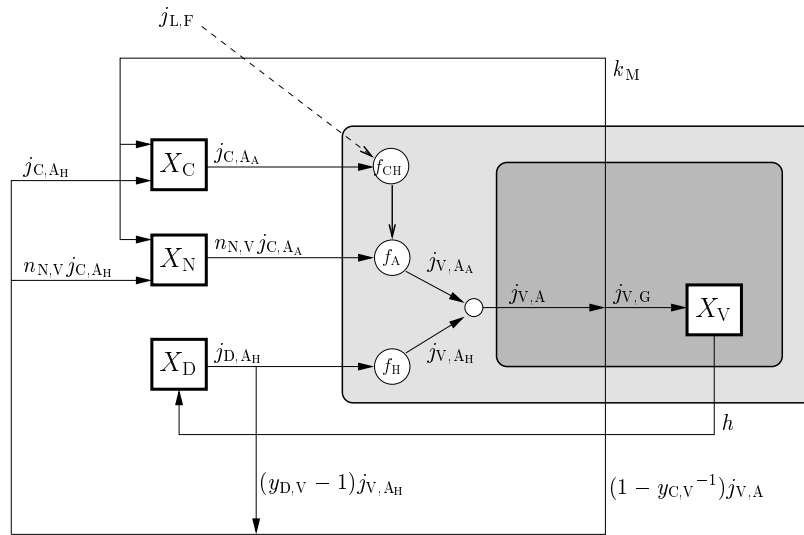


Figure 2.1: Diagram of the metabolism of a mixotroph. The shaded box encloses the organism, the lighter part of which denotes its membranes containing the assimilatory machinery; circles denote a synthesizing unit. The organism has one state variable X_V for biomass; the environment consists of the other three states: dissolved inorganic carbon X_C , dissolved inorganic nitrogen X_N and detritus X_D . Arrows indicate the structure-specific transformation fluxes.

Table 2.1: Table of symbols used for transformations and compounds.

Index	Transformation	Index	Compound
A	assimilation	C	DIC
A_A	autotr. assim.	N	DIN
A_H	heterotr. assim.	V	biomass
M	maintenance	D	detritus
H	death	I	intermediary product
G	growth		

Table 2.2: Table of frequently used symbols for variables. Index m refers to the maximum value. In the dimension column, l means length, t time.

symbol	dim	interpretation
t	t	time
X_i	$\text{mol } l^{-3}$	concentration of compound i
K_i	$\text{mol } l^{-3}$	saturation constant for compound i
$y_{i,j}$	$\frac{\text{mol } i}{\text{mol } j}$	mol compound i required per mol compound j
$J_{i,j}$	$\text{mol } i \ t^{-1}$	flux of compound i associated with transformation j
$j_{i,j}$	$\frac{\text{mol } i}{\text{mol } V} \ t^{-1}$	structure-specific flux of compound i
$j_{i,\text{Am}}$	$\frac{\text{mol } i}{\text{mol } V} \ t^{-1}$	struct-spec. max assimilation flux of compound i
$j_{i,\text{AK}}$	$\frac{\text{mol } i}{\text{mol } V} \ t^{-1}$	struct-spec. max saturation flux of compound i
$n_{i,j}$	–	chemical coefficient for element i in compound j
h	t^{-1}	hazard rate
k_M	t^{-1}	maintenance rate
p_i	–	affinity for assimilatory route i (A = autotrophic, H = heterotrophic route)
z_i	–	flux ratio $j_{i,\text{Am}}/j_{i,\text{AK}}$ for compound i
z	–	determines the curvature of the cost function
f_i	–	scaled functional response for element/process i
r	t^{-1}	struct-spec. growth rate
s	t^{-1}	invasion fitness
s_i	t^{-1}	potential fitness contributed by assimilation via route i (A or H)

yield coefficient denotes the amount of detritus that is required per amount of biomass. The gross growth flux $j_{V,G}$ consists of the total assimilation flux $j_{V,A}$ corrected for maintenance and again the overhead costs. Carbon and nitrogen fluxes due to overhead costs and stoichiometric constraints are included in the heterotrophic assimilation flux $j_{C,AH}$, which simply follows from the difference between incoming (assimilation) fluxes and the production flux of biomass, $j_{V,G}$.

$$j_{C,AA} = -j_{V,AA}, \quad (2.2)$$

$$j_{C,AH} = -j_{D,AH} - \frac{j_{V,AH}}{y_{D,V}}, \quad (2.3)$$

$$j_{D,AH} = -y_{D,V} j_{V,AH}, \quad (2.4)$$

$$j_{V,G} = \frac{j_{V,A}}{y_{D,V}} - k_M. \quad (2.5)$$

The deviation in $j_{C,AH}$ from the model of Kooijman et al. [9] is caused by the extra overhead costs at the transition from assimilates to biomass. The autotrophic and heterotrophic assimilation fluxes $j_{V,AA}$ and $j_{V,AH}$, and the way the total assimilation flux $j_{V,A}$ depends on these two are discussed below.

Assimilation. Mixotrophs have the ability to produce assimilates via two separate pathways, the autotrophic and heterotrophic pathway. In the model, a



Table 2.3: Table of default values.

Control parameters:							
X_{C+}	800	μM					
X_{N+}	150	μM					
$j_{L,F}$	-5	mol/mol d					
Evolutionary parameters:							
ρ_A	0 - 1	-					
ρ_H	0 - 1	-					
Cost levels and function:							
y^0	1.1	mol/mol					
y^A	2.5	mol/mol					
y^H	2.5	mol/mol					
y^{AH}	0.0	mol/mol					
z	1	-					

K_C	500	μM	z_C	10	-	$y_{D,I}$	1.3	mol/mol
K_N	0.1	μM	z_N	10	-	$n_{N,V}$	0.15	-
K_D	2500	μM	z_{CH}	10	-	k_M	0.1	d^{-1}
$j_{V,A_A m}$	2.6	mol/mol d	$j_{L,FK}$	25	mol/mol d	h	0.1	d^{-1}
$j_{V,A_H m}$	2.6	mol/mol d						

central role is played by the affinity that the organisms have for each of these two assimilatory pathways, ρ_A for the autotrophic route and ρ_H for the heterotrophic route. These affinities represent binding probabilities and therefore their values range from 0 to 1. A higher affinity may be interpreted as an increase or an improvement in the assimilation machinery that results in a higher binding probability, which in turn will lead to a higher assimilation flux.

Autotrophic and heterotrophic assimilation fluxes j_{V,A_A} and j_{V,A_H} are calculated by multiplying the affinities with the corresponding maximum assimilation rates $j_{V,A_A m}$ and $j_{V,A_H m}$, and the functional responses f_A and f_H :

$$j_{V,A_A} = \rho_A j_{V,A_A m} f_A, \quad (2.6)$$

$$j_{V,A_H} = \rho_H j_{V,A_H m} f_H. \quad (2.7)$$

In [9], these affinities were not included in the assimilation fluxes, but in the gross growth flux $j_{V,A}$. Another difference is that here we assume that no limitation exists to the maximum flux of processing gross assimilates ($k \rightarrow \infty$). The total assimilation flux $j_{V,A}$ then simply becomes:

$$j_{V,A} = j_{V,A_A} + j_{V,A_H}. \quad (2.8)$$

The functional responses are modeled with use of Synthesizing Units (SUs) cf. Kooijman [7, 8], which provide a simple and realistic method for calculating production fluxes at simultaneous nutrient and light limitations. Planktonic protists have a photosynthetic system that consists of two photosystems, with which they stepwise convert carbon dioxide, nitrogen and light into assimilates. First, carbon dioxide and photons are bound by carriers. Then, the carbon dioxide is reduced into a carbohydrate. Nitrogen is bound, and together the

carbohydrates and nitrogen are synthesized into biomass. This process can be modeled by coupling several SUs: The binding fluxes of carbon f_C and nitrogen f_N can be calculated by a simple one-substrate SU; the reduction rate of carbon f_{CH} can be calculated by a complementary SU for which both carbon and electrons are essential. Finally, f_A can be calculated with again a complementary SU. These processes are represented by the following equations:

$$\begin{aligned}
 f_C &= \frac{X_C}{K_C + X_C}, \\
 f_{CH} &= \frac{1 + z_C^{-1}}{1 + a^{-1} + b^{-1} - (a + b)^{-1}}; \quad a = z_C f_C; \quad b = \frac{-J_{L,F}}{J_{L,FK}}, \\
 f_N &= \frac{X_N}{K_N + X_N}, \\
 f_A &= \frac{1 + z_N^{-1} + z_{CH}^{-1} - (z_N + z_{CH})^{-1}}{1 + a^{-1} + b^{-1} - (a + b)^{-1}}; \quad a = z_N f_N; \quad b = z_{CH} f_{CH},
 \end{aligned} \tag{2.9}$$

where K_i is the saturation constant for compound i and z_i a scaling parameter that weighs the contributions of carbon C , carbohydrates CH and nitrogen N . Light influx $J_{L,F}$ (negative, because photons flow in) is scaled with parameter $J_{L,FK}$, so that a multiplication of these two fluxes with an arbitrary number (different from zero) has no effect. The light influx can be taken proportional to the solar irradiance (photon flux per unit of surface area of water/ air boundary layer). For a detailed discussion on modeling photosynthesis by means of SUs the reader is referred to Kooijman (2000) and Kooijman et al. (2002).

The functional response of the heterotrophic route f_H depends on the binding of detritus, which can be represented by a one-substrate SU:

$$f_H = \frac{X_D}{K_D + X_D}, \tag{2.10}$$

where K_D is the saturation constant for detritus. In [9] a parallel processing SU was used that complemented detritus with DIN to synthesize assimilates; the two models are equal when nitrogen density does not limit the heterotrophic assimilation flux ($K_{N_V} \rightarrow 0$).

At the transformation of assimilates into biomass, overhead costs have to be paid; these were quantified by the yield coefficient $y_{D,V}$ (2.11). This yield coefficient is assumed to be related to the affinities for assimilation, as among the overhead costs are the costs that are associated with building of the assimilation machinery. Depending on the mechanisms assumed, various relations between overhead costs and affinities result. These costs were modeled as to consist of three parts: (1) a constant ‘base’ cost y^0 , specifying the costs involved in biomass production apart from the assimilation machinery; (2) costs associated with the increase in or the improvement of the assimilation machinery, a relation that can be either linear ($z = 1$), convex ($z < 1$) or concave ($z > 1$); the absolute increase in these costs are specified by the parameters y^H and y^A ; (3) other costs, in this case we consider costs proportional to the product of



the two affinities; their relative increase is specified by the parameter y^{AH} . Together, these three parts make up the (flexible) function for the yield coefficient $y_{\text{D,V}}$ that quantifies the overhead costs for growth:

$$\begin{aligned} \text{costs} &= \text{base costs} + \text{costs for ass.machinery } (A_{\text{A}} \text{ and } A_{\text{H}}) + \text{extra costs} \\ y_{\text{D,V}} &= y^0 + y^{\text{A}}(1 - (1 - \rho_{\text{A}})^z) + y^{\text{H}}(1 - (1 - \rho_{\text{H}})^z) + y^{\text{AH}} \rho_{\text{H}} \rho_{\text{A}}. \end{aligned} \quad (2.11)$$

Population and ecosystem. The DEB theory takes the organism's uptake to be proportional to its surface area and maintenance to be proportional to its (structural) mass. Because we assume here that an organism's surface area is proportional to its mass, the distinction between the individual and the population is eliminated in the expressions for the fluxes. The system is closed for mass, but open for energy and is started up containing only one (monomorphic) population of mixotrophs. Because the mixotrophs are capable of both autotrophic and heterotrophic assimilation, all essential recycling of carbon and nutrients is installed and a continuous material cycling through the ecosystem is possible. So, although only a single population is involved, we may regard the mixotrophs and their environment as a complete ecosystem.

Evolution and Specialization. Evolution is included in the system in the form of random but small mutations, i.e. heritable changes in parameters values. The mutations occur (independently) in the values of the two affinities ρ_{A} and ρ_{H} that the mixotrophs have for the two assimilatory pathways. A time scale separation is assumed between the evolutionary time scale and the population dynamical time scale, so that mutations occur only after the system has reached a steady state. Our main goal is then to derive under which conditions for the affinities the mixotroph population specializes into two populations of separate autotrophs and heterotrophs.

2.2.2 Predicting the evolutionary outcome

Predictions of the evolutionary outcome of the system are made with use of AD theory [2, 13]. The fitness s of an organism with a certain phenotype $(\rho_{\text{A}}, \rho_{\text{H}})$ is defined as its long-term average per capita growth rate r . An important concept in AD theory is the feedback loop between population and environment; the resident population is said to 'set' the environment, which is then denoted by E_{res} . The resident population that has reached a steady state with its environment, does not grow or shrink so that phenotypes $(\rho_{\text{A}_{\text{res}}}, \rho_{\text{H}_{\text{res}}})$ belonging to this population by definition have an invasion fitness of zero:

$$s_{\text{res}} = r(\rho_{\text{A}_{\text{res}}}, \rho_{\text{H}_{\text{res}}}, E_{\text{res}}) = 0. \quad (2.12)$$

When a mutant phenotype arises, it will be rare and is therefore assumed not to affect the environment in the short term. Its invasion fitness will thus be

determined by its phenotype $(\rho_{A_{\text{mut}}}, \rho_{H_{\text{mut}}})$, and by the environment which was set by the residents:

$$s_{\text{mut}} = r(\rho_{A_{\text{mut}}}, \rho_{H_{\text{res}}}, E_{\text{res}}). \quad (2.13)$$

Mutants of a phenotype having a positive invasion fitness may be able to invade, those having a negative invasion fitness will die out. Following the invasion, a mutant may replace the resident population and become the new resident or live on in coexistence with the original population. Together, the changed population and the environment will reach a new steady state, in which the new residents will have a growth rate of zero again. It is by a series of such invasions and replacements that the population evolves towards a ‘singular strategy’ at which both the fitness gradients have vanished:

$$\frac{\partial s_{\text{mut}}}{\partial \rho_{A_{\text{mut}}}} = 0 \quad \text{and} \quad \frac{\partial s_{\text{mut}}}{\partial \rho_{H_{\text{mut}}}} = 0. \quad (2.14)$$

A phenotype is a combination of the properties or ‘traits’ that characterize the organisms, and all phenotypes together form the organisms’ trait space. In this trait space, fitness-contour lines connect all combinations of traits that have the same invasion fitness. Such a contour plot is often thought of as a ‘fitness landscape’, with peaks at phenotypes that have a high fitness and valleys at those of small fitness. As invasion fitness depends on the mutant’s trait values but also on the environment which was set by the resident, this landscape is different for different resident populations. The sequence of resident replacements typical to the evolutionary process then gives rise to the concept of ‘changing fitness landscapes’.

The model presented here differs from the simple ‘toy’ models that are often used in AD theory. Not only is the mixotroph model physiologically based, but also is it two-dimensional, meaning that the organisms have two traits that are subject to evolution instead of one. The standard graphical approach in AD that uses Pairwise Invasibility Plots (PIP’s) is only appropriate for one-dimensional cases and comments on the extension of the theory for multiple traits are rare [12, 13]. Therefore, we use an alternative method based on Levin’s graphical approach, which was extended for AD theory by Rueffler and van Dooren [15]. The classical approach [11] is based on fixed fitness landscapes, but the extended approach does include density dependence, which leads to the changing fitness landscapes that are conditional on the resident type. With this method it is possible to classify the evolutionary behavior as a function of the curvature of the invasion boundary and the shape of the trade-off function.

Invasion boundaries are the zero-fitness contours, consisting of all those phenotypes that are selectively neutral, i.e. which neither grow nor shrink in numbers under the conditions set by the resident population. Strategies at one side of the invasion boundary will have invasion fitness smaller than zero and mutants at this side will all die out. Strategies at the other side of the invasion boundary will have invasion fitness higher than zero and mutants at that side will potentially be able to invade.



Trade-offs exist between two (beneficial) processes or traits of which not all combinations are feasible for the organism. Together, the feasible phenotypes constitute the feasibility set, which is a subset of the total trait space. The trade-off function is shaped by the boundary of this feasibility set. For strategies on the trade-off curve an increase in either of the two traits results in a decrease of the other.

Rueffler and van Dooren (2002) explained that under certain assumptions a series of mutations will always lead towards this trade-off curve, and once it has been reached, evolution is assumed to proceed along it. The direction of further trait substitutions depends on whether the derivative of the invasion boundaries is smaller or larger than that of the trade-off curve. Whereas the trade-off curve does not depend on the environment, the invasion boundaries do depend on the environment and so they will change every time the resident population is replaced by a new population. The process of mutations followed by the replacement of the resident population will continue until the invasion boundary becomes tangent to the trade-off curve or until the border of the feasibility set is reached. In the first case the fitness gradient vanishes and a singular strategy is reached. From the shapes of trade-off curve and invasion boundaries, it can then be determined if such a singular strategy is an attractor (convergence stable) and whether it is invadable (evolutionarily stable).

Two of the possible outcomes of evolution are continuously stable strategies (CSS's) and evolutionary branching points (EBP's). The former are convergence stable and evolutionarily stable strategies. In other words these are attractors that can not be invaded by any mutant; the population will remain on such a strategy. The latter are convergence stable but evolutionarily unstable strategies. When arriving at a branching point, the population will suffer from heavy intraspecific competition. Any mutant is able to invade, and disruptive selection will induce the population to split up into two populations. For the mixotrophs such branching points form opportunities to specialize into separate autotrophs and heterotrophs.

In terms of Levins' extended approach a singular strategy is an *attractor* if the slope of the invasion boundaries above this strategy is larger (more negative) than the slope of the trade-off curve at the place where the two intersect; below the singular strategy the slope of the invasion boundaries must be smaller (less negative) than that of the trade-off curve. A singular strategy is *invadable* if the second derivative of the invasion boundaries is smaller (more negative) than that of the trade-off curve. From this it follows that, when the invasion boundaries are known to be linear and the singular strategy is an attractor, the trade-off curve has to be convex in order to give rise to a branching point.

2.2.3 Levins' graphical approach applied to the mixotroph model

To find the conditions under which evolutionary branching occurs in the mixotroph model, we must first define the mixotrophs' traits, invasion fitness and

trade-off function. As was discussed above, every model organism is characterized by its two trait values ρ_A and ρ_H . The values of the affinities range between 0 and 1, so the organism's trait space is the set $\mathcal{T} = \{\rho_A, \rho_H \mid 0 \leq \rho_A \leq 1 \wedge 0 \leq \rho_H \leq 1\}$. The invasion fitness s_{mut} of a mutant strategy $(\rho_{A_{\text{mut}}}, \rho_{H_{\text{mut}}})$ in an environment that is set by the resident population E_{res} is defined as its specific growth rate. This can be rewritten from equations (2.1d) and (2.5) as follows:

$$s_{\text{mut}} = \frac{1}{X_V} \frac{d}{dt} X_V = \frac{j_{V,A}(\rho_{A_{\text{mut}}}, \rho_{H_{\text{mut}}}, E_{\text{res}})}{y_{D,V}(\rho_{A_{\text{mut}}}, \rho_{H_{\text{mut}}})} - k_M - h, \quad (2.15)$$

in which we now denoted explicitly the arguments of the variables. $j_{V,A}$ again is the total gross assimilation flux, $y_{D,V}$ the yield coefficient for biomass out of assimilates, k_M the maintenance costs and h the death rate.

As the affinities are related to both costs and benefits, they are no direct measures for invasion fitness. An expression is needed in which the affinities are translated into a partial fitness contributed by the autotrophic route and a partial fitness contributed by the heterotrophic route. By substituting (2.6) and (2.7) via (2.8) in (2.15) the separate contributions of the two trophic pathways to total invasion fitness become explicit:

$$\begin{aligned} s_{\text{mut}} &= \frac{j_{V,AA}(\rho_{A_{\text{mut}}}, \rho_{H_{\text{mut}}}, E_{\text{res}}) + j_{V,AH}(\rho_{A_{\text{mut}}}, \rho_{H_{\text{mut}}}, E_{\text{res}})}{y_{D,V}(\rho_{A_{\text{mut}}}, \rho_{H_{\text{mut}}})} - k_M - h, \\ &= f_{A_{\text{mut}}}(E_{\text{res}}) \frac{j_{V,AA} \rho_{A_{\text{mut}}}}{y_{D,V}(\rho_{A_{\text{mut}}}, \rho_{H_{\text{mut}}})} + f_{H_{\text{mut}}}(E_{\text{res}}) \frac{j_{V,AH} \rho_{H_{\text{mut}}}}{y_{D,V}(\rho_{A_{\text{mut}}}, \rho_{H_{\text{mut}}})} - k_M - h, \\ &= f_{A_{\text{mut}}}(E_{\text{res}}) s_A(\rho_{A_{\text{mut}}}, \rho_{H_{\text{mut}}}) + f_{H_{\text{mut}}}(E_{\text{res}}) s_H(\rho_{A_{\text{mut}}}, \rho_{H_{\text{mut}}}) - k_M - h, \end{aligned} \quad (2.16)$$

in the last step of which we rename the grouped terms as the potential autotrophic fitness s_A and the potential heterotrophic fitness s_H . These contributions are called 'potential' because they do not include the functional responses f_A and f_H , and thus stand for the maximally attainable fitness of each trophic route.

Now that the contributions of autotrophy and heterotrophy to the invasion fitness have been separated and can be expressed in s_A and s_H , the shape of the trade-off curve and the invasion boundaries can be found much more easily. Equation (2.16) shows that the invasion boundaries are linear in s_A and s_H . Because of this, the evolutionary stability of the singular strategies can be predicted on basis of the shape of the trade-off curve alone: if the trade-off curve is concave the singular strategy will be evolutionarily stable; if it is convex the singular strategy will be evolutionarily unstable. Note that all singular strategies are also attracting (convergence stable), because autotrophs and heterotrophs are mutually dependent; their products serve as each others substrates. This means that the shape of the trade-off curve now fully determines the qualitative evolutionary outcome of the system: if the trade-off curve is concave the population will evolve towards a CSS; if the trade-off curve is convex a branching point will arise.



The trade-off curve can be visualized indirectly by the feasibility set, because it consists of this set's boundary. The feasibility set consists of all possible combinations of s_A and s_H . It is obtained by calculating for every combination of the two affinities the potential autotrophic fitness s_A and the potential heterotrophic fitness s_H ; it thus is the set $\mathcal{F} = \{s_A, s_H \mid 0 \leq \rho_A \leq 1 \wedge 0 \leq \rho_H \leq 1\}$. The feasibility set can be shown by means of a contour or surface plot of the invasion fitness s_{mut} plotted against the two potential fitnesses s_A and s_H ; its boundary is the trade-off curve. A complicating factor in showing the trade-off curve is that the invasion fitnesses of the mutants lying on this curve change with every resident. This can be solved by using the 'total potential fitness' instead of the invasion fitness; the total potential fitness s_{pot} is simply the sum of the two partial potential fitnesses:

$$s_{\text{pot}} = s_A(\rho_A, \rho_H) + s_H(\rho_A, \rho_H). \quad (2.17)$$

Putting the total potential fitness on the z-axis of the contour plot (instead of the invasion fitness) will not affect the feasibility set \mathcal{F} and thus not the shape of the trade-off curve. However, the total potential fitness is independent of the resident strategy, which makes it an obvious and easy method for graphically representing the trade-off curve. In terms of the total potential fitness, the trade-off curve can be described as to consist of those strategies that combine a given value of ρ_H with a value of ρ_A such that the total potential fitness s_{pot} is maximal, provided that ρ_H lies between 0 and the value at which s_{pot} is highest; vice versa, it also consists of the strategies that combine a given ρ_A with a ρ_H such that s_{pot} again is maximal and ρ_A lies between 0 and the value at which s_{pot} is highest. The trade-off curve thus is the set $\mathcal{C} = \{s_A, s_H \mid (0 \leq \rho_A \leq \rho_{A_{\text{pot}}} \wedge \rho_H \mid s_{\text{pot}} = \text{maximal}) \vee (\rho_A \mid s_{\text{pot}} = \text{maximal} \wedge 0 \leq \rho_H \leq \rho_{H_{\text{pot}}})\}$.

The relation between the traits ρ_A and ρ_H and potential fitnesses s_{pot} is illustrated in Figure 2.2, in which surface and (base-)contour plots of the total potential fitness are shown. The figures on the left show the total potential fitness for every combination of ρ_A and ρ_H ; on the right these strategies have been translated into potential fitnesses s_A and s_H , and the total potential fitness was then plotted against these two. In the base-contour plots, the feasibility sets \mathcal{F} now become visible, as do their boundaries \mathcal{C} , which form the trade-off curves between autotrophy and heterotrophy. Each grid cell consists of a different combination of the two affinities and thus denotes a different strategy, and each grid cell in the surface plot on the left corresponds with a grid cell in the surface plot on the right. Although on the left these strategies are shown in terms of affinity values and on the right they are shown in terms of potential autotrophic and heterotrophic fitnesses, corresponding strategies have the same total potential fitness in both plots. In the first example (A) potential fitness increases monotonously in both affinities; in the second example (B) fitness maxima lie at intermediate affinities.

In the plots on the right of Figure 2.2 it can be seen that total potential fitness increases when approaching the trade-off curve. Another feature illustrated in these plots is the role of the constraints on the affinity trait space

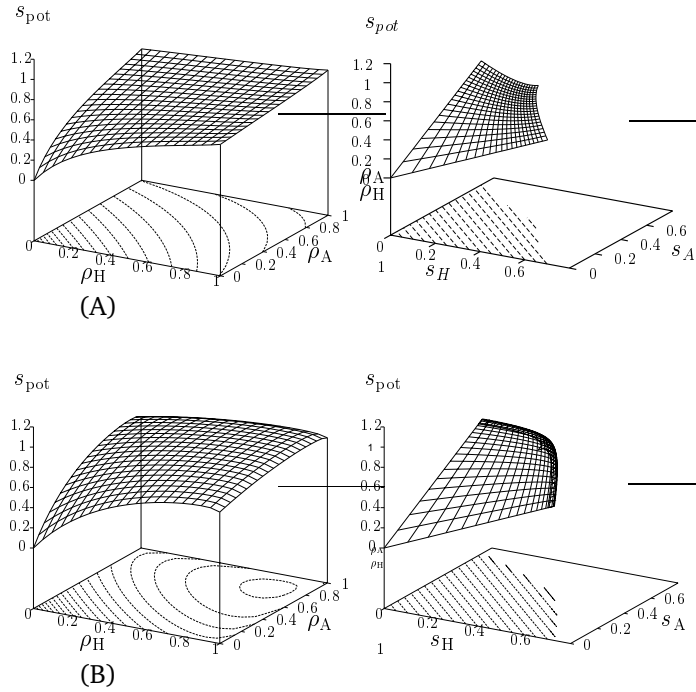


Figure 2.2: Surface plots and (base-)contour plots of total potential fitness s_{pot} (2.17). On the left, total potential fitness is plotted for every combination of the two affinities ρ_A and ρ_H ; on the right these strategies are translated into the potential autotrophic and heterotrophic fitnesses s_A and s_H , and the total potential fitness is then plotted against these two. The base-contour plots in the latter figures show the feasibility sets \mathcal{F} , and their upper boundary is the tradeoff curve \mathcal{C} . (A) Maxima in total potential fitness lie at the extremes of affinity trait space; the trade-off curve coincides with the boundaries of the trait space ($\mathcal{C} = \mathcal{B}$). (B) Maxima in total potential fitness lie at intermediate trait values; on the right the fitness surface folds back onto itself, so that the boundaries of the trait space end up within the feasibility set.



\mathcal{T} . At its boundaries, either of the affinities has a constant value of 1, while the other affinity varies. These boundaries are given by the set $\mathcal{B} = \{s_A, s_H \mid (0 \leq \rho_A \leq 1 \wedge \rho_H = 1) \vee (\rho_A = 1 \wedge 0 \leq \rho_H \leq 1)\}$. In example (A) the trade-off curve coincides with the boundary of the trait space, $\mathcal{C} = \mathcal{B}$. In this case the shape of this trade-off curve is governed by the constraints on the affinities. In example (B) the best strategies lie at intermediate trait values, and limitations to affinity trait space do not play a role in shaping the trade-off curve.

To study the effect of various cost functions, we tested four different cost functions (2.11) and three levels of the costs: For the first three cost functions, costs are related to the trait values ($y^A > 0, y^H > 0, y^{AH} = 0$). For the first cost function a convex relation between affinity and costs was assumed ($z = 0.7$). This cost function implies relatively low costs for small affinities but leads to increasingly higher costs at higher affinities. For the second cost function a linear relation between affinity and costs was assumed ($z = 1$). For the third cost function a concave relation between affinity and costs was assumed ($z = 1.3$), which implies that small affinities are relatively expensive but for higher affinities costs will level off. The fourth cost function does not assume a relation between affinities and costs as such, but is related to the combination of two affinities ($y^A = 0, y^H = 0, y^{AH} > 0$). These costs might for instance be coupled to interference of intermediary products of the two pathways. The amount of costs are in this case proportional to the product of the affinities. Finally, three additional cost functions, consisting of a combination of the fourth costs function with one of the first three ($y^A > 0, y^H > 0, y^{AH} > 0$), were tested for their effect on the shape of trade-off curve. The parameters y^A, y^H and y^{AH} were set to low (1.0), intermediate (2.5) or high values (5.0).

2.3 Results

In Figure 2.3, feasibility sets \mathcal{F} and trade-off curves \mathcal{C} for various cost functions (rows) and at three levels of costs (columns) are shown. In the first three rows, costs are related to trait value. In the fourth row, costs are related to the combination of the two affinities. Arrows indicate the strategies where the population will end up, which in case of a CSS is at the location of the singular strategy (which may be a boundary optimum) and in case of an EBP at the two end strategies that result after evolutionary branching. In the figures also the boundaries of the affinity trait space \mathcal{B} are shown, which are marked by thick continuous curves. It can be seen that in many of these figures, the trade-off curve coincides with these boundaries, $\mathcal{C} = \mathcal{B}$. Although not shown, invasion boundaries are all linear, and they all intersect the feasibility set such that all singular strategies are attracting.

The figure shows that for low cost levels the feasibility sets are large, and that their size decreases and their shape flattens with increasing cost level. At low costs the singular strategy is a boundary optimum that lies in the middle of the trade-off curve; this is an attractor and it is evolutionarily stable (CSS). At high levels of costs the upper-left extreme of the trade-off curve is reached.

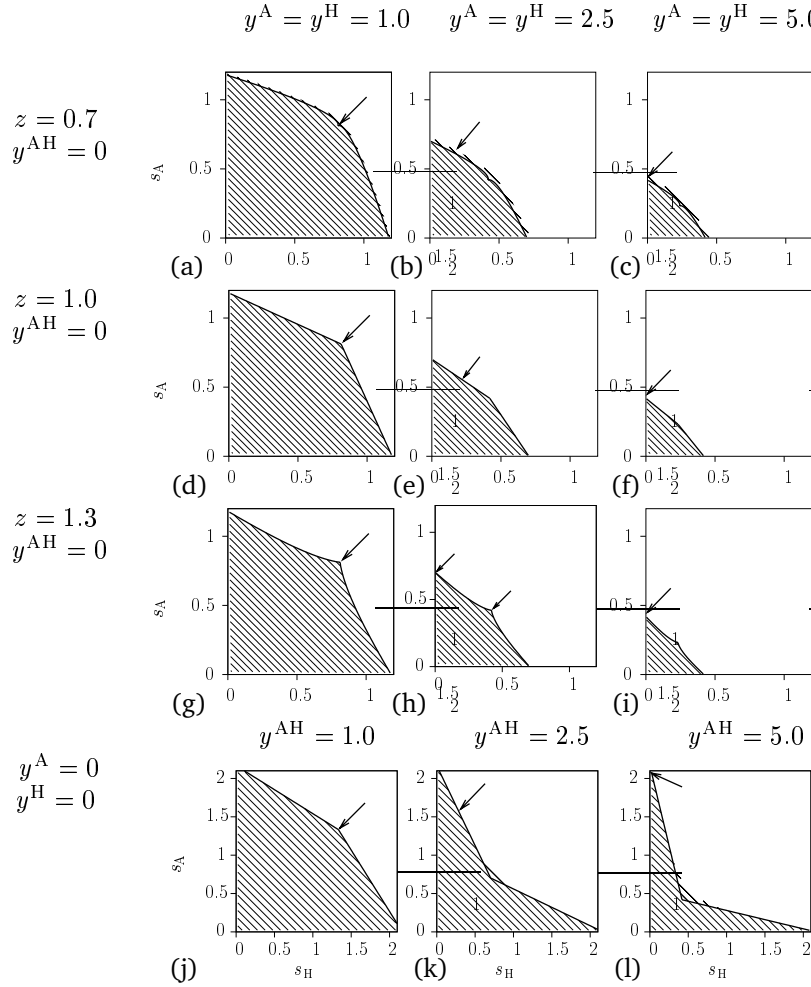


Figure 2.3: Contour plots of total potential fitness s_{pot} (2.17) for various cost functions (rows), and for three levels of costs (columns). The contours give shape to the feasibility sets \mathcal{F} ; their boundaries form the trade-off curves \mathcal{C} . Arrows indicate the evolutionary end strategies. The thick continuous curve shows the boundary of the affinity trait space \mathcal{B} , which in some cases coincides with the trade-off curve. In the first three rows, costs (2.11) are related to the trait values ($y^A > 0$, $y^H > 0$, $y^{AH} = 0$); these relations are convex ($z = 0.7$), linear ($z = 1.0$) or concave ($z = 1.3$). In the fourth row, costs are related to interference of intermediary products ($y^A = 0$, $y^H = 0$, $y^{AH} > 0$). The three levels of costs are low (1.0), intermediate (2.5) and high (5.0). At low costs (left column), the singular strategy is a CSS, with $\rho_H = 1$ and $\rho_A = 1$. At intermediate costs (center column), the singular strategy has shifted to the upper left of the trade-off function. Its evolutionary behavior depends on the specific cost function; At high costs (right column) the evolutionary end point has come to lie at the extreme of the trade-off curve where $\rho_H = 0$. This population is not viable and will die out.



Although this strategy is attracting and evolutionarily stable, it is non viable. Intermediate levels of costs will lead to a singular strategy that lies somewhere in-between, and which is in some cases again a boundary optimum. Its evolutionary behavior, however, is not set by the level of costs; rather it depends on the specific cost function that is assumed.

At convex cost functions for which $z = 0.7$, the resulting trade-off curves are concave; for linear cost functions in which $z = 1$, they consist of two linear parts and for concave cost functions in which $z = 1.3$ they consist of two convex parts. For the fourth type of cost function, resulting trade-off curves consist of two linear parts again. None of these cost functions results in a convex trade-off curve; hence, none of these will lead to evolutionary branching.

The upper row of Figure 2.4 shows the feasibility sets \mathcal{F} and trade-off curves \mathcal{C} resulting from the combined cost functions. In these cost functions the three relations between costs and trait values (convex $z = 0.7$, linear $z = 1$ and concave $z = 1.3$) were combined with extra costs for interference; all costs were set to intermediate levels ($y^i = 2.5$). Again, arrows show the strategies at which the population will end up. The lower row shows the corresponding contour plots in the affinity trait space. Here, dots indicate the end strategies.

It can be seen that for the first combined cost function (Figure 2.4a) the trade-off curve is convex and does not coincide with the trait boundaries. Evolutionary branching may occur and simulations show that the population will then end up consisting of pure autotrophs ($\rho_A = 0.8$, $\rho_H = 0$) and pure heterotrophs ($\rho_A = 0$, $\rho_H = 0.8$); notice that eventually both types have a sub-maximal affinity for the function in which they specialize. A combined cost function with $z = 1$ leads to a trade-off function that consists of two linear parts, resulting in a singular strategy that also is a boundary optimum (CSS) (Fig. 2.4b). The shape of this curve coincides largely with the boundaries of affinity trait shape; only its center does not. A combined cost function with $z = 1.3$ leads to a trade-off that is convexly shaped (Fig. 2.4c) and completely coincides with the boundaries of the affinity values. For this trade-off curve the population will evolve towards a branching point at which the population splits up. Eventually it will end up in pure autotrophs ($\rho_A = 1$, $\rho_H = 0$) and pure heterotrophs ($\rho_A = 0$, $\rho_H = 1$); both types will then have a maximum affinity for the function in which they specialize.

2.4 Discussion

2.4.1 Intrinsic vs. extrinsic properties

Intrinsic properties affect the organism's *potential* fitness, while extrinsic properties affect the environment and therefore the *actual* fitness of the organism. Intrinsic properties considered in this study are the level of the costs, the mechanisms underlying these costs and the constraints on the affinity trait space. With extrinsic properties are meant external environmental properties such as the total carbon or nitrogen content and the incoming light intensity.

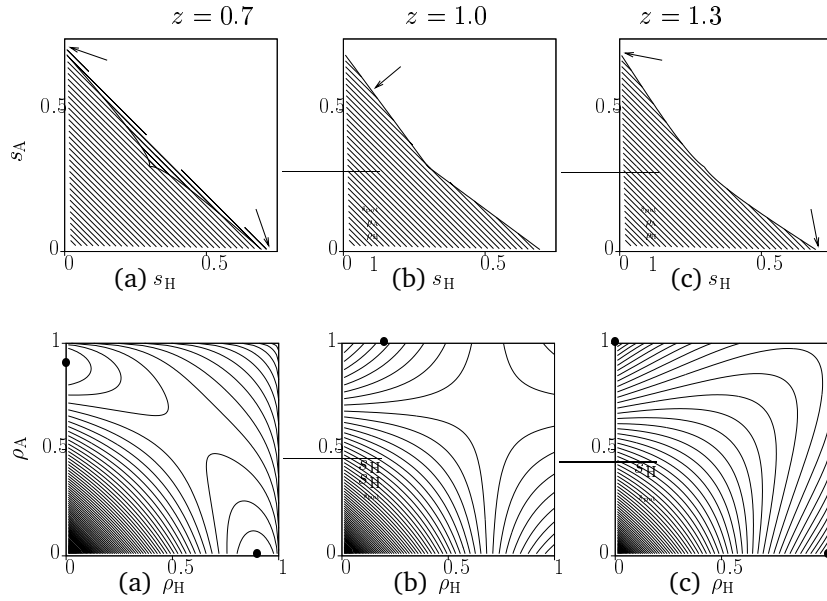


Figure 2.4: Contour plots of total potential fitness s_{pot} (2.17) for the ‘combined’ cost functions. Costs parameters are all set to the intermediate level of 2.5, and are related both to interference of intermediary products and to trait value ($y^A > 0$, $y^H > 0$, $y^{AH} > 0$) (2.11). Latter relation is (a) convex ($z = 0.7$), (b) linear ($z = 1.0$) or (c) concave ($z = 1.3$). The upper row shows the fitness contours in terms of potential autotrophic and heterotrophic fitness, s_A and s_H . Here the feasibility sets \mathcal{F} become visible; their boundaries form the trade-off curves \mathcal{C} . The thick continuous curves show the boundaries of affinity trait space \mathcal{B} . Arrows indicate the evolutionary end strategies. The lower row shows the fitness contours in terms of the affinities, ρ_A and ρ_H . Here, dots indicate the end points of evolution; these correspond to the arrows above. (a) The resulting trade-off is, although only slightly curved, convexly shaped. Evolutionary branching will occur and the population will end up at pure strategies with sub-maximal affinity values. (b) The trade-off curve consists of two linear parts. The population will remain on the boundary maximum; (c) The trade-off curve is convex. The singular strategy is a branching point, at which the population may split up into pure autotrophs and pure heterotrophs with maximal affinity values.



The intrinsic and extrinsic properties affect the system's evolutionary behavior each in a different way. Following Levins' extended approach, the evolutionary outcome of a system is determined by the shape of the trade-off curve and that of the invasion boundaries. As was discussed above, the trade-off curve is based on the boundaries of the feasibility set and is therefore only affected by intrinsic properties. In contrast, invasion boundaries do depend on the environment and theoretically they can thus be affected by extrinsic properties.

Remarkably, however, it was found that the environmental properties do not have any effect on the evolutionary outcomes at all, which was derived mathematically in Appendix I. This result is explained by the mass balance that was respected in the model: the feedback mechanisms that take care of the full material recycling in the system couple the steady state densities of the environment such that even under different environmental conditions the mixotrophs will evolve to the same strategy.

Although this result was derived for a closed system, it can be easily extended to open systems. Changing the closed system into an open system can be done by adding in- and output fluxes to the equations that describe the changes in the state variables (2.1a – 2.1d). For the mixotroph system, an obvious choice would be to have DIC and DIN enter the system, and to have detritus removed as is often the case in the surface layer of a water column. Another possibility would be a constant flow of water in and out of the system, carrying a certain concentration of compounds, such as in a chemostat environment. By consequently adjusting the equations in the appendix as to include these in- and output fluxes, it can be shown that in such open systems the evolutionary behavior would be affected not only by intrinsic parameter values, but also by the parameters that determine these in- and output fluxes (e.g. the dilution rate). If these fluxes are very large, they will come to dominate the system's evolutionary behavior. For example, when the influx of DIC and DIN is very large as well as the outflux of detritus, the autotrophs will be no longer dependent on heterotrophs and are able to survive on their own. Surely, in such an environment it will be advantageous to specialize into more autotrophic organisms. On the other hand, as the in- and output fluxes go to zero, the evolutionary behavior of the system will be dominated more and more by intrinsic parameters. Eventually, the system will be completely closed as the one studied in this paper, and its evolutionary behavior will be determined by intrinsic parameters only.

2.4.2 Boundaries of the affinities' trait space

Figure 2.3 shows that many of the trade-off curves \mathcal{C} coincide with the boundaries of affinity trait space \mathcal{B} . This happens if fitness increases monotonously in both affinities, instead of having an internal optimum. If coinciding with the trade-off curve, these boundaries determine to what value the fitness can increase. Singular strategies on such trade-off curves will thus always lie on (one of) the extremes of the affinity trait space, and will in that sense be boundary

maxima. Usually, at a singular strategy both the fitness gradients vanish (2.14). At the singular strategies that lie at a boundary of the affinity trait space, only one of these gradients will be zero.

The influence of the trait space boundaries becomes apparent in the shape of the trade-off curve, and explains the pointed shapes that many of them have. Along the boundaries of the affinity trait space, one of the traits is held constant at a value of 1. At their ‘tips’, which in affinity trait space corresponds to a strategy of ($\rho_A = 1, \rho_H = 1$), the control of the trade-off curve switches from one boundary to another. At such a tip, neither of the fitness gradients is zero.

This illustrates that the constraints on the affinities can greatly control the location of the singular strategy and the shape of the trade-off curve. In this way they can have considerable effect on the evolutionary outcomes of the system.

2.4.3 Cost level

The level of the costs also has considerable effects on the evolutionary behavior of the system. If costs are small relative to the benefits, the trade-off between autotrophic assimilation and heterotrophic assimilation will be very weak, which results in a feasibility set that is ‘pointing outward’, as can be seen in the first column of Figure 2.3. As small costs hardly put any constraints on the affinity values, it is advantageous to increase these affinities to their maximum, which explains why in these cases the evolutionary behavior is governed completely by the limitations on the range of the trait values. The corresponding evolutionary outcome will be a population ending up at the boundary optimum lying at the ‘tip’ of the trade-off curve which, as mentioned above, corresponds to a strategy of ($\rho_A = 1, \rho_H = 1$).

At intermediate costs, the trade-off is stronger which is visible from the feasibility set that has become smaller and has flattened. In some cases (Figures 2.3e and h) the trade-off curve is still determined by the constraints on affinities; this is, however, largely related to the cost function at hand. In other cases (Figures 2.3b and k), the trade-off curve is (at least partially) governed by the relation of affinities with costs and benefits. The singular strategy has shifted over the trade-off curve in the upper left direction, which in terms of trait values means that the affinity for the heterotrophic route has decreased.

If costs are high, the population will evolve to ‘the extreme’ of the trade-off curve, where the affinity for the heterotrophic route has decreased to zero ($\rho_H = 0$) and organisms are pure autotrophs. Monomorphic populations consisting of a strategy in which one of the trait values is zero are not viable as they can not maintain a complete nutrient cycle; as a consequence such populations will die out. The phenomenon in which the population evolves towards a non viable strategy is called evolutionary suicide [3, 4]. As low costs lead to a boundary optimum that is a CSS while high costs lead to evolutionary suicide, a branching point can only be found at intermediate cost levels.



2.4.4 Cost function

The cost function specifies the relation between costs and affinity. To a large extent, this relation determines whether a trade-off curve is controlled by the boundaries of affinity trait space or not. Costs that increase with affinity in a convex manner ($z > 1$) turn out relatively high for small affinities but level off for higher affinities. Therefore, high affinities will be relatively cheap and these strategies will naturally lead to the highest potential fitnesses. As in such case the potential fitness will be increasing monotonously in the two affinities, it are the boundaries set to the affinity trait space that determine the curvature of the trade-off curve (Figure 2.3, third row). In contrast, concave cost functions ($z < 1$) lead to relatively low costs at small affinities. This leads to a fitness optimum at intermediate affinities, in which case the boundaries of the trait space do not affect the trade-off curve (Figure 2.3, first row). Also for linear cost functions ($z = 1$), high affinities are relatively cheap. This is a consequence of the division of the assimilation flux $j_{V,A}$ by the yield coefficient $y_{D,V}$ (2.5): whereas both the assimilation flux and the costs depend linearly on ρ , only the assimilation flux goes through the origin; the cost function is set off by the base cost y^0 , which is always larger than zero (2.11). Therefore, also for linear cost functions the trade-off function is controlled by the boundaries of affinity trait space (Figure 2.3, second row).

The effect that the cost function has on the evolutionary behavior can be read from the shape of the trade-off curve. For costs that increase with trait values in a convex manner ($z < 1$) the trade-off curve is concavely shaped (Figure 2.3, first row). In combination with invasion boundaries that are linear and singular strategies that are attracting, concave shaped trade-off curves will always lead to continuously stable strategies (CSS's).

For costs that are linearly related to trait value ($z = 1$), trade-off curves consist of two straight lines connected at a blunt angle (Figure 2.3, second row). Linear costs put an advantage to higher affinities; at the boundaries, where one of the affinities is constant, these costs increase linearly with the other affinity. This explains why the two parts of the trade-off curve are linear as well (Figure 2.3d-f). At intermediate costs the singular strategy will lie somewhere on the upper segment of the trade-off curve. Once such a strategy is reached, the invasion boundary coincides with this straight part of the trade-off curve which means that all strategies on this part of the trade-off curve will then have the same invasion fitness. In practice, the population will remain on such a strategy.

Concavely shaped cost functions ($z > 1$) will give rise to trade-off curves that consist of two segments that are both convexly curved (Figure 2.3, third row). This is because at the boundaries, where one of the affinities is held constant, costs still increase convexly and specialized strategies are favored over mixed ones. Like before, at intermediate cost levels, the singular strategy will have shifted to the middle of the upper segment of the trade-off curve. Once the population has reached this strategy, this segment will lie above the invasion boundary, and all strategies on this part of the trade-off function are

able to invade. This combination of trade-off curve and invasion boundary indicates that the system has a branching point at which the population will split into two populations. However, the two resulting populations will consist not of pure autotrophs and pure heterotrophs, but of pure autotrophs ($\rho_A = 1$, $\rho_H = 0$) on the one hand and mixotrophs ($\rho_A = 1$, $\rho_H = 1$) on the other. So basically, only one of the traits is involved in the process of evolutionary branching, while the other trait remains constant.

Trade-off curves resulting from the fourth cost function ($y^{AH} > 0$), in which costs are related to the interference of intermediate products, consist of two straight parts again (Figure 2.3, fourth row); this is because these costs are proportional to the product of the two affinities, and at the boundaries these costs will increase linearly. This cost function only affects mixed strategies; strategies towards the zero-boundaries are much less affected and completely pure strategies are not affected at all, which explains why the extremes of the trade-off curve are equal at all three levels of costs. It also explains that, at the higher cost levels, only these extremes are controlled by the boundaries of affinity trait space and its center is not. At intermediate costs, the singular strategy will lie somewhere at the upper segment of the trade-off curve and the population will remain on this singular strategy.

2.4.5 Evolutionary branching

None of the simple cost functions discussed above leads to a convex trade-off curve; and thus, none of them leads to a branching point. Figure 2.4, however, shows that some of their combinations do lead to convex trade-off curves. In these ‘combined’ cost functions, two mechanisms are assumed to underlie the costs simultaneously: one part of the costs is related to the value of the affinities, and another part is related to the interference between the two affinities. As discussed earlier, the relation between affinities and costs determines whether the fitness optimum lies at intermediate affinities or at maximum affinities values. The costs for interference put a disadvantage to maximizing both traits at the same time, which favors pure strategies over mixed ones. Apparently, it is the combination of these costs that make a convex trade-off curve possible and thus evolutionary branching. To understand this finding, we will discuss the different combinations one by one.

In the first case (Figure 2.4a), the costs of interference are combined with a concave cost function ($z = 0.7$). Owing to the contribution of the concave cost function, the potential fitness maxima come to lie at intermediate affinity values, and the boundaries of the trait space do not play a role in shaping the trade-off curve. Simultaneously, the costs for interference favor pure strategies over mixed ones, which in this case is enough to provide an advantage to specialization. Indeed this cost function leads to a trade-off curve that, although only slightly curved, is clearly convexly shaped and may lead to evolutionary branching of the population.

In the other cases (Figure 2.4b and c), the boundaries of the trait space do affect the trade-off curve, and the formation of its curvature is more complic-



ated. When the trait space boundaries control the trade-off curve, the behavior of the cost function at these boundaries is important. At the boundaries one of the affinities is constant; for the costs related to interference, which are proportional to the product of the affinities, this means that they will increase linearly with the other affinity. Hence, in contrast to the previous case, these costs will now not induce an advantage to specialization. Costs that are related linearly to affinity ($z = 1$) will not favor specialization either. As a result, the trade-off curve will consist of two linear parts (Figure 2.4b). Consequently, the boundary optimum will not be a branching point, and the population will remain on this strategy. However, if the costs related to affinity are concave ($z > 1$), these will favor specialized strategies over mixed ones, even at the boundaries of trait space. Standing alone, these costs led to a trade-off curve that resulted in branching in only one of the traits (see Figure 2.3h); however, in combination with costs for interference that discourages mixed strategies, the two convex parts are connected such that a completely convex trade-off curve results (Figure 2.4c). This gives rise to a branching point and specialization may now occur.

In summary, a single mechanism underlying the costs will not result in evolutionary branching; it is the combination of two mechanisms with complementary effects that can lead to a convex trade-off curve and thus to a branching point. In the first case, the convex relation between costs and affinities leads to a fitness optimum at intermediate affinity values, which is complemented by the costs related to interference that favors pure strategies. In the second case, the concave relation between costs and affinities puts an advantage to maximizing each trait, whereas the costs related to interference makes it disadvantageous to maximize both affinities simultaneously. In both these cases, the mechanisms together combine into an explicit advantage to specialization. Apparently, such an advantage must exist in the underlying metabolic mechanisms in order to obtain evolutionary branching. In many toy models, a single trait value may determine the shape of the trade-off curve. For the studied system, however, two traits are involved that are coupled indirectly via the cost function; constraints imposed on the affinities complicate things even further. As a result, only some of the more complicated cost functions may induce evolutionary branching. This clearly illustrates the considerable consequences that indirect trade-offs and constraints on the trait space can have for the evolutionary outcomes of the system.

2.5 Conclusions

We have studied a DEB model of a population of mixotrophs and the conditions under which this population will specialize into separate autotrophs and heterotrophs. For the mixotrophic organisms a trade-off exists between autotrophy and heterotrophy, which was derived from the physiological mechanisms in the DEB model. Difficulties in applying the AD theory, which were inherent to the model's complexity and its two-dimensionality of the trait space,

could be solved by using the extended version of Levins' graphical approach. This approach was particularly helpful in providing more insight in the effects of the various mechanisms on the curvature of the trade-off function, and therefore on the system's evolutionary outcome.

The evolutionary behavior of the mixotrophic population was found to depend only on intrinsic properties such as the cost function (the relation between the costs and the affinities for assimilation) and the level of these costs; also the boundaries of the affinity trait space were found to play an important role. Evolutionary branching was found to occur only at intermediate cost levels and for cost functions that create an explicit advantage to specialization. Although this might seem obvious, it may not always be realized when assuming a specific trade-off function without considering the underlying mechanisms.

Furthermore, it was found that indirect trade-offs and constraints on the affinities can greatly affect the location of the singular strategy and the shape of the trade-off curve. As such they can considerably complicate the requirements for evolutionary branching. This result should be taken into account when considering trade-offs from real systems, because in the natural situation many constraints and indirect couplings might exist on or between physiological processes.

In contrast to the intrinsic properties, extrinsic properties such as total nutrient content were found to have no effect on the evolutionary outcomes of the model at all; this was related to the mass balance and the feedback mechanisms in the system. Therefore, our analysis suggests that evolutionary branching of the mixotrophic population is not a common feature of the system and that it is not related to the environment. This, perhaps, explains the observations in the introduction that many organisms are in fact mixotrophic, and that mixotrophs are found in a range of eutrophic to oligotrophic waters. However, assumptions such as homogeneity and the application of the mass balance may limit the possibilities for evolutionary branching and specialization. Additional research could therefore study the effects that for instance spatial structure has on the evolutionary behavior of the system.

Another line of research could make use of the fact that the mixotroph model presented in this study consists of only a single population, which makes it one of the smallest non-degenerative ecosystems that we can think of. Evolutionary branching into separate autotrophic and heterotrophic populations forms the first step in the evolution of the ecosystem to develop from a very simple to a more complex (and realistic) ecosystem, purely by self organization. It would be interesting to study this process of self-organization, and to follow the developments that take place in the cycling of energy and nutrients.

Appendix

In this appendix we show that in a homogeneous system, the singular strategy and its evolutionary stability are determined only by parameters that are intrinsic to the organisms. This means that they are not affected by system



properties such as the total nitrogen content, the total carbon content or the incoming light intensity. This can be shown as follows:

As a time scale separation is assumed between the evolutionary and ecological dynamics, the resident population is considered to be always in steady state with its environment. The resident's fitness s_{res} is equal to its specific growth rate (2.15), which in steady state must be equal to zero (2.12):

$$s_{\text{res}} = \frac{j_{V,A}(\rho_{A_{\text{res}}}, \rho_{H_{\text{res}}}, E_{\text{res}})}{y_{D,V}(\rho_{A_{\text{res}}}, \rho_{H_{\text{res}}})} - k_M - h = 0. \quad (2.18)$$

This can be rewritten into the following expression for the total assimilation flux: (The star denotes that a flux is constant on a ecological time scale, but may vary on an evolutionary time scale.)

$$j_{V,A}^* = (k_M + h) y_{D,V}(\rho_{A_{\text{res}}}, \rho_{H_{\text{res}}}) \quad (2.19)$$

Since the system is assumed to be in steady state, the density of detritus is constant; $\frac{d}{dt} X_D = 0$. The detritus density depends on the specific detritus uptake flux (for autotrophic assimilation) $j_{D,AH}$ and the specific influx of detritus, which is equal to the specific death rate h (2.1c). Therefore, in steady state $j_{D,AH}^* = -h$. The uptake flux of detritus is determined by the heterotrophic assimilation flux $j_{V,AH}$ and the yield coefficient of assimilates from detritus $y_{D,I}$ (2.4). With the steady state assumption, (2.1c) and (2.4) can be combined into an expression for the heterotrophic assimilation flux:

$$j_{V,AH}^* = \frac{h}{y_{D,I}}. \quad (2.20)$$

By substituting (2.19) and (2.20) in (2.8), an expression for the autotrophic assimilation flux can now be given as well:

$$(h + k_M) y_{D,V}(\rho_{A_{\text{res}}}, \rho_{H_{\text{res}}}) - \frac{h}{y_{D,I}}. \quad (2.21)$$

Substituting (2.20) and (2.21) in respectively (2.6) and (2.7) yields expressions for the steady state functional responses f_A^* and f_H^* :

$$\begin{aligned} f_A^* &= \frac{(h + k_M) y_{D,V}(\rho_{A_{\text{res}}}, \rho_{H_{\text{res}}}) - \frac{h}{y_{D,I}}}{\rho_{A_{\text{res}}} j_{V,AA}^m}, \\ f_H^* &= \frac{\frac{h}{y_{D,I}}}{\rho_{H_{\text{res}}} j_{V,AH}^m}. \end{aligned} \quad (2.22)$$

The steady state values of both these functional responses can thus be fully expressed in terms of $\rho_{A_{\text{res}}}$ and $\rho_{H_{\text{res}}}$ and other intrinsic parameters that are constant both on an ecological and an evolutionary time scale (h , k_M , $y_{D,I}$, z , $j_{V,AA}^m$, $j_{V,AH}^m$, y^0 , y^A , y^H and y^{AH}).

In turn, the functional responses determine the steady state densities of DIC (X_C), DIN (X_N) and detritus (X_D). This is done via equations (2.9) and

(2.10), such that for a given set of system properties (C^+ , N^+ , and $j_{L,F}$) the invasion fitness of the residents is exactly zero:

$$E_{\text{res}} = \{X_C, X_N, X_D | C^+, N^+, j_{L,F}, s_{\text{res}} = 0\}. \quad (2.23)$$

As follows from (2.13) and (2.15), the invasion fitness of a mutant invading in a resident population depends on its phenotype ($\rho_{A_{\text{mut}}}, \rho_{H_{\text{mut}}}$) but also on the environment as was set by the residents E_{res} and thus on the environmental properties. However, from (2.9) and (2.10) it can be seen that the mutants have exactly the same steady state functional responses as the residents; (2.22) showed that these functional responses do not depend on environmental properties but only on intrinsic parameters:

$$f_{A_{\text{mut}}} = f_A^* \quad \text{and} \quad f_{H_{\text{mut}}} = f_H^*. \quad (2.24)$$

By substituting (2.24) in (2.16), the environmental properties can be ‘bypassed’ in calculating the invasion fitness of the mutants. That is, we do not need the steady state values of DIC, DIN and detritus to calculate the steady state functional responses and the associated invasion fitnesses. Equation (2.13) can thus be replaced by

$$s_{\text{mut}} = r(\rho_{A_{\text{mut}}}, \rho_{H_{\text{mut}}}, \rho_{A_{\text{res}}}, \rho_{H_{\text{res}}}). \quad (2.25)$$

The invasion fitness of a mutant invading a resident population can thus be fully expressed by intrinsic parameters. From the invasion fitness the fitness gradients can be calculated (2.14), as well as the location of the singular strategies and their evolutionary stability. Therefore, predictions on the evolutionary outcomes of the system, which are based on the fitness function, can also be done from intrinsic parameters alone. In other words, the evolutionary outcomes of the system are not affected by the environmental properties at all.

This result can be explained by the feedback mechanisms in the system, which couple the densities of detritus (needed for heterotrophy) with the densities of DIC and DIN (needed for autotrophy). As a consequence, these densities can not vary independently; changing one of the system properties will directly or indirectly affect *all* densities. Because the system is closed, for any set of environmental properties a balance is sought between autotrophy and heterotrophy, which apparently always results in the same evolutionary outcome.

Acknowledgments

We would like to thank Hans Metz, Claus Rueffler and Michel Durinx for their help and suggestions on this work.



References

- [1] Bockstahler, K. R. and Coats, D. W. (1993). Spatial and temporal aspects of mixotrophy in Chesapeake Bay dinoflagellates. *J. Euk. Microbiol.*, 40(1):49–60.
- [2] Geritz, S. A. H., Kisdi, E., Meszéna, G., and Metz, J. A. J. (1998). Evolutionary singular strategies and the adaptive growth and branching of the evolutionary tree. *Evolutionary Ecology*, (12):35–57.
- [3] Gyllenberg, M. and Parvinen, K. (2001). Necessary and sufficient conditions for evolutionary suicide. *Bulletin of Mathematical Biology*, 63:981–993.
- [4] Gyllenberg, M. and Parvinen, K. (2002). Evolutionary suicide and evolution of dispersal in structured metapopulations. *Journal of Mathematical Biology*, 45:79–105.
- [5] Hartman, H. (1998). Photosynthesis and the origin of life. *Origins of Life and evolution of the biosphere*, 28:515–521.
- [6] Holen, D. A. (2000). The relative abundance of mixotrophic and heterotrophic ciliates in an oligotrophic lake. *Arch. Hydrobiol.*, 150(1):1–15.
- [7] Kooijman, S. A. L. M. (1998). The synthesizing unit as model for the stoichiometric fusion and branching of metabolic fluxes. *Biophysical Chemistry*, 73:179–188.
- [8] Kooijman, S. A. L. M. (2000). *Dynamic Energy and Mass Budgets in Biological Systems*. Cambridge University, 2nd edition.
- [9] Kooijman, S. A. L. M., Dijkstra, H. A., and Kooij, B. W. (2002). Light-induced mass turnover in a mono-species community of mixotrophs. *Journal of Theoretical Biology*, 214:233–254.
- [10] Kooijman, S. A. L. M. and Hengeveld, R. (2003). The symbiotic nature of metabolic evolution. *Acta Biotheoretica*, submitted.
- [11] Levins, R. (1962). Theory of fitness in a heterogeneous environment. i. the fitness set and adaptive function. *American Naturalist.*, 96:361–373.
- [12] Meszéna, G., Kisdi, E., Dieckmann, U., Geritz, S. A. H., and Metz, J. A. J. (2001). Evolutionary optimisation models and matrix games in the unified perspective of adaptive dynamics. *Selection*, 2:193–210.
- [13] Metz, J. A. J., Geritz, S. A. H., Meszéna, G., Jacobs, F. J. A., and van Heerwaarden, J. S. (1996). Adaptive dynamics, a geometrical study of the consequences of nearly faithful reproduction. In van Strien, S. J. and Verduyn Lunel, S. M., editors, *Stochastic and spatial structures of dynamical systems*, pages 183–231. Elsevier.

- [14] Raven, J. A. (1997). Phagotrophy in phototrophs. *Limnol. Oceanogr.*, 42:198–205.
- [15] Rueffler, C., van Dooren, T., and Metz, J. A. J. (2004). Adaptive walks on changing landscapes: Levins' approach extended. *Theoretical Population Biology*, 65:165–178.
- [16] Stickney, H. L., Hood, R. R., and Stoecker, D. K. (2000). The impact of mixotrophy on planktonic marine ecosystems. *Ecol. Modelling*, 125:203–230.
- [17] Stoecker, D. K. (1998). Conceptual models of mixotrophy in planktonic protists and some ecological and evolutionary implications. *Europ. J. Protistol.*, 34:281–290.
- [18] Thingstad, T. F., Havskum, H., Garde, K., and Riemann, B. (1996). On the strategy of "eating your competitor": a mathematical analysis of algal mixotrophy. *Ecology*, 77:2108–2118.
- [19] Wachtershauser, G. (1988). Pyrite formation, the first energy source for life: A hypothesis. *Systematic and Applied Microbiology*, 10:207–210.



3

Bifurcation analysis of ecological and evolutionary processes in ecosystems

Tineke A. Troost, Bob W. Kooi and Sebastiaan A.L.M. Kooijman

Abstract

Bifurcation theory is commonly used to study the dynamical behavior of ecosystems. It involves the analysis of points in the parameter space where the stability of the system changes qualitatively. Generally, such changes are related only to changes in environmental parameters, while the organism's trait values are assumed to be constant. In reality, however, these values also change, though on a longer (evolutionary) time scale. On an ecological time scale, evolutionary changes come down to mutants invading a resident population. Points in the trait space where invasibility changes correspond to transcritical bifurcations. Therefore, bifurcation theory may also be used to study the evolutionary dynamics of ecosystems. By analyzing an exemplary system, the advantages of this approach and differences with the Adaptive Dynamics approach are discussed. We will elaborate the evolutionary course of an ecosystem consisting of a mixotroph population. Mixotrophs use inorganic resources for their autotrophic assimilation pathway, and organic material for their heterotrophic pathway. The adaptive traits are the affinities for these two pathways, which also affect the overhead costs for growth. We will show that the shape of the cost-function determines whether the evolutionary end-point is a monomorphic (mixotroph) population, or a dimorphic (autotroph, heterotroph) population.

3.1 Introduction

In biological modeling studies the model behavior is often studied by means of bifurcation analysis. This technique involves the analysis of qualitative changes in the stability of the system. Generally, such changes are related only to changes in environmental parameters such as the total nutrient content or the ambient temperature. The corresponding dynamics all take place on an ecological time-scale, at which the organisms' phenotypes or traits are assumed to be fixed. In reality, however, these traits may also change, though on a much longer, evolutionary, time-scale. As such, evolution provides an additional 'dimension' to the system. In contrast to environmental parameters, however, the trait values cannot be forced externally. Instead, they are the result of an evolutionary process involving mutation and natural selection. Therefore, insight in the evolutionary dynamics of a system is essential for its full understanding.

On an ecological time-scale, evolution consists of mutants trying to invade a resident population. When the mutant is successful, it may replace the residents or coexist with them. This marks a change at the evolutionary time-scale. A common method to analyze evolutionary population dynamics is the Adaptive Dynamics theory [12, 23]. In this approach the invasion fitness of the mutant depends not only on its own trait values, but also on those of the residents, as these interactively determine the environment. Two time-scales are distinguished, the ecological and the evolutionary time-scale. On the ecological time-scale the dynamics of the resident species, as well as other ecosystem species, are generally formulated with difference equations, or with ordinary, delay or partial differential equations. The time-independent parameters that occur in these equations, such as vital rates, depend on the organism's trait values. These traits, in turn, form the state variables in the evolutionary model. Their changes can be described by a set of ordinary differential equations, the so-called 'canonical equations' [7], in which the (stable) equilibrium state variables of the ecological model are parameters.

Points in the trait space where the invasion fitness of the mutant changes sign are the values where the system changes stability. Here a mutant can invade the resident(s) population, which corresponds to an evolutionary change of the ecosystem. In bifurcation theory, these points are called transcritical bifurcation points. This indicates that bifurcation analysis techniques can be used to analyze evolutionary dynamics. The vital parameters which described the ecological function of the populations are now used as bifurcation parameters, instead of the normally used environmental parameters [15]. In [1, 2], the rate of change of a population behavioral trait alters at the ecological time-scale instead of at the evolutionary time-scale. That is, the ecological model is augmented with the equations which describe the dynamics of the adaptive traits. This is the hybrid case where species traits and environmental parameters can be used as bifurcation parameters simultaneously.

The main goal of the paper is to apply bifurcation analysis to both the ecological and the evolutionary dynamics of a simple ecosystem. The stand-



ard graphical approach in Adaptive Dynamics uses Pairwise Invasibility Plots (PIP's). Here we put more information into these diagrams by including bifurcation curves of the ecological model at which the long-term dynamical behavior changes when a parameter is varied. Furthermore we extend the graphical approach for the dimorphic resident population case. Finally, we discuss the advantages of applying bifurcation analysis to evolutionary models.

We use a model considering a mixotroph population in an environment closed for mass and open for energy (incoming sunlight and heat loss). The organisms use light, inorganic carbon and nitrogen to produce carbohydrates via the autotrophic metabolic pathway. Dead organisms are recycled: detritus is consumed and used via the heterotrophic metabolic pathway. Assimilates produced by both the metabolic pathways are used for growth. Organic matter is re-mineralized via overhead costs and maintenance. A system of ODES describes the dynamics at the ecological time-scale. The model is a simplified version of the one used by Kooijman et al. [21], which was also used in [30] and [29]. The adaptive traits ρ_A and ρ_H control the efforts to process assimilates via the autotrophic and heterotrophic metabolic pathways. The model is simplified by assuming a trade-off between the investment into these two pathways, which makes the trait space one-dimensional. Consequently, more results can be obtained analytically, and the standard AD approach using PIP's can be applied.

The evolutionary behavior of this system depends on the shape of the cost function. When it is convex the singular strategy is uninvadable. This is an evolutionary end-point at which the population remains mixotrophic. When the cost function is concave the singular strategy is an evolutionary branching point. Detailed descriptions of the evolutionary course before branching (one resident and one mutant) and after branching (two residents and one mutant) are given. After branching the uninvadable evolutionary end-point is dimorphic in which case autotrophs and heterotrophs coexist.

3.2 The ecological model formulation

The ecosystem is described by four state variables: the mass densities of Dissolved Inorganic Carbon (DIC) X_C , Dissolved Inorganic Nitrogen (DIN) X_N , detritus X_D , and biomass X_V . The state variables partake in 5 transformations: autotrophic and heterotrophic assimilation \mathcal{A} , maintenance \mathcal{D} , growth \mathcal{G} and death \mathcal{H} . The material flows are depicted in Figure 3.1 and the notation is introduced in Table 5.1.

3.2.1 The population model

The conversion of the resources X_C and X_N into biomass occurs via two assimilation pathways, an autotrophic (using inorganic sources) and a heterotrophic one (using organic sources).

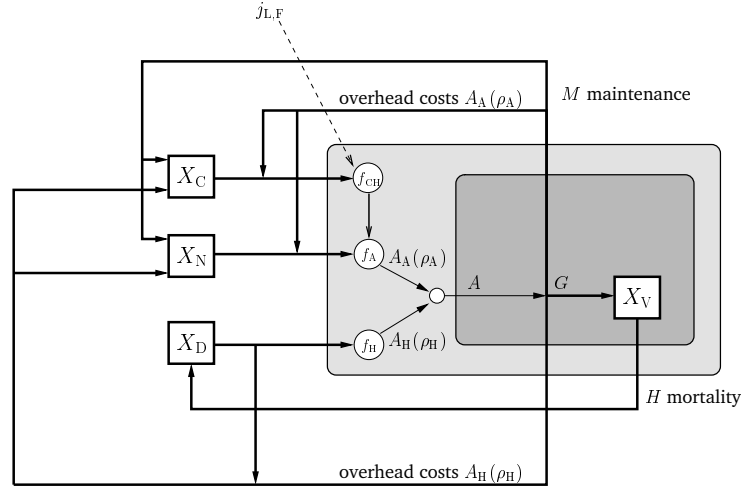


Figure 3.1: Schematic representation of the mass fluxes through the mixotroph system, after Troost et al. [29].

Autotrophic pathway. DIC and DIN are used for assimilation via the autotrophic pathway. The corresponding functional responses for their uptake are Holling type II

$$f_C = \frac{X_C}{K_C + X_C}, \text{ and } f_N = \frac{X_N}{K_N + X_N}, \quad (3.1)$$

where K_C and K_N are the saturation constants. Light is treated as a nutrient, and is stoichiometrically coupled with carbon to form carbohydrates C_H . The corresponding functional response reads

$$f_{CH} = \frac{1 + z_C^{-1}}{1 + z_C^{-1} f_C^{-1} + x_L^{-1} - (z_C f_C + x_L)^{-1}} \quad \text{with } x_L = \frac{-J_{L,F}}{J_{L,FK}}, \quad (3.2)$$

where the light influx $J_{L,F}$ is taken to be proportional to the solar irradiance. The parameter z_C weighs the relative contribution of DIC in the florescence process. The expression (3.2) is proposed by Kooijman [20] to model assimilation and growth and is called a Synthesizing Unit (SU). The light influx is scaled with parameter $J_{L,FK}$, which quantifies the maximum phototrophic assimilation rate. Observe that this functional response (3.2) differs from the Liebig's minimum law formulation [13, 28] in which growth is limited by only one nutrient at a time. The SU-formulation provides a more realistic description of multiple nutrient limitation, and avoids switches in the model that hamper the application of bifurcation theory. Under Liebig's minimum law the Jacobian matrix evaluated at an equilibrium will generally be discontinuous at points at which another resource becomes limiting [19].



Table 3.1: Parameters where element $\mathcal{E} \in \{C, N, \}$ (carbon, nitrogen), compounds $\mathcal{C} \in \{C, \mathcal{N}, \mathcal{D}, \mathcal{V}\}$ (DIC, DIN, detritus, biomass) and transformation $\mathcal{P} \in \{A, H\}$ assimilation processes.

Symbol	Dim	Interpretation
t, τ	t	ecological and evolutionary time scales
X_C	$\text{mol } l^{-3}$	concentration of compound C
K_C	$\text{mol } l^{-3}$	saturation constant for compound C
x_L	–	scaled light influx: $\frac{-J_{L,F}}{J_{L,FK}}$
yc_i, c_j	$\frac{\text{mol } c_i}{\text{mol } c_j}$	mol compound C_i required per mol compound C_j
$j_{C,P}$	$\frac{\text{mol } C}{\text{mol } V} t^{-1}$	structure-specific flux of compound C and process \mathcal{P} : $J_{C,P}/X_V$
$j_{C,Am}, j_{P,AK}$	$\frac{\text{mol } C}{\text{mol } V} t^{-1}$	struct-spec. max assim. & satur. flux, of compound C
$n_{\mathcal{E},C}$	–	chemical coefficient for element \mathcal{E} in compound C
h	t^{-1}	mortality rate
k_M	t^{-1}	maintenance rate coefficient
ρ_A, ρ_H	–	affinities for auto- and heterotrophic assimilation route
z_C	–	assimilation preference for compound C
f_P	–	scaled functional response for transformation \mathcal{P}

Nitrogen and carbohydrates are combined as follows

$$f_A = \frac{(1 + z_N^{-1} + z_{CH}^{-1} - (z_N + z_{CH})^{-1})}{1 + z_N^{-1} f_N^{-1} + z_{CH}^{-1} f_{CH}^{-1} - (z_N f_N + z_{CH} f_{CH})^{-1}}, \quad (3.3)$$

where z_N and z_{CH} weigh the relative contributions of nitrogen and carbohydrates.

Heterotrophic pathway. In [21], the heterotrophic assimilation fluxes are associated with the complementary detritus-nitrogen SU which depends on both detritus and DIN. Here we will follow [30], assuming the more simple Holling type II functional response f_H

$$f_H = \frac{X_D}{K_D + X_D}. \quad (3.4)$$

Growth, maintenance and mortality. Functional responses for the autotrophic and heterotrophic assimilation pathways f_A and f_H determine the two flows $j_{V,AA}$ and $j_{V,AH}$ from the two pathways as follows

$$j_{V,AA} = \rho_A j_{V,AAm} f_A, \quad (3.5a)$$

$$j_{V,AH} = \rho_H j_{V,AHm} f_H. \quad (3.5b)$$

where ρ_A and ρ_H are the organism's affinities for each pathway, and $j_{V,Am}$ and $j_{V,AHm}$ are the corresponding maximum assimilation rates. The two affinities are assumed to be traded off, such that the trait space becomes one-dimensional: $\rho_A + \rho_H = 1$. The value ρ , used from this point on, effectively

Table 3.2: Parameter reference values, after [29].

Symbol	Value	Unit	Symbol	Value	Unit	Symbol	Value	Unit
$j_{L,F}$	-1	mol/mol d	X_{C+}	2400	μM	X_{N+}	40	μM
z_C	0.1	-	z_N	0.1	-	z_{CH}	0.01	-
y^0	1.1	mol/mol	y^A	0.5	mol/mol	y^H	0.1	mol/mol
$j_{V,A_{Am}}$	4.5	mol/mol d	$j_{V,A_{Hm}}$	4.0	mol/mol d	$j_{L,FK}$	50	mol/mol d
$y_{D,V}$	1.3	mol/mol	n_{NV}	0.15	-			
K_C	500	μM	K_N	0.1	μM			
K_{NV}	0.0	μM	K_D	2500	μM			
k_M	0.15	1/d						
h	0.1	1/d						

corresponds to the affinity for the autotrophic pathway, while $(1 - \rho)$ corresponds to the affinity for the heterotrophic pathway. The two assimilation fluxes are then summed to form the total assimilation flux $j_{V,A}$:

$$j_{V,A} = j_{V,A_A} + j_{V,A_H}. \quad (3.6)$$

The conversion of assimilates into new biomass comes with overhead costs $y_{C,V} > 1$. The conversion coefficient $y_{C,V}(\rho)$ is assumed to depend on trait ρ as follows [30]:

$$y_{C,V}(\rho) = y_{C,V}^0 + y^A (1 - (1 - \rho)^z) + y^H (1 - \rho^z). \quad (3.7)$$

Parameter z determines the shape of this cost-function, for $z = 0.7$ it is convex, for $z = 1$ it is linear, and for $z = 1.3$ it is concave. For the parameter values given in Table 3.2 the cost function is increasing for $0.7 < z < 1.3$.

Due to the overhead costs, part of the growth flux ($j_{V,A}(1 - 1/y_{C,V})$) is excreted in the environment. Part of the remaining assimilates are used to pay maintenance costs, which are proportional to the biomass and to the maintenance rate k_M . Death occurs at rate h .

3.2.2 The ecosystem model

We study a system consisting of n populations denoted by V_i , $i = 1 \dots n$. The populations are characterized by their affinity for the assimilatory pathways, ρ_i . Apart from this value, all populations are assumed to have the same set of parameter values. Because the trait value differs per population, also their assimilation rates differ. This, however, does not affect their chemical compositions, nor those of their assimilation and maintenance products. Hence, we can assume that the dead individuals of all populations are converted into the common detritus pool with biomass X_D . This leads to the following state



equations

$$\frac{dX_C}{dt} = \sum_{i=1}^n X_{Vi} \left(-\frac{j_{V,A}^i}{y_{C,V}(\rho_i)} + y_{D,V} j_{V,AH}^i \right) + X_V k_M, \quad (3.8a)$$

$$\frac{dX_N}{dt} = n_{NV} \left(\sum_{i=1}^n X_{Vi} \left(-\frac{j_{V,A}^i}{y_{C,V}(\rho_i)} + y_{D,V} j_{V,AH}^i \right) + X_V k_M \right), \quad (3.8b)$$

$$\frac{dX_D}{dt} = -y_{D,V} \sum_{i=1}^n X_{Vi} j_{V,AH}^i + X_V h, \quad (3.8c)$$

$$\frac{dX_{Vi}}{dt} = X_{Vi} \left(\frac{j_{V,A}^i}{y_{C,V}(\rho_i)} - k_M - h \right), \quad (3.8d)$$

where t is the time at the ecological time scale.

The last term of Eqs. (3.8a) and (3.8b) are due to recycling of the maintenance products. Detritus is produced at a rate equaling the mortality rate of the organism, described by the last terms of Eqs. (3.8c) and (3.8d). Via the heterotrophic pathway the detritus may be converted into biomass again, enabling mass recycling. The resulting assimilates are used for growth and maintenance (see Eq. (3.8d)). The assimilation and maintenance products excreted by the organisms into the environment are instantaneously mineralized.

The system is closed for mass but open for energy, such as light input and heat production. Environmental parameters are the light influx constant $J_{L,F}$, and the total amounts of carbon X_C^+ and nitrogen X_N^+ ,

$$X_{C+} = X_C + X_D + \sum_{i=0}^n X_{Vi}, \quad (3.9a)$$

$$X_{N+} = X_N + n_{NV} \left(X_D + \sum_{i=0}^n X_{Vi} \right), \quad (3.9b)$$

which act as external forcing on the system. The model conserves carbon and nitrogen, so the dimension of the systems equals the number of state variables minus these two ($n + 1$). The initial conditions for X_D and X_V have to be chosen such that all state variables of the full system are always non-negative.

3.2.3 Numerical bifurcation analysis of the ecosystem

To study the ecological dynamics of the system, we first consider one population only ($n = 1$). The steady-state equations are obtained from (3.8) by taking the right-hand sides to be zero. The roots of the resulting set of four non-linear equations have to fulfill the constraints (3.9a) and (3.9b).

$$(1 - \rho) j_{V,AHm} f_H^* = \frac{h}{y_{D,V}}, \quad (3.10a)$$

$$\rho j_{V,AAm} f_A^* = -\frac{h}{y_{D,V}} + y_{C,V} (k_M + h). \quad (3.10b)$$

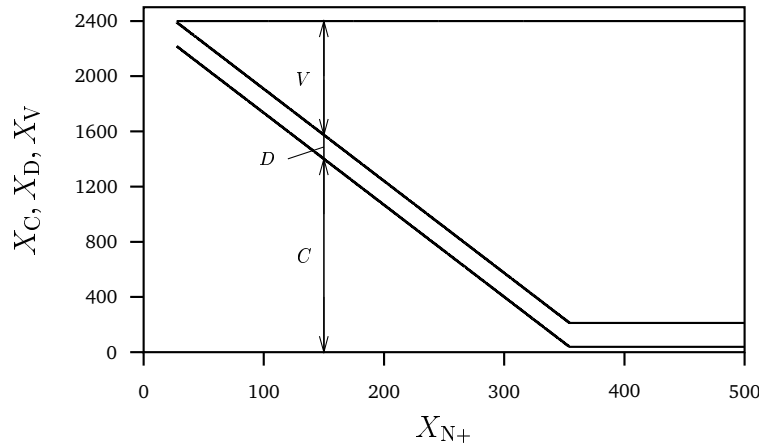


Figure 3.2: The steady-state distribution of carbon in the mixotroph community, plotted for a range of total nitrogen contents, X_{N+} . The non-changed amounts are $X_{C+} = 2400$ C-mol for carbon and $J_{L,F} = 1$ for light. Carbon can occur in the form of DIC, (X_C), detritus (X_D) and biomass (X_V). The amount of C-moles in these state variables are plotted cumulatively. The affinity is taken equal to $\rho = 0.7038$ and $z = 1.3$. All other parameter values are given in Table 3.2.

Equations (3.10a) and (3.1) give an explicit formulation for X_D^* . Equation (3.10b), together with (3.9), determines the remaining three state variables X_C^* , X_N^* and X_V^* . For the parameter values given in Table 3.2 all positive equilibria are stable.

Figure 3.2 shows the bifurcation diagram where the total amount of nitrogen, X_{N+} , is varied. Roughly speaking, DIN is the most limiting nutrient for $X_{N+} \lesssim 350$, and DIC for $X_{N+} \gtrsim 350$. The results are similar to those reported in [21], where the costs for growth $y_{C,V}$ were constant.

In Figure 3.3 the equilibrium values of the four state variables X_C^* , X_N^* , X_D^* and X_V^* are depicted as a function of the single trait value ρ . For a fixed environment with $X_{N+} = 40$, $X_{C+} = 2400$, the population can only exist for a restricted range of affinities ($0.2 \lesssim \rho \lesssim 0.8$).

3.3 The evolutionary model formulation

Now, we consider the parameter ρ to be an adaptive trait whose value may change on the evolutionary time scale τ . The affinity ρ is a genetic trait that is inherited from parent to offspring. A new value of ρ may enter the population through mutation. A mutant may just die out, or it may invade and replace the resident population. A series of such replacements is called a ‘trait-substitution

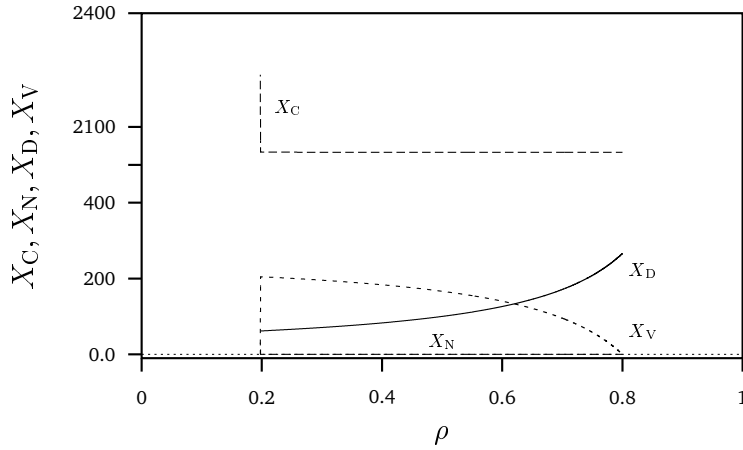


Figure 3.3: The steady-state distributions in the mixotroph community as a function of trait ρ . The non-changed amounts are $X_{C+} = 2400$ C-mol for carbon, $X_{N+} = 40$ N-mol for nitrogen, and $J_{L,F} = 1$ for light. The amount carbon (DIC X_C) nitrogen (DIN X_N), detritus (structural X_D) and biomass (structural X_V) are plotted. All other parameter values are given in Table 3.2.

sequence' and corresponds to evolution of the population.

3.3.1 Invasion of a monomorphic resident population

To study the invasibility of the population we consider two populations ($n = 2$), a resident population with trait value ρ_r and a mutant population with trait value ρ_m . In AD theory, the resident population is assumed to be in equilibrium with its environment, and is therefore said to 'set' the environment, which we denote by $E(\rho_r)$. Mutants are assumed to be rare ($X_{V_m} = 0$), so that initially they do not yet have any affect on their environment. The mutant invasion fitness $s(\rho_m, E(\rho_r))$ is then defined as its long-term per capita growth rate calculated in the equilibrium environment as is set by the resident population, with $X_{V_m} = 0$ [24]. As the resident is in steady state with its environment, its specific growth rate is zero, which leads to the conclusion that the invasion fitness of the resident is always zero, $s(\rho_r, E(\rho_r)) = 0$. The assimilation fluxes for the resident and mutant population read

$$j_{V,A}^r(\rho_m, E(\rho_r)) = \rho_r j_{V,A_{Am}} f_A(\rho_r) + (1 - \rho_r) j_{V,A_{Hm}} f_H(\rho_r), \quad (3.11)$$

$$j_{V,A}^m(\rho_r, E(\rho_r)) = \rho_m j_{V,A_{Am}} f_A(\rho_r) + (1 - \rho_m) j_{V,A_{Hm}} f_H(\rho_r), \quad (3.12)$$

where f_A and f_H are given in Eqs. (3.4) and (3.3). These assimilation fluxes depend only on the trait value of the resident population since the mutant

biomass was set to zero. The mutant invasion fitness is

$$s(\rho_m, E(\rho_r)) = \frac{j_{V,A}^m(\rho_r, \rho_m)}{y_{C,V}(\rho_m)} - k_M - h, \quad (3.13a)$$

$$= \frac{h}{y_{D,V} y_{C,V}(\rho_m)} \left(\frac{1 - \rho_m}{1 - \rho_r} - \frac{\rho_m}{\rho_r} \right) + (k_M + h) \left(\frac{\rho_m y_{C,V}(\rho_r)}{\rho_r y_{C,V}(\rho_m)} - 1 \right). \quad (3.13b)$$

When the invasion fitness is positive, the mutant may invade and may then replace the residents, or it may coexist together with them. When the invasion fitness is negative, the mutant will just die out.

By a series of invasions and replacements of the residents, the population evolves. The direction and speed with which this happens depends on the local ‘invasion gradient’. This gradient reads

$$\left. \frac{\partial s(\rho_m, E(\rho_r))}{\partial \rho_m} \right|_{\rho_m = \rho_r} = \frac{y_{C,V}(\rho_r) \left(\frac{-h}{y_{D,V}(1-\rho_r)\rho_r} + (k_M + h) \left(\frac{y_{C,V}(\rho_r)}{\rho_r} - \frac{\partial y_{C,V}(\rho_r)}{\partial \rho_r} \right) \right)}{(y_{C,V}(\rho_r))^2}, \quad (3.14)$$

where

$$\left. \frac{\partial y_{C,V}(\rho_m)}{\partial \rho_m} \right|_{\rho_m = \rho_r} = y^A z (1 - \rho_r)^{z-1} - y^H z \rho_r^{z-1}. \quad (3.15)$$

The dynamics of the trait ρ_r and the full evolutionary trajectory of the population are then described by the canonical equation [4, 5, 7]

$$\frac{d\rho_r}{d\tau} = \kappa X_{V_r}^* \left. \frac{\partial s(\rho_r, \rho_m)}{\partial \rho_m} \right|_{\rho_m = \rho_r}, \quad (3.16)$$

where τ is the time at the evolutionary time scale; κ is the invasion rate coefficient and describes the frequency and variance of the mutations.

Evolution continues until the invasion gradient (3.14) becomes zero. This occurs when

$$\frac{h}{y_{D,V}(k_M + h)} = y_{C,V}(\rho_r)(1 - \rho_r) - y^A z (1 - \rho_r)^z \rho_r + y^H (1 - \rho_r) z \rho_r^z, \quad (3.17)$$

where $y_{C,V}(\rho_r)$ is given by Eq. (3.7). The root of this equation is called the ‘singular strategy’ SS, denoted by ρ_r^* . Figure 3.4 plots the invasion fitness $s(\rho_m, E(\rho_r^*))$ of a range of mutants while the resident has a trait value equal to the SS, for three values of z : $z = 0.7$ (continuous curve), $z = 1$ (dashed curve) and $z = 1.3$ (dotted line).

The evolutionary stability of the SS can be determined by the second derivative of the fitness function with respect to the mutant trait, evaluated in the SS:

$$\left. \frac{\partial^2 s}{\partial \rho_m^2} \right|_{\rho_m = \rho_r} = \left. \frac{\partial^2 s(\rho_r, \rho_m)}{\partial \rho_m^2} \right|_{\rho_m = \rho_r}. \quad (3.18)$$

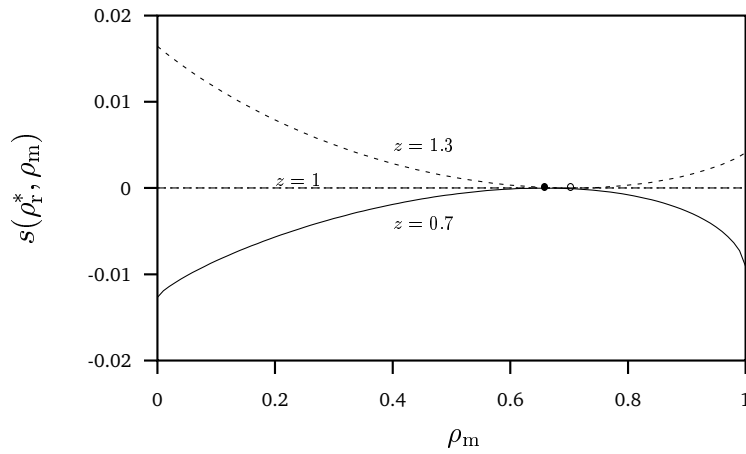


Figure 3.4: Invasion fitnesses $s(\rho_m, E(\rho_r))$ for mutants with a range of trait values ρ_m in the resident population at the ss ρ_r^* , for $z = 0.7$ (continuous curve where $\rho_r^* = 0.6578$, CSS), and $z = 1.3$ (dotted curve where $\rho_r^* = 0.7038$, EBP). For $z = 1$ the invasion fitness is zero (dashed curve) and the singular strategy becomes $\rho_r^* = 0.67948$. The symbols (filled circle for $z = 1.3$ and open circle for $z = 0.7$) indicate the singular strategy ss values ρ^* . All other parameter values are given in Table 3.2.

If this derivative is negative, residents with this strategy cannot be invaded by any mutant. Hence, the ss is evolutionarily stable and the population will remain on this strategy, which is a ‘continuously stable strategy’ (css) [12]. On the other hand, if the derivative is positive, the residents on this strategy are invadable by any mutant. The ss is evolutionarily unstable and is now called an ‘evolutionary branching point’ (EBP) [12]. Once the population has reached this strategy, disruptive selection will induce the population to split up and into two coexisting subpopulations. The evolutionary dynamics of the resulting dimorphic system are discussed further in section 3.3.5. First, however, we study how the stability of the ss depends on a change of the coefficient z and we present the corresponding bifurcation diagrams.

3.3.2 Bifurcation analysis of the evolutionary model

In terms of bifurcation analysis, the invasibility of the resident is determined by the system’s stability. As the resident is assumed to be in equilibrium with its environment, the system without the mutant is stable. If the stability does not change when a mutant is added to the system, this mutant will just die out. If the stability does change, however, the mutant may be able to invade. The stability is obtained by evaluation of the Jacobian matrix of system (3.8) with $n = 2$, evaluated in the equilibrium point X_D^* , $X_{V_r}^*$ and $X_{V_m}^* = 0$. Since the system is closed for mass we can eliminate the equations for the two nutrients X_C and X_N . Hence, the Jacobian matrix is a 3×3 matrix, where the detritus X_D and biomasses of the resident and mutant populations X_{V_i} , $i = r, m$ are the state variables.

The determinant of the Jacobian matrix evaluated at the equilibrium is factorizable. That is, it equals the determinant of the system where the mutant population is not considered, times the long term specific growth rate (invasion fitness) of the mutant. Since we assumed that the system without mutant is in stable equilibrium, the real part of the roots of the characteristic equation of this system are all negative. Consequently, the stability of the system including the mutant is completely determined by the sign of the invasion fitness s . Therefore, the adaptive dynamics approach and the bifurcation approach come down to the same thing: $s < 0$ gives stability in which case the mutant cannot invade, while $s > 0$ means instability and thus invasibility of the resident population. Notice that there are two additional zero eigenvalues when the two nutrients are included.

Computer packages LOCBIF [14], CONTENT [22] and AUTO, [9, 10] can be used to calculate the transcritical bifurcation curves. We found that it was not possible to use the standard procedure in AUTO. Obviously, the fact that two transcritical curves intersect in the ss causes a problem. This was solved as follows. Since we are interested in the situation where the biomass of the mutant population is zero we can skip the equation for the mutant population from Eq. (3.8) while still the equilibrium values for the resident populations are determined as equilibria of the resulting system. In order to fix a transcritical bifurcation point in that point where the invasion rate of the mutant is zero we



append Eq. (3.19c) to that system where the trait of the mutant ρ_m is taken as a state variable. Though this equation does not have an interpretation, it can be used to continue the transcritical bifurcation.

$$\frac{dX_D}{dt} = -y_{D,V} \sum_{i=1}^n X_{Vi} j_{V,AH}^i + X_V h, \quad (3.19a)$$

$$\frac{dX_{Vri}}{dt} = X_{Vri} \left(\frac{j_{V,A}^{ri}}{y_{C,V}(\rho_{ri})} - k_M - h \right), \quad (3.19b)$$

$$\frac{d\rho_m}{dt} = \frac{j_{V,A}^m}{y_{C,V}(\rho_m)} - k_M - h, \quad (3.19c)$$

where $y_{C,V}(\rho)$ is given by (3.7) and the growth flux $j_{V,A}^i$ by (3.6). Both X_C and X_N are eliminated using mass conservation. The trait ρ_r is the free bifurcation parameter with the continuation of the so-called fold bifurcation where one eigenvalue of the Jacobian matrix evaluated at the equilibrium equals zero.

To calculate the evolutionary dynamics, the fitness gradient with respect to the trait of the two residents has to be evaluated, for which at each instant the equilibrium values of the state variables of the ecological system (3.8) have to be calculated. This can be avoided by integrating both the ecological and evolutionary model simultaneously for $t = \varepsilon\tau$, $\varepsilon \ll 1$ by implementing an approximation of the time-scale separation. Symbolic expressions for the invasion gradients can be obtained using symbolic computer packages. We used Maple (Maplesoft, Waterloo, Canada) together with AUTO.

3.3.3 Bifurcation diagrams for the monomorphic resident population

The Pairwise Invasibility Plot (PIP) in Figure 3.5 shows the invasibility of a rare mutant with trait value ρ_m in a resident population with trait value ρ_r [3, 12] for $z = 1.3$ (continuous curves) and $z = 0.7$ (dashed curves). The vertical lines are the mutant zero invasion fitness isoclines ($s(\rho_m, E(\rho_r)) = 0$). The horizontal lines denote the zero fitness isoclines for the residents when the roles of mutant and resident are interchanged ($s(\rho_r, E(\rho_m)) = 0$); these are easily obtained by mirroring the mutant isocline over the diagonal. On the diagonal, mutant and resident have the same trait value, and therefore their invasion fitnesses are zero as well. Together, these lines bound six regions: two with a ‘+’ where the mutant invasion fitness is positive in which case the mutant may invade and replace the resident; two with a ‘-’ where the mutant invasion fitness is negative in which case it cannot invade; and two with ‘++’ in which case the mutant may invade but cannot replace the resident: when invaded by the mutant, the resident may invade ‘back’, which is called ‘mutual invasibility’. The ss lies at the trait value ρ_r^* where the local fitness gradient (Eq. 3.14) is zero.

With $z = 0.7$ we have $\rho_r^* = 0.6578$ and at this point the second derivative (Eq. 3.18) is negative. Hence, the ss is a CSS [12] on which the population will

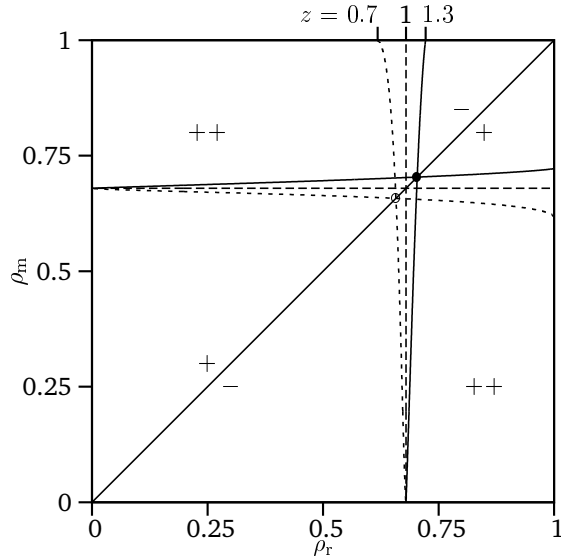


Figure 3.5: Pairwise Invasibility Plot (PIP) plotting the invasion fitness of a mutant with trait value ρ_m invading a resident population with trait value ρ_r . It shows the zero fitness isoclines for $z = 0.7$ (dotted lines), $z = 1.0$ (dashed curves) and $z = 1.3$ (continuous curves). The intersection of the diagonal with the other two curves corresponds to a singular strategy (SS). ‘-’ denotes the area in which the mutant cannot invade the resident, ‘+’ denotes the area in which the mutant may invade and replace the resident, and ‘++’ denotes the area of mutual invasibility in which the mutant may invade but cannot replace the residents.

remain. For $z = 1.3$ we have $\rho_r^* = 0.7038$. At this point the second derivative is positive and therefore the SS is an (EBP) at which the population will split up into two coexisting subpopulations.

The two-parameter bifurcation diagram in Figure 3.6 uses as bifurcation parameters the affinities of two competing populations, ρ_1 and ρ_2 . Though it looks very similar to the PIP in Figure 3.5, its interpretation is different. Instead of a resident population and a rare mutant with traits, the bifurcation diagram treats the two populations as equals. The lines now denote transcritical bifurcation curves, which are the boundaries in trait space where the system changes stability. Formally, these boundaries correspond not to zero invasion fitnesses, but to zero biomass of (one of) the populations. In the trait space below TC_1^- no population can exist. Above TC_1^- one population can exist stably. At TC_2^- the biomass of population 2 is zero ($X_{V_2} = 0$), while above TC_3^- the biomass of population 1 is zero ($X_{V_1} = 0$). Between these lines both populations can coexist. Coexistence in this figure corresponds to mutual invasibility in the PIP-plot (Figure 3.5). Above TC_4^- no population can exist. At the diagonal line Z ,

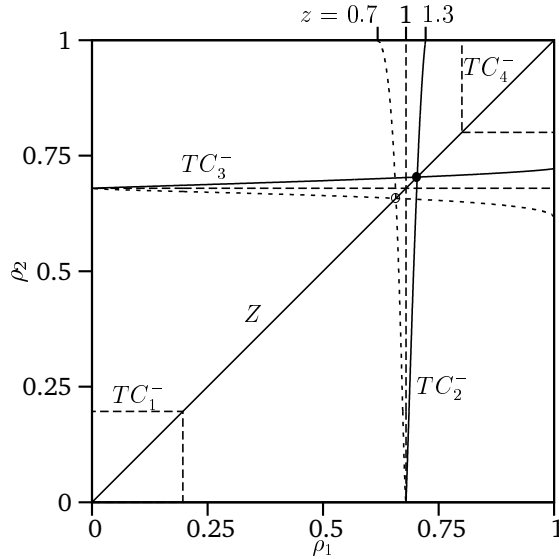


Figure 3.6: Two-parameter bifurcation diagram, using as bifurcation parameters the affinities of two competing populations, ρ_1 and ρ_2 . Transcritical bifurcation curves are shown for three z -values, $z = 1.3$ (continuous curve), $z = 1$ (dashed curve) and $z = 0.7$ (dotted curve). At TC_1^- and at TC_4^- , one of the populations has zero biomass and can establish itself. At TC_2^- population 2 has zero biomass, and can establish itself next to population 1. At TC_3^- population 1 has zero biomass and can establish itself next to population 2; between these two bifurcation curves both populations can exist.

the two populations exchange roles. Crossing this line in a vertical direction corresponds to the replacement of population 2 by population 1. At this point the biomass of population 1 goes from zero to an equilibrium value, while at the same time the biomass of population 2 goes to zero. As these changes in equilibrium biomass densities are not smooth, Z is a catastrophic bifurcation. Moreover, points on Z are also structurally unstable, as the biomasses of the two populations are undetermined, only their total biomass is known.

When interpreting the two populations as residents and mutants, the bifurcation plot provides information about the evolutionary dynamics of the system. The change in stability to which the transcritical bifurcations correspond, may be interpreted in terms of invasibility. Crossing TC_2^- corresponds to the mutant invading the resident, while crossing the TC_3^- corresponds to the resident invading the mutant. The ss lies at the point where the two transcritical bifurcations intersect, which thus is a degenerated point. Introducing a mutant in a system with residents that have the ss, corresponds to moving up or down in the strictly vertical direction in the plot. Evolutionary stability is en-

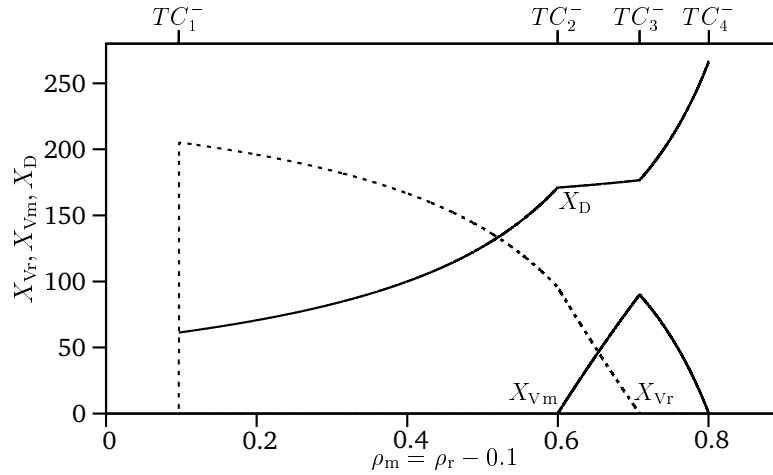


Figure 3.7: Steady-state distributions of detritus X_D , resident X_{Vr} and mutant X_{Vm} biomass as function of trait $\rho_m = \rho_r - 0.1$ for a monomorphic resident population, where $z = 1.3$.

sured when we do not end up in the region where coexistence is possible. This holds true for $z = 0.7$. Because the transcritical bifurcation curve for $z = 0.7$ does not intersect with the vertical line through the ss, this also holds for large mutational steps. With $z = 1.3$, such movements end up in the region of coexistence. Hence in this case the ss is evolutionarily unstable and thus an EBP. For a linear cost function ($z = 1$), numerical evaluation of the expression for the invasion fitness in its singular strategy $\rho_r^* = 0.67948$ equals zero, independent of the trait value of the mutant ρ_m . Hence, when the resident population possesses the singular strategy, all mutants have a zero invasion fitness.

The one-parameter bifurcation diagram in Figure 3.7 depicts the equilibrium detritus X_D and biomasses X_{Vi} along the subdiagonal curve, $\rho_m = \rho_r - 0.1$. At the two transcritical bifurcation points TC_1^- and TC_4^- , biomasses are zero of the mutant and the resident populations, respectively. Between TC_1^- and TC_2^- only the resident population exists, while between TC_3^- and TC_4^- only the mutant population exists. Between TC_2^- and TC_3^- both populations coexist. We remark that for $\rho_m = \rho_r + 0.1$ (the line symmetric with respect to the diagonal, $\rho_m = \rho_r$) the same results hold when X_{Vr} and X_{Vm} are interchanged, that is, the two populations change role.

Figure 3.8 is again a one-parameter bifurcation diagram where now $\rho_r = 0.7$ and ρ_m is the bifurcation parameter. The range of parameter ρ_m is divided in four subregions. Coexistence of the resident and mutant population occurs for low ($\rho_m < TC_2^-$) and high ($\rho_m > TC_3^-$) values. In the intermediate range the mutant is extinct, while at crossing the diagonal (Z) in region the mutant replaces the resident. As a result of the small mutational step assumption the value of the mutant never lies in the two outer regions during a monomorphic

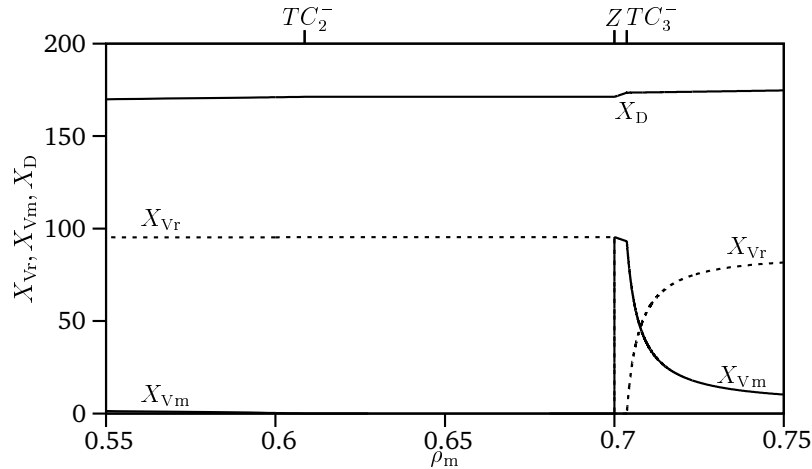


Figure 3.8: Steady-state distributions of detritus X_D , resident X_{Vr} and mutant X_{Vm} biomass as function of the trait ρ_m , where $\rho_r = 0.7$ and $z = 1.3$ for a monomorphic resident population. Note that the plot shows a limited range of values for ρ_m .

evolutionary sequence. Figure 3.8 illustrates what happens on the diagonal Z , where $\rho_m = \rho_r$. Here, the steady state biomasses of the two populations X_{Vr}^* and X_{Vm}^* themselves are not fixed, only their sum is. This shows that the diagonal is a structurally unstable point where the dependence of the state variables is not smooth with respect to a parameter change. A similar bifurcation point was found in [17] where the effects were studied of predation of two prey populations living on a single nutrient in a chemostat environment, a phenomenon called ‘predator-mediated coexistence’.

3.3.4 Invasion of the dimorphic resident population

We have seen that when $z = 0.7$ the singular strategy is a CSS. Hence, the population will evolve towards it and then remain on it. However, for $z = 1.3$ the singular strategy was an EBP. This means that the population will evolve towards it, but not remain on it. When it has reached the ss, disruptive selection will split up the population such that it becomes dimorphic. To study the evolutionary dynamics in this post-branching period, we will study the invasibility of a dimorphic resident population. Therefore, we now consider a trimorphic population ($n = 3$), consisting of two resident populations and one mutant population. In Figure 3.9 the region of coexistence of the two residents in the three dimensional parameter space is drawn. Two subdiagonal planes are important, one where $\rho_m = \rho_{r1}$ and ρ_{r2} is free, and the other where $\rho_m = \rho_{r2}$ and ρ_{r1} is free. So on these planes the mutant is equal to one of the residents. Since we may restrict ourselves to the invasion of a rare mutant which differs slightly

from one of the two residents we are interested in the part of the diagram close to these two subdiagonal planes which intersect in the diagonal line Z where $\rho_m = \rho_{r1} = \rho_{r2}$. Pre-branching dynamics is restricted to this diagonal line on which the point $\rho_{r1} = \rho_{r2} = \rho_m = \rho_r^*$ is the singular strategy. In a similar way, the post-branching process is restricted to the two subdiagonal planes.

The invasion fitness for the mutant invading the resident population $i = 1, 2$ with trait ρ_{ri} equals

$$s_i(\rho_m, E(\rho_{r1}, \rho_{r2})) = \left. \frac{j_{V,A}^m(\rho_{r1}, \rho_{r2}, \rho_m)}{y_{C,V}(\rho_m)} \right|_{\rho_m=\rho_{ri}} - k_M - h. \quad (3.20)$$

The invasion gradients for the mutant invading the resident populations $i = 1, 2$ with trait ρ_{ri} read

$$\left. \frac{\partial s_i(\rho_m, E(\rho_{r1}, \rho_{r2}))}{\partial \rho_m} \right|_{\rho_m=\rho_{ri}} = \left. \frac{y_{C,V}(\rho_m) \frac{\partial j_{V,A}^m(\rho_{r1}, \rho_{r2}, \rho_m)}{\partial \rho_m} - j_{V,A}^m(\rho_{r1}, \rho_{r2}, \rho_m) \frac{\partial y_{C,V}(\rho_m)}{\partial \rho_m}}{(y_{C,V}(\rho_m))^2} \right|_{\rho_m=\rho_{ri}}, \quad (3.21)$$

with $\partial y_{C,V}(\rho_m)/\partial \rho_m|_{\rho_m=\rho_{ri}}$ given by (3.15).

The dynamics of the two traits ρ_{ri} are described by the canonical equation

$$\frac{d\rho_{ri}}{d\tau} = \kappa X_{V_{ri}}^* \left. \frac{\partial s_i(\rho_m, E(\rho_{r1}, \rho_{r2}))}{\partial \rho_m} \right|_{\rho_m=\rho_{ri}}, \quad (3.22)$$

where the parameter κ is the invasion rate coefficient of the mutant.

To calculate the evolutionary dynamics we have to solve ODE-system (3.22). Evaluation of the right-hand side of these ODEs requires the calculation of the invasion gradient $\partial j_{V,A}^m(\rho_{r1}, \rho_{r2}, \rho_m)/\partial \rho_m$ which depends on the three equilibrium values for detritus X_D^* and the biomasses of the two residents $X_{V_i}^*$, $i = 1, 2$. (We recall that since the system is closed for mass we can eliminate the two nutrients equilibrium densities X_C^* and X_N^* .) This means that in each time step of the procedure to solve the ODE-system, the equilibria of the ecological model have to be solved numerically.

The ss for the monomorphic resident population is also a ss for the dimorphic resident population. However, when we allow infinitesimally small evolutionary changes, this point is never reached in the pre-branching episode. Therefore, Geritz et al. [12] explicitly do not allow ‘infinitesimally small evolutionary changes’ and the biologically more realistic assumption is made that the mutations are small but discrete. As a result, evolution does not stop after reaching (a point close to) the ss, but continues as a development of a dimorphic resident population.

3.3.5 Bifurcation diagrams for the dimorphic population

To study invasibility of the dimorphic resident population we calculated one-parameter diagrams for pairs of residents (ρ_{r1}, ρ_{r2}) with $\rho_r^* < \rho_{r1} \leq 1$ and

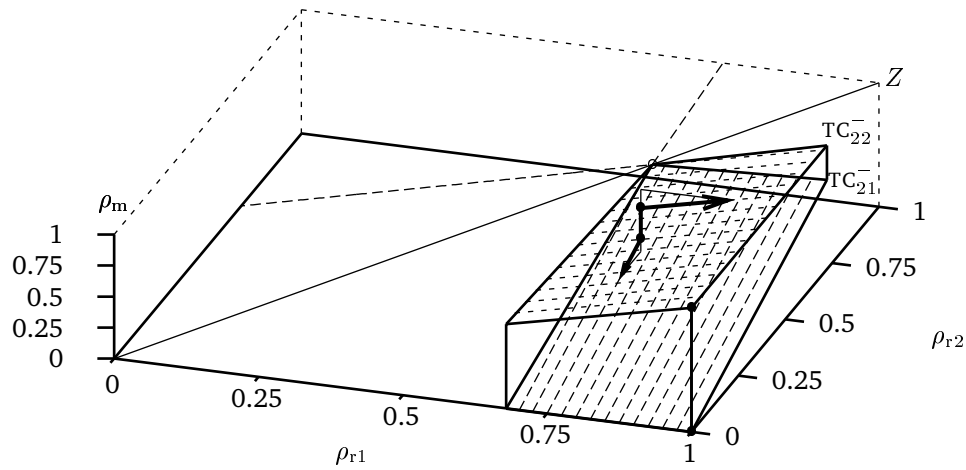
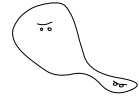


Figure 3.9: Three-dimensional PIP for the dimorphic resident population. Evolutionary changes of the resident with trait ρ_{r1} take place in the lower dashed plane, and those due to changes of the resident with trait ρ_{r2} in the upper dashed plane. These planes correspond to transcritical bifurcation sheets, denoted by TC_{21}^- and TC_{22}^- . The arrows denote the direction of evolution in each plane. The bullet on diagonal Z indicates the ss of the monomorphic population. The two filled circles in the corners indicate the evolutionary end-points.

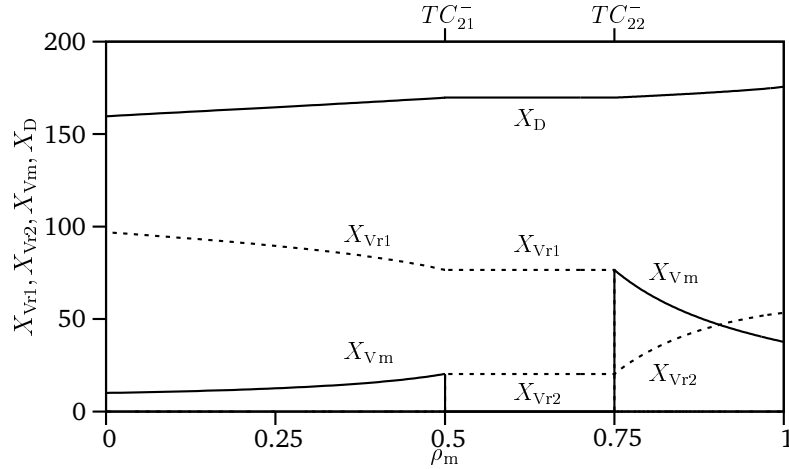


Figure 3.10: Steady-state distributions of detritus X_D , resident X_{Vr} and mutant X_{Vm} biomass as function of the traits ρ_m , for a dimorphic resident population with $\rho_{r1} = 0.75$, $\rho_{r2} = 0.5$ and $z = 1.3$.

$\rho_r^* < \rho_{r2} \leq 1$. Figure 3.10 is one of these diagrams where $\rho_{r1} = 0.75$, $\rho_{r2} = 0.5$, and ρ_m is the bifurcation parameter. The range of parameter ρ_m is divided into three subregions. In the intermediate range for $\rho_{r2} = 0.5 < \rho_m < \rho_{r1} = 0.75$ the steady state with $X_{Vm} = 0$ is stable; here, the mutant cannot invade. For $\rho_m < 0.5$ and $\rho_m > 0.75$ the equilibrium with $X_{Vm} = 0$ is unstable and the mutant may invade. Like in the monomorphic case, these subregions are divided by transcritical bifurcations, which we denote by TC_{21}^- and TC_{22}^- .

Figure 3.11 depicts the corresponding mutant invasion fitness as a function of the mutant trait ρ_m . We found the same pattern for all (ρ_{r1}, ρ_{r2}) in the range with coexistence. Thus, a mutant is unable to invade when $\rho_{r1} < \rho_m < \rho_{r2}$, but able to invade when this value is greater or smaller than those of both residents: $\rho_m < \rho_{r1}$ or $\rho_{r2} < \rho_m$. In our case this is true for all two-resident-mutant combinations inside the region between the two subdiagonal planes, except at the ss $\rho_{r1} = \rho_{r2} = \rho_r^*$ and in the corner of the trait-space ($\rho_{r1} = 1$ and $\rho_{r2} = 0$ or $\rho_{r2} = 1$ and $\rho_{r1} = 0$). Apparently, the trait values of the residents coincide with transcritical bifurcation points. This implies that the subdiagonal surfaces in the 3-dimensional representation of Figure 3.9 act as ‘transcritical bifurcation sheets’.

Invasion is thus possible if the mutant has a trait value above this region (when the resident is on the upper plane) or below it (when the resident is on the lower plane). This is illustrated by the arrows in Figure 3.9. The trait substitution sequence will lead to the corner coalition $\rho_{r1} = 1$, $\rho_{r2} = 0$ (or to $\rho_{r2} = 1$, $\rho_{r1} = 0$). These boundary coalitions are evolutionary attainable and uninvadable, and thus they are evolutionary end-points. No interior protected dimorphisms exist, because no point exists where both invasion gradients are

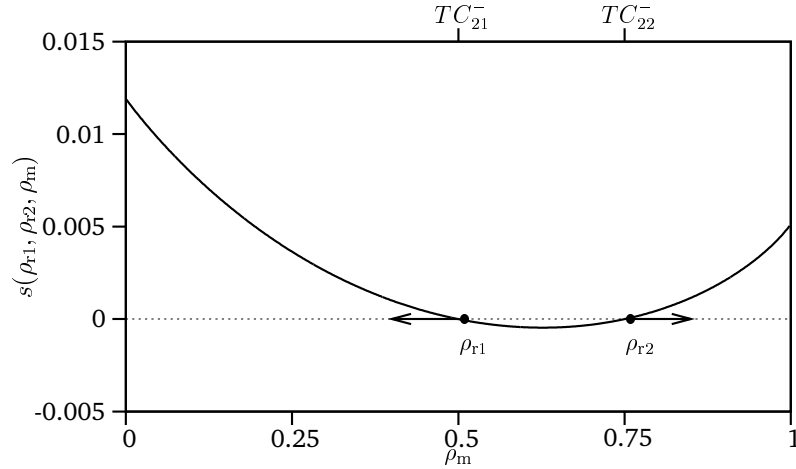
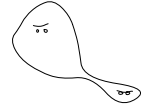


Figure 3.11: The invasion fitness $s(\rho_m, E(\rho_{r1}, \rho_{r2}))$ as function of the traits ρ_m , for a dimorphic resident population with $\rho_{r1} = 0.75$, $\rho_{r2} = 0.5$ and $z = 1.3$. Arrows indicate the direction of evolution.

simultaneously zero. This could already be seen from the PIP's in Figure 3.5, because none of the zero fitness isoclines contains points where the fitness gradient is zero.

For completeness, Figure 3.12 shows the evolutionary course for the mixotroph starting with a resident population with $\rho_r(\tau = 0) = 0.3$. A deterministic and a stochastic realization are shown. In the deterministic case the evolutionary steps are continuous. After evolutionary branching both subpopulations start from a point close to the ss point and initially diverge slowly. In the stochastic case the mutations are assumed to be uniformly distributed around the trait of the progenitor resident population. In this simulation, new mutants are introduced already before the equilibrium state is attained, so that the mutants do not always have completely replaced the residents, which explains why polymorphism occurs. In both types of realizations the population eventually consists of pure autotrophs ($\rho = 1$) and pure heterotrophs ($\rho = 0$).

3.4 Discussion and conclusions

We studied the application of bifurcation analysis to the ecological and the evolutionary dynamics of a mixotrophic population in a closed system. We found that bifurcation analysis is very suitable to determine the evolutionary behavior of a model. This is because the derivation of the evolutionary invasion criterion can be based on the stability of the extended system including the mutant. The standard AD approach partly stems from bifurcation techniques, and therefore both approaches and their results show substantial overlap. This

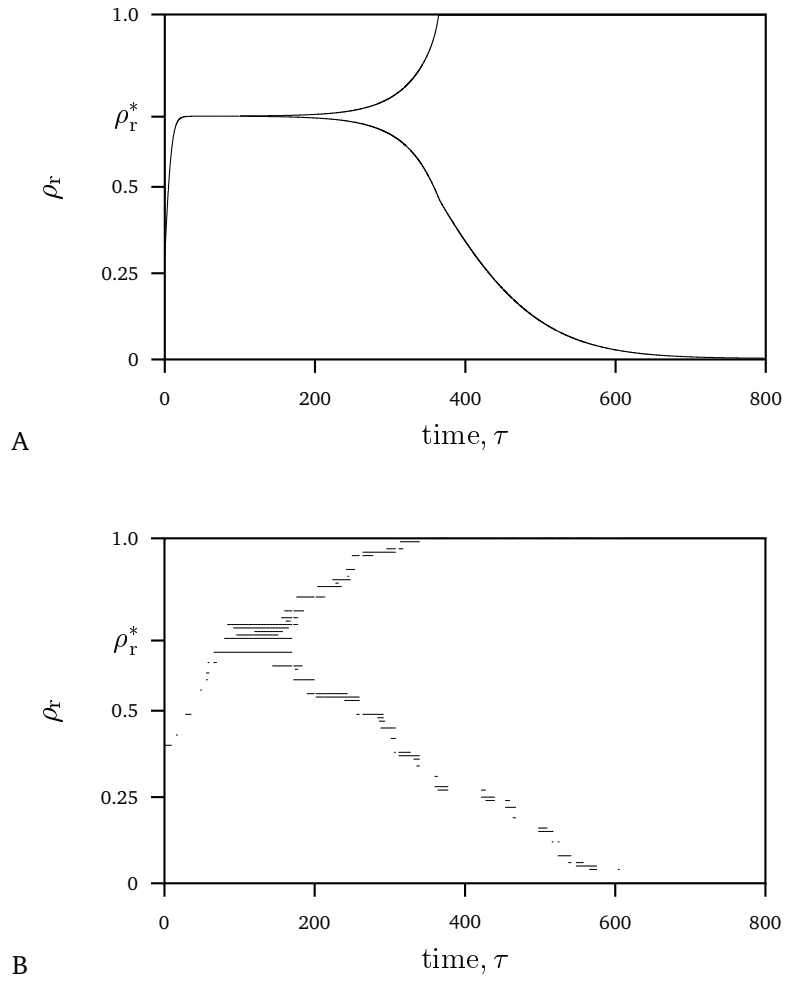
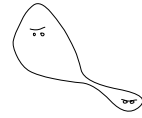


Figure 3.12: Evolution predicted by a deterministic (A) and a stochastic model (B). When $\rho = 1$ the population is purely autotrophic, and when $\rho = 0$ it is purely heterotrophic.



is illustrated by the fact that the zero invasion fitness isoclines in the PIP's can also be calculated on basis of transcritical bifurcations.

The application of bifurcation techniques to evolutionary problems is not new but has also been used by other authors, such as [6, 8]. However, when the underlying ecological model is based on the classical Lotka-Volterra population dynamics, often analytical solutions are available and bifurcation analysis is more straightforward. Dercole [4, 5] used the standard Rosenzweig-MacArthur prey-predator model [27], which also has simple ecological equilibria. He used, however, bifurcation analysis intensively to study the evolution of complex trait dynamics such as evolutionary branching-extinction cycles. In our case, numerical bifurcation analysis is needed because the ecosystem model itself is more complex, due to the explicit formulation of the environment. Other sources of complexity may be a large system dimension, such that the determination of the attractor to which the system will evolve after invasion becomes non-trivial [16, 18]. Finally, numerical bifurcation techniques may be needed when analyzing models that have multiple ecological equilibria or non-equilibrium attractors, such as limit cycles (see also [7, 11]).

Numerical bifurcation analyzes are made easy by standard computer packages such as LOCBIF [14], CONTENT [22] and AUTO, [9, 10]. For their application, however, the models need to be continuously differentiable. Switches, such as are needed when for example using Liebig's minimum law, provide problems. A suitable alternative to Liebig's law is provided by the Synthesizing Unit [20], which models multiple nutrient limitation in a continuous fashion. Similarly, the reserve dynamics of the Dynamic Energy Budget theory (DEB) gives a continuous description of the formation and use of energy storages, for which no threshold values or model switches are needed. This makes DEB-models very suitable for evolutionary studies that need bifurcation techniques.

In addition to facilitating the analysis of large ecosystems and complex evolutionary dynamics, bifurcation diagrams were also found to provide additional information. For example, they may show the areas in the trait space where no population can exist. Also, bifurcation diagrams of the ecological model in the neighborhood of the singular strategy can show the equilibrium biomasses of the competing residents and mutants, which may help to understand how evolution continues after evolutionary branching.

Another advantage of bifurcation analysis is that the results are valid for both small and large mutational steps. This enables a comparison between an evolutionary approach and the assembly process approach [25, 26]. In adaptive evolution, mutants differ in one or a few trait values from one of the resident populations. This process consists of small mutational steps, which lead to an (almost) continuous change of the trait value. Therefore, the course of the evolution of the system can be described deterministically. In contrast, with an ecosystem assembly process, populations from a pool are introduced. These populations may have very different parameter values, so that the changes in the parameter space may be in big steps. This means that in Figure 3.6 the trait value of the introduced population may be on the entire range along the vertical line. Coexistence can already occur after one step and this may already

be the end-point. Therefore, the succession sequence of the assembly process can be very irregular and can not be approximated deterministically.

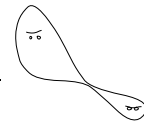
Evolutionary analysis of the mixotroph model showed that for convex cost functions ($z < 1$) a CSS was found; the population will evolve towards this point and then remain on it. For concave cost functions ($z > 1$) an EBP was found. In this case the population will first evolve towards this point and then split up into two coexisting subpopulations. These will then evolve to a pure autotrophic and a pure heterotrophic subpopulation. This holds for both increasing and decreasing cost functions and even for costs functions with interior local extrema.

3.5 Acknowledgments

The authors would like to thank Frans Jacobs for valuable discussions.

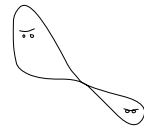
References

- [1] Abrams, P. A. (1999). The adaptive dynamics of consumer choice. *The American Naturalist*, 153(1):83–97.
- [2] Abrams, P. A. and Matsuda, H. (2004). Consequences of behavioral dynamics for the population dynamics of predator-prey systems with switching. *Population Ecology*, 46(1):13–25.
- [3] Christiansen, F. B. and Loeschcke, V. (1980). Evolution and intraspecific exploitative competition I, one-locus theory for small additive gene effects. *Theoretical Population Biology*, 18:297–313.
- [4] Dercole, F. (2003). Remarks on branching-extinction evolutionary cycles. *Journal of Mathematical Biology*, 47(6):569–580.
- [5] Dercole, F., Irisson, J.-O., and Rinaldi, S. (2003). Bifurcation analysis of a prey-predator coevolution model. *SIAM J. Appl. Math.*, 63(4):1378–1391.
- [6] Dieckmann, U. and Doebeli, M. (1999). On the origin of species by sympatric speciation. *Nature*, 400:354–357.
- [7] Dieckmann, U. and Law, R. (1996). The dynamical theory of coevolution: a derivation from stochastic ecological processes. *Journal of Mathematical Biology*, 34:579–612.
- [8] Doebeli, M. and Dieckmann, U. (2000). Evolutionary branching and sympatric speciation caused by different types of ecological interactions. *The American Naturalist*, 156:S77–S101.
- [9] Doedel, E. and Kernévez, J. (1986). Auto: Software for continuation problems in ordinary differential equations with applications. Technical report, California Institute of Technology, Applied Mathematics.



- [10] Doedel, E. J., Champneys, A. R., Fairgrieve, T. F., Kuznetsov, Y. A., Sandstede, B., and Wang, X. (1997). *Auto 97: Continuation and bifurcation software for ordinary differential equations*. Technical report, Concordia University, Montreal, Canada.
- [11] Geritz, S. A. H. (2005). Resident-invader dynamics and the coexistence of similar strategies. *Journal of Mathematical Biology*, 50(1):67–82.
- [12] Geritz, S. A. H., Kisdi, É., MeszÉna, G., and Metz, J. A. J. (1998). Evolutionarily singular strategies and the adaptive growth and branching of the evolutionary tree. *Evol. Ecol.*, 12:35–57.
- [13] Grover, J. P. (1997). *Resource Competition*. Population and Community Biology series. Chapman & Hall, London.
- [14] Khibnik, A. I., Kuznetsov, Y. A., Levitin, V. V., and Nikolaev, E. V. (1993). Continuation techniques and interactive software for bifurcation analysis of ODEs and iterated maps. *Physica D*, 62:360–371.
- [15] Kooi, B. W. (2003). Numerical bifurcation analysis of ecosystems in a spatially homogeneous environment. *Acta Biotheoretica*, 51(3):189–222.
- [16] Kooi, B. W., Boer, M. P., and Kooijman, S. A. L. M. (1999). Resistance of a food chain to invasion by a top predator. *Mathematical Biosciences*, 157:217–236.
- [17] Kooi, B. W. and Kooijman, S. A. L. M. (2000). Invading species can stabilize simple trophic systems. *Ecological Modelling*, 133(1-2):57–72.
- [18] Kooi, B. W., Kuijper, L. D. J., Boer, M. P., and Kooijman, S. A. L. M. (2002). Numerical bifurcation analysis of a tri-trophic food web with omnivory. *Mathematical Biosciences*, 177:201–228.
- [19] Kooi, B. W., Kuijper, L. D. J., and Kooijman, S. A. L. M. (2004). Consequence of symbiosis for food web dynamics. *Journal of Mathematical Biology*, 49(3):227–271.
- [20] Kooijman, S. A. L. M. (2000). *Dynamic Energy and Mass Budgets in Biological Systems*. Cambridge University Press, Cambridge.
- [21] Kooijman, S. A. L. M., Dijkstra, H. A., and Kooi, B. W. (2002). Light-induced mass turnover in a mono-species community of mixotrophs. *Journal of Theoretical Biology*, 214(2):233–254.
- [22] Kuznetsov, Y. A. and Levitin, V. V. (1997). *CONTENT: Integrated environment for the analysis of dynamical systems*. Centrum voor Wiskunde en Informatica (CWI), Kruislaan 413, 1098 SJ Amsterdam, The Netherlands, 1.5 edition.

- [23] Metz, J. A. J., Geritz, S. A. H., Meszéna, G., Jacobs, F. J. A., and van Heerwaarden, J. S. (1996). Adaptive dynamics, a geometrical study of the consequences of nearly faithful reproduction. In Strien, S. J. van and Verduyn Lunel, S. M., editors, *Stochastic and spatial structures of dynamical systems*, pages 183–231. North-Holland, Amsterdam.
- [24] Metz, J. A. J., Geritz, S. A. H., and Nisbet, R. M. (1992). How should we define ‘fitness’ for general ecological scenarios? *Trends Ecol. Evol.*, 7:198–202.
- [25] Morton, R. D., Law, R., Pimm, S. L., and Drake, J. A. (1996). On models for assembling ecological communities. *Oikos*, 75(3):493–499.
- [26] Post, W. M. and Pimm, S. L. (1983). Community assembly and food web stability. *Mathematical Biosciences*, 64(1):169–192.
- [27] Rosenzweig, M. L. and MacArthur, R. H. (1963). Graphical representation and stability conditions of predator-prey interactions. *The American Naturalist*, 97:209–223.
- [28] Tilman, D. (1982). *Resource competition and community structure*. Princeton University Press, Princeton.
- [29] Troost, T. A., Kooi, B. W., and Kooijman, S. A. L. M. (2005a). Ecological specialization of mixotrophic plankton in a mixed water column. *The American Naturalist*, 166:E45–E61.
- [30] Troost, T. A., Kooi, B. W., and Kooijman, S. A. L. M. (2005b). When do mixotrophs specialize? Adaptive Dynamics theory applied to a Dynamic Energy Budget model. *Mathematical Biosciences*, 193:159–182.



4

Ecological specialization of mixotrophic plankton in a mixed water column

Tineke A. Troost, Bob W. Kooi, Sebastiaan A.L.M. Kooijman
Published in *American Naturalist* 163 (2003): 19-32

Abstract

In recent years, the population dynamics of plankton in light- or nutrient-limited environments have been studied extensively. Their evolutionary dynamics, however, have received much less attention. Here, we used a modeling approach to study the evolutionary behavior of a population of plankton living in a mixed water column. Initially, the organisms are mixotrophic and thus have both autotrophic and heterotrophic abilities. Through evolution of their trophic preferences, however, they can specialize into separate autotrophs and heterotrophs. It was found that the light intensity gradient enables evolutionary branching and thus may result in the ecological specialization of the mixotrophs. By affecting the gradient, also other environmental properties acquire influence on this evolutionary process. Intermediate mixing intensities, large mixing depths and high nutrient densities were found to facilitate evolutionary branching and thus specialization. Latter result may explain why mixotrophs are often more dominant in oligotrophic systems while specialist strategies are associated with eutrophic systems.

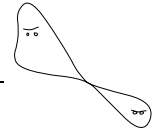
4.1 Introduction

We study the evolution of trophic preference of a population of mixotrophic plankton in a mixed water column by means of a modeling approach. Mixotrophs are capable of both auto- and heterotrophy, which means that they can use both organic and inorganic sources for the production of biomass. We enable the mixotrophs to specialize into pure auto- and heterotrophs by allowing their trophic preferences to evolve. Nitrogen content, mixing intensity and mixing depth are environmental properties that are typical to aquatic systems, and are known to have a large impact on the ecological dynamics of plankton. Here, we study their effects on the evolution of trophic preferences and thus the ecological specialization of the mixotrophs.

The focus is on mixotrophic organisms for two reasons. Firstly, because the phenomenon of mixotrophy is widespread. Eukaryotes acquired photo-autotrophy via the uptake of chloroplasts [36]; in most taxa, however, this did not result in the loss of heterotrophy. Hence, many typical photo-autotrophs are able to use organic compounds as an energy, carbon and/or nitrogen source [46] and basically they are mixotrophs. This seems to be the case especially in algae. Algae are not a natural group, but a collection of unrelated taxa that each have fully heterotrophic close relatives; this applies to blue green bacteria, chlorophytes, rhodophytes, euglenophytes, dinoflagellates, chlorarachniids, cryptophytes, haptophytes and heterokonts (see for example Cavalier-Smith [3]). This suggests that, in addition to their well known autotrophic abilities, many algae may also have some (unknown) heterotrophic abilities. Many other organisms, including plants, some animals, fungi, forams and radiolarians, acquired phototrophy via symbiosis [30]; these are again mixotrophs. Although the practical importance of either of the assimilatory routes in these organisms is often small or depends on environmental conditions, mixotrophy is thus much more common than is generally recognized.

The second reason for studying mixotrophs is because of their autotrophic and heterotrophic abilities, which enable a complete recycling of matter and nutrients. Therefore, they form the simplest, non-degenerate ecosystem possible. Such single-species mixotrophic communities share many characteristics with the canonical communities [28, 31], i.e. a three-species systems consisting of producers, consumers and decomposers. We, therefore, believe that these very much simplified theoretical single-species ecosystems do capture some of the basic features of all ecosystems. From this it also follows that specialization of mixotrophs into auto- and heterotrophs corresponds to the first steps in the evolution of the ecosystem to develop from a very simple to a more complex ecosystem. Studying this process may therefore provide insight in the evolution of food webs and ecosystems.

In recent years, an extensive amount of research has been done on the effects of chemical and physical properties on plankton blooms and species composition. Obviously, nutrients and light play a large role; they affect the abundance and the species composition of phytoplankton communities through their ratio [16, 24], as well as through their absolute supply [22]. Physical proper-



ties, on the other hand, affect the *availability* of nutrients and light and therefore, they can have a great impact on the dynamics and species composition as well [22]. The vertical turbulent diffusion coefficient and the mixing depth were found to define critical conditions for phytoplankton blooms [10, 18–20]. Diehl [7] explained how the primary causes of biomass limitation shift with increasing mixing depth. Yet other factors were found to determine the species composition, such as for instance fluctuations in light intensity [33, 34].

While the research on phytoplankton has thus been centered around ecological dynamics, their evolutionary dynamics have received considerably less attention. Although several studies have been done to assess the effects of resource gradients on evolutionary outcomes, these studies were of a more general character [2, 4, 8, 13, 14, 32, 38, 41]. Analysis of the evolutionary dynamics of a more specific and realistic system is expected to lead to more specific results and additional insights. Also, many of the studied systems have self-growing, reproducing lowest trophic levels (the logistic growth model is very popular) and are based on implicit assumptions about their food dynamics; frequently, they are at odds with conservation of mass [25]. In reality, however, all trophic levels are closely interlinked, including that of the zero trophic (abiotic) level. These assumptions can have considerable effects on the evolutionary dynamics of the system, as already became apparent in a previous study on mixotrophs in a closed and homogeneous system [44]. In the present study we again take into account explicitly the dynamics of the lowest trophic level, but now we consider the mixotrophs to live in a mixed water column with a light intensity gradient; this is a closed but heterogeneous system.

The paper is organized as follows: first we give a short description of the mixotroph model and the methods used for analyzing its evolutionary outcomes. Then we discuss the general effects of a light intensity gradient on the ecological and evolutionary dynamics of the mixotroph system. Thereafter we explain how system characteristics such as spatial structure and mass balances affect the evolutionary outcomes. Finally we discuss the specific effects of mixing intensity, mixing depth and nitrogen content on the evolution of specialization.

4.2 Modeling mixotrophs in a water column

We model a mixotrophic population in a water column, which is based on the mixotroph model presented by Kooijman et al. [29]. The model is based on the Dynamic Energy Budget (DEB) theory, which is a modeling framework for metabolic processes based on physiological rules for uptake and use of energy and nutrients [27]. It respects the principles of energy and mass conservation, and stoichiometric constraints on the synthesis of biomass. The population dynamics of the mixotrophs were simplified according to the same assumptions that were done by Troost et al. [44], which were found to have no qualitative effect and only a small quantitative effect on the evolutionary outcomes of the system. The model has only one state variable for the mixotrophic organisms

Table 4.1: Symbols for transformations and compounds.

Index	Transformation	Index	Compound
A	assimilation	C	DIC
A_A	autotr. assim.	N	DIN
A_H	heterotr. assim.	V	biomass
M	maintenance	D	detritus
G	growth		

(biomass X_V), and three state variables to describe the abiotic environment: detritus X_D , dissolved inorganic carbon (DIC) X_C and nitrogen (DIN) X_N . The latter two states consist of one nutrient only, while biomass and detritus are thought of as generalized compounds containing both carbon and nitrogen and other elements in a fixed chemical composition. It is assumed that elements other than carbon and nitrogen are not limiting the growth of the organisms. The system is closed for mass, but open to energy (light and heat production).

The four state variables partake in five transformations: assimilation A (autotrophic A_A and heterotrophic assimilation A_H), growth G , maintenance M and death H (see Table 4.1). A diagram of these transformations is shown in Figure 4.1. The mixotrophic organisms are capable both of autotrophic and heterotrophic assimilation, for both of which they have a certain affinity, denoted by ρ_A and ρ_H respectively. The mixotrophs use DIC, DIN and light for the autotrophic pathway, and detritus for the heterotrophic pathway. Once taken up, these resources are synthesized into basic building blocks. Part of the assimilates are used for maintenance; the rest is turned into biomass. When an organism dies, its biomass turns into detritus and becomes available for its conspecifics. Maintenance costs, overhead costs for growth and stoichiometric constraints take care of the conversion of organic carbon and nitrogen back into their inorganic form; other means of mineralization of detritus such as decomposition by bacteria are not considered. A brief description of the main growth fluxes and evolutionary processes is given below, which is followed by a section on the spatial structure of the water column and the equations for the vertical transport. A detailed discussion on the growth equations of the mixotrophs is given in the Appendix.

4.2.1 Assimilation and evolution

The mixotrophs are capable of both autotrophy and heterotrophy and therefore they are assumed to use light, carbon, nitrogen and detritus for assimilation. The corresponding functional responses (f_A for the uptake of nutrients involved in the autotrophic route and f_H for uptake of nutrients involved in the heterotrophic route) are calculated with use of synthesizing units (SU) cf. Kooijman [26], which provide a simple and realistic method for calculating production fluxes at simultaneous limitations. This method provides a more realistic alternative for Liebig's law which assumes that only one resource is

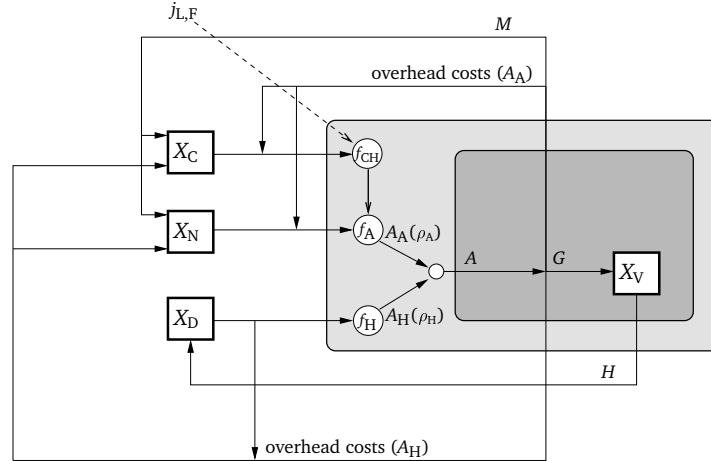
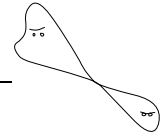


Figure 4.1: Diagram of the metabolism of a mixotroph. The shaded box encloses the organism, the lighter part of which denotes its membranes containing the assimilatory machinery. A circle denotes a Synthesizing Unit (only SUs with two or more substrates are shown). The organism has one state variable for biomass X_V ; the environment consists of three states: dissolved inorganic carbon X_C , dissolved inorganic nitrogen X_N and detritus X_D . Arrows indicate the structure-specific transformation fluxes.

limiting at a time.

The mixotrophs are characterized by their affinities for the autotrophic and heterotrophic assimilatory pathway ρ_A and ρ_H , which together represent the trophic preference of the organisms. These affinities affect the organism's autotrophic and heterotrophic assimilation rates j_{V,A_A} and j_{V,A_H} , and consequently the total assimilation rate $j_{V,A}$ (4.16-4.18). Affinities for either pathway are assumed to entail costs for building the necessary machinery, which are included by means of the yield coefficient $y_{C,V}$, which consists of certain base costs y^0 , increased by extra costs for building the assimilation machineries y^A and y^H , which for both pathways is proportional to the corresponding affinity (4.24). The parameter z determines the shape of the cost function; convex cost functions ($z > 1$) give the organisms an intrinsic advantage to evolve to specialized strategies, while concave cost functions ($z < 1$) give them an intrinsic advantage to evolve to mixotrophic strategies. 'Intrinsic advantage' means that it is naturally inherent to the physiology of the organism, and thus not induced by the external environment. As a default the cost function is chosen to be linear ($z = 1$), because this gives a neutral trade off which does not favor mixotrophic nor specialized strategies [44].

The two affinities are assumed to be traded off, following the requirement

that

$$\rho_H + \rho_A = 1. \quad (4.1)$$

That is, we effectively have a one-dimensional trait space, which is denoted by $\rho = \rho_A$; Organisms that have a ρ of unity are thus pure autotrophs, those that have a zero ρ are pure heterotrophs; strategies in-between correspond to mixotrophic organisms with a range of different trophic preferences.

The trophic preference ρ of the mixotrophs is genetically determined, and in combination with their abiotic environment it determines the fitness of the organisms. The mixotrophs reproduce asexually and a parent passes its trophic preference on to its offspring; sloppy heredity may however introduce small changes in the trophic preference. These mutations give rise to differences in fitness between the organisms, and mutants with a higher fitness can replace (or coexist with) the resident population; it is by a series of such replacements that the population evolves. A time scale separation is assumed to exist between the ecological and the evolutionary time scale, so that mutations occur only after the system has reached a steady state.

4.2.2 Spatial structure, light gradient and vertical transport

The aquatic environment in which the mixotrophs live is modeled as a one-dimensional water column. $\mathbf{X}(L_z, t)$ denotes the vector of the densities of the compounds (X_C, X_N, X_D, X_V) at depth L_z and time t . $L_z \in (-L_m, 0)$ where L_m is the maximum depth of the water column. Mass transport through the column is possible, but the column as a whole is closed for mass. Hence, the total carbon content X_{C+} and the total nitrogen content X_{N+} of the system are constant; they consist of the amounts of carbon (or nitrogen) in each of the four compounds, integrated over the depth of the water column:

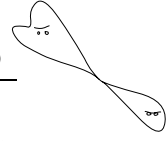
$$X_{C+} = \int_0^{-L_m} \left(X_C(L_z, t) + X_D(L_z, t) + X_V(L_z, t) \right) dL_z, \quad (4.2)$$

$$X_{N+} = \int_0^{-L_m} \left(X_N(L_z, t) + n_{N,V}(X_D(L_z, t) + X_V(L_z, t)) \right) dL_z, \quad (4.3)$$

in which $n_{N,V}$ is the fixed amount of nitrogen per mole carbon in biomass and detritus.

The system is open to energy; light comes in at the surface and is absorbed by biomass, detritus and non-plankton components. According to Lambert-Beer's law, the light absorption is proportional to the density of biomass and detritus and to the background turbidity. The change in light intensity is given by:

$$\frac{\partial J_{L,F}}{\partial L_z}(L_z, t) = -(\alpha + \beta_V X_V(L_z, t) + \beta_D X_D(L_z, t)) J_{L,F}(L_z, t), \quad (4.4)$$



where α denotes the background turbidity; β_V and β_D are the specific absorption coefficients for biomass and detritus. Integrating this equation over depth gives the following light intensity $J_{L,F}$ at depth L_z and time t :

$$J_{L,F}(L_z, t) = J_{L,F}(0) \exp \left\{ \alpha L_z + \int_0^{L_z} \left(\beta_V X_V(l, t) + \beta_D X_D(l, t) \right) dl \right\}, \quad (4.5)$$

where $J_{L,F}(0)$ is the amount of incoming light at the surface. Diurnal changes in incoming light intensity are not taken into account.

As a default, self shading (light absorption by plankton components) is neglected ($\beta_V = 0$, $\beta_D = 0$), and Equation (4.5) can be simplified into:

$$J_{L,F}(L_z) = J_{L,F}(0) \exp \{ \alpha L_z \}. \quad (4.6)$$

The value of the background turbidity ($\alpha = 0.07 \text{ m}^{-1}$) was chosen such that the light intensity is reduced to about 6% at 40 m depth. In the oligotrophic/eutrophic scenarios, where self shading is taken into account, the specific absorption coefficients of biomass and detritus were set to values of $\beta_V = 0.1$ and $\beta_D = 0.05 \text{ m}^2 \text{ mol}^{-1}$, respectively. The specific absorption coefficient of biomass was assumed to be higher than that of detritus due to the presence of photosynthetic pigments in biomass; these pigments are largely broken down in detritus. Values of the specific absorption coefficients were based on those presented by Falkowski and Woodhead [11] and Valiela [45].

The decrease in light intensity affects the autotrophic assimilation rate; density gradients build up as a consequence and induce diffusive transport through the water column. This diffusive transport is modeled as a down-gradient mixing process, which uses a finite mixing coefficient. Therefore, a density gradient is retained throughout the mixed layer even at considerable turbulence levels. The phytoplankton cells are assumed to be neutrally buoyant, i.e. there is no advection. The reaction-diffusion equation for the change in density of the compounds amounts to:

$$\frac{\partial \mathbf{X}}{\partial t}(L_z, t) = \mathbf{F} + K_V \frac{\partial^2}{\partial L_z^2} \mathbf{X}(L_z, t), \quad (4.7)$$

where the growth term \mathbf{F} is a vector consisting of the righthand sides of Equations (4.11a-4.11d); $K_V = 0.5 \text{ m}^2 \text{ d}^{-1}$ and denotes the vertical mixing coefficient that is assumed to be the same for all compounds, and uniform over the whole depth of the water column. Mixing is thus not hindered by a thermo- or pycnocline and the mixing depth of the water column is equal to its maximum depth. Neumann boundary conditions are imposed; this implies no material fluxes at the surface and the maximum depth of the water column:

$$\frac{\partial \mathbf{X}}{\partial L_z}(L_z, t) = 0 \text{ for } L_z = -L_m, 0. \quad (4.8)$$

4.2.3 Evolutionary analysis

Predictions of the evolutionary outcome of the system are made with use of Adaptive Dynamics (AD) theory [5, 6, 15, 37]. In this theory the invasion fitness of a mutant invading in a resident population $s_{\rho_{\text{res}}}(\rho_{\text{mut}})$ is defined as its long-term average per capita growth rate. The resident population is assumed to have reached a steady state with its environment so that resources are reduced to a level that just covers the costs of exploitation; the residents thus have by definition a zero invasion fitness: $s_{\rho_{\text{res}}}(\rho_{\text{res}}) = 0$. A mutant is assumed to be rare and will therefore not affect the environment in the short term. Mutants that have a positive invasion fitness (specific growth rate) may be able to invade, those that have a negative invasion fitness will just die out. Following the invasion, a mutant may replace the resident population and become the new resident or live on in coexistence with the original population. Together, the changed population and the environment will reach a new steady state, in which the new residents will again have a net specific growth rate of zero.

The evolutionary process can be illustrated by means of ‘adaptive landscapes’, of which some examples are given in Figure 4.2. Adaptive landscapes plot invasion fitness to strategy; they visualize by which mutants a resident population can be invaded. The residents (denoted by a black dot) have, as was discussed above, a zero invasion fitness. Evolution is directed towards strategies with a higher invasion fitness than the resident strategy, and will therefore follow the fitness gradient D_1 , i.e. the derivative of the fitness function with respect to the trait of the mutant ρ_{mut} :

$$D_1 = \frac{\partial s_{\rho_{\text{res}}}}{\partial \rho_{\text{mut}}}(\rho_{\text{mut}}). \quad (4.9)$$

In Figure 4.2, the direction of evolution is indicated by arrows. Evolution will drive the population to a singular strategy (SS) at which the fitness gradient vanishes ($D_1 = 0$); this is an evolutionary equilibrium.

The evolutionary stability of such an SS is determined by the second derivative (D_2) of the fitness function:

$$D_2 = \frac{\partial^2 s_{\rho_{\text{res}}}}{\partial \rho_{\text{mut}}^2}(\rho_{\text{mut}}). \quad (4.10)$$

Two types of singular strategies that are most relevant to this study are the continuously stable strategies (CSS) and the evolutionary branching points (EBP). CSS’s are attractors and lie at a fitness maximum at which the second derivative of the fitness gradient is negative ($D_2 < 0$); this is an evolutionarily stable situation and the population will remain at such a strategy (Figure 4.2B). EBP’s are attractors as well, but these lie at a fitness minimum at which the second derivative of the fitness gradient is positive ($D_2 > 0$); now any nearby mutant is able to invade (Figure 4.2E). In this case disruptive selection will induce the population to split up and become dimorphic. In the remainder of the paper, the adaptive landscapes and the vertical profiles only show the system for residents that have already reached an SS.

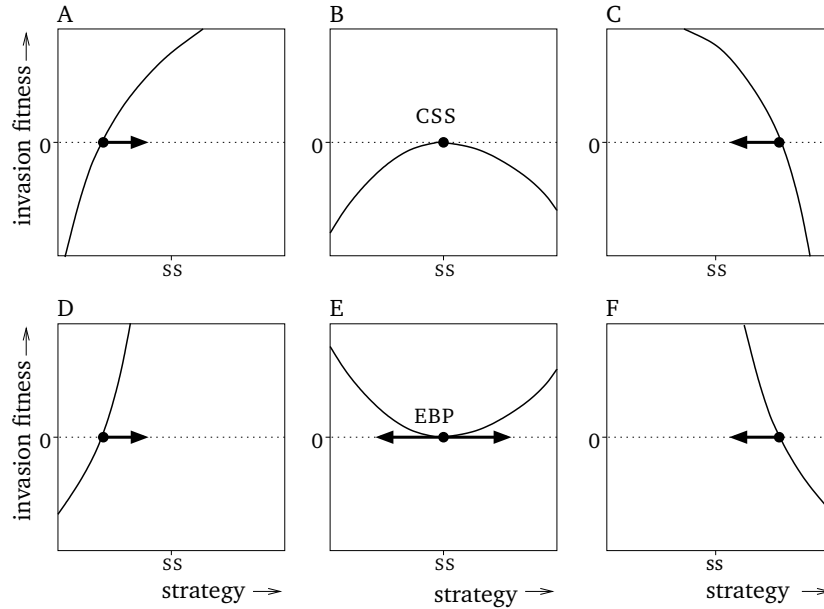
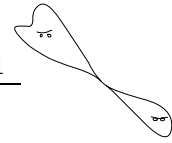


Figure 4.2: Schematic examples of adaptive landscapes; the residents are denoted by a dot and the arrows indicate the direction in which the population will evolve. (A,D) The strategy of the residents is smaller than the singular strategy (ss); (B,E) the resident strategy is equal to the ss ; (C,F) the resident strategy is larger than the ss . (B) represents an adaptive landscape of a ss that is evolutionarily stable (CSS), while (E) represents an adaptive landscape of a ss that is evolutionarily unstable (EBP).

4.3 Results and discussion

4.3.1 Vertical profiles and evolutionary outcomes

When no light intensity gradient is present, the system is spatially homogeneous. In this case, and if costs for autotrophy and heterotrophy are neutral with respect to specialization ($z = 1$), the population will evolve to a trophic preference of $\rho = 0.68$. This is a singular strategy that lies at a fitness maximum and thus is evolutionarily stable (CSS); the corresponding adaptive landscape is almost flat (Figure 4.3F, dotted curve). When imposing a light intensity gradient (Figure 4.3E), the system becomes heterogeneous, which has both ecological and evolutionary consequences.

On an ecological time scale, the autotrophic production rate begins to vary throughout the system and becomes highest in the euphotic surface layer. Here, nutrients will get depleted while biomass and detritus densities will increase. The resulting differences in concentrations will cause net movement due to diffusion. Imposing a light intensity gradient thus triggers a cascade of dens-

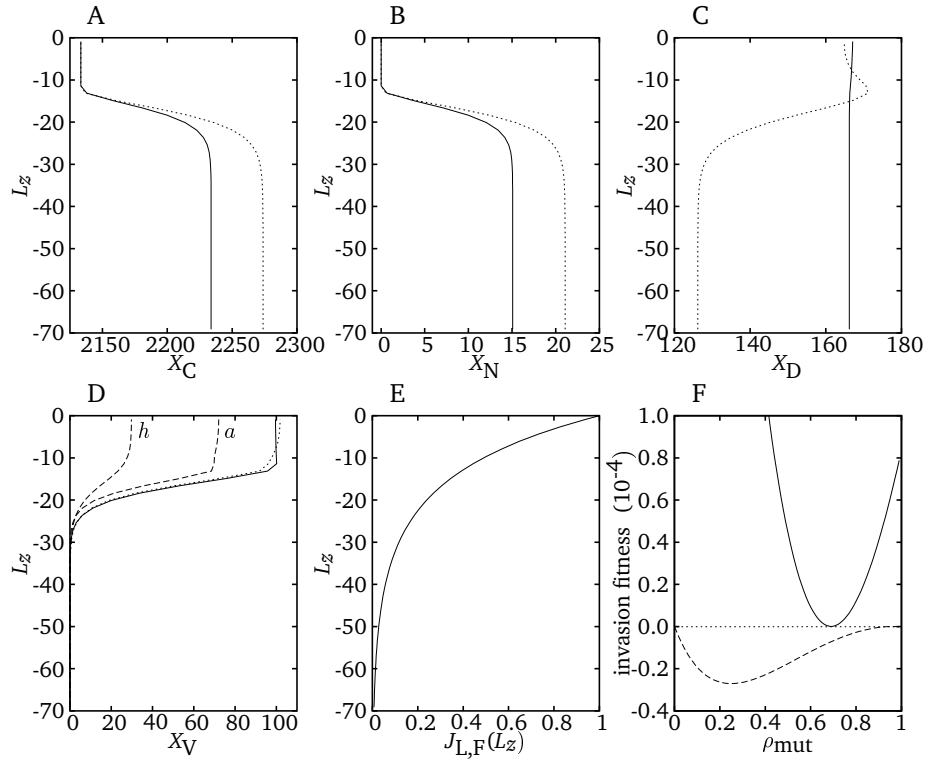
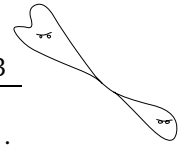


Figure 4.3: Vertical profiles and adaptive landscape for the monomorphic population (continuous curves) and those for the dimorphic population after evolutionary branching has taken place (dotted and dashed curves). The former consists of mixotrophs that have reached the singular strategy; the latter population consists of separate heterotrophs (dashed curve h) and almost pure autotrophs (dashed curve a) that have reached an evolutionarily stable coexistence. In (A-E) are shown the densities of DIC (X_C), DIN (X_N), detritus (X_D), biomass (X_V) and the light intensity gradient (X_L), plotted against the depth L_z . The adaptive landscapes in (F) plot invasion fitness $s_{\rho_{res}}(\rho_{mut})$ against a range of mutant strategies ρ_{mut} ; the dashed curve shows the adaptive landscape with two resident strategies after branching, the dotted curve shows the (almost flat) adaptive landscape at the singular strategy for a homogeneous system.



ity gradients, locally limiting factors and diffusive transport processes. This results in the steady state profiles that are shown by the continuous curves in Figure 4.3A-D. These profiles correspond well to the typical vertical structure of the water column in tropical latitudes (TTS) [35]: the light intensity is highest at the surface, while the source of nutrients is at depth; at the surface a nitrogen depleted layer exists. The model also captures the observed sharp gradient in the nitrogen density, and the shallow peak of autotrophic production (not shown).

On an evolutionary time scale, the light intensity gradient induces the ss to shift to a slightly more autotrophic value ($\rho = 0.69$), which now comes to lie at a fitness minimum (Figure 4.3F, continuous curve). This is an evolutionary branching point (EBP), at which the mixotrophic population may split up into two specialized subpopulations. Here, evolutionary branching is expected to result in (almost) pure autotrophs ($\rho = 0.97$) and heterotrophs ($\rho = 0.0$), as these form an evolutionarily stable coexistence; this coexistence was found by manually adjusting the traits of the two strategies until they were at the boundary or at a ESS. The autotrophs in this coexistence are at a fitness optimum with a fitness gradient of zero, while the heterotrophs are at a fitness boundary maximum (Figure 4.3F, dashed curve). The dotted curves in Figure 4.3A-D show the profiles that result after evolutionary branching has taken place. The total amount of biomass is not very different from that of the mixotrophic population, and the distribution has changed slightly. DIC and DIN densities have increased, but the depth of the nitrogen depleted layer is unchanged.

An intuitive explanation for the occurrence of the evolutionary branching and the resulting ecological specialization of the mixotrophs is related to their lack of flexibility. Each variation in habitat can be optimally exploited by a different phenotype. However, the mixotrophs have a fixed phenotype with a constant ratio of the two affinities which they can not adjust on an ecological time scale. Neither can autotrophs and heterotrophs, but by changing their abundances relative to the other they are able of changing the ratio of autotrophy to heterotrophy. Together, they can adjust themselves to any habitat, which gives them an advantage over mixotrophic phenotypes.

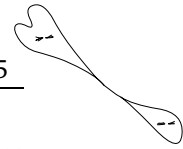
The result that a light intensity gradient induces evolutionary branching is consistent with previous, more general studies on the effects of spatial (or temporal) heterogeneity on evolutionary outcomes. Some of these studies [13, 32] assumed two, three or a range of habitats with for instance different resource types or productivities that lead to differences in demographic parameters that are consistent across genotypes; in these studies, the genotype determines the habitat choice or preference. Other studies [2, 4, 8, 14, 38, 41] assumed that no habitat was intrinsically more productive than another but that different genotypes achieve different growth rates, carrying capacities or mortality rates (genotype by environment interaction) [2, 4, 8, 14, 38, 41]; here, the habitat choice is passive, like in the present paper. In these studies it was found that heterogeneity of the environment facilitates evolutionary branching. Doebeli and Dieckmann [8] explained that the underlying mechanism is an enhanced degree of frequency dependence.

4.3.2 Open and closed systems

A remarkable difference between this and earlier studies becomes apparent when the locally different habitats, present in the heterogeneous systems, are considered in isolation. When isolated, these habitats resemble homogeneous systems with different environments. In most studies, the populations will adapt to these different environments, resulting in a different phenotype per habitat. By contrast, in the mixotroph system, the population will always evolve to one and the same mixotrophic strategy, regardless of its habitat. The difference lies in the fact that the mixotroph system is closed for mass. The isolated habitats can thus be considered as closed and homogeneous systems, for which we showed that their evolutionary outcomes are not affected by environmental properties indeed [44]. This result was explained by the feedback mechanisms of the mixotrophs and the recycling processes in the system that couple the steady state densities of the environment such that they can not change independently. Changing an environmental property does not affect one, but all of the steady state densities. Ultimately, the feedback fluxes produced by the mixotrophs determine the steady states of the environment, and not vice versa. Therefore, the evolutionary outcome is determined only by the organism's intrinsic properties quantifying these feedback fluxes. Organisms with equal properties will thus always evolve towards the same (mixotrophic) strategy.

Apparently, the light intensity gradient not only facilitates evolutionary branching, but also provides the degrees of freedom that enable phenotypic variation (and thus ecological specialization) to occur. This freedom is associated with the vertical transport in the water column. Although the transport of the organisms is analogous to the migrational or dispersal processes considered in previous studies, transport of other compounds in the environment is generally not taken into account. For the mixotrophs, however, such transport is essential, because the system is closed for mass and a full recycling of material has to take place. Transport between the layers relaxes the requirement of mass conservation, which now has to be respected only at the level of the whole water column. As a consequence, complementary processes such as autotrophic and heterotrophic assimilation can be carried out at different locations, as long as their products are exchanged. It is also possible to induce evolutionary branching in homogeneous systems, but then an intrinsic advantage is required which favors specialism over mixotrophy. Such an advantage can for example be induced by a non-linear cost function ($z > 1$). The spatial gradient in this study, however, induces evolutionary branching without an intrinsic advantage ($z = 1$). In some cases, it even induces evolutionary branching with an intrinsic disadvantage ($z < 1$), as will be discussed later on.

Whereas in closed and homogeneous systems the environmental properties have no effect on the evolutionary outcomes at all, in a closed and spatially heterogeneous environment these properties may acquire influence through their effect on the spatial gradient. Examples of such environmental properties are mixing intensity, mixing depth and total nutrient content, which are discussed



in the following sections. In homogeneous systems, environmental properties can only induce phenotypic variation when the system is opened for mass [44]. Opening the system for mass relaxes the requirement of full material recycling, and thus reduces the effect of the feedback mechanisms. As a consequence, the environmental properties that determine the in- and outfluxes of the system can affect the steady state densities of the environment and as such they acquire influence on the evolutionary outcomes as well [44].

Another difference with previous studies is the occurrence of habitat segregation. Doebeli and Dieckmann [8] showed that branching induced by spatial heterogeneity and local adaptation is often accompanied by geographical segregation. This is because the local environment at the one end of the gradient is more favorable for one of the morphs, while the local environment at the other end is more favorable for the other morph. Basically, such a single spatial gradient thus provides two opposite gradients, which results in a clear habitat segregation of the two morphs. Figure 4.3D, however, shows that after mixotrophs have specialized into separate autotrophs and heterotrophs, habitat segregation does not occur. Although the autotrophs are more abundant at the surface and the heterotrophs are (relatively) more abundant at the bottom of the column, the geographical differentiation is not sharp and far from complete. This is because the light intensity gradient has a direct effect only on the autotrophs; these autotrophs produce the substrates for the heterotrophs, so that the resulting detritus gradient is closely related to that of the light intensity gradient, and certainly not opposite to it. The mutual dependency of the two phenotypes, and thus that of the two substrate gradients, restricts the degree of the spatial heterogeneity. This explains why a clear habitat segregation does not occur. Probably, it also explains why the fitness differences between the various strategies are not very large, and why the spatial profiles of the mixotrophs before branching are so similar to the profiles of the auto- and heterotrophs after branching.

To induce and maintain two opposite substrate gradients (more spatial heterogeneity) in the studied system, we will need additional mechanisms that actively separate autotrophic and heterotrophic substrates. These mechanisms could for instance be a downward transport (sinking) of detritus, in combination with upward diffusion of DIC and DIN. The upward diffusion of DIC and DIN can probably also be replaced by the more effective alternative of a continuous influx of these nutrients at the surface of the water column. This would imply opening the system for mass and thus reducing the mutual dependency of the two phenotypes. This could be taken a step further by assuming a 'lateral' in- and outflux, i.e. in- and outputs of material over the whole depth of the column, which would totally eliminate the mutual dependency between the auto- and heterotrophs, and readily increase the degree of spatial heterogeneity. Because in studies of open systems recycling is not necessary, feedback loops and mutual dependencies are often not considered. Hence, habitat segregation will be found more often in those studies than in studies considering closed systems.

4.3.3 The role of diffusion and turbulent mixing

Figure 4.4A shows the evolutionary stability of the system when the mixing intensity is varied simultaneously with z . We recall that values of z larger than one give the organisms an intrinsic advantage to specialize into autotrophic and heterotrophic strategies, while values smaller than one provide a disadvantage to specialization. In the figure it can be seen that when only molecular diffusion takes care of the vertical transport ($K_V = 9 \cdot 10^{-5} \text{m}^2 \text{d}^{-1}$), the evolutionary equilibrium (ss) will be stable unless z becomes equal to or larger than unity. This implies that, if they have an intrinsic disadvantage to specialization, the organisms will always evolve to a mixotrophic strategy and remain on it. Apparently, the substrate gradients resulting from molecular diffusion are not sufficient to ‘counteract’ such a disadvantage.

In real life, however, vertical transport is not restricted to molecular diffusion. Eddy or turbulent diffusion is due to external sources such as wind stress, and mixes the water much more effectively than does the molecular motion. Figure 4.4A shows that at higher mixing intensities, the ss becomes unstable, even though $z < 1$. In this case, the population may thus split up and specialize into autotrophs and heterotrophs, regardless of their intrinsic disadvantage to specialization. Clearly, increasing the mixing intensity makes the singular strategy more susceptible to invasion and thus facilitates ecological specialization.

Although it was shown that an increase in the mixing intensity facilitates evolutionary branching, it can be theorized that the effect will be reduced at very high intensities. This is because at high mixing intensities, the water column will lose its heterogeneous character; even though the light intensity gradient will still be present, the organisms will be circulating randomly through the column and will on average be exposed to a same amount of light. Effectively, a completely mixed system will thus be equal to a homogeneous system, which by definition has no spatial gradient.

However, it was found that high mixing coefficients ($K_V > 102$) lead to the extinction of the population. At these mixing intensities, the phytoplankton cells are mixed to great depths and will on average be exposed to light intensities that are too small to allow a net positive population growth. Apparently, the depth of the water column exceeds the critical depth, which for neutrally buoyant phytoplankton is equal to the ‘Sverdrup depth’ [21]. This is the depth at which the integrated autotrophic production exactly equals the integrated respiration.

To test the effects of a high mixing intensity, we thus needed to reduce the mixing depth to prevent the population from extinction. In natural systems, the mixing depth is limited by a thermo- or pycnocline. Here, we simply reduced the maximum depth of the water column to 40 and 30 m, respectively; the steepness of the light intensity gradient and the grid cell size used for discretization were unchanged; the cost function was assumed to be neutral with respect to specialization ($z = 1$). Figure 4.5 shows that high mixing intensities indeed result in a decrease of the second derivative of the fitness function

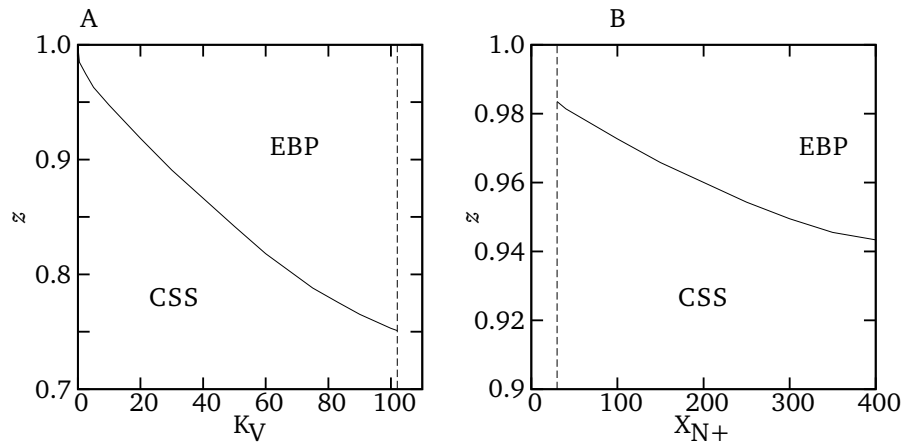


Figure 4.4: Bifurcation diagrams showing the evolutionary outcomes of the mixotroph system when the shape coefficient z (Equation (4.24)) is varied simultaneously with (A) the mixing intensity K_v and (B) the total nutrient content X_{N+} ; ‘CSS’ denotes that for these parameter values the organisms will evolve towards a mixotrophic strategy at which they will remain; ‘EBP’ denotes that the singular strategy is evolutionarily unstable so that the population may split up and evolve into specialists; the dashed curve in (A) denotes the critical mixing intensity above which the system is not viable and in (B) it denotes the critical nutrient content below which the system is not viable.

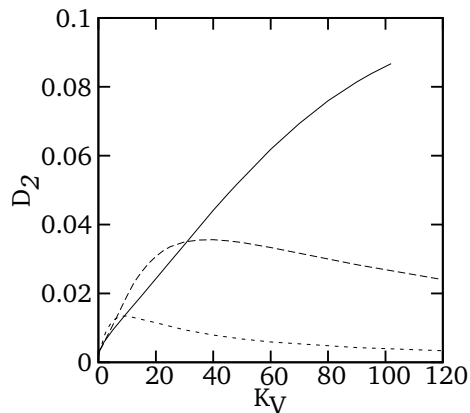


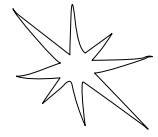
Figure 4.5: The second derivative of the fitness function D_2 for a range of mixing intensities and at various mixing depths: $L_m = 70$ m (continuous curve), $L_m = 40$ m (dashed curve) and $L_m = 30$ m (dotted curve); in this graph the cost function is assumed to be neutral with respect to specialization ($z = 1$).

(dashed curve for $L_m = 40$ m, dotted curve for $L_m = 30$ m). This suggests that facilitation of evolutionary branching is highest at intermediate mixing intensities. As intermediate mixing intensities result in intermediate gradients of DIN and ‘light-exposure’, this is in agreement with Doebeli and Dieckmann [8] who find that at intermediate gradients the facilitation of evolutionary branching is highest. From the figure it also follows that an increase in the mixing depth positively affects evolutionary branching and thus supports ecological specialization.

While increasing the mixing coefficient was thus found to facilitate the process of evolutionary branching, it seems to have only a small effect on the final evolutionary outcomes that result after branching has taken place. The mixotrophs again specialize into pure heterotrophs and almost pure autotrophs. The corresponding adaptive landscape is qualitatively also very similar to the landscape that was found at the default parameter values (Figure 4.3E, dashed curve); at higher mixing intensities it just becomes more pronounced, with a deeper fitness valley between the two coexisting strategies.

4.3.4 Effects of the total nutrient content

Nutrients such as nitrogen and phosphorus are important limiting factors in aquatic systems. The mixotrophs in our model are nitrogen limited, as can be seen from the nitrogen depleted layer in the vertical profiles (Figure 4.3B). Although an increase in the total amount of DIN in the system does lead to an



increase in the amount of biomass, it does not affect the depth of the nitrogen depleted layer and neither does it affect the evolutionary outcomes (not shown). This is because nitrogen does not directly interfere with the light intensity and its gradient.

However, when taking into account self shading, nitrogen content will affect the light intensity gradient indirectly. Self shading decreases the total amount of available light, and alters the light intensity gradient. In eutrophic systems (which have a larger total nutrient content) organisms are more abundant, so that a larger proportion of the incoming light is absorbed than in oligotrophic systems (with smaller nutrient contents). Figure 4.4B shows the evolutionary stability of the system when X_{N+} and z are varied simultaneously. Below a critical nitrogen content ($X_{N+} < 28$), the system is not viable. At small nitrogen contents, the singular strategies are evolutionarily unstable (EBPS) only at a narrow range of z -values where the intrinsic disadvantage to specialization is small. At higher nutrient contents, the range of z -values under which branching will occur has increased. High nutrient contents may thus lead to ecological specialization under a larger range of cost functions.

This result links evolutionary branching and specialized strategies to higher nutrient contents and thus to eutrophic systems, while it links mixotrophic strategies to oligotrophic systems. Indeed, mixotrophs are observed to be most dominant in oligotrophic environments [1, 17]. This is mostly explained by the fact that mixotrophs have access to two food sources, which is assumed to increase their chances of survival when resources are limited [9, 39, 40, 43]. The present result that evolutionary branching is facilitated by eutrophic conditions more than by oligotrophic conditions may provide an additional mechanism underlying the association between mixotrophs and oligotrophic environments.

4.4 Conclusions

4.4.1 Evolution of specialization

The light intensity gradient makes evolutionary branching possible, such that mixotrophs living in a mixed water column may specialize into separate autotrophs and heterotrophs. Because the system is closed for mass, the diffusive transport of all compounds through the system is essential and makes ecological specialization possible. By affecting the light intensity gradient, also other environmental properties can acquire influence on the evolutionary behavior of the system. It was found that evolutionary branching, and thus ecological specialization, is facilitated most by intermediate mixing intensities and large mixing depths. Under these circumstances, evolutionary branching may occur even when the organisms have an intrinsic disadvantage to specialization ($z < 1$). If self shading is taken into account, higher nutrient densities will facilitate specialization as well. This may provide an explanation for the observation that mixotrophs are more dominant in oligotrophic systems while

specialized autotrophs and heterotrophs are more often found in eutrophic systems. Ecological specialization of mixotrophs results in a very simple food web of autotrophs and heterotrophs, and thus may correspond to the first steps in the evolution of an ecosystem. As the results show how various environmental properties facilitate ecological specialization, they provide insight in how the environment affects the organization of food webs and which environmental conditions favor the development of ecosystems.

Although nitrogen content and mixing intensity can increase the ranges of z -values for which evolutionary branching occurs, this increase is not very large when compared to the full range of possible z -values (Figure 4.4). This suggests that the shape of the cost function is more important than the environmental parameters in determining the evolutionary outcomes of the system. However, the quantitative impact of the spatial heterogeneity, and that of the environmental properties, may well depend on the degree of heterogeneity itself; including additional mechanisms that increase the spatial heterogeneity (e.g. sinking of detritus) may therefore be of importance before reaching quantitative conclusions. Also, the quantitative impact of the environmental parameters depends on the used parameter values, while the model was not tested against (nor fitted to) empirical data and not all of the parameter values were empirically based. Therefore, we focus on the qualitative rather than on the quantitative results of the model. It would be interesting, however, to test the model predictions experimentally, such that the relative impact of environmental parameters can be quantified. Unfortunately, such experiments are difficult to realize. Experimental work with closed few-species ecosystems is rare; Kawabata et al. [23] managed to maintain a three-species community of heterotrophic protozoa, saprotrophic bacteria and mixotrophic euglena, but experiments involving closed systems with only mixotrophs are not known to the authors. Furthermore, the predictions involve evolutionary processes which requires experiments that continue over long time periods. However, we are optimistic about future possibilities, as in various experiments microbial populations limited by a single resource have been observed to evolve into stable dimorphisms [12, 42].

4.4.2 Concluding remarks on system structure

The study revealed that the assumptions on mass conservation and spatial structure can greatly affect the evolutionary outcomes. This should be taken into account when choosing or developing a model for the study of evolutionary behavior. In this final section, we summarize these effects and indicate their significance with respect to evolutionary speciation processes.

In closed and homogeneous systems, evolutionary branching does not occur unless the organisms have an intrinsic advantage to specialization ($z > 1$) [44]. Moreover, for $z \leq 1$ phenotypic variation is not possible at all: the population always evolves to the same (mixotrophic) strategy. Environmental properties do not have any effect on this.

Opening the system for mass makes phenotypic variation possible, and populations living in a different environment may now each evolve to a different trophic preference. This process of ‘local adaptation’ of the asexual mixotrophs may correspond to a speciation process in sexually reproducing organisms. Such a speciation process would be ‘allopatric’, as the reproductive isolation of the two descendent species is initially due to their geographical separation.

Introducing a spatial heterogeneity (spatial gradient) in the system, as was done in the present study, may induce evolutionary branching, even when the organisms have an intrinsic disadvantage to specialization ($z \leq 1$). Hence, it may cause the mixotrophs to specialize into separate autotrophs and heterotrophs. Like local adaptation, evolutionary branching of the asexual mixotrophs may correspond to a speciation process in sexual organisms. In this case, however, speciation would be ‘sympatric’, as the two descendant species live in the same or in overlapping areas and geneflow is thus not hindered by geographical barriers.

Finally, we showed that habitat segregation resulting from a spatial heterogeneity will be found more often in studies of open systems than in those considering closed systems. This is related to the mutual dependencies and feed back loops inherent to the full mass recycling which may restrict the degree of spatial heterogeneity and its effects. Evolutionary branching resulting in habitat segregation suggests the possibility of an adaptive route to allopatric or parapatric speciation [38].

Appendix: The mixotroph model

State variables and ODEs

This appendix gives a detailed discussion on the growth equations of the mixotroph model. The spatial structure and vertical transport are discussed in the main text. Although all state variables depend on time t and on depth L_z , here we discuss only how they depend on the time, while their depth is considered to be fixed. The model is based on the mixotroph model presented by Kooijman et al. [29] and is based on the Dynamic Energy Budget (DEB) theory. The population dynamics of the mixotrophs were simplified according to the same assumptions made by Troost et al. [44], which are discussed in appendix 4.4.2.

The model has only one state variable for the mixotrophic organisms (biomass X_V), and three state variables to describe the abiotic environment (detritus X_D , dissolved inorganic carbon (DIC) X_C and nitrogen (DIN) X_N). The latter two states consist of one nutrient only, while biomass and detritus are thought of as generalized compounds containing both carbon and nitrogen and other elements in a fixed chemical composition. It is assumed that elements other than carbon and nitrogen are not limiting the growth of the organisms. The system is closed for mass, but open to energy (light and heat production).

The four state variables partake in five transformations: assimilation A (autotrophic A_A and heterotrophic assimilation A_H), growth G , maintenance

Table 4.2: Symbols used for variables.

Symbol	Dimension	Interpretation
t	t	Time
L_z	l	Depth below water surface
X_i	$\text{mol } l^{-3}$	Concentration of compound i
X_{i+}	mol	Total amount of compound i
f_i	–	Scaled functional response for element/process i
h	t^{-1}	Hazard rate
$J_{i,j}$	$\text{mol } i \text{ } t^{-1}$	Flux of compound i associated with transformation j
$j_{i,j}$	$\frac{\text{mol } i}{\text{mol } V} t^{-1}$	Structure-specific flux of compound i : $J_{i,j}/M_V$
$j_{i,\text{Am}}$	$\frac{\text{mol } i}{\text{mol } V} t^{-1}$	Struct-spec. max assimilation flux, of compound i
$j_{i,\text{AK}}$	$\frac{\text{mol } i}{\text{mol } V} t^{-1}$	Struct-spec. max saturation flux, of compound i
K_i	$\text{mol } l^{-3}$	Saturation constant for compound i
K_V	$l^2 t^{-1}$	Turbulent mixing coefficient
k_M	t^{-1}	Maintenance rate
$n_{i,j}$	–	Chemical coefficient for element i in compound j
$y_{i,j}$	$\frac{\text{mol } i}{\text{mol } j}$	Mol compound i required per mol compound j
z	–	Shape coefficient for the cost function
z_i	–	Flux ratio $j_{i,\text{Am}}/j_{i,\text{AK}}$ for compound i
α	l^{-1}	Background turbidity coefficient
β_i	$l^2 \text{mol } i^{-1}$	Specific absorption coefficient for compound i
ρ_i	–	Affinity for assimilation route i (autotrophic or heterotrophic)

M and death H . An overview of these transformations was already given in the main text, accompanied by Figure 4.1. A more detailed diagram is given in Figure A1, which shows the symbols for all fluxes. DIC and DIN are assimilated via the autotrophic route and their specific uptake fluxes are denoted by $j_{C,\text{AA}}$ and $j_{N,\text{AA}}$; the resulting autotrophic assimilation flux is $j_{V,\text{AA}}$. Detritus is taken up by the heterotrophic route, whose uptake flux is denoted by $j_{D,\text{AH}}$; the resulting heterotrophic assimilation flux is $j_{V,\text{AH}}$. The two assimilation fluxes are combined into a total production rate $j_{V,\text{A}}$. Part of these assimilates are transformed into biomass ($j_{V,\text{G}}$); maintenance costs ($j_{V,\text{M}}$) and overhead costs take care of the conversion of organic material back into inorganic nutrients ($(1 - y_{C,V}^{-1})j_{V,\text{AA}}$, $(y_{D,V} - 1)j_{V,\text{AH}}$ and $(1 - y_{C,V}^{-1})j_{V,\text{AH}}$). The biomass density is diminished through mortality ($j_{V,\text{H}}$); upon death, the biomass of these organisms turns into detritus ($j_{D,\text{H}}$). The notation of these fluxes and the corresponding equations are introduced in Table 4.2; default values of the parameters are given in 4.3.

The amounts of biomass, detritus and DIC are all expressed in the number of moles of carbon. Therefore, at transformations without additional costs or losses, the production flux equals minus its associated uptake flux: $j_{V,\text{H}} = -j_{D,\text{H}}$ and $j_{V,\text{M}} = -j_{C,\text{M}}$. Also, biomass is assumed to have a constant chemical composition, and $n_{N,V}$ specifies the fixed amount of nitrogen per mole carbon. As a result, the uptake flux of DIN $j_{N,\text{AA}}$ equals $n_{N,V}$ times $j_{C,\text{AA}}$; similarly, also other fluxes involving nitrogen can be rewritten: $j_{N,\text{M}} = n_{N,V} j_{C,\text{M}}$ and $j_{N,\text{AH}} = n_{N,V} j_{C,\text{AH}}$. Finally, the specific maintenance and death rates of

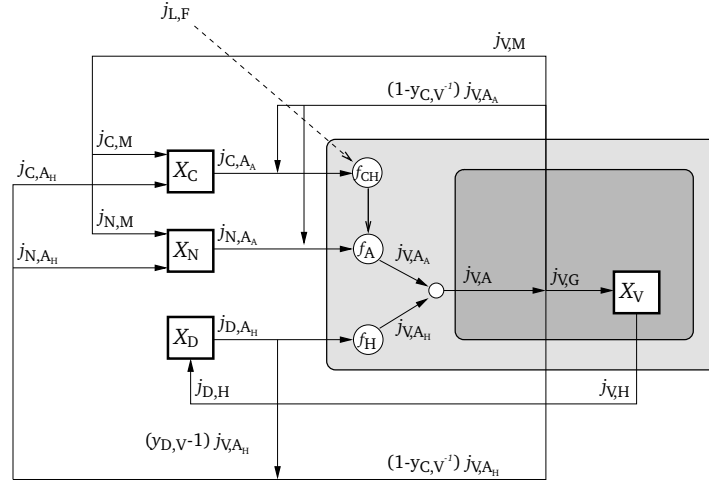


Figure 4.6: Detailed diagram of the metabolism of a mixotroph, showing the symbols of the fluxes. The shaded box encloses the organism, the lighter part of which denotes its membranes containing the assimilatory machinery. A circle denotes a Synthesizing Unit (only SUs with two or more substrates are shown). The organism has one state variable for biomass X_V ; the environment consists of three states: dissolved inorganic carbon X_C , dissolved inorganic nitrogen X_N and detritus X_D . Arrows indicate the structure-specific transformation fluxes.

the mixotrophs are assumed to be constant, so that $j_{V,M} = k_M$ and $j_{V,H} = h$. The temporal changes in state variables can now be summarized as follows:

$$\frac{d}{dt} X_C = X_V (j_{C,A_A} + j_{C,A_H} + k_M), \quad (4.11a)$$

$$\frac{d}{dt} X_N = X_V (j_{C,A_A} + j_{C,A_H} + k_M) n_{N,V}, \quad (4.11b)$$

$$\frac{d}{dt} X_D = X_V (j_{D,A_H} + h), \quad (4.11c)$$

$$\frac{d}{dt} X_V = X_V (j_{V,G} - h), \quad (4.11d)$$

where X_i is the concentration of state variable i and $j_{i,j}$ is the specific flux of

Table 4.3: Default parameter values.

Parameter	Value	Dimension
h	0.1	d^{-1}
$j_{L,F(0)}$	-1	$\text{mol mol}^{-1} \text{d}^{-1}$
$j_{L,FK}$	50	$\text{mol mol}^{-1} \text{d}^{-1}$
$j_{V,AAm}$	4.5	$\text{mol mol}^{-1} \text{d}^{-1}$
$j_{V,AHm}$	4.0	$\text{mol mol}^{-1} \text{d}^{-1}$
K_C	500	μM
K_N	0.1	μM
K_D	2500	μM
K_V	0.5	$\text{m}^2 \text{d}^{-1}$
k_M	0.1	d^{-1}
L_m	70	m
n_{NV}	0.15	-
X_{C+}	2400	μM
X_{N+}	40	μM
y^0	1.1	mol mol^{-1}
y^A	0.5	mol mol^{-1}
y^H	0.1	mol mol^{-1}
$y_{D,V}$	1.3	-
z	1	-
z_C	0.1	-
z_N	0.1	-
z_{CH}	0.01	-
α	0.07	m^{-1}
β_D	0.1	$\text{m}^2 \text{mol}^{-1}$
β_V	0.05	$\text{m}^2 \text{mol}^{-1}$

compound i partaking in transformation j . The fluxes are given by:

$$j_{C,AA} = -\frac{j_{V,AA}}{y_{C,V}}, \quad (4.12)$$

$$j_{C,AH} = -j_{D,AH} - \frac{j_{V,AH}}{y_{C,V}}, \quad (4.13)$$

$$j_{D,AH} = -y_{D,V} j_{V,AH}, \quad (4.14)$$

$$j_{V,G} = \frac{j_{V,A}}{y_{C,V}} - k_M. \quad (4.15)$$

The transformation of detritus into assimilates comes with overhead costs. The yield coefficient $y_{D,V}$ determines the fraction of detritus required per amount of produced assimilates. To compensate for the loss in this transformation, an additional amount of detritus is taken up. Therefore, the uptake flux of detritus $j_{D,AH}$ is equal to minus the amount of assimilates that is used for heterotrophic assimilation $j_{V,AH}$ times the yield factor $y_{D,V}$ (equation (4.14)).

From the assimilation products, maintenance costs are paid; the resulting amount of material is used for growth (see equation (4.15)). At the transformation of assimilates into biomass, again overhead costs have to be paid again, which is in this case taken care of by means of the yield coefficient $y_{C,V}$. DIC is

thus taken up by autotrophic assimilation, but due to the overhead costs, not all of the carbon becomes biomass; the ‘lost’ carbon is released in the environment in its inorganic form again. The same goes for DIN and detritus: part of these resources that are taken up for assimilation are released again into the environment in the form of DIC and DIN.

It is assumed that the overhead costs are paid from the assimilates produced in both assimilatory routes, and in proportion to the two assimilatory fluxes. DIC and DIN fluxes due to overhead costs paid by the autotrophic route come back into the environment in the same form (inorganic) as they were taken from it. Therefore, these can be ‘bypassed’ in calculating $j_{C,AA}$. This flux is then equal to minus the amount of DIC that is taken up is from the environment for assimilation ($j_{V,AA}$), plus the amount of DIC that is released through overhead costs; latter amount can be calculated by subtracting the amount that is actually transformed into biomass ($j_{V,AA}/y_{C,V}$) from the amount that is taken up ($j_{V,AA}$). This results in the following equation: $j_{C,AA} = -j_{V,AA} + (j_{V,AA} - j_{V,AA}/y_{C,V})$, which can be simplified into $j_{C,AA} = -j_{V,AA}/y_{C,V}$ (equation (4.12)).

Similarly, the amount of DIC that is released from the heterotrophic route $j_{C,AH}$ is equal to the difference between the amount taken up for assimilation $j_{V,AH}$ and the amount that is actually transformed into biomass: $j_{V,AH} - j_{V,AH}/y_{C,V}$. But, also at the transformation of detritus into assimilates, overhead costs had to be paid and DIC and DIN were released. These losses are equal to the difference between the amount that is taken up for assimilation ($y_{D,V} j_{V,AH}$) and the amount that is actually transformed into assimilates ($j_{V,AH}$). Combining these two release fluxes of DIC in the environment results in the following equation: $j_{C,AH} = (y_{D,V} - 1)j_{V,AH} + (j_{V,AH} - j_{V,AH}/y_{C,V})$. This equation can be simplified as $j_{C,AH} = y_{D,V} j_{V,AH} - j_{V,AH}/y_{C,V}$ in which the first term can be substituted by $-j_{D,AH}$ (equation (4.13)).

The deviation in equations (4.12-4.15) from Kooijman et al. [29] is caused by the extra overhead costs that were included for the production of biomass by means of $y_{C,V}$. These costs were introduced by Troost et al. [44] as to provide a trade-off between autotrophy and heterotrophy. Without such costs, the mixotrophs could increase both their assimilatory capabilities without any negative consequences. Although in the present study yet another trade-off is assumed (see Equation (4.1)), these additional overhead costs were maintained. This provides the possibility to include an intrinsic advantage to either mixotrophic or specialist strategies, and makes it better possible to compare the present results with those of the previous study. In the next section these costs and the assimilation fluxes $j_{V,AA}$, $j_{V,AH}$ and $j_{V,A}$ are explained.

Assimilation

Mixotrophs have two assimilatory pathways, the autotrophic and the heterotrophic one, of which the products are combined substitutably for biomass production. In the model, a central role is played by the affinities that the organisms have for each of these two assimilatory pathways; ρ_A for the autotrophic

route and ρ_H for the heterotrophic route. A higher affinity may be interpreted as an increase or an improvement in the assimilation machinery that results in a higher assimilation flux.

Autotrophic and heterotrophic assimilation fluxes j_{V,A_A} and j_{V,A_H} are proportional to the affinities, to the maximum assimilation rates $j_{V,A_{Am}}$ and $j_{V,A_{Hm}}$, and to the functional responses f_A and f_H :

$$j_{V,A_A} = \rho_A j_{V,A_{Am}} f_A, \quad (4.16)$$

$$j_{V,A_H} = \rho_H j_{V,A_{Hm}} f_H. \quad (4.17)$$

In Kooijman et al. [29] the affinities were not included in the assimilation fluxes, but in the gross growth flux $j_{V,A}$. Another difference is that here we assume that no limitation exists to the total assimilation flux (see section 4.4.2). The total assimilation flux then becomes:

$$j_{V,A} = j_{V,A_A} + j_{V,A_H}. \quad (4.18)$$

The functional responses f_A and f_H are modeled with use of Synthesizing Units (SUs) cf. Kooijman [26, 27], which provide a simple and realistic method for calculating production fluxes at simultaneous nutrient and light limitations. Planktonic protists have a photosynthetic system that consists of two photosystems, with which they stepwise convert carbon dioxide, nitrogen and light into biomass. First, carbon dioxide and photons are bound by carriers. Then, the carbon dioxide is reduced into a carbohydrate. Nitrogen is bound and, together with the carbohydrates, synthesized into biomass. This process can be modeled by coupling several SUs. Binding fluxes of carbon f_C and nitrogen f_N can be calculated by a simple one-substrate SU; the reduction rate of carbon f_{CH} can be calculated by a complementary SU for which both carbon and electrons are essential. Finally, f_A can be calculated with again a complementary SU for which both carbohydrate and nitrogen are essential:

$$f_C = \frac{X_C}{K_C + X_C}, \quad (4.19)$$

$$f_N = \frac{X_N}{K_N + X_N}, \quad (4.20)$$

$$f_{CH} = \frac{(1 + z_C^{-1})}{1 + z_C^{-1} f_C^{-1} + x_L^{-1} - (z_C f_C + x_L)^{-1}}; \quad \text{with } x_L = \frac{-J_{L,F}}{J_{L,FK}} \quad (4.21)$$

$$f_A = \frac{(1 + z_N^{-1} + z_{CH}^{-1} - (z_N + z_{CH})^{-1})}{1 + z_N^{-1} f_N^{-1} + z_{CH}^{-1} f_{CH}^{-1} - (z_N f_N + z_{CH} f_{CH})^{-1}}, \quad (4.22)$$

where K_i is the saturation constant for compound i and z_i a scaling parameter that weighs the contributions of carbon C , carbohydrates CH and nitrogen N . Light influx $J_{L,F}$ (negative, because photons flow in) is scaled with parameter $J_{L,FK}$ so that a multiplication of these two fluxes with an arbitrary number (different from zero) has no effect. At the surface of the water column, the light influx can be taken proportional to the solar irradiance (photon flux per

unit of surface area of water/ air boundary layer). Below the surface the light influx depends on the depth according to equation (4.5) (with selfshading) or to equation (4.6) (without self shading). The functional response of the heterotrophic route f_H depends on the binding of detritus, which can be represented by a one-substrate SU:

$$f_H = \frac{X_D}{K_D + X_D}, \quad (4.23)$$

in which K_D is the saturation constant for detritus.

Affinities for either pathway are assumed to entail costs for building the necessary machinery, which are taken care of by means of the yield coefficient $y_{C,V}$. This yield coefficient consists of certain base costs y^0 , increased by extra costs for building the assimilation machineries y^A and y^H , which for both pathways is proportional to the corresponding affinity:

$$y_{C,V} = y^0 + y^A(1 - (1 - \rho_A)^z) + y^H(1 - (1 - \rho_H)^z). \quad (4.24)$$

We recall that in this paper we took $\rho = \rho_A = 1 - \rho_H$. The parameter z determines the shape of the cost function; convexly shaped cost functions ($z > 1$) give the organisms an intrinsic advantage to specialized strategies, while concave cost functions ($z < 1$) give them an intrinsic advantage to mixotrophic strategies. The fourth term in the cost function (y_{AH}) as it was used by Troost et al. [44], involving costs due to the interaction between the two assimilatory routes, was for simplicity not taken into account ($y^{AH} = 0$). Based on Raven [40], the costs related to the autotrophic machinery y^A were assumed to be higher than the costs related to the heterotrophic machinery y^H . The costs are paid by both assimilatory pathways ($j_{V,AA}$ and $j_{V,AH}$), proportional to the contribution of these pathways to the total assimilation flux $j_{V,A}$, see equations (4.12), (4.13) and (4.18).

Simplifications

As mentioned above, the population dynamics of the mixotrophs were simplified according to the same assumptions that were done in [44]. These assumptions were found to have no qualitative and only a small quantitative effect on the evolutionary outcomes, while they simplify the model considerably.

The first simplification concerns the structure of the organisms. The mixotrophs are assumed to consist only of structural biomass and not to have storage pools or reserves. Reserves may be very important when studying the transient behavior and ecological dynamics of a system and in particular when considering a fluctuating environment. However, here we assume a constant environment; in addition, we study the evolutionary dynamics of the system for which we assume that the system is always in steady state at an ecological time scale.

Secondly, it is assumed that no limit exists to the total assimilation rate $j_{V,A}$, which was done by increasing the maximum assimilation rates (k_A and

$k_H \rightarrow \infty$). As a consequence, the total assimilation flux $j_{V,A}$ can be calculated by simply adding the autotrophic and heterotrophic assimilation rates $j_{V,AA}$ and $j_{V,AH}$. This makes the maximum assimilation rates (k_A and k_H) as well as the intermediary assimilation fluxes that were used in [29] ($j_{V_A,AA}$ and $j_{V_H,AH}$) redundant, and thus leads to a simpler formulation. Again, this assumption mainly affects the transient dynamics of the system.

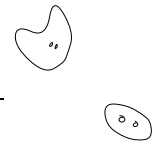
Thirdly, DIN was assumed not to play a role in the heterotrophic assimilation route. In the model of Kooijman et al. [29], detritus was complemented with DIN in order to synthesize the nitrogen-rich reserves. Here, we assume that DIN does not affect the heterotrophic route at all, and the flux is removed from the equations. In the base model, the saturation constant for the uptake of DIN via the heterotrophic route K_{N_V} was already set to a small value, such that the heterotrophic assimilation rate was hardly affected by DIN. Since the two models become equal when the saturation constant goes to zero ($K_{N_V} \rightarrow 0$), they are effectively very similar.

Finally, we used a more common formulation of Lambert-Beer's law (4.5) by removing the maximum depth L_m out of the equation. This resulted in a different interpretation and dimension of α .

Numerical methods

To calculate the steady state vertical profiles of the four variables (X_C , X_N , X_D , X_V), the equations are solved with the method of lines: first the spatial derivatives are discretized using central differences on a regular grid consisting of N cells; then, the resulting system of $4N$ ordinary differential equations is solved by numerical integration. For this we use a standard FORTRAN routine from the IMSL library for implicit integration of ODEs (DIVPAG), which can handle stiff systems. To speed up the calculations, the routine is set to select the chord method in which the Jacobian is replaced by a diagonal approximation based on a directional derivative. It turns out that a value of $N = 40$ gives sufficiently accurate results. Because the plankton cells are assumed to be neutrally buoyant, we do not have an advection term in the reaction-diffusion equations. This makes it rather straightforward to solve them. When taking into account self shading, the depth integral in Equation (4.5) classifies the PDE model as an integro-PDE, which is computationally more demanding than simulation of standard PDEs [19]. Calculations, however, did not raise any problems.

To calculate the evolutionary outcomes, we need to calculate the invasion fitness of potential mutants. In the heterogeneous environment, the specific growth rate of the mutants varies with depth. Therefore, we can not use their specific growth rate as the invasion criteria straight away, but we have to take into account the distribution of the resident and the mutant population over the depth of the water column. Mathematically, this comes down to calculating the dominant eigenvalue λ , evaluated in the ss of the linearized discretized system that includes the mutant. If λ is negative, the mutant cannot invade; if λ is positive, the mutant is able to invade. Therefore, an additional state variable



for the mutant is included in the model; its density was set to zero ($X_{V_{\text{mut}}} = 0$) as mutants are assumed to be rare. The resulting system now consists of $5N$ ODEs.

The Jacobian of this system is calculated with a FORTRAN routine (again from the IMSL library) that uses forward differences (DFDJAC), and the associated eigenvalues are found with the routine DEVLRG. Because mass balances are applied to the total carbon and nitrogen content in the system, always two of the resulting eigenvalues are zero. The resident population is assumed to be in stable equilibrium with its environment, so all other eigenvalues of the system without the mutant are negative. For the system including the mutant, the largest eigenvalue (other than the two zeros) represents the long term growth rate of the mutant and thus its invasion fitness: $s_{\rho_{\text{res}}}(\rho_{\text{mut}}) = \lambda$. The evolutionary equilibria, at which the first derivative of the fitness function at the strategy of the resident is equal to zero ($D_1 = 0$), were found with the bisection method. The second derivatives of the fitness function (D_2) are determined quantitatively by taking second order central finite differences.

Acknowledgments

We are grateful for the thorough comments by two anonymous referees and the editor E.J. Weissing which have considerably improved the contents and presentation of the paper.

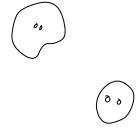
References

- [1] Beaver, J., Crisman, T., and Bienert, R. J. (1988). Distribution of planktonic ciliates in highly coloured subtropical lakes: comparison with clear-water ciliate communities and the contribution of myxotrophic taxa to total autotrophic biomass. *Freshwater Biology*, 20:51–60.
- [2] Brown, J. S. (1996). Coevolution and community organization in three habitats. *OIKOS*, 75(2):193–206.
- [3] Cavalier-Smith, T. (1998). A revised six-kingdom system of life. *Biological reviews*, 73:203–266.
- [4] Day, T. (2000). Competition and the effect of spatial resource heterogeneity on evolutionary diversification. *American Naturalist*, 155(6):790–803.
- [5] Dieckmann, U. (1997). Can adaptive dynamics invade? *Trends in Ecology and Evolution*, 12:128–131.
- [6] Dieckmann, U. and Law, R. (1996). The dynamical theory of coevolution: a derivation from stochastic ecological processes. *Journal of Mathematical Biology*, 34:579–612.

- [7] Diehl, S. (2002). Phytoplankton, light, and nutrients in a gradient of mixing depths: Theory. *Ecology*, 83(2):386–398.
- [8] Doebeli, M. and Dieckmann, U. (2003). Speciation along environmental gradients. *Nature*, 421:259–264.
- [9] Dolan, J. R. and Perez, M. T. (2000). Costs, benefits and characteristics of mixotrophy in marine oligotrichs. *Freshwater Biology*, 45(2):227–238.
- [10] Ebert, U., Arrayas, M., Temme, N. M., Sommeijer, B. P., and Huisman, J. (2001). Critical conditions for phytoplankton blooms. *Bulletin of Mathematical Biology*, 63:1095–1124.
- [11] Falkowski, P. G. and Woodhead, A. D., editors (1992). *Primary productivity and biochemical cycles in the sea*, volume 43 of *Environmental Science Research*. Plenum Press.
- [12] Friesen, M. L., Saxer, G., Travisano, M., and Doebeli, M. (2004). Experimental evidence for sympatric ecological diversification due to frequency-dependent competition in *Escherichia coli*. *Evolution*, 58(2):245–260.
- [13] Fryxell, J. M. (1997). Evolutionary dynamics of habitat use. *Evolutionary Ecology*, 11(6):687–701.
- [14] Geritz, S. A. H., Kisdi, E., Meszéna, G., and Metz, J. A. J. (1998). Evolutionary singular strategies and the adaptive growth and branching of the evolutionary tree. *Evolutionary Ecology*, (12):35–57.
- [15] Geritz, S. A. H., Metz, J. A. J., Kisdi, É., and Meszéna, G. (1997). Dynamics of adaptation and evolutionary branching. *Physical Review Letters*, 78:2024–2027.
- [16] Hall, S. R., Leibold, M. A., Lytle, D. A., and Smith, V. H. (2004). Stoichiometry and planktonic grazer composition over gradients of light, nutrients and predation risk. *Ecology*, 85(8):2291–2301.
- [17] Holen, D. (2000). The relative abundance of mixotrophic and heterotrophic ciliates in an oligotrophic lake. *Archiv fuer Hydrobiologie*, 150:1–15.
- [18] Huisman, J., Arrayas, M., Ebert, U., and Sommeijer, B. P. (2002). How do sinking phytoplankton species manage to persist? *American Naturalist*, 159(3):245–254.
- [19] Huisman, J. and Sommeijer, B. P. (2002). Maximal sustainable sinking velocity of phytoplankton. *Marine Ecology-Progress series*, 244:39–48.
- [20] Huisman, J., Van Oostveen, P., and Weissing, F. J. (1999a). Critical depth and critical turbulence; two different mechanisms for the development of phytoplankton blooms. *Limnology and Oceanography*, 44(7):1781–1787.

- [21] Huisman, J., Van Oostveen, P., and Weissing, F. J. (1999b). Species dynamics in phytoplankton blooms: incomplete mixing and competition for light. *American Naturalist*, 154(1):46–68.
- [22] Huisman, J. and Weissing, F. J. (1995). Competition for nutrients and light in a mixed water column: a theoretical analysis. *American Naturalist*, 146(4):536–564.
- [23] Kawabata, Z., Matsui, K., Okazaki, K., Nasu, M., Nakano, N., and Sugai, T. (1995). Synthesis of a species-defined microcosm with protozoa. *Journal for Protozoology Research*, 5:23–26.
- [24] Klausmeier, C. A., Litchman, E., Daufresne, T., and Levin, S. A. (2004). Optimal nitrogen-to-phosphorus stoichiometry of phytoplankton. *Nature*, 429:171–174.
- [25] Kooi, B. W., Boer, M. P., and Kooijman, S. A. L. M. (1998). On the use of the logistic equation in models of food chains. *Bulletin of Mathematical Biology*, 60:231–246.
- [26] Kooijman, S. A. L. M. (1998). The synthesizing unit as model for the stoichiometric fusion and branching of metabolic fluxes. *Biophysical Chemistry*, 73:179–188.
- [27] Kooijman, S. A. L. M. (2000). *Dynamic Energy and Mass Budgets in Biological Systems*. Cambridge University, 2nd edition.
- [28] Kooijman, S. A. L. M., Andersen, T., and Kooi, B. W. (2004). Dynamic energy budget representations of stoichiometric constraints on population dynamics. *Ecology*, 85(5):1230–1243.
- [29] Kooijman, S. A. L. M., Dijkstra, H. A., and Kooi, B. W. (2002). Light-induced mass turnover in a mono-species community of mixotrophs. *Journal of Theoretical Biology*, 214:233–254.
- [30] Kooijman, S. A. L. M. and Hengeveld, R. (2005). The symbiotic nature of metabolic evolution. In Reydon, T. A. C. and Hemerik, L., editors, *Current Themes in Theoretical Biology: A Dutch perspective.*, pages 159–202. Springer, Dordrecht.
- [31] Kooijman, S. A. L. M. and Nisbet, R. M. (2000). How light and nutrients affect life in a closed bottle. In Jørgensen, S. E., editor, *Thermodynamics and ecological modelling*, pages 19–60, Boca Raton, FL, USA. CRC Publ.
- [32] Krivan, V. and Sirot, E. (2002). Habitat selection by two competing species in a two-habitat environment. *American Naturalist*, 160(2):214–234.
- [33] Litchman, E. (1998). Population and community responses of phytoplankton to fluctuating light. *Oecologia*, 117:247–257.

- [34] Litchman, E. and Klausmeier, C. A. (2001). Competition of phytoplankton under fluctuating light. *American Naturalist*, 157(2):170–187.
- [35] Mann, K. H. and Lazier, J. R. N. (1996). *Dynamics of marine ecosystems; Biological-Physical interactions in the oceans*. Blackwell Science, 2nd edition.
- [36] Margulis, L. (1993). *Symbiosis in Cell Evolution*. Freeman, New York.
- [37] Metz, J. A. J., Geritz, S. A. H., Meszéna, G., Jacobs, F. J. A., and van Heerwaarden, J. S. (1996). Adaptive dynamics, a geometrical study of the consequences of nearly faithful reproduction. In van Strien, S. J. and Verdun Lunel, S. M., editors, *Stochastic and spatial structures of dynamical systems*, pages 183–231. Elsevier.
- [38] Mizera, F. and Meszéna, G. (2003). Spatial niche packing, character displacement and adaptive speciation along an environmental gradient. *Evolutionary Ecology Research*, 5(3):363–382.
- [39] Nygaard, K. and Tobiesen, A. (1993). Bacterivory in algae: A survival strategy during nutrient limitation. *Limnology and Oceanography*, 38(2):273–279.
- [40] Raven, J. A. (1997). Phagotrophy in phototrophs. *Limnol. Oceanogr.*, 42:198–205.
- [41] Ronce, O. and Kirkpatrick, M. (2001). When sources become sinks: Migrational meltdown in heterogeneous habitats. *Evolution*, 55(8):1520–1531.
- [42] Rozen, D. E. and Lenski, R. E. (2000). Long-term experimental evolution in escherichia coli. viii dynamics of a balanced polymorphism. *American Naturalist*, 155(1):24–35.
- [43] Thingstad, T. F., Havskum, H., Garde, K., and Riemann, B. (1996). On the strategy of ‘eating your competitor’: a mathematical analysis of algal mixotrophy. *Ecology*, 77:2108–2118.
- [44] Troost, T. A., Kooi, B. W., and Kooijman, S. A. L. M. (2005). When do mixotrophs specialize? Adaptive dynamics theory applied to a dynamic energy budget model. *Mathematical Biosciences*, 193(2):159–182.
- [45] Valiela, I. (1995). *Marine ecological processes*. Springer, 2nd edition.
- [46] Zajic, J. E., editor (1970). *Properties and products of algae*. Plenum Press, New York.



5

Joint evolution of predator body size and prey-size preference

Tineke A. Troost, Bob W. Kooi, Ulf Dieckmann

Abstract

We studied the joint evolution of predator body size and prey-size preference based on Dynamic Energy Budget theory. The predators' demography and their functional response are based on general eco-physiological principles involving the size of both predator and prey. While our model can account for qualitatively different predator types by adjusting parameter values, we mainly focused on 'true' predators that kill their prey. The resulting model explains various empirical observations, such as the triangular distribution of predator-prey size combinations, the island rule, and the difference in predator-prey size ratios between filter feeders and raptorial feeders. The model also reveals key factors for the evolution of predator-prey size ratios. Capture mechanisms turned out to have a large effect on this ratio, while prey-size availability and competition for resources only help explain variation in predator size, not variation in predator-prey size ratio. Furthermore, predation among predators is also identified as an important factor.

5.1 Introduction

The range of body sizes encountered in nature is enormous. A bacterium with full physiological machinery has a volume of $0.25 \times 10^{-18} \text{ m}^3$, while a blue whale has a volume of up to 135 m^3 . These body sizes are associated with the different scales in time and space in which organisms live, and reflect the differences in physiological processes and life histories. A wide range is also found in the prey-size preference of predators: consider, for example, whales feeding on plankton and hyena eating zebra. Like body size, the prey-size preference is an important ecological property, as it determines which trophic links between predators and prey are established. Together, the body size and the prey-size preference of predators largely define the structure of a community. While the effects of body size on individuals and populations has been investigated from many angles [4, 25, 40, 49], general relationships between a predator's body size and its prey-size preference are more difficult to find.

Various mechanisms have been proposed that attempt to explain predator-prey size ratios and prey-size preferences. These include passive selection mechanisms such as prey visibility [41, 43] or gape limitation [17, 24, 35, 41]. Active selection mechanisms, on the other hand, underlie optimal foraging theory, which assumes that predators select prey sizes that provide the best energy returns. Several mechanisms based on active selection are discussed in [16, 23, 30, 32, 42, 44]. However, since results vary both within and between predator-prey systems and the found relationships are greatly species-specific, it is difficult to extract general rules from them.

In recent years, several models have been developed that focus on general large-scale patterns of feeding links in food webs. Some of these models, such as the cascade model [8] and the niche model [48], are able to generate food webs that approximate many features observed in real food webs. However, these models are often descriptive and predator-prey pairs are assigned at random. Other models do have a more mechanistic basis and include physiological relations based on body size, but assume a fixed predator-prey size ratio [31]. Aljetlawi et al. [1] derived a functional response that accounts for both predator and prey size: the derived relation is sufficiently flexible to be adjusted to many different specific predator-prey systems. This very flexibility, however, limits the scope for deriving general rules.

In this study we combine a process-based eco-physiological model with a functional response that depends on the size of both predator and prey. The model is based on Dynamic Energy Budget (DEB) theory [28, 29], a versatile framework for modeling metabolic processes with physiological rules for uptake and use of material and energy. DEB theory does not specify all details of the size-dependence of the functional response. One of our aims here is to make the terms underlying this functional response explicit and, where necessary, include additional terms, while staying as close to DEB theory as possible.

We do not arbitrarily choose predator-prey size ratios, but instead allow the predator size and its prey-size preference to evolve independently. The objective is to study which size combinations between predators and preys are

feasible and to which predator-prey size ratios the considered population or community will eventually evolve. More specifically, we study how patterns of predator size and prey-size preference depend on various factors, given a fixed prey-size distribution; the examined factors include environmental parameters and ecological parameters, with the latter describing predation as well as competition. The model focuses on a generalized predator with two life stages, and therefore is not intended to replace more species-specific studies on size-selective prey choice. By retaining a general perspective, we hope that the results reported below will provide insights into the various factors determining predator-prey size ratios, and thereby will help understanding of predator-prey size patterns observed in nature.

5.2 Model description

5.2.1 Population dynamics

We consider a predator-prey model in which a population of predators feed on one or more populations of prey. The predators are described by one state variable, their biomass density X_A (given by the total amount of structural biovolume per unit of system volume), and by two adaptive traits, their adult length ℓ_A and their preference for a prey length ℓ_P . The two adaptive traits remain constant throughout an individual's life, but may change from parent to offspring through mutation. Prey populations are described by their biomass density X_i per volume, and consist of organisms of length ℓ_i , with $i = 1, \dots, n$. The prey populations do not directly interact with each other.

Our model is based on a model of a size-structured rotifer population [26, 27], of which we use a simplified version that includes only two life stages for the predator, embryos and adults. Embryos do not feed, but grow by using the reserves they got from their mothers when eggs were produced. Adults, in contrast, do not grow but they do feed; the acquired energy is used for maintenance and egg production. Separating the functions of growth and feeding simplifies the model, but also removes intraspecific body size scaling relations. The interspecific scaling relations, however, are maintained. These include a size-dependent egg-production period a_A and a size-dependent developmental period of the embryo a_b . A continuous function for reproduction allows the system to be expressed in terms of delay differential equations (DDEs). The dynamics of the system can then be described as follows,

$$\frac{d}{dt}X_i(t) = (X_{r,i} - X_i(t))D - I_i f_i(t)X_A(t), \quad (5.1a)$$

$$\frac{d}{dt}X_A(t) = R(t - a_b) \exp(-ha_b) X_A(t - a_b) - hX_A(t), \quad (5.1b)$$

where $X_{r,i}$ is the incoming density of prey i , f_i is the predator's functional response to prey i (to be further discussed in Section 6.2), I_i is the maximum

volume-specific ingestion rate of prey i (which equals the inverse of the handling time $[t_{h,i}]$ multiplied by the probability ρ_s that an attack is successful, $I_i = \rho_s/[t_{h,i}]$, where the square brackets indicate that the handling time is expressed on a volume-specific basis), D is the dilution rate of prey, and h is the predator's mortality rate. The predator's egg development time a_b depends on the specific energy conductance k_E , $a_b = 3/k_E$ [26]. The predator's reproduction rate is given by

$$R(t) = \frac{h}{\exp(ha_A(t)) - 1}, \quad (5.2)$$

(see [26]), which depends on the mortality rate h to account for the removal of unhatched eggs due to mortality of their mothers. For small mortality rates, the reproduction rate equals the inverse of the egg-production period, $R(t) = 1/a_A(t)$.

An expression for $a_A(t)$ was derived by Kooi and Kooijman [26]. Their expression is given by the ratio between the amount of energy needed per egg and the rate with which energy becomes available for reproduction. The latter depends on the scaled energy density e of the mother (i.e., on the volume-specific amount of energy $[E]$ divided by the maximum energy content $[E_{\max}]$) and on the specific energy conductance k_E . At equilibrium, the scaled energy density e of an adult equals its scaled functional response f , so that the amount of mobilized energy equals $k_E f$. From the mobilized energy, the costs of maintenance have to be paid, calculated by multiplying the maintenance rate coefficient k_M (ratio of costs for maintenance per unit of time to costs for growth) with the energy investment ratio g (the proportion of the total amount of available energy that is used for growth). The scaled energy density required to produce an egg consist of the costs for the structural biomass of a newborn individual and the costs for growth and maintenance during the embryonic period, $g^+ = g + \frac{3}{4}gk_M/k_E$ [26], as well as the energy density of a newborn individual itself, \hat{e} . Based on these considerations, the egg-production period is obtained as

$$a_A(t) = \frac{g^+ + \hat{e}(t)}{k_E f(t) - k_M g}, \quad (5.3)$$

[26]. For a more detailed explanation of the model, including derivations of a_b , R , a_A , and g^+ , readers may want to consult [26] and [27]. All parameters and variables of the model are summarized in Table 5.1, with all default parameter values listed in Table 5.2.

5.2.2 Scaling considerations

Because this study considers adult length to be subject to evolution, some body-size scaling relations had to be included that were not taken into account in the original model [26, 27], where body size was fixed. First, the energy investment ratio g was no longer assumed to be constant, but instead becomes

Table 5.1: Parameters and state variables of the model.

Symbol	Dimension	Interpretation
<i>Physiological parameters</i>		
a_b, a_A	t	Egg-development time and egg-production time; $a_b = 3/k_E$
e, \hat{e}	–	Scaled energy density, of adult and of newborn individuals; $e = [E]/[E_{\max}] = f$
$[E], [E_{\max}], [E_{\max}]_{\text{ref}}$	eL^{-3}	Volume-specific energy density; actual, maximum, and reference
g, g^+	–	Energy investment ratio for biomass and embryo growth; $g^+ = g + \frac{3}{4}gk_M/v$
h	t^{-1}	Mortality rate
k_E	t^{-1}	Specific energy conductance; $k_E = v/\ell_A$
k_M	t^{-1}	Maintenance rate coefficient
R	t^{-1}	Reproduction rate
α	–	Proportion of the maximum size that is reached; $\alpha = \ell_A/\ell_{\max}$
v	Lt^{-1}	Energy conductance
<i>Trophic parameters</i>		
b, b_0	$l^3L^{-3}t^{-1}$	Volume-specific encounter rate and encounter rate coefficient
D	t^{-1}	Dilution rate
f, f_i	–	Functional response; overall, and with respect to prey population i
I_i	$L^3L^{-3}t^{-1}$	Maximum volume-specific intake rate for prey population i
$\ell_i, \ell_{\max}, \ell_{\text{ref}}$	L	Length of individuals of prey population i ; maximum length of predator; reference length
t_g, t_c, t_h	t	Ingestion, capture, and handling time
$[t_h], [t_{h,i}], [t_h]_{\text{ref}}$	$L^3L^{-3}t$	Volume-specific handling time: actual, with respect to prey population i , and minimum.
$[t_{g,0}], [t_{c,0}]$	$L^3L^{-3}t$	Coefficients for volume-specific ingestion and capture time
$X_{r,i}, X_{r,0}$	L^3l^{-3}	Incoming prey density; function, and scaling coefficient
δ	L	Distance between the successive lengths of incoming prey-size distribution
μ	L	Mean length of incoming prey-size distribution
σ_p, σ	–	Standard deviation; of attack probability (niche width), and of incoming prey-size distribution
ρ_a, ρ_s	–	Attack probability and capture efficiency
<i>Ecological state variables</i>		
X_A, X_i	L^3l^{-3}	Structural volume density of (adult) predators and of prey population i
<i>Evolutionary state variables</i>		
ℓ_A	L	Adult length of predator
ℓ_p	L	Prey-size preference of predator

Units: t , time; L , length of individual; l , length of reactor; e , energy.

Table 5.2: Default parameter values.

Parameter	Default value
\tilde{b}_0	1000
\tilde{D}	0.1
$\tilde{\ell}_{\text{ref}}$	1
$[\tilde{\ell}_{\text{c},0}]$	3.5
$[\tilde{\ell}_{\text{g},0}]$	0.77
α	0.1
σ_{p}	0.05
$\tilde{\sigma}$	0.25
ρ_{s}	1
$\tilde{\mu}$	0.5

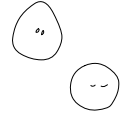
Tildes indicate that parameters are scaled by v , k_{M} and/or $X_{\text{r},0}$ to make them dimensionless.

dependent on body volume ℓ^3 m, following an expression central to DEB theory, $g = v/(k_{\text{M}} \ell_{\text{max}})$ [28]. Note that the adult body size ℓ_{A} of the predators is a fixed proportion α of their maximum size, $\ell_{\text{A}} = \alpha \ell_{\text{max}}$. This enables the model to cope with predators that quickly grow to adult size, without slowing down as would be expected from an asymptotic growth curve.

Second, the specific energy conductance k_{E} is equal to the energy conductance v divided by the size of the organism, $k_{\text{E}} = v/\ell_{\text{A}}$. The rationale behind this scaling relation is that energy is mobilized across membranes, which have a surface area proportional to that of the organism. As a result, the developmental period of the embryo becomes dependent on adult body size as well, $a_{\text{b}} = 3\ell_{\text{A}}/v$. Third, the mortality rate h was assumed to scale with length, such that larger organisms have a longer life span, $h = D \ell_{\text{ref}}/\ell_{\text{A}}$; at the reference length ℓ_{ref} mortality rate h is equal to dilution rate D . As such, the dilution rate serves as a measure for the harshness of the environment.

Like in the original model [26, 27], the scaled energy density of the eggs \hat{e} is assumed to depend on the scaled energy density e of the mother. However, the present study considers various prey sizes, and the scaled energy density e varies with prey size. Therefore, we assume that the mother does not provide her eggs with an energy density $[E]$ that equals e when scaled to her own maximum energy density $[E_{\text{max}}]$ (which depends on the actual prey availability). Instead she assumes the worst-case scenario for her eggs, and provides them with an energy density $[\hat{E}]$ that equals e when scaled against the maximum possible energy density $[E_{\text{max}}]_{\text{ref}}$. This ensures that the model does not allow for the unrealistic scenario in which mothers deliberately lower their energy densities by choosing prey with large handling times, in order to increase their reproduction rates. The scaled energy density of eggs is thus given by

$$\hat{e} = \frac{[\hat{E}]}{[E_{\text{max}}]} = \frac{[\hat{E}]}{[E_{\text{max}}]_{\text{ref}}} \frac{[E_{\text{max}}]_{\text{ref}}}{[E_{\text{max}}]} = \frac{[E_{\text{max}}]_{\text{ref}}}{[E_{\text{max}}]} e. \quad (5.4a)$$



If we again use $e = f$, this can be rewritten as

$$\frac{[E_{\max}]_{\text{ref}}}{[E_{\max}]} e = \frac{[E_{\max}]_{\text{ref}}}{[E_{\max}]} f = \frac{[t_{\text{h}}]}{[t_{\text{h}}]_{\text{ref}}} f, \quad (5.4b)$$

where the last step follows from the fact that the maximum energy density is proportional to the maximum ingestion rate, while the maximum ingestion rate is the inverse of the handling time, so that $[E_{\max}] \propto 1/[t_{\text{h}}]$, [28], p. 269.

5.2.3 Incoming prey densities

The model introduced above can be analyzed either for a single or for multiple prey populations. In the latter case, the incoming prey densities $X_{r,i}$ were assumed to vary gradually across prey populations, following a distribution with mean prey size μ , (dimensionless) standard deviation σ , and maximum density $X_{r,0}$,

$$X_{r,i} = X_{r,0} \frac{\delta}{\sigma \sqrt{2\pi}} \exp\left(-\frac{1}{2} \frac{\ln(\ell_i/\mu)^2}{\sigma^2}\right), \quad (5.5)$$

where δ denotes the distance between the successive lengths of prey. For numerical purposes, this prey-size distribution was truncated at $+3$ and at -3 times the standard deviation σ , thus representing 98% of the total distribution. We found that a resolution of $n = 50$ was sufficient to ensure that results were essentially unaffected by discretization of the prey-size distribution.

5.2.4 Functional responses

The sequence of capturing a prey consists of encounter, attack, and handling. These interactions between predator and prey are assumed to follow a Holling type-II functional response,

$$f = \sum_{i=1}^n f_i, \text{ with } f_i = \frac{X_i/K_i}{1 + \sum_{j=1}^n X_j/K_j} \text{ and } 1/K_j = \rho_{a,j} b_j [t_{\text{h},j}], \quad (5.6)$$

where K_i is the half-saturation constant of the functional response to prey i , b_i is the volume-specific encounter rate of the predator with prey i , $\rho_{a,i}$ is the attack probability for prey i , and $[t_{\text{h},i}]$ is the volume-specific time required for handling prey i . These terms and their dependencies on the body sizes of both predator and prey, ℓ_{p} and ℓ_i , as well as on the prey-size preference of the predator, ℓ_{p} , are discussed below. In line with DEB theory, we base these relationships on general scaling principles involving the lengths ℓ , surface areas ℓ^2 , or volumes ℓ^3 of the involved organisms. As a result, the relations derived here are less detailed than the relations derived by, e.g., Aljetlawi et al. (2004); our assumption below of fixed scaling exponents also avoids problems with varying dimensions, and thus interpretations, of scaling coefficients.

Encounter rate b . The encounter rate b_i of a predator with a prey of size ℓ_i arises from encounters within the predator's search area. This search area is assumed to be proportional to the predator's surface area, $b \propto \ell_A^2$, as is the case, for instance, for sessile filter feeders that orient their arms perpendicular to the current. For filter feeders that generate their own current, the encounter rate equals the filter rate. Their flapping or beating frequency is observed to be independent of their size [28], such that the generated current is proportional to the surface area of their extremities, and thus again to their surface area. Other organisms may lay in ambush and capture prey that come within reach, i.e., within a distance that is proportional to the length of a leg or jaw or tongue, such that also here the encounter rate scales with surface area. Mobile organisms generally move with a speed proportional to their length: if the width of the path searched for food is proportional to length, this again leads to an encounter rate that scales with surface area. The encounter rate also scales with the surface area of the prey ℓ_i^2 , as the prey's visibility or detectability is assumed to be proportional to the prey cross-sectional area or silhouette. In summary, we assume $b_i \propto \ell_A^2 \ell_i^2$. Because the population dynamics above were expressed on a per-volume basis, b_i is divided by the volumes of predator and prey, leading to the following relationship,

$$b_i = b_0 \frac{\ell_{\text{ref}}^2}{\ell_A \ell_i}, \quad (5.7)$$

where the lengths are measured relative to a reference length ℓ_{ref} , so that the encounter rate coefficient b_0 , which controls the absolute value of the encounter rate, has the same dimensions as b_i . Without any loss of generality, reference lengths were taken as equal for predator and prey.

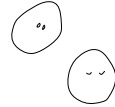
Attack probability ρ_a . The predator prey-size preference ℓ_p is assumed to evolve separately from the predator's adult body size ℓ_A and is not imposed by morphological constraints such as limited gape size. Even though such structural limits may exist, we assume here that they are adjusted to the prey-size preference, rather than vice versa. The probability ρ_a with which a predator attacks a prey of size ℓ_i is assumed to be log-normally distributed and depends on the prey-size preference ℓ_p and (dimensionless) niche width σ_p ,

$$\rho_{a,i} = \exp\left(-\frac{1}{2} \frac{\ln(\ell_i/\ell_p)^2}{\sigma_p^2}\right). \quad (5.8)$$

On encounter, a prey exactly of the preferred size ℓ_p will thus be attacked with certainty.

Handling time t_h . In general, the time required for handling each prey item comprises the time needed for capture and ingestion.

Ingestion is the process by which the prey is physically taken up into the body of the predator, passing through, for instance, its outer membrane or



its gut wall. First of all, ingestion time t_g is assumed to be proportional to the amount of prey biomass that has to be ingested, and thus, for one prey individual, proportional to the prey volume, $t_{g,i} \propto \ell_i^3$.

In addition, for *intraspecific* comparisons, DEB theory assumes the ingestion time to be inversely proportional to the surface area through which the intake occurs, and this surface area is assumed to scale with the total surface area ℓ_A^2 of the predator. For small individuals, which have a favorable ratio between surface-area and volume, the ingestion time will thus be small, while for larger individuals, it will be large. In this study, however, we assume all adult individuals of a population to have the same size, ℓ_A . For *interspecific* comparisons, DEB theory assumes ingestion rates to be proportional to maximum length, ℓ_{\max} , which implies that $t_g \propto \ell^{-1}$ m. Such a scaling may, for instance, be related to gut capacity (body plan) or diet composition of the predator.

Capture time is assumed to depend on the relative sizes of predator and prey. Larger prey require a longer capture time because they may be better protected, resisting more strongly, or have to be cut into chunks before being ingested. Specifically, we assume that the capture time increases faster with prey size than does the corresponding yield, which implies that it is proportional to size with an exponent larger than 3; as a default, here, we assume an exponent of 4, $t_c \propto (\ell_i/\ell_A)^4$.

The total handling time t_h equals the mean length of the handling process, consisting of capture and ingestion,

$$\begin{aligned} t_{h,i} &= t_{c,i} + \rho_s t_{g,i} \\ &= t_{c,0} \left(\frac{\ell_i}{\ell_A}\right)^4 + \rho_s \frac{t_{g,0}}{\ell_{\max}} \frac{\ell_i^3}{\ell_A^2}, \end{aligned} \quad (5.9)$$

where $t_{g,0}$ and $t_{c,0}$ are the ingestion and capture coefficients, and ρ_s is the fraction of attacked prey that is actually captured; only this fraction has to be ingested. As a default, all attacks are assumed to be successful, $\rho_s = 1$; the effects of reduced capture efficiencies are studied in Section 5.5.5.

Because adult size increases with maximum size, and since all adult organisms are assumed to possess adult size, ℓ_{\max} can be substituted with ℓ_A/α . The time $t_{h,i}$ that a predator needs for handling an individual of prey i can be converted into the volume-specific handling time $[t_{h,i}]$, which measures the time that a volume-unit of predator needs for handling a volume-unit of prey i , through multiplication with $(\ell_A/\ell_i)^3$,

$$[t_{h,i}] = [t_{c,0}] \frac{\ell_i}{\ell_A} + \rho_s \alpha [t_{g,0}]. \quad (5.10)$$

The total handling time $[t_h]$ given the actual prey-size availability is the sum of prey-size specific handling times $[t_{h,i}]$ weighted with the fraction θ_i of all attacks that are directed at prey i ,

$$[t_h] = \sum_{i=1}^n \theta_i [t_{h,i}], \quad \text{with } \theta_i = \frac{\rho_{a,i} b_i X_i}{\sum_{j=1}^n \rho_{a,j} b_j X_j}. \quad (5.11)$$

Finally, $[t_h]_{\text{ref}}$ (5.4a) is the absolute minimum, or reference, handling time, which equals $[t_{h,i}]$ at infinitely small prey-sizes, $[t_h]_{\text{ref}} = [t_{h,i}]|_{\ell_i=0} = \rho_s \alpha t_{g,0}$, and thus only depends on predator size.

5.2.5 Choice of units

The model presented above was scaled by maintenance rate k_M , energy conductance v , and incoming prey density coefficient $X_{r,0}$. Scaling renders the outcomes independent of these parameters. The unit of time, t , is chosen as k_M^{-1} , the unit of predator and prey length, L , is chosen as v/k_M , and the unit of reactor length, l , is chosen as $\sqrt[3]{X_{r,0}} k_M/v$; the latter unit, however, only features in the dimensions of biomass-volume densities, $L^3 l^{-3}$, which are made dimensionless simply through division by $X_{r,0}$.

The remaining variables and parameters, which then become dimensionless, are denoted by a tilde: for instance, the predator size ℓ_A (dim: L) was divided by v (dim: Lt^{-1}) and multiplied by k_M (dim: t^{-1}) so that the scaled length $\tilde{\ell}_A$ is dimensionless. The scaled predator and prey densities are indicated by x instead of X , e.g., $x_A = X_A/X_{r,0}$, and the scaled time t is indicated by τ . The default values of the scaled parameters are shown in Table 5.2. The scaled model can thus be written as follows,

$$\frac{dx_i}{d\tau} = (x_{r,i} - x_i)\tilde{D} - \tilde{I}_i f_i x_A(\tau), \quad (5.12a)$$

$$\frac{dx_A}{d\tau} = \tilde{R}(\tau - \tilde{a}_b) \exp(-\tilde{h}\tilde{a}_b) x_A(\tau - \tilde{a}_b) - \tilde{h}x_A(\tau). \quad (5.12b)$$

The scaled reproduction rate \tilde{R} is given by

$$\tilde{R}(\tau) = \frac{\tilde{h}}{\exp(\tilde{h}(g^+ + \hat{e}(\tau))(f(\tau)/\tilde{\ell}_A - g)^{-1}) - 1}, \quad (5.13)$$

where \tilde{D} and \tilde{h} are the scaled dilution and mortality rates and \tilde{a}_b is the scaled egg development rate, $\tilde{a}_b = 3\tilde{\ell}_A$. Furthermore, f is the functional response, g is the energy investment ratio, $g = \alpha/\tilde{\ell}_A$, g^+ is the difference in reserve density between the beginning and end of egg development, $g^+ = g + \frac{3}{4}\alpha$, and \hat{e} is the energy density of an egg. Note that f , g and \hat{e} already were dimensionless variables before, and are therefore not affected by any choice of units.

5.3 Methods

5.3.1 Ecological analysis

The coexistence set is the region in the trait space of the predator's body size $\tilde{\ell}_A$ and its prey-size preference $\tilde{\ell}_P$ in which the predator and prey populations can coexist, i.e., where $x_i^* > 0$ for $i = 1, \dots, n$ and $x_A^* > 0$ (here and below, a superscripted asterisk indicates a population dynamical equilibrium). At each



point of this trait space there also exists a boundary equilibrium, $x_A^* = 0$ and $x_i^* = x_{r,i}$ for $i = 1, \dots, n$, which is unstable for trait combinations within the coexistence set and stable for those outside. In other words, the boundary of the coexistence set is formed by trait combinations for which the boundary equilibrium changes stability.

To determine the coexistence set for the model introduced above, only one prey population was assumed to be available in the system. When the prey-size preference of the predator matches the one available prey size, $\tilde{\ell}_p = \tilde{\ell}_i$, the predator's niche width σ_p is not relevant and a point on the boundary of the coexistence set is given by $(\tilde{\ell}_A, \tilde{\ell}_p = \tilde{\ell}_i)$ for which $x_A^* = 0$ and $\tilde{R} \exp(-\tilde{h}\tilde{a}_b) = \tilde{h}$, with \tilde{R} in (5.13). The remaining points $(\tilde{\ell}_A, \tilde{\ell}_p \neq \tilde{\ell}_i)$ of the boundary of the coexistence set were then determined by numerically continuing this condition using standard continuation software.

5.3.2 Adaptive Dynamics theory

For the evolutionary analysis of our model we utilized adaptive dynamics theory, a general framework that helps analyze phenotypic evolution under frequency dependent selection [12, 13, 20, 38]. This approach assumes a time scale separation between the ecological and evolutionary dynamics, so that mutations in adaptive traits occur sufficiently rarely for the considered resident population always to be close to its population dynamical equilibrium when probed by a mutant. Mutants with a positive invasion fitness may replace the resident population. A series of such replacements leads to phenotypic change of the population. The directions and endpoints of phenotypic change depend on the invasion fitness-gradient and are calculated by means of the so-called canonical equation of Adaptive Dynamics [13]. Below we specify, in turn, these general notions for the model analyzed in this study.

Invasion fitness. The invasion fitness of a mutant is defined by its long-term per capita growth rate $r(\tilde{\ell}_m, E_r(\tilde{\ell}_r))$ while being rare in the environment E_r set by the resident population at its ecological equilibrium. Here, $\tilde{\ell}$ is the vector of the predator's adaptive traits $\tilde{\ell} = (\tilde{\ell}_A, \tilde{\ell}_p)$ and the subscripts 'r' and 'm' indicate resident and mutant trait values, respectively. To calculate the invasion fitness of the mutant we extend Equations (5.12a) by including the dynamics of the mutant predator,

$$\frac{dx_{A,m}}{d\tau} = \tilde{R}_m(\tau - \tilde{a}_{b,m}) \exp(-\tilde{h}_m \tilde{a}_{b,m}) x_{A,m}(\tau - \tilde{a}_b) - \tilde{h}_m x_{A,m}(\tau). \quad (5.14)$$

Introducing a mutant in the system also requires a feeding term to be added to Equation (5.12a), as shown in Equation (5.21a).

As explained in detail in the appendix, the invasion fitness of the mutant is thus given by

$$s(\tilde{\ell}_m, \tilde{\ell}_r) = \tilde{R}_m(\exp(-3\tilde{h}\tilde{\ell}_{A,m}) - \tilde{h}), \quad (5.15)$$

where \tilde{R}_m is the mutant's reproduction rate,

$$\tilde{R}_m = \frac{\tilde{h}}{\exp(\tilde{h}(g_m^+ + \hat{e}_m)/(f_m/\tilde{\ell}_{A,m} - g_m)) - 1}. \quad (5.16)$$

Here the functional response f_m of the mutant depends on the adaptive traits of both mutant and resident, because the resident predator sets the environment E_r and thus determines the equilibrium prey density in the system.

Selection gradient. The expected direction of phenotypic change is proportional to the selection gradient, i.e., to the derivative of invasion fitness with respect to the adaptive traits of the mutant, evaluated at the trait values of the resident. For a monomorphic resident population, this selection gradient is denoted by

$$\nabla_m s(\tilde{\ell}_m, \tilde{\ell}_r) = \left(\frac{\partial}{\partial \tilde{\ell}_{A,m}} s(\tilde{\ell}_m, \tilde{\ell}_r), \frac{\partial}{\partial \tilde{\ell}_{P,m}} s(\tilde{\ell}_m, \tilde{\ell}_r) \right) \Big|_{\tilde{\ell}_m = \tilde{\ell}_r}. \quad (5.17)$$

Canonical equation. A deterministic approximation of the stochastic evolutionary trajectories of body size and prey-size preference, jointly driven by mutation and selection, is provided by the canonical equation of adaptive dynamics [13], which for our system is given by

$$\frac{d\tilde{\ell}_r}{dt} = \rho(\tilde{\ell}_r) \frac{x_{A,r}^*}{\tilde{\ell}_{A,r}^3} \nabla_m s(\tilde{\ell}_m, \tilde{\ell}_r). \quad (5.18)$$

Here ρ is a rate factor that depends on the fraction of mutations per birth, on the coefficient of variation in the distribution of offspring numbers, on the mean size of mutational steps, and on the multiplier that transforms $x_{A,r}^*/\tilde{\ell}_{A,r}^3$ into the abundance of resident predators. The precise value of ρ is irrelevant for this study as we are only interested in evolutionary equilibria, and not in the timing of the trajectories leading towards them.

Evolutionary outcomes. Eventually, the population will reach a combination of trait values $\tilde{\ell}_r$ at which the selection gradient vanishes,

$$\nabla_m s(\tilde{\ell}_m, \tilde{\ell}_r) = 0. \quad (5.19)$$

Such an evolutionary equilibrium may be either stable or unstable according to Equation (6.7). An evolutionary equilibrium may also be situated at a fitness maximum, a fitness minimum, or a fitness saddle according to Equation (6.5). In the latter cases, the evolutionary equilibrium is not locally evolutionarily stable, so that the resident population may split up and evolve into two or more subpopulations through a process known as evolutionary branching [19, 20, 37, 38].



5.3.3 Evolutionary analysis

Single-trait evolution. As a preparatory step in the evolutionary analysis of our model, only the predator's body size was allowed to evolve, while its prey-size preference was fixed. In this case, the evolutionary dynamics are reduced to the single trait $\tilde{\ell}_A$. For this purpose we assumed, like in the ecological analysis, that only a single prey population existed and that the predator's prey-size preference matched this prey size, $\tilde{\ell}_P = \tilde{\ell}_i$. The evolutionary outcome in $\tilde{\ell}_A$ was then found numerically by integrating the dynamics of $\tilde{\ell}_A$ according to the canonical equation of adaptive dynamics, Equation (6.7), while keeping $\tilde{\ell}_P$ fixed, until an evolutionary equilibrium was reached. This evolutionary equilibrium was determined for a range of prey-size preferences within the coexistence region.

Two-trait evolution. The full evolutionary dynamics were studied by allowing the two adaptive traits of the predator to evolve jointly. In this case, a range of prey sizes was assumed to be available to the predator according to Equation (5.5). The evolutionary equilibrium was again found numerically, by solving Equation (6.8).

Evolutionary branching. To study the evolutionary process after an evolutionary equilibrium had been reached, an extended numerical analysis was carried out. This analysis consisted of integrating Equation (6.7) until reaching an evolutionary equilibrium. If this equilibrium was evolutionarily unstable, i.e., if it corresponded to a fitness minimum, the original predator population was equally split into two predator populations and the two corresponding canonical equations were considered further. The trait values of the two predator populations were chosen to deviate slightly from that of their ancestor in the two (opposite) directions of highest fitness increase around the ancestral combination of trait values. The two canonical equations were integrated, and new predator populations were added analogously if applicable, until an evolutionarily stable evolutionary equilibrium was reached, corresponding to a fitness maximum in all introduced predator populations. Due to the deterministic nature of the adaptive dynamics, more than one predator population may branch at the same time.

Mutual predation. Finally, to explore the effects of predation among predators, the functional response f was calculated as the sum of partial functional responses f_i , where i now consisted of all prey populations ($1, \dots, n$) as well as of all predator populations ($1, \dots, p$),

$$f = \sum_{i=1}^{n+p} f_i. \quad (5.20)$$

Stochastic evolution. As a further robustness test, we used a stochastic simulation process instead of the deterministic dynamics in Equation (6.8). For this purpose, we integrated the ecological dynamics of the system for 10^4 time steps, followed by the addition of a new mutant predator population to the system. The trait values of the mutant were drawn at random from a normal distribution around the trait values of its ancestor with a standard deviation of 10^{-3} . The initial biomass of the mutant population was set to a very small value, $x_{A,m} = 10^{-20}$, which was also the cutoff biomass density below which a population was assumed to go extinct. In the case of extinction, the affected population was removed from the system.

5.4 Results

5.4.1 Ecological analysis

We start by studying which predator-prey size combinations can coexist. These combinations are referred to as ‘feasible’ and shown in Figure 5.1. For this analysis, the predator’s prey-size preference equals the single available prey size assumed to be available, $\tilde{\ell}_p = \tilde{\ell}_i$. Figure 5.1 can be interpreted in two ways: vertically, as the feasible range of predator body sizes for a given prey size (illustrated by arrow 1), and horizontally, as the feasible range of prey-size preferences for a given predator body size (illustrated by arrow 2).

We separately determined the coexistence set for two different functional responses. First, only the basic handling processes of encountering and ingesting prey were assumed to play a role in the functional response of the predator ($[\tilde{t}_{c,0}] = 0$, for other parameter values, see Table 5.2). In this case, Figure 5.1 shows that the maximum feasible predator body size is inversely related to the maximum feasible prey size (dashed line). Second, the model was extended by including a capture time that depends on the predator-prey size ratio. Now, large predator-prey size ratios are no longer feasible, and the boundary of the coexistence set become curvilinear (continuous curve).

Figure 5.2 shows a set of empirically observed combinations of predator-prey sizes that were presented by Cohen et al. [9], together with the coexistence set of our model based on a size-ratio-dependent capture time (continuous curve). The empirical data set consists of 478 size combinations from 30 food webs. In the doubly logarithmic plot, these are distributed over a triangular area that is bounded above by a maximum predator size, bounded below by the equality of predator and prey sizes, and bounded on the left by the minimum prey size. The coexistence sets in Figures 5.1 and 5.2 (continuous curves) are identical, but in Figure 5.2 the axes are translated back from dimensionless variables into lengths expressed in centimeters. For the two relevant scaling parameters, k_M and v , reasonable values were chosen that lie well within the range of empirically observed values ($k_M = 1.44 \text{ d}^{-1}$, $v = 0.3 \text{ cm d}^{-1}$ [28]); the dilution rate was adjusted ($\tilde{D} = 0.05$) so as to obtain a slightly better fit for the upper boundary of the coexistence set.

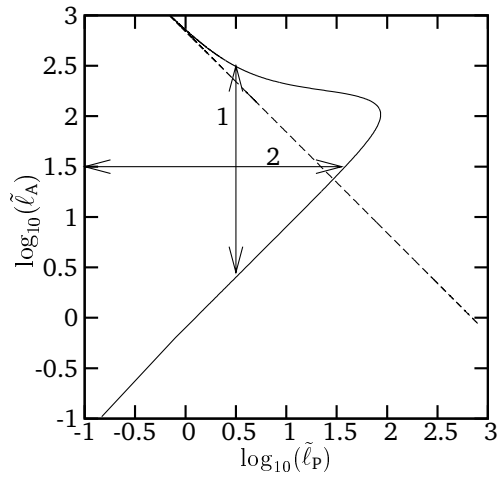


Figure 5.1: Coexistence set of the investigated predator-prey system. Combinations of scaled predator body size $\tilde{\ell}_A$ (vertical) and prey-size preference $\tilde{\ell}_P$ (horizontal) are shown logarithmically, assuming that the preferred prey size equals the one available prey size ($\tilde{\ell}_P = \tilde{\ell}_i$). The dashed curve depicts the boundary of this coexistence set when only ingestion and encounter times are considered, while the continuous curve shows this boundary when capture times are considered as well. The two arrows indicate the graph's two possible interpretations: (1) the feasible range of predator body sizes for a given prey size, and (2) the feasible range of prey-size preferences for a given predator size.

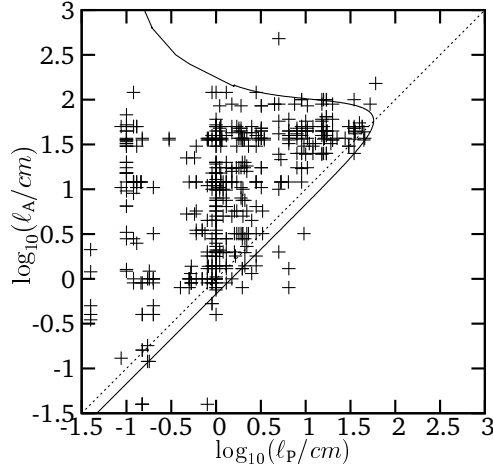


Figure 5.2: Comparison of the coexistence set predicted by our model (continuous curve) with empirical data presented by Cohen et al. [9]. The logarithm of the length of the predator is plotted against the logarithm of the length of the prey, with both lengths being expressed in centimeters. Along the dotted line, body sizes of prey and predator are equal. The dimensionless variables $\tilde{\ell}_A$ and $\tilde{\ell}_P$ were translated back into lengths using the two relevant scaling parameters, $k_M = 1.44 \text{ d}^{-1}$ and $v = 0.3 \text{ cm d}^{-1}$; the dilution rate was set to $\tilde{D} = 0.05$.

5.4.2 Evolutionary analysis

After having established which combinations of a predator's body size and its prey-size preference are ecologically feasible, we also studied the evolutionary dynamics of these adaptive traits. Figure 5.3 again shows the coexistence set (continuous curve) and the diagonal along which predator size and prey-size preference are equal (dotted line). The dashed line shows the body size to which the predator will evolve when feeding on a prey of a given size. In other words, it shows how the evolutionary equilibrium depends on prey size. This line results from single-trait evolution in ℓ_A , and applies when only one prey size is available and $\tilde{\ell}_P = \tilde{\ell}_i$. The figure shows that the evolved predator size is positively correlated with prey size, and that the slope of the correlation line is equal to unity.

When, instead of one prey size, a range of prey sizes is available simultaneously to the predator, as described in Section 5.2.3, and both traits are allowed to jointly evolve, the predator population evolves to an evolutionary equilibrium within the coexistence set, which in Figure 5.3 is denoted by an asterisk.

However, after this evolutionary equilibrium is reached, evolution continues. Since the evolutionary equilibrium does not correspond to an evolutionarily stable fitness maximum, the originally monomorphic predator population

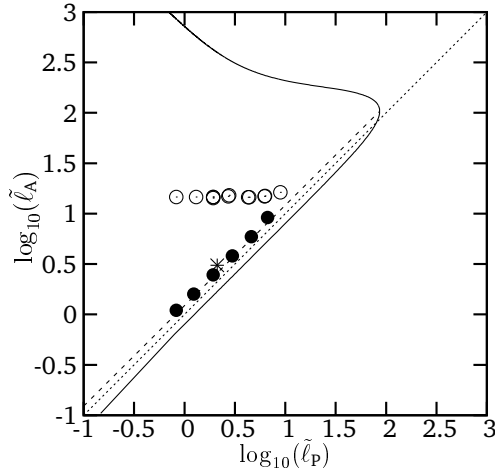
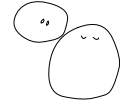


Figure 5.3: Evolutionary outcomes of scaled predator body size $\tilde{\ell}_A$ and prey-size preference $\tilde{\ell}_P$. The continuous curve depicts the boundary of the coexistence set, while the dotted line depicts the diagonal along which predator size and prey-size preference are equal. The dashed line shows the outcome of single-trait predator evolution in $\tilde{\ell}_A$, for a single prey size, with $\tilde{\ell}_P = \tilde{\ell}_i$. The asterisk indicates the initial evolutionary equilibrium (and primary evolutionary branching point) of two-trait evolution in the predator when considering a range of available prey sizes. The filled circles show the composition of the predator community after evolutionary branching (deterministic evolution), while the open circles depict this composition when predation among predators was also taken into account (stochastic evolution).

splits up into two populations and thus becomes dimorphic. This process of evolutionary branching is repeated several times, such that the predator population cascades into a range of populations with different trait combinations, until an evolutionarily stable predator community is eventually reached. In Figure 5.3 the trait combinations realized in this evolved community are shown by filled circles.

Inclusion of predation among predators also leads to sequential evolutionary branching. The trait combinations resulting under stochastic evolution after 5000 mutations are shown in as open circles in Figure 5.3; at this point in time the system is close to an evolutionarily stable equilibrium. The slightly irregular spacing of the realized trait combinations reflects the stochastic nature of the evolutionary process.

Figure 5.4 (pg. 115) shows how the predator's body size and prey-size preference at the initial evolutionary equilibrium (i.e., before evolutionary branching) are affected by the availability of prey sizes. Specifically, the three panels show how the predator's adaptive traits vary with three features of the prey: the mean $\tilde{\mu}$ and standard deviation σ of the prey-size distribution, and the

prey's dilution rate \tilde{D} . Analogously, Figure 5.5 (pg. 116) shows the variation of the predator's adaptive traits with two features of the predator: its niche width σ and its probability ρ_s of successfully capturing an attacked prey.

5.5 Discussion

In the first two subsections below we discuss the results of our ecological analysis, followed by three subsections of discussion on the results of our evolutionary analysis.

5.5.1 True predators versus parasitic predators

When taking into account only the basic handling processes of encountering and ingesting of prey, small predator-prey size ratios are feasible (Figure 5.1, dashed line). Clearly, this does not agree with the distribution of empirically observed predator-prey sizes shown in Figure 5.2. However, small size ratios are typically found in parasite-host systems [36], which were not included in the empirical dataset of Cohen et al. (1993). Parasites are organisms that obtain their nutrients from one or very few host individuals, causing harm but no (immediate) death. True predators, in contrast, continuously require new prey individuals, which are killed at attack or quickly thereafter. Because parasites do not have to overpower their prey, capture times may be neglected. Under these circumstances, our model predicts that small predator-prey size ratios are feasible, in qualitative agreement with empirical data.

The transition between parasites and true predators, however, is gradual. This is illustrated by the typical classification of a bird-egg eating snake as a predator, while the sea-cucumber-egg eating pearlfish is classified as a parasite. Examples of the wide range of parasitic relationships are discussed in [10]. Whatever classification rules are defined, many exceptions can be found, pointing to the fact that these boundaries are essentially artificial. DEB theory assumes that predators and parasites are basically of the same kind, and thus that they can be described by the same model; their differences in physiology only require different parameter values. The differences in these parameter values, however, may lead to considerable, even qualitative, differences in the feasibility of predator-prey size combinations. In the results of our model, this is reflected by the qualitative change in the shape of the coexistence set when capture times are considered (Figure 5.1, continuous curve). In this case, the coexistence set is shrunk and it is no longer feasible for small predators to feed on large prey.

Hence, by adjusting capture times in our model (e.g., by varying the capture time coefficient), we can account for both parasites and true predators. Similarly, by adjusting other parameter values, our model may also be expected to account for other types of predators, such as grazers or parasitoids. As a default, however, we considered a capture time coefficient that is relatively large, so that the model corresponds mainly to true predators.



5.5.2 Imperfect upper triangularity

When including in our model a capture time that depends on the predator-prey size ratio, the feasible set becomes triangularly shaped (Figure 5.1, continuous curve), which matches the empirical distribution of observed predator-prey size combinations presented by Cohen et al. [9] (Figure 5.2). This so-called ‘upper triangularity’ is often found in real food webs [7, 9, 47]. The term stems from considering a food web’s matrix of trophic interaction coefficients, in which species are arranged in hierarchical order, such that all of the non-zero matrix elements lie above the main diagonal. In the present study, the emergence of upper triangularity implies that larger predators can feed on a wider range of prey sizes and that for smaller prey sizes, the feasible range of predator sizes is wider. It also implies that a given species essentially does not eat other species that are larger than itself, which suggests a body-size-based hierarchy. Body size has been suggested previously to provide a mechanistic interpretation for the hierarchy assumption in the cascade model [8], both by Warren and Lawton [47] and by Cohen [6]. However, in our analysis we did not postulate a size hierarchy as such: instead, this hierarchy naturally results from the scaling relations and size-dependent functional response suggested by DEB theory, and in particular from the considered proportionality of capture time to predator-prey size ratio.

The value of the capture time coefficient $[\tilde{t}_{c,0}]$ considerably affects the shape of the coexistence set. Yet, when plotted on a doubly logarithmic scale, different values of $[\tilde{t}_{c,0}]$ all result in a lower boundary of the coexistence set given by a straight line with slope one, corresponding to a fixed predator-prey size ratio. Although these lines have different intercepts, they lie rather close to each other and to the main diagonal for a relatively large range of values for $[\tilde{t}_{c,0}]$, especially when large predator and prey size ranges are considered. This finding would explain why, across many natural systems, the distribution of body size combinations involved in predator-prey links seems to be essentially the same.

Although the predicted boundaries of the coexistence set fit the empirical data reasonably, the fit is not perfect. For example, part of the predicted curvilinear upper boundary of the coexistence set, corresponding to combinations of small prey sizes with large predator sizes, is not observed in the considered empirical dataset. Instead, the upper boundary in the empirical dataset may be described simply by the body size of predators maxing out at about 150 cm to 200 cm. In the model, this curvilinear upper boundary is mainly determined by the encounter rate between predator and prey being proportional to the prey’s surface area. Apparently, in natural systems, this is not realistic for large predators in combination with small prey. Probably, at these size ratios, the prey is not detected by vision, and the detectability may not be proportional to a prey’s silhouette. This implies that the model’s fit in this range of size combinations could be improved by including additional mechanisms. However, we chose to keep our model simple and to stay in line with DEB theory by including as few additional assumptions as possible.

An interesting property of the model is that the predicted lower boundary of the predicted coexistence set (Figure 5.2, continuous curve) does not coincide with the diagonal along which predator and prey sizes are equal (dotted line), but instead lies below it (as discussed above, the exact location of this lower boundary depends on parameter values, and especially on the capture time coefficient $[\tilde{t}_{c,0}]$). The coexistence set thus extends to predators feeding on prey individuals that are larger than themselves.

Cohen et al. [9] found that, in their dataset, approximately 10% of all predators fed on larger prey. Empirical studies have demonstrated this effect also for other natural food webs. Because of these consistent observations, the simple cascade model [8] has been extended, resulting in the more general niche model [48], which is viewed as providing better matches with empirical food web data [7, 39, 47]. The proposed explanations are all based on the assumption that a certain hierarchy exists, but that the measures or variables used to characterize it may be imperfect. In contrast, the size-ratio-dependent capture time assumed in our model provides a mechanism that naturally explains a body-size-based hierarchy while also allowing for ‘exceptional’ predator-prey links. This result suggests that not the measures or the variables, but rather the hierarchy itself is imperfect.

5.5.3 Evolution under increased levels of ecological realism

Our approach allows us to study and disentangle the evolutionary effects caused by the successive incorporation into our model of increased levels of ecological realism. Five such steps have been taken. First, we started out from a system in which a single predator adapts to a single prey. Second, we investigated the joint evolution of the body size and prey-size preference of a single predator confronted with a range of prey sizes. Third, we considered the adaptive radiation of predator types caused by resource competition. Fourth, we included trophic interactions among predators to examine their effects on the outcomes of predator radiation. Fifth, we included evolutionary stochasticity in our model, to corroborate the robustness of our deterministic predictions.

Figure 5.3 shows that when a single predator adapts to a single prey, predator body size is positively correlated with prey body size, with a slope equal to 1. This implies that the predators evolve to a fixed predator-prey size ratio that is constant across predator sizes. A positive correlation between body sizes of predator and prey is indeed found in vertebrates [21, 46] and invertebrates [47], as well as in planktonic predators [22]. Even though these studies underscore that a general and fixed size ratio does not exist, they do find a constant size ratio within each trophic or taxonomic group.

When, instead of one prey size, a range of prey sizes is available simultaneously to the predator, and the body size and prey-size preference of a single predator evolve jointly, the size ratio at the resultant evolutionary equilibrium (asterisk in Figure 5.3) is slightly different than that resulting from single-trait evolution (dashed line in Figure 5.3). This is because now a range of prey sizes



is available, so that the predator's niche width comes to play a role. The effects of varying this niche width are discussed in detail in Section 5.5.5.

Were the range of prey sizes not bounded, the predators would evolve towards ever smaller body sizes. This is inherent to their physiology, which favors small sizes over large ones: large organisms have relatively more energy reserves, and therefore a relatively longer egg-production period, which negatively affects their reproduction rate. Also, smaller organisms have a relatively large surface area, which is favorable with respect to the encounter and ingestion rates that both scale with surface area. Apparently, many physiological mechanisms favor a smaller size. Two factors that, by contrast, may induce evolution towards larger body sizes are heat loss and environmental variability. The tendency of organisms living at high latitudes to evolve to large body sizes has become known as Bergmann's rule [3, 33, 34], and is often ascribed to the favorable effects of lower surface-area-to-volume ratios on heat loss. Environmental variability, on the other hand, implies periods of starvation for which a large body size is favorable, as larger organisms have larger energy reserves. These two factors, however, were not considered in the present study.

Figure 5.3 (filled circles) shows the trait combinations of the predator populations that will eventually result from deterministic evolution when adaptive radiations are considered. The mechanism underlying the evolutionary branching events is competition for resources, which leads to disruptive selection. The evolutionary branching process affects both adaptive traits: under the force of disruptive selection, some populations evolve towards smaller body sizes *and* smaller prey-size preferences, while others evolve to larger body sizes *and* larger prey-size preferences. When they are isolated, each of the populations (filled circles) will again evolve towards the first evolutionary equilibrium (asterisk). This may correspond to evolutionary processes on some islands, where small mammal species have been observed to evolve to a larger size and larger species to a smaller size. Such a tendency has become known as the 'island rule' [45], and can thus be understood by the evolutionary dynamics in our model. Figure 5.3 also shows that all resulting populations retain the same predator-prey size ratio. From this it can be concluded that competition for resources may lead to the differentiation of predator body sizes and prey-size preferences, but not to a differentiation of predator-prey size ratios.

In determining these evolutionary outcomes, direct interactions among predators, either through predation or through interference competition, were not taken into account. Therefore, these outcomes clearly correspond to idealized conditions. Real organisms may only conform to the resultant predictions in situations in which competition and predation among predators are naturally absent, such as on (small) islands.

Predation among predators or direct (interference) competition, on the other hand, may give an additional advantage to large body sizes: larger organisms can be preyed upon by a smaller range of predators and are thus less vulnerable to predation (as follows from the triangular distribution of empirical predator-prey combinations), and they may also have an advantage in the direct competition for food or territory. As such, these processes may be expec-

ted to cause organisms to depart from the predator-prey size ratios predicted above.

Figure 5.3 (open circles) shows that predation among predators does indeed lead to much larger predator-prey size ratios than would be expected on the basis of resource competition alone. Predation among predators may thus indeed be an important factor for explaining the large variation of predator-prey size ratios found in nature. Direct (interference) competition is expected to have a similar effect as predation among predators. Both factors help explain Cope's rule [2, 11], which states that natural selection will tend to produce large-bodied species.

Predictions of deterministic and stochastic renderings of the evolutionary dynamics in our model agree almost completely, even though the stochastic dynamics expectedly induce a slight amount of jitter in the evolved predator populations (open circles in Figure 5.3).

5.5.4 Evolutionary effects of environmental factors

Figures 5.4a and 5.4b show how the outcomes of evolution in predator body size and prey-size preference are affected by the availability of prey sizes. An increase in the mean $\tilde{\mu}$ of the prey-size distribution causes both traits to increase (Figure 5.4a), while the response to variations in the standard deviation σ of the prey-size distribution turns out to be hump-shaped (Figure 5.4b). Although the evolved values of the scaled predator body size $\tilde{\ell}_A$ and prey-size preference $\tilde{\ell}_p$ change, their ratio remains essentially constant across a large range of the studied parameter values. Changes in the prey-size distribution, expressed in terms of $\tilde{\mu}$ and σ , may thus induce shifts in predator body sizes and prey-size preferences, but cannot explain the variation observed in predator-prey size ratios.

In contrast, an increase in dilution rate does change the evolved size ratio by making it larger. The evolved body size of predators is affected by the dilution rate through changes food abundance: smaller dilution rates reduce both the rate at which new prey enter the system and the mortality of predators, thus intensifying conspecific competition for resources. The resulting decrease in evolved predator body size may correspond to the tendency to dwarfism on islands, which also has been related to limited food resources [5].

5.5.5 Evolutionary effects of feeding modes

Ecological factors, such as the predator's feeding mode, may also affect the evolutionary outcomes of predator body size and prey-size preference. In particular, a difference between the predator-prey size ratio of filter feeders and raptorial feeders is seen across taxonomic groups. Hansen et al. [22] found that the optimal size ratio of filter feeders is larger than that of raptorial feeders. They also found that filter feeders generally feed on a larger range of prey sizes than raptorial feeders. To examine whether the wider prey range can explain

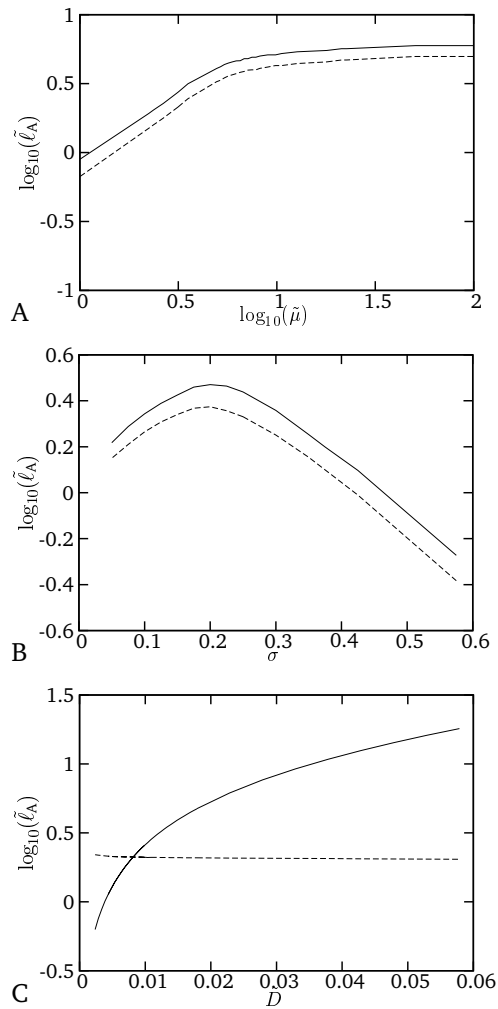


Figure 5.4: Effects of environmental parameters on the evolutionary outcomes of scaled predator body size ℓ_A (continuous curve) and prey-size preference $\tilde{\ell}_P$ (dashed curve). The three panels show the evolutionary equilibrium values (a) for a range of means of the available prey-size distribution $\tilde{\mu}$, (b) for a range of standard deviations of this distribution σ , and (c) for a range of dilution rates \tilde{D} .

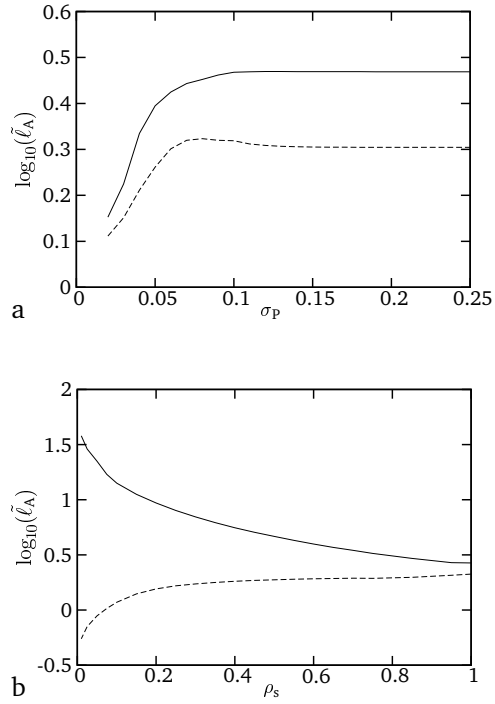
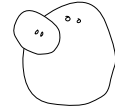


Figure 5.5: Effects of ecological parameters on the evolutionary outcome of scaled predator body size \tilde{l}_A (continuous curve) and prey-size preference \tilde{l}_p (dashed curve). The two panels show the evolutionary equilibrium values (a) for a range of niche widths σ_p and (b) for a range of capture efficiencies ρ_s .



the differences in size ratios, we studied the evolutionary effects of varying the niche width σ_p of the predator. Figure 5.5a shows that the predator-prey size ratio first increases with niche width and then stabilizes. As the niche width goes to zero, the predator evolves towards a preference for the smallest prey size that is still available. In this case, the predator-prey size ratio becomes equal to the size ratio that was predicted from single-trait evolution; this is expected, as in that analysis the predator was assumed to feed on one prey size only, which corresponds to vanishing niche width.

Although raptorial feeders may be more size-selective, it is conceivable that they are also more efficient predators, with a larger fraction of their attacks being successful. Therefore, we also studied the evolutionary effects of varying the capture efficiency ρ_s . Figure 5.5b shows that when a predator is less successful, its body size will become larger, while its prey-size preference will become smaller. Successful predators will thus evolve towards smaller predator-prey size ratios. Combining a large niche width with a small capture efficiency will lead to an even stronger increase in predator-prey size ratio, which may explain the large size ratio often encountered in filter feeders. These mechanisms might also provide an explanation for the tendency of the predator-prey size ratio to decrease with trophic level [7], as predators at higher trophic levels may more often be raptorial feeders than filter feeders.

5.6 Conclusions

A size-dependent functional response was developed and combined with body-size scaling relationships from DEB theory to establish a physiologically motivated eco-evolutionary model of adaptations in the body sizes and prey-size preferences of predators. To obtain a realistic coexistence set for feasible predator-prey size combinations, we included capture times that depend on predator-prey size ratios. The resulting model exhibits many features, both ecological and evolutionary, that match empirical observations, such as the triangular distribution of predator-prey size combinations, the island rule, dwarfing, and the difference in predator-prey size ratio between filter feeders and raptorial feeders.

The coexistence set predicted by our model accommodates a wide range of predator-prey size ratios. By contrast, the evolutionary outcomes in the simplest versions of our model, in which a single predator adapts either to a single prey or to a range of prey, imply a fixed predator-prey size ratio. Even though such a fixed size ratio often exists within trophic and taxonomic groups, it certainly does not apply across these groups. We therefore introduced and examined various factors that help explain variation in predator-prey size ratios. These factors can be organized into three different classes (Figure 5.6).

First, some factors may change the size ratio predicted for single-predator adaptation (Figure 5.6a). Therefore, these factors can have a large impact on observed patterns of predator-prey size combinations. Examples include changes in physiology and feeding mode, but also changes in the harshness of

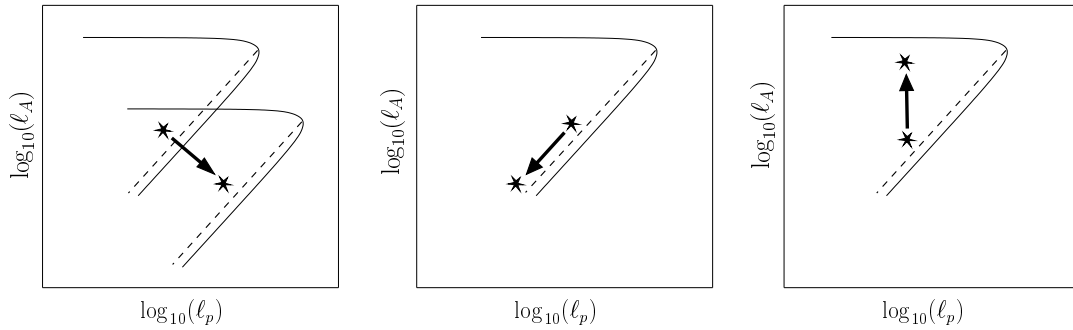


Figure 5.6: Three different types of change in evolved predator-prey patterns. Continuous curves delineate the boundaries of the coexistence set, dashed lines show the outcomes of single-trait evolution, and asterisks indicate the evolutionary outcome of two-trait predator evolution when a range of prey types is present. Arrows depict changes in the predator's two adaptive traits \tilde{l}_A (vertical) and prey-size preference \tilde{l}_p (horizontal): (a) the expected outcome of evolution in predator body size and predator-prey size ratio is changed, together with the coexistence set; (b) predator body size evolves, while the size ratio remains the same; (c) the predator evolves away from the body size and size ratio predicted by single-trait predator evolution.

the environment (dilution rate). Within taxonomic or trophic groups, organisms often possess a relatively similar physiology, which may therefore explain the constant size-ratio that is observed within such groups. It should be noted that factors in this class, in contrast to those listed further below, may also affect the boundaries of the coexistence set. Yet, on the logarithmic scale used in Figures 5.1 to 5.3, the resultant lower boundaries of the coexistence set lie close to each other for a relatively large range of parameter values.

Second, there are factors that cause predators to change their body size and prey-size preference without changing their predator-prey size ratio (Figure 5.6b). These include, for example, changes in the range of available prey sizes. Also, the patterns of size combinations resulting from resource competition conform to a fixed predator-prey size ratio. In addition, our analysis has demonstrated that competition for resources induces differentiation, rather than mere shifts, in predator body sizes and prey-size preferences. Changes in available range in prey sizes and resource competition may thus explain the range of predator body sizes and prey-size preferences observed in nature, but cannot explain the large variation in predator-prey size ratios.

Third, some factors may systematically induce organisms to depart from the predator-prey size ratio predicted for single-prey-single-predator adaptation (Figure 5.6c). We have found that predation among predators, as well as



interference competition, can cause this effect, by giving an additional advantage to large body sizes. As such, these processes may provide an explanation for the tendency of natural selection to produce large-bodied species (Cope's rule). Factors from this third class also help us understand the diversity of predator-prey size ratios encountered in nature.

Distinguishing which of these types of processes is causing the variation in specific empirical predator-prey size combinations will not be easy. Several parameters and processes have similar, or compensatory, effects that are difficult to separate, even in experiments. For example, in most cases it will be problematic to assess the evolutionary outcome of single-prey-single-predator adaptation. This is because the organism will usually have adapted evolutionarily to its specific environment, which typically includes predation and competition. These limitations should be taken into account when trying to explain empirical predator-prey patterns, or when measuring predator-prey size ratios in experimental setups.

Appendix: Derivation of invasion fitness

In this appendix we show that for determining the coexistence set and the invasion fitness of the DDE system (5.12) one can use an ODE formulation without delay. For this purpose, below we first derive the invasion fitness of a mutant predator trying to invade a given resident population of predators.

We start from DDE system (5.12), consisting of a prey population x_1 and a resident predator population $x_{A,r}$, and introduce a mutant predator population $x_{A,m}$, according to Equation (5.14). For the sake of clarity, we consider only a single prey population and leave out the tildes that denote scaled parameters in the main text. The resulting system is given by

$$\frac{dx_1}{dt} = (x_{r,1} - x_1(t))D - I_{1,r}f_{1,r}(t)x_{A,r}(t) - I_{1,m}f_{1,m}(t)x_{A,m}(t), \quad (5.21a)$$

$$\frac{dx_{A,r}}{dt} = \exp(-ha_{b,r})R_r(t - a_{b,r})x_{A,r}(t - a_{b,r}) - hx_{A,r}(t), \quad (5.21b)$$

$$\frac{dx_{A,m}}{dt} = \exp(-ha_{b,m})R_m(t - a_{b,m})x_{A,m}(t - a_{b,m}) - hx_{A,m}(t), \quad (5.21c)$$

where $I_{1,x} = 1/t_h(\tilde{\ell}_x)$, with $x = r,m$.

The subsequent analysis can be outlined as follows. In order to derive the mutant's invasion fitness, we study the stability of the resident after the mutant has been introduced. We assume that there is a stable resident equilibrium when the mutant is absent. The full system above is then linearized around this equilibrium, and the characteristic equation of the resultant linear system is analyzed. When the real parts of all roots of this equation are negative, the resident is stable and the mutant cannot invade. By contrast, when the dominant root is positive, the resident is unstable and the mutant can invade. In particular, we will determine the combinations of trait values at which this stability changes.

Below, a superscripted asterisk indicates that the considered variable is at equilibrium under constant environmental conditions. We now introduce new variables that denote displacements from this equilibrium,

$$\xi_1 = x_1 - x_1^*, \quad (5.22a)$$

$$\xi_{A,r} = x_{A,r} - x_{A,r}^*, \quad (5.22b)$$

$$\xi_{A,m} = x_{A,m} - x_{A,m}^*. \quad (5.22c)$$

The linearized model at equilibrium then reads

$$\begin{aligned} \frac{d\xi_1}{dt} = & -\xi_1(t)D - I_{1,r}(\xi_1(t))\frac{df_{1,r}}{dx_1}(x_1^*)x_{A,r}^* + f_{1,r}(x_1^*)\xi_{A,r}(t) \\ & - I_{1,m}(\xi_1(t))\frac{df_{1,m}}{dx_1}(x_1^*)x_{A,m}^* + f_{1,m}(x_1^*)\xi_{A,m}(t), \end{aligned} \quad (5.23a)$$

$$\frac{d\xi_{A,r}}{dt} = \exp(-ha_{b,r})(\xi_1(t - a_{b,r}))\frac{dR_r}{dx_1}(x_1^*)x_{A,r}^* + R_r(x_1^*)\xi_{A,r}(t - a_{b,r}) - h\xi_{A,r}(t), \quad (5.23b)$$

$$\frac{d\xi_{A,m}}{dt} = \exp(-ha_{b,m})(\xi_1(t - a_{b,m}))\frac{dR_m}{dx_1}(x_1^*)x_{A,m}^* + R_m(x_1^*)\xi_{A,m}(t - a_{b,m}) - h\xi_{A,m}(t). \quad (5.23c)$$

In the following we use the shorthand notations $R_r^* = R_r(x_1^*)$ and $R_m^* = R_m(x_1^*)$.

Since we are interested in the invasion by a rare mutant predator population, we take $x_{A,m}^* = 0$. Then the matrix \mathcal{P} , defined by

$$\mathcal{P} \begin{pmatrix} \xi_1 \\ \xi_{A,r} \\ \xi_{A,m} \end{pmatrix} = \begin{pmatrix} 0 \\ 0 \\ 0 \end{pmatrix} \quad (5.24)$$

in conjunction with Equations 5.23, is obtained by substituting ξ_i in Equations (5.23) by $\zeta_i \exp(\lambda t)$, $i = 1(A, r), (A, m)$ and division by $\exp(\lambda t) > 0$,

$$\mathcal{P} = \begin{pmatrix} \mathcal{J}_1 & -I_{1,m}f_{1,m}(x_1^*) \\ 0 & 0 \\ 0 & \mathcal{J}_2 \end{pmatrix}. \quad (5.25a)$$

The 2×2 matrix \mathcal{J}_1 is given by

$$\mathcal{J}_1 = \begin{pmatrix} -(\lambda + h) - I_{1,r}\frac{df_r}{dx_1}(x_1^*)x_{A,r}^* & -I_{1,r}f_{1,r}(x_1^*) \\ \exp(-(\lambda + h)a_{b,r})\frac{dR_r}{dx_1}(x_1^*)x_{A,r}^* & -(\lambda + h) + \exp(-(\lambda + h)a_{b,r})R_r^* \end{pmatrix} \quad (5.25b)$$

and the 1×1 matrix \mathcal{J}_2 by

$$\mathcal{J}_2 = \exp(-(\lambda + h)a_{b,m})R_m^* - (\lambda + h). \quad (5.25c)$$



The characteristic equation is obtained by the requirement that the determinant of the matrix \mathcal{P} be equal to zero. Then the ζ_i play the role of eigenvector components and the complex number λ plays the role of eigenvalue, which is now a root of the characteristic equation.

Since the mutant is assumed to be rare, the determinant of \mathcal{P} factorizes, being given by the product of $\det \mathcal{J}_1$ and $\det \mathcal{J}_2 = \mathcal{J}_2$, with these two factors corresponding to the two decoupled systems: the prey-resident-predator system, described by \mathcal{J}_1 , and the mutant-predator population, described by \mathcal{J}_2 . The first factor yields the characteristic equation of the prey-resident-predator system, $\det \mathcal{J}_1 = 0$. This characteristic equation belongs to the eigenvalue problem for the set of one ODE and one DDE (Equations 5.23a and 5.23b) evaluated at the resident equilibrium without the mutant (i.e., $x_{A,m}^* = 0$). The second factor yields the characteristic equation $\det \mathcal{J}_2 = \mathcal{J}_2 = 0$ of the first-order linear homogeneous DDE (Equation 5.23c) describing the dynamics of the mutant population. The expression for \mathcal{J}_2 in Equation (5.25c) is of a form discussed extensively in [14, page 312]. For this case, the complex roots of the characteristic equation can be obtained analytically.

The function $\mathcal{J}_2(\lambda)$ with $\lambda \in \mathbb{R}$ is monotonically decreasing, $d\mathcal{J}_2/d\lambda < 0$. Therefore there is one unique real root λ_0 . Since $\mathcal{J}_2(0) = \exp(-ha_{b,m})R_m^* - h$, the real eigenvalue equals zero, $\lambda_0 = 0$, if and only if $\exp(-ha_{b,m})R_m^* = h$. Thus, Equation (5.25c) has exactly one positive real solution, $\lambda_0 > 0$, when $\exp(-ha_{b,m})R_m^* > h$ and exactly one negative real solution, $\lambda_0 < 0$, when $\exp(-ha_{b,m})R_m^* < h$. In [15, page 321] it is shown that infinitely many complex roots exist. Let $\lambda_k = \mu_k + i\omega_k$, then substitution of this into the characteristic equation $\mathcal{J}_2 = 0$ and separately equating real and imaginary parts gives

$$\mu_k = -h + \exp(-ha_{b,m})R_m^* \exp(-\mu_k a_{b,m}) \cos(a_{b,m}\omega_k), \quad (5.26a)$$

$$\omega_k = -\exp(-ha_{b,m})R_m^* \exp(-\mu_k a_{b,m}) \sin(a_{b,m}\omega_k). \quad (5.26b)$$

Clearly, if Equation (5.26b) holds for ω_k , it holds also for $-\omega_k$, so the complex conjugate $\lambda_k^* = \mu_k - i\omega_k$ is also a root of the characteristic equation. Furthermore, the unique real root λ_0 is the dominant eigenvalue, i.e., the real parts of all other roots are smaller than λ_0 . Comparison of Equation (5.26a) with the characteristic equation for λ_0 gives

$$\lambda_0 - \mu_k = \exp(-ha_{b,m})R_m^* (1 - \exp((\lambda_0 - \mu_k)a_{b,m}) \cos(a_{b,m}\omega_k)). \quad (5.27)$$

Suppose that $\cos(a_{b,m}\omega_k) = 1$, then $\sin(a_{b,m}\omega_k) = 0$, and hence $\omega_k = 0$, which contradicts the fact that $\lambda_k = \mu_k + i\omega_k$ has non-zero imaginary part. We can thus conclude that $\cos(a_{b,m}\omega_k) < 1$. Now assume that $\lambda_0 - \mu_k \leq 0$, then, with $R_m^* > 0$ (since $R_m^* \approx R_r^* > 0$ due to small mutational steps), Equation (5.27) implies $1 \leq \exp((\lambda_0 - \mu_k)a_{b,m}) \cos(a_{b,m}\omega_k)$, and also this leads to a contradiction. This shows that $\text{Re}(\lambda_k) < \lambda_0$, $k = 1, 2, \dots$, or in other words: the real eigenvalue λ_0 is the dominant root of the characteristic equation $\det \mathcal{P} = 0$.

Above, we assumed that the system comprising the resident predator and the prey has a positive stable equilibrium. We checked this assumption numerically for the coexistence set shown in Figure 5.1 using the default parameter

values given in Table 5.2: under these circumstances, the real parts of the eigenvalues of \mathcal{J}_1 are strictly negative. Thus, the dominant eigenvalue λ_0 of \mathcal{J}_2 will also be the dominant eigenvalue of $\det \mathcal{P}$, if λ_0 exceeds the largest real part of the eigenvalues of \mathcal{J}_1 . Hence, for $\exp(-ha_{b,m})R_m^* = h$ the dominant eigenvalue is zero, $\lambda_0 = 0$, and at trait values for which this holds the prey-resident-predator system changes stability, so that the system becomes invadable by the mutant predator.

Now suppose that the real eigenvalue λ_0 is positive but small. Then the characteristic equation gives

$$\begin{aligned} \lambda_0 = & -h + \exp(-(\lambda_0 + h)a_{b,m})R_m^* \\ & - h + \left(1 - \lambda_0 a_{b,m} + \frac{1}{2} \lambda_0^2 a_{b,m}^2 + \dots\right) \exp(-ha_{b,m})R_m^*, \end{aligned} \quad (5.28a)$$

so that, for $\lambda_0 a_{b,m} \ll 1$, we have

$$\lambda_0 = -h + \exp(-ha_{b,m})R_m^*. \quad (5.28b)$$

Consequently, the rate λ_0 is the invasion fitness of the mutant predator at the equilibrium of the prey-resident-predator system, $(x_1^*, x_{A,r}^*, x_{A,m}^* = 0)$.

We have thus shown that $\exp(-ha_{b,m})R_m^* - h$ can be used as a test function for a continuation procedure to calculate the boundary of the coexistence set. Furthermore, if $\lambda_0 a_{b,m} \ll 1$, which holds for small mutational steps, $\exp(-ha_{b,m})R_m^* - h$ is the mutant's invasion fitness. The rare mutant ($x_{A,m} = 0$) will be able to invade the stable prey-resident-predator system if and only if $\exp(-ha_{b,m})R_m^* > h$. The biological interpretation of this inequality is clear: the mutant's effective birth rate has to exceed the dilution rate. After successful invasion, the mutant generally replaces the resident; around evolutionary branching points they can coexist, leading to a dimorphic predator population [18].

Acknowledgments

T.A. Troost thanks the International Institute for Applied Systems Analysis (IIASA) in Austria for providing the possibility of a three-month stay during which the basis for this paper was laid out, and the Netherlands Organization for Scientific Research (NWO) for financing this stay. The authors are very grateful for the data kindly provided by J. Cohen, S. Pimm, P. Yodzis, and J. Saldaña, previously published in [9], and for their approval to use them in Figure 5.2. We also would like to thank M. Boer, O. Diekmann, F. Kelpin, and M. Kirkilionis for helpful discussions on delay differential equations.



References

- [1] Aljetlawi, A. A., Sparrevik, E., and Leonardsson, K. (2004). Prey-predator size-dependent functional responses: derivation and rescaling to the real world. *Journal of Animal Ecology*, 73:239–252.
- [2] Benton (2002). *Encyclopedia of evolution*, chapter Cope's rule, pages 209–210. Oxford University Press, Oxford, U.K.
- [3] Bergmann, C. (1847). Über die Verhältnisse der Wärmeökonomie der Thiere zu ihre Grösse. *Göttinger Studien*, 3:595–708.
- [4] Brown, J. H., Marquet, P. A., and Taper, M. L. (1993). Evolution of body size: Consequences of an energetic definition of fitness. *American Naturalist*, 142(4):573–584.
- [5] Case, T. J. (1978). Body size, endothermy, and parental care in the terrestrial vertebrates. *American Naturalist*, 112:861–874.
- [6] Cohen, J. E. (1989). *Perspectives on Ecological Theory*, chapter Food webs and community structure., pages 181–202. Princeton University Press, Princeton.
- [7] Cohen, J. E., Jonsson, T., and Carpenter, S. R. (2003). Ecological community description using the food web, species abundance, and body size. *PNAS*, 100(4):1781–1786.
- [8] Cohen, J. E. and Newman, C. M. (1985). A stochastic theory of community food webs i. models and aggregated data. *Proceedings of the Royal Society of London B*, 224:449–461.
- [9] Cohen, J. E., Pimm, S. L., Yodzis, P., and Saldana, J. (1993). Body sizes of animal predators and animal prey in food webs. *Journal of Animal Ecology*, 62:67–78.
- [10] Combes, C. (2001). *Parasitism; the ecology and evolution of intimate interactions*. University Chicago Press.
- [11] Cope, E. D. (1896). *The primary factors of organic evolution*. The Open Court Publishing Company, Chigago.
- [12] Dieckmann, U. (1997). Can adaptive dynamics invade? *Trends in Ecology and Evolution*, 12:128–131.
- [13] Dieckmann, U. and Law, R. (1996). The mathematical theory of coevolution: a derivation from stochastic processes. *J. Math. Biol.*, 34:579–612.
- [14] Diekmann, O., van Gils, S. A., Verduyn Lunel, S. M., and Walther, H.-O. (1995). *Delay Equations*, volume 110 of *Applied Mathematical Sciences*. Springer-Verlag, New York.

- [15] Driver, R. D. (1977). *Ordinary and Delay Differential Equations*, volume 20 of *Applied Mathematical Sciences*. Springer-Verlag, New York.
- [16] Ellison, T. and Gibson, R. N. (1997). Predation of 0-group flatfishes by 0-group cod: Handling times and size-selection. *Marine Ecology - Progress Series*, 149(1-3):83–90.
- [17] Forsman, A. (1996). Body size and net energy gain in gape-limited predators: A model. *Journal of Herpetology*, 30(3):307–319.
- [18] Geritz, S. A. H., Gyllenberg, M., Jacobs, F. J. A., Parvinen, K., (2002). Invasion dynamics and attractor inheritance. *J. Math. Biol.*, 44:548–560.
- [19] Geritz, S. A. H., Kisdi, É., Meszéna, G. and Metz, J. A. J. (1998). Dynamics of adaptation and evolutionary branching. *Evolutionary Ecology*, 12:35–57.
- [20] Geritz, S. A. H., Metz, J. A. J., Kisdi, É., and Meszéna, G. (1997). Dynamics of adaptation and evolutionary branching. *Physical Review Letters*, 78:2024–2027.
- [21] Gittleman, J. L. (1985). Carnivore body size: Ecological and taxonomic correlates. *Oecologia*, 67:540–554.
- [22] Hansen, B., Bjornsen, P. K., and Hansen, P. J. (1994). The size ratio between planktonic predators and their prey. *Limnology and Oceanography*, 39(2):395–403.
- [23] Husseman, J. S., Murray, D. L., Power, G., Mack, C., Wenger, C. R., and Quigley, H. (2003). Assessing differential prey selection patterns between two sympatric large carnivores. *OIKOS*, 101(3):591–601.
- [24] Karpouzi, V. and Stergiou, K. I. (2003). The relationships between mouth size and shape and body length for 18 species of marine fishes and their trophic implications. *Journal of Fish Biology*, 62(6):1353–1365.
- [25] Kooijman, S. A. L. M. (1986). Energy budgets can explain body size relations. *Journal of Theoretical Biology*, 121:269–282.
- [26] Kooi, B. W. and Kooijman, S. A. L. M. (1997). Population dynamics of rotifers in chemostats. *Nonlinear Analysis, Theory, Methods & Applications*, 30(3):1687–1698.
- [27] Kooi, B. W. and Kooijman, S. A. L. M. (1999). Discrete event versus continuous approach to reproduction in structured population dynamics. *Theoretical Population Biology*, 56(1):91–105.
- [28] Kooijman, S. A. L. M. (2000). *Dynamic Energy and Mass Budgets in Biological Systems*. Cambridge University Press.
- [29] Kooijman, S. A. L. M. (2001). Quantitative aspects of metabolic organization; a discussion of concepts. *Phil. Trans. R. Soc. B*, 356:331–349.



- [30] Kristiansen, J. N., Fox, T., and Nachman, G. (2000). Does size matter? maximising nutrient and biomass intake by shoot size selection amongst herbivorous geese. *ARDEA*, 88(2):119–125.
- [31] Loeuille, N. and Loreau, M. (2005). Evolutionary emergence of size-structured food webs. *PNAS*, 102(16):5761–5766.
- [32] Manatunge, J. and Aseada, T. (1998). Optimal foraging as the criteria of prey selection by two centrarchid fishes. *Hydrobiologica*, 391(1-3):223–240.
- [33] Mayr, E. (1956). Geographical charactergradients and climatic adaptation. *Evolution*, 10:105–108.
- [34] Mayr, E. (1963). *Animal species and evolution*. Harvard University Press, Cambridge, Mass.
- [35] Mehner, T., Plewa, M., Hulsmann, S., and Worischka, S. (1998). Gape-size dependent feeding of age-0 perch (*perca fluviatilis*) and age-0 zander (*stizostedion lucioperca*) on *daphnia galeata*. *Archiv fuer Hydrobiologie*, 142(2):191–207.
- [36] Memmott, J., Martinez, N. D., and Cohen, J. E. (2000). Predators, parasitoids and pathogens: species richness, trophic generality and body sizes in a natural food web. *Journal of Animal Ecology*, 69:1–15.
- [37] Metz, J. A. J., Nisbet, R. and Geritz, S. A. H (1992). How should we define ‘fitness for general ecological scenarios? *Trends in Ecology and Evolution*, 7:198–202.
- [38] Metz, J. A. J., Geritz, S. A. H., Meszéna, G., Jacobs, F. J. A and van Heerwaarden, J. S. Adaptive Dynamics, a geometrical study of the consequences of nearly faithful reproduction. In: van Strien, S. J. and Verduyn Lunel, S. M. (Eds.). *Stochastic and Spatial structures of dynamical systems*. KNAW Verhandelingen, Amsterdam, 1996 pp. 183–231.
- [39] Neubert, M. G., Blumenshine, S. C., Duplisea, E. D., Jonsson, T., and Rashleigh, B. (2000). Body size and food web structure: testing the equiprobability assumption of the cascade model. *Oecologia*, 123:241–251.
- [40] Peters, R. H. (1983). *The Ecological Implications of Body Size*. Cambridge University Press, New York.
- [41] Rincon, P. A. and Loboncervia, J. (1995). Use of an encounter model to predict size-selective predation by a stream-dwelling cyprinid. *Freshwater Biology*, 33(2):181–191.
- [42] Rytkonen, S., Kuokkanen, P., Hukkanen, M., and Huhtala, K. (1998). Prey selection by sparrowhawks *accipiter nisus* and characteristics of vulnerable prey. *Ornis Fennica*, 75(2):77–87.

- [43] Svensson, J. E. (1997). Fish predation on eudiaptomus gracilis in relation to clutch size, body size, and sex: A field experiment. *Hydrobiologica*, 344:155–161.
- [44] Turesson, H., persson, A., and Bronmark, C. (2002). Prey size selection in piscivorous pikeperch (stizostedion lucioperca) includes active prey choice. *Ecology of Freshwater Fish*, 11(4):223–233.
- [45] Van Valen, L. (1973). Pattern and the balance of nature. *Evolutionary Theory*, 1:31–49.
- [46] Vezina, A. F. (1985). Empirical relationshi[s between predator and prey size among terrestrial vertebrate predators. *Oecologia*, 67:555–565.
- [47] Warren, P. H. and Lawton, J. H. (1987). Invertebrate predator-prey body size relationships: an explanation for upper triangular food webs and patterns in food web structure? *Oecologia*, 74(231-235).
- [48] Williams, R. J. and Martinez, N. D. (2000). Simple rules yield complex food webs. *Nature*, 404:180–183.
- [49] Yodzis, P. and Innes, S. (1992). Body size and consumer-resource dynamics. *American Naturalist*, 139(6):1151–1175.



6

Seasonality as a driver of body size evolution

Tineke A. Troost, Jan A. van Dam, Bob W. Kooi, Erik Tuenter

Abstract

The seasonality hypothesis states that variable climates, characterized by large annual cycles, select for large body sizes. Therefore, it provides an alternative explanation for the observed increase of body size with latitude, which phenomenon is known as 'Bergmann's rule', and is traditionally explained by differences in temperatures. So far, experimental and field data do not unambiguously support the seasonality hypothesis, and neither do models. In order to study the effects of seasonality on the evolution of body size, we use a physiologically based model for rodents. Model results show that seasonality may lead to larger body sizes indeed; for this, relative amplitude rather than absolute amplitude is decisive. Our model is the first to support the seasonality hypothesis and, as such, shows the importance of basing model dynamics on physiological processes. Simulations across geological time scales illustrate that evolutionary patterns in body size may be a response to temporal variability in seasonality related to the Milankovitch cycles.

6.1 Introduction

Temporal and geographical trends in body size are still not fully understood. A famous example is Bergmann's rule, describing an increase of size with latitude [5, 42, 43]. The latitudinal trend in body size is often attributed to the latitudinal gradient in temperatures, but Lindstedt and Boyce [40] suggested it to be related to seasonality. Their so-called 'seasonality hypothesis' states that seasonal environments select for large body sizes [6, 7]. The underlying mechanism is thought to be related to starvation, as larger organisms have larger energy reserves that will last longer under starvation conditions [39, 51].

So far, however, experimental and field data do not unambiguously support the seasonality hypothesis. The hypothesis has been tested against field data by searching for geographical gradients in body size that correlate with gradients in seasonality, but the results are non-decisive. Positive relations between body size and seasonality were found for muskrats [6], western bobcats [57], western rattlesnake [2], weevils [8] and sifakas [37]. In contrast, data on moose [19] and thirteen species of western palearctic carnivores [44] did not show clear correlations and thus did not support the hypothesis. The variability of the results may be explained by the fact that body size is not only related to starvation, but also to a range of other physiological processes such as ingestion, maintenance, reproduction and thermo-regulation. As was previously pointed out by Dunsbrack and Ramsay [18], these (inter)relationships and processes may cloud the specific effects of seasonality.

Mathematical models may help to study the many interrelationships between body size and physiological processes. Various models have been developed to study the effect of seasonality on a variety of life history parameters and storage dynamics. Yet, like the empirical data mentioned above, existing model results do not clearly support the seasonality hypothesis either. Cohen and Parnas [9, 50] used a model to study the relation between variability and storage level, and optimized allocation patterns. They found that variability leads to higher levels of storage, but they make no predictions on body size. Boyce [7] studied the relation between seasonality and life history parameters (*r*- versus *K*-selection), and his results can be interpreted as being consistent with the seasonality hypothesis. Finally, Shertzer and Ellner [53] found that variable environments select for *smaller* body sizes. Clearly, their result does not support the hypothesis.

The present paper aims to study again the effects of seasonality on the evolution of body size by means of a modeling approach. Our model distinguishes itself from the previously mentioned models because it is fully based on physiological rules for uptake and use of energy and material; the dynamics of biomass and reserves are derived from first principles and tested against a large amount of experimental data, which modeling framework is referred to as Dynamic Energy Budget (DEB) theory [33].

The resulting model is tested under different values of seasonality. Traditionally, different seasonalities are sought in a geographical context. In this study, however, we focus on *temporal* variations in seasonality. An advantage



of studying temporal variability in seasonality is that the body size response can be followed for a single species or lineage, occurring at one location. Geographical comparisons, in contrast, need often be corrected for interspecific differences, or for environmental differences other than those in seasonality. Also, studying temporal variation allows for additional testing, as not only the evolutionary equilibria, but also the evolutionary trajectories, can be compared against empirical data.

A particularly strong temporal forcing of seasonality exists on the scale of 20,000-400,000 years, the scale of Milankovitch cycles [34, 47], which have been extensively documented in the geological record [25, 26, 49]. Solar insolation reaching the earth's atmosphere is a function of three orbital parameters: the wobbling of the earth's axis (*precession*, mean period 21,000 years), the tilt of the axis (*obliquity*, 41,000 year period), and the shape of the earth orbit around the sun (*eccentricity*, main periods 100,000 and 400,000 years). The effect of precession is that the distance from earth to sun varies for each of the seasons. The climatic effects of precession on seasonality are relatively strong on low and middle latitudes, with periods of high seasonality alternating with periods of low seasonality. Obliquity creates seasons, and its effect is largest on high latitudes. Obliquity-variations in the geological past have been particularly linked to glaciations. The direct contribution of eccentricity to insolation is low, but because eccentricity modulates precession (there is no precession effect with zero eccentricity, i.e. a circular earth orbit), 100,000 and 400,000 year periodicities are also well recorded in the geological record. In addition, the primary Milankovitch cycles are modulated by longer cycles with periods of 1.2 and 2.4 million years [34].

The fossil record shows that organisms respond to Milankovitch cycles by changes in their distribution (habitat tracking) [3]. Body size response is to be expected as well, but until now there are surprisingly few studies which have addressed changes in body size on Milankovitch time scales. Given the widespread recognition of climate cycles in sediments throughout the earth's history, the body size response is expected to show a cyclical component. This can be tested only in cases where an excellent fossil record is available. Because rodents have such an excellent fossil record, and because their population dynamics are well known, and are often driven by periodic environmental factors such as rainfall [15, 38, 41, 52], we have based our model on these animals. Results are compared with data on body size changes of small rodents belonging to the family of Muridae during the late Miocene (10-8 million years ago), which are based on fossil teeth collected from fluvial and lacustrine (lake) sediments in Central Spain.

6.2 Methods

6.2.1 Model description

We use a model that is based on the model developed by Kooijman and Kooi [29, 30], and adjusted it to account for rodents living in a generalized reactor, with a resource entering the system with a periodically varying density. The rodent population is described by two state variables, their ‘structural biomass’ (the total amount of biovolume per hectare X_1) and their ‘reserve density’ (energy per structural volume $[E_1] = E_1/X_1$). The energy density is scaled by the maximum energy density $[E_m]$, so that the resulting scaled energy density $e_1 = [E_1]/[E_m]$ is dimensionless and may range between 0 to 1. Adults are assumed to all have the same energy density e_1 , as well as the same body size ℓ_A . The model was simplified by assuming that the delay in birth due to the embryonal period is negligible, which reduces the equations into ordinary differential equations (ODEs):

$$\frac{dX_0}{dt} = (X_{0,\text{in}}(t) - X_0)D - f(X_0)\{I_m\}X_1/\ell_A, \quad (6.1a)$$

$$\frac{de_1}{dt} = k_E(f(X_0) - e_1), \quad (6.1b)$$

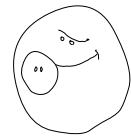
$$\frac{dX_1}{dt} = (R(e_1) - h)X_1, \quad (6.1c)$$

where X_0 is the resource density in the system, and $X_{0,\text{in}}$ is the resource density that enters the system at rate D ; the periodic forcing of the incoming resource density is discussed in section 6.2.2. k_E is the energy turnover rate and h the rodent mortality rate. $\{I_m\}$ is the surface-area-specific maximum ingestion rate and X_1/ℓ_A is the rodent surface-area per hectare. The function f is their functional response, which is assumed to be of Holling type-II ,

$$f = \frac{X_0}{K + X_0}, \quad (6.2)$$

where K is the saturation constant.

The continuous expression for the reproduction rate R is derived in [29, 30], which is the ratio between the amount of energy needed per egg and the rate with which energy becomes available for reproduction. The latter depends on the scaled energy density e_1 of the mother, and on the energy conductance k_E . From the mobilized energy, first the costs for maintenance have to be paid, calculated by multiplying the maintenance rate k_M (i.e. the ratio of costs for maintenance per unit of time to costs for growth) with the energy investment ratio g (i.e., the proportion of the total amount of available energy that is used for growth). The scaled energy density required to produce an embryo consists of the costs for the structural biomass of a newborn individual, the cost for growth and maintenance during the embryonic period, $g^+ = g + \frac{3}{4}gk_M/k_E$ [29, 30], as well as of the energy density of a newborn individual, e_1 . The



reproduction rate is thus given by:

$$R(e_1) = \frac{k_E e_1 - k_M g}{g^+ + e_1}. \quad (6.3)$$

Rodents quickly grow into their adult size. Therefore, the juvenile stage can be neglected and all individuals are assumed to be adults, and thus have the same body size, which simplifies the model considerably. To model the corresponding steep growth curve, the adult size was assumed to lie at a fraction α of the maximum size: $\ell_A = \alpha \ell_m$.

Parameter values for physiological processes were based on average values for rodent species found in literature. Weights were converted to biovolumes using a volume-specific density $[M_V]$ of 1 g cm^{-3} . The average incoming resource density or productivity, $\bar{X}_{0,\text{in}}$, was set to 10 kg ha^{-1} , as to result in realistic rodent densities. The saturation constant K was chosen as one-tenth of the maximum possible food density, such that the scaled functional response f could range from 0 to a value close to 1. For a more detailed explanation of the model, including derivations of R and g^+ , readers may want to consult [29, 30]. Parameters and variables of the model are summarized in Table 6.1, with all default parameter values listed in Table 6.2.

Reproduction rate under starvation conditions. During the winter, the rodents may deplete their energy storage. In case they can no longer meet their maintenance requirements ($R(e_1) < 0$), death due to starvation will start to occur. Note that the reserve density does not need to be zero for such shortages to arise, as it is not only the reserve density but also its mobilization rate k_E that is physiologically limiting. In a physiologically-structured model organisms generally have different energy reserves and such shortages would mean that some organisms or cohorts would die. However, in our simplified model all organisms have the same size and energy reserves and deplete these reserves at the same time. Instead of having the total population die, we assume that the change in the structural biomass of the population is proportional to the reproduction rate, also when this becomes negative. The resulting decrease in biomass implies that the organisms use their structural biomass for paying their maintenance costs. A more liberal interpretation could be that, due to the natural variation in energy density, part of the population dies while the rest survives. As a result, the average reserve density, and thus the reproduction rate, increase again. When it is very inefficient to use structural biomass to pay maintenance costs, the body size at the evolutionary equilibrium would shift towards a size at which the reserves are always sufficient to pay the maintenance needs. Therefore, together with the evolutionary size, we present this ‘adequate’ body size in our results.

Scaling considerations. In the present study, body size ℓ_A is assumed to be subject to evolution. Therefore, various body-size scaling relationships were included that were not considered in the original DEB model [29, 30], where

Table 6.1: Used symbols; t=time, L=length of individual, l =length of area, m=mass, e=energy.

Symbol	Dimension	Interpretation
D	t^{-1}	'Dilution' rate
$[E], [E_m]$	$e L^{-3}$	Energy density, and maximum (storage capacity)
f	–	Scaled functional response
g, g^+	–	Energy investment ratio; $g + \frac{3}{4} gm/\nu$
$\{I_m\}$	$L^3 L^{-2} t^{-1}$	Surface-area-specific maximum intake rate $\{I_m\} = \ell_A [I_m]$
$[I_m]$	$L^3 L^{-3} t^{-1}$	Volume-specific maximum intake rate.
k_E	t^{-1}	Specific energy conductance: v/ℓ_A
k_M	t^{-1}	Maintenance rate coefficient
$[M_V]$	$m L^{-3}$	mass per unit of structural body volume
R	t^{-1}	Reproduction rate
T_0, T_p	t	Period length of seasonal cycle, and of precession cycle
T_s	t	Starvation period
$X_{0,in}(t), \bar{X}_{0,in}$	$L^3 l^{-2}$	Incoming resource density, function and average
α	–	Fraction of the asymptotic size that is reached
ϵ, ϵ_p	–	Amplitude of the seasonal cycle, and of the precession cycle
v	$L t^{-1}$	Energy conductance
γ	–	Shape coefficient of environmental cycle
State Variables		
X_1, X_0	$L^3 l^{-2}$	Rodent and resource biovolume density
e_1	–	Scaled energy density
Adaptive traits		
ℓ_A	L	Adult rodent length $\ell_A = \alpha \ell_m$
ℓ_m	L	Maximum rodent length

Table 6.2: Default parameter values

Symbol	Value	Unit	Reference (if relevant)
D	0.01	d^{-1}	
h	0.002	d^{-1}	[20]
$[I_m]$	0.05	$mg ml^{-1} d^{-1}$	[35]
k_M	0.5	d^{-1}	[33]
K	1	$kg ha^{-1}$	1/10 of $\bar{X}_{0,in}$
$[M_v]$	1	$g cm^{-3}$	
T_0	365	d	
T_s/T_0	0.5	–	
v	0.2	$cm d^{-1}$	[33]
$\bar{X}_{0,in}$	10	$kg ha^{-1}$	
α	0.25	–	–
ϵ	1	–	



body size was assumed to be fixed. First, the energy investment ratio g was no longer constant, but comes to depend on body volume ℓ_m^3 , following an expression central to DEB theory, $g = v/(k_M \ell_m)$ [33]. Second, the specific energy conductance k_E is equal to the energy conductance v divided by the size of the organism, $k_E = v/\ell_A$. The rationale behind this scaling relation is that energy is mobilized across membranes, which have a surface area proportional to that of the organism. Third, the surface-area specific ingestion rate is proportional to size $\{I_m\} = \ell_A[I_m]$, in which $[I_m]$ is the (constant) volume-specific ingestion rate, following a primary scaling relationship in DEB theory.

6.2.2 The periodic environment

The resource density X_0 is externally forced by the incoming resource density function $X_{0,\text{in}}(t)$. This incoming density has a sinoidal shape which is specified by the amplitude ϵ , the average incoming resource density or productivity $\bar{X}_{0,\text{in}}$ and the period length T_0 , such that the density is always positive:

$$X_{0,\text{in}}(t) = \begin{cases} \bar{X}_{0,\text{in}}(1 + \epsilon \sin(2\pi t/T_0)) & , 1 + \epsilon \sin(2\pi t/T_0) > 0 \\ 0 & , 1 + \epsilon \sin(2\pi t/T_0) \leq 0. \end{cases} \quad (6.4)$$

The relative starvation period T_s/T_0 is defined as the fraction of the total period in which the incoming resource density $X_{0,\text{in}}$ is lower than its average $\bar{X}_{0,\text{in}}$. This fraction can be changed by deforming the sinus, while keeping amplitude, offset and total period constant. This is done by taking the i^{th} power of the resource function as follows: $X_{0,\text{in}}(t) = \bar{X}_{0,\text{in}}(1 + 2\epsilon(((1 + \sin(2\pi t/T_0))/2)^i - 1/2))$, with $i = 0, 1000$. For $i = 1$ this equation becomes equation (6.4). Then, the relative starvation period corresponding to each i was calculated with an empirically fitted function: $T_s/T_0 = 1 - (1 + \sqrt{i})^{-1}$.

The shape coefficient γ is a measure for the shape of the environmental cycle: at $\gamma = 1$ it is a perfect sinus, while at $\gamma = 0$ it is block-shaped. The shape deformation was done by taking the j^{th} root of the sinus: $X_{0,\text{in}}(t) = \bar{X}_{0,\text{in}}(1 + \epsilon \sin(2\pi t/T_0)^{1/j})$ for $\sin(2\pi t/T_0) > 0$, and $X_{0,\text{in}}(t) = \bar{X}_{0,\text{in}}(1 - \epsilon \sin(-2\pi t/T_0)^{1/j})$ for $\sin(2\pi t/T_0) < 0$, with $j = 1, 100$. Then, j was converted into γ to correspond linearly to the range of shapes: $\gamma = \exp\{-0.15(j - 1)\}$. Figure 6.3A shows how amplitude, period and offset and the other properties are defined.

6.2.3 Evolutionary equilibria

In nature, body size is the result of several interrelated factors. Here, however, we treat it as a single ‘compound’ trait that is subject to evolution. Body size is inherited from parents to offspring, but due to sloppy heredity small differences may occur. Mutants with a different body size may invade and replace the resident population or simply go extinct. A series of such replacements will lead to phenotypic change of the population. To find the evolutionary equilibrium, i.e. the body size to which the organisms will eventually evolve, we use Adaptive Dynamics (AD) theory; this theory helps to analyze phenotypic

evolution under frequency-dependent selection [16, 17, 23, 45]. The invasion fitness of a mutant s_{mut} is defined as its long-term per capita growth rate r while being rare in the environment $E(\ell_{\text{res}})$ set by the resident population at its ecological equilibrium: $s_{\text{mut}} = r(\ell_{\text{mut}}, E(\ell_{\text{res}}))$, where ℓ_{res} and ℓ_{mut} are the trait values ℓ_A of the resident and the mutant population, respectively. Because the resident population is at its ecological equilibrium, individuals belonging to this population always have a zero invasion fitness, $s_{\text{res}} = r(\ell_{\text{res}}, E(\ell_{\text{res}})) = 0$. Mutants with a negative invasion fitness will die out, but mutants with a positive invasion fitness may replace or coexist with the resident population.

In constant environments, the mutant invasion fitness is equal to the specific growth rate of the mutant: $s_{\text{mut}} = R_{\text{mut}}(\ell_{\text{mut}}, E(\ell_{\text{res}})) - h$. In this paper, however, we study a system in which the incoming resource density is not constant but periodic; as a result, the environment does not only depend on the resident trait value ℓ_{res} , but also on time t . This makes the calculation of the mutant invasion fitness more complicated, but in [31, 46] it is shown that it comes down to the mutant's growth rate averaged over the environmental cycle period T_0 :

$$s_{\text{mut}} = T_0^{-1} \int_0^{T_0} R_{\text{mut}}(\ell_{\text{mut}}, E(t, \ell_{\text{res}})) dt - h. \quad (6.5)$$

The expected direction of phenotypic change is proportional to the local fitness or selection gradient, i.e. the derivative of the fitness function with respect to the body size of the mutant evaluated at the body size of the resident:

$$\frac{\partial}{\partial \ell_{\text{mut}}} s_{\text{mut}} = \left. \frac{\partial}{\partial \ell_{\text{mut}}} s(\ell_{\text{mut}}, E(t, \ell_{\text{res}})) \right|_{\ell_{\text{mut}} = \ell_{\text{res}}}. \quad (6.6)$$

A deterministic approximation of the evolutionary trajectory of the body size can be obtained with use of the ‘canonical equation’ of Adaptive Dynamics [17]. For periodic systems this involves the additional assumption that the mutant invasion is slow with respect to the dynamics of the periodic attractor. For a monomorphic population this comes down to:

$$\frac{d\ell_{\text{res}}}{dt} = \frac{1}{2} k \frac{X_1}{\ell_{\text{res}}^3} \frac{\partial}{\partial \ell_{\text{mut}}} s_{\text{mut}}, \quad (6.7)$$

where k is the mutation-rate parameter involving the fraction of mutations per birth and the mean size of the mutational step; X_1/ℓ_{res}^3 is the mean population size (in number of rodents per hectare).

Eventually, the population will reach a body size at which the fitness gradient has vanished:

$$\frac{\partial}{\partial \ell_{\text{mut}}} s_{\text{mut}} = 0. \quad (6.8)$$

Such a ‘singular strategy’ is an evolutionary equilibrium, which is found by integration of the canonical equation. In a constant environment, the population



will continue to evolve until reaching this equilibrium body size. The used methods and the evolutionary dynamics of this system are discussed in more detail in [31].

6.2.4 Evolutionary trajectories

Evolution is a slow process, and the environment (seasonality) may change faster than the phenotype of the organisms. As a result, the evolutionary equilibrium may never be reached. In these cases, not only the evolutionary equilibrium discussed above, but also the evolutionary trajectories of body size are of interest. These trajectories can be deterministically approximated with use of the canonical equation of AD theory (Equation (6.7)). However, in AD theory, it is assumed that mutations are rare, such that the resident population has reached a population-dynamical equilibrium before a next mutation occurs. This implies that, by that time, all other populations consisting of individuals with smaller invasion fitnesses have gone extinct. This may be unrealistic, especially when studying evolution in a changing environment. Therefore, the evolutionary trajectories were determined by means of stochastic simulations instead, in which no equilibrium assumption is required.

In the first simulation, the body size response of rodents was studied over a period of almost one precession cycle (from 20,000 years ago until now). The temporal change in seasonality during this interval was incorporated in the function for the incoming resource density by multiplying the amplitude ϵ of the seasonal cycle by the precession cycle β_p , which thus amounted to: $X_{0,\text{in}}(t) = \bar{X}_{0,\text{in}}(1 + \beta_p \epsilon \sin(2\pi t/T_0))$. The precession cycle was calculated as $\beta_p = 1 + \epsilon_p \sin(2\pi t/T_p)$, with a period T_p of 21,000 yr. Because no resource or precipitation data were available for this area at this interval, values for the amplitudes, ϵ and ϵ_p , had to be assumed. The amplitude ϵ of the seasonal cycle was set to $\epsilon = 0.7$, to study specifically the evolutionary dynamics in the vicinity of the bifurcation point. The amplitude ϵ_p of the precession cycle was set to a value smaller than one, $\epsilon_p = 0.25$, so that a certain amount of seasonality remained throughout the whole period. Note that, on the northern hemisphere, seasonality is high at precession minima (e.g., at 11,000 years ago), while it is low at precession maxima. Seasonality thus follows a pattern that is opposite to precession.

Mutations in the maximum body size were assumed to be normally distributed around the parent maximum body size with $\sigma = 0.02$. Mutants were assumed to enter the system with the same reserve density as their parent and, because they were assumed to be rare, with a very low initial biomass density, corresponding to that of 10^{-20} adults per hectare; the threshold for extinction was also set to 10^{-20} individuals per ha. To limit the number of potential lineages, they were grouped in size classes with a width of $\log_{10}(0.005)$. The mutation rate k was set to 0.5×10^{-4} per birth.

In the second simulation, we focus on a longer interval in the late Miocene in Central Spain (10-8 million years ago, Teruel Basin) [13]. For this interval and area, theoretical precipitation values were calculated at the most

extreme precession maxima and minima of the last million years, and at zero precession. These precipitation values were calculated with a climate model of intermediate complexity using present-day boundary conditions [55]. The use of these boundary conditions is not problematic, as small-mammal community structure shows that Late Miocene levels of rainfall in Spain were not very different from today's levels [14]. Obliquity was considered fixed in these calculations and was set to the lowest value found in the last million years.

The climate model results show (relative) amplitudes of precipitation rates of 0.62 at precession minima, 0.34 at precession maxima, and 0.37 at zero precession. To translate the precipitation rate into the incoming resource densities, it was assumed that a minimum of 1 mm d^{-1} of precipitation was minimally required for resources to be produced. Above this minimum precipitation value, the incoming resource density was assumed to be linearly related to precipitation rate. Calculated as such, one arrives at amplitudes of 1.05 at the most extreme precession minima, 0.51 at the most extreme precession maxima, and 0.68 at zero precession.

The temporal change in seasonality was calculated by modifying the precession cycle β_p by three longer cycles: $\beta_p = 1 + \beta_1\beta_2\beta_3(\theta + \sin(2\pi t/T_p))$. These cycles, calculated as $\beta_i = \frac{1}{2}(1 + \epsilon_i \sin(2\pi(t + T_{d_i})/T_i))$, have periods T_i of {100, 400, 2400} kyr, and delays T_{d_i} of {20, 0, 1100} kyr, respectively [34]. Their amplitudes, $\epsilon_i = \{0.6, 0.8, 0.6\}$, were based on the relative importance of the three cycles calculated by Laskar et al. [34] and, for their absolute values, on the differences in amplitudes of the incoming resource densities calculated above; θ was set to a value of 0.2 as to incorporate the asymmetry in the distribution of precipitation minima and maxima around the average precipitation as appeared in the theoretical precipitation values predicted by the climate model. The amplitude of the incoming resource density function was set to $\epsilon = 0.68$, which is the amplitude in incoming resource density at zero precession calculated above.

Simulation results were compared to data on rodent teeth sizes from this period, derived from an exceptionally dense and well-dated record (24.5-2.5 million years ago) of fossil small teeth. These fossil teeth were collected from fluvial and lacustrine (lake) sediments in Central Spain [11]. Tooth size changes were traced in the two best-represented *Progonomys-Occitanomys* and *Hispanomys* lineages (mouse- and hamster-like forms, respectively, belonging to the family Muridae). Changes in lake and small-river sediments have been found to be controlled by astronomically-forced climate change [1], and tooth size is a good estimator for body size [36].

6.3 Results

6.3.1 Effects of seasonality

Figure 6.1 shows the density fluctuations of resources and rodents on a population-dynamical time scale, at which the adult body size is constant. Re-

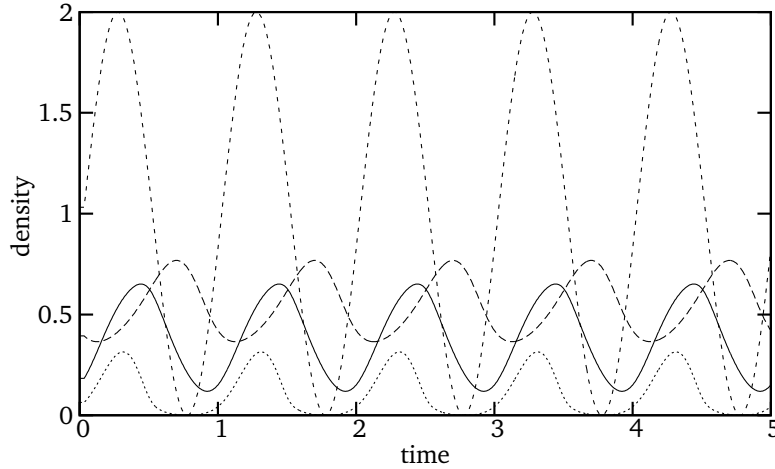


Figure 6.1: Density fluctuations on an ecological time scale: Incoming resource density $X_{0,in}$ (short-dashed curve), resource density X_0 (dotted curve), rodent energy density e_1 (continuous curve) and rodent biovolume density X_1 (long-dashed curve) plotted against time (years); energy density is a dimensionless variable, the other variables were normalized to the average incoming resource density $\bar{X}_{0,in}$.

sources X_0 (dotted curve) are transformed into rodent reserves e_1 (continuous curve) and then into rodent biovolume X_1 (long dashes). It can be seen that all variables follow the forced fluctuations of the incoming resource density $X_{0,in}$ (short dashed curve), though each with an increased delay and a decreased amplitude. This illustrates the buffering function of the reserves, smoothing out variations in the resource availability. Muller and Nisbet [48] studied the physiological response on an ecological time scale, of an organism following DEB-rules, in more detail. They showed that a variable food supply stimulates growth, increases mortality and may enhance reproduction.

Figure 6.2 shows the evolutionary equilibria of body size (continuous and dashed curves) against the amplitude ϵ of the environmental cycle; both period length and offset are kept constant. When the amplitude becomes larger than the offset, periods with zero food occur. The evolutionary equilibrium at the continuous curve is stable, and thus an ‘evolutionary attractor’, which means that the population will evolve towards it. The dashed curve denotes an unstable equilibrium, or an ‘evolutionary repeller’: above the line evolution is directed towards larger body sizes, whereas below the line it is directed towards smaller body sizes. The dotted curve denotes the body sizes above which reproduction is never smaller than zero, such that the organisms always have sufficient energy reserves to pay their maintenance; this curve was named the ‘adequate’ body size. The figure shows that body size value at the evolutionary equilibrium increases with amplitude. At $\epsilon = 0.75$, the stable and unstable

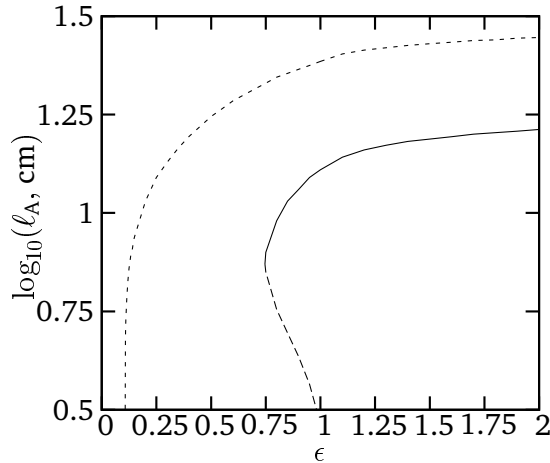


Figure 6.2: The effect of seasonality on the evolutionary equilibrium of body size. The figure plots the logarithm of the body length in centimeters against the amplitude ϵ of the environmental cycle. The continuous curve denotes the stable evolutionary equilibrium (attractor); the dashed curve denotes the unstable evolutionary equilibrium (repellor); dotted curves denote the ‘adequate’ body size, above which the reserves always suffice to pay the maintenance costs.

equilibria (continuous and dashed curves) come together and the evolutionary equilibria ‘disappear’; this is a so-called ‘tangent bifurcation’. At this and smaller amplitudes, the environment will select for ever smaller body sizes. A similar phenomenon was also found in [22].

Figure 6.3B-E show how the evolutionary equilibrium of body size is affected by various other cycle characteristics (Figure 6.3A), while the unchanged characteristics are kept at their default values. The evolutionary equilibrium increases considerably with cycle period T_0 (Figure 6.3B). Productivity (offset) has a much smaller effect (Figure 6.3C); only at small productivities that are on average below the saturation constant, the body size at the evolutionary equilibrium decreases. At very small offsets, the population goes extinct. Relative starvation period ρ_s has a two-sided effect (Figure 6.3E): body size decreases both for shorter and for longer starvation periods. The shape of the environmental periodicity γ has only a small effect on body size. At sharper transitions between the good and the bad season (smaller values of γ) the evolutionary equilibrium increases slightly in value.

6.3.2 Effects of variations in seasonality

Figure 6.4 shows the results of the first simulation. In response to the sinusoidal change in seasonality (lower continuous curve), the body size also

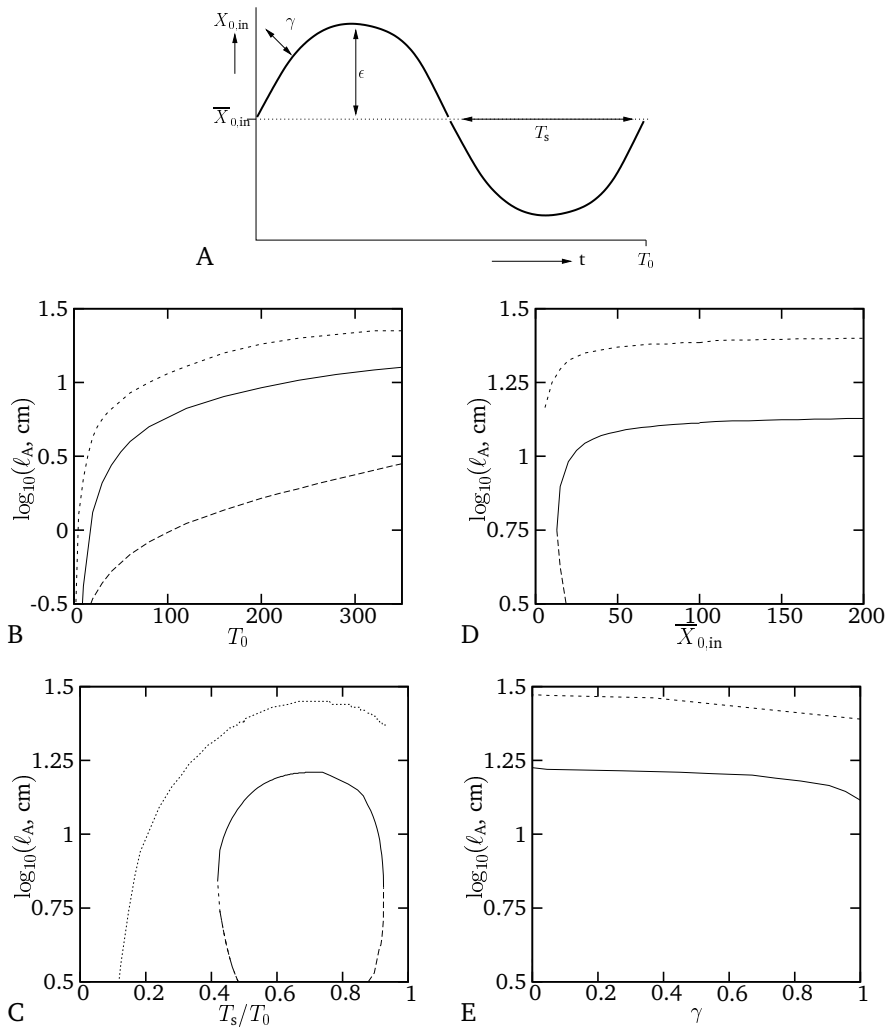
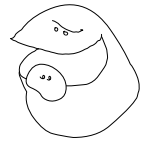


Figure 6.3: The effect of various environmental cycle characteristics (A) on the evolutionary equilibria of body size (B-E). The figures plot the logarithm of body size in centimeters against period length T_0 (B), average incoming resource availability $\bar{X}_{0,in}$ (C), the relative starvation period T_s/T_0 (D), and the shape coefficient γ (E). Continuous curves denote the stable evolutionary equilibrium (attractor); dashed curves denote the unstable evolutionary equilibrium (repellor); dotted curves denote the 'adequate' body size above which the reserves always suffice to pay the maintenance costs.

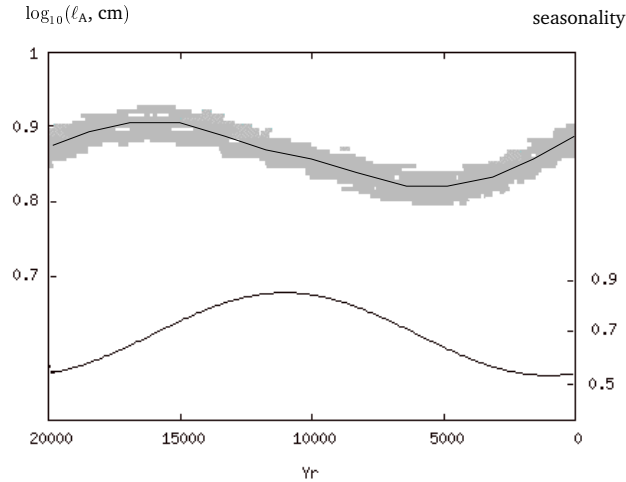


Figure 6.4: Average adult body sizes predicted (upper continuous curve) in the last 20000 years, resulting from a simulation in which the seasonality (lower continuous curve) is varied according to the changes in precession. The gray areas around the average size indicate the range of body sizes that are present in the system simultaneously.

changes sinusoidally. Grey tones indicate the range of body sizes simultaneously present in the system. Note that the body size response is out of phase with the change in seasonality.

Figure 6.5 shows the results of the second simulation, together with rodent teeth sizes of *Progonomys-Occitanomys* and *Hispanomys* lineages derived from fossil teeth from the late Miocene period. Tooth size in both lineages shows a drop in all studied elements (first and second upper and lower molars) between 9.7 and 8.9 million years ago. The model simulates this drop very well.

6.4 Discussion

Model results show a positive relation between the amplitude of the environmental cycle and the body size at the evolutionary equilibrium (Figure 6.2). As amplitude corresponds to the variability and therefore to the seasonality of the environment, these results support the seasonality hypothesis. This, in turn, implies that latitudinal differences in body size (Bergmann's rule) may be attributed to differences in seasonality indeed.

Our model is the first model that clearly supports the seasonality hypothesis, contrasting most sharply with that of [53], who found that variability selects for *smaller* sizes. The contrasting results originate from the structural differences between the models that were used. In the model of Shertzer and Ellner [53], energy storage is treated as an additional feature that is only used

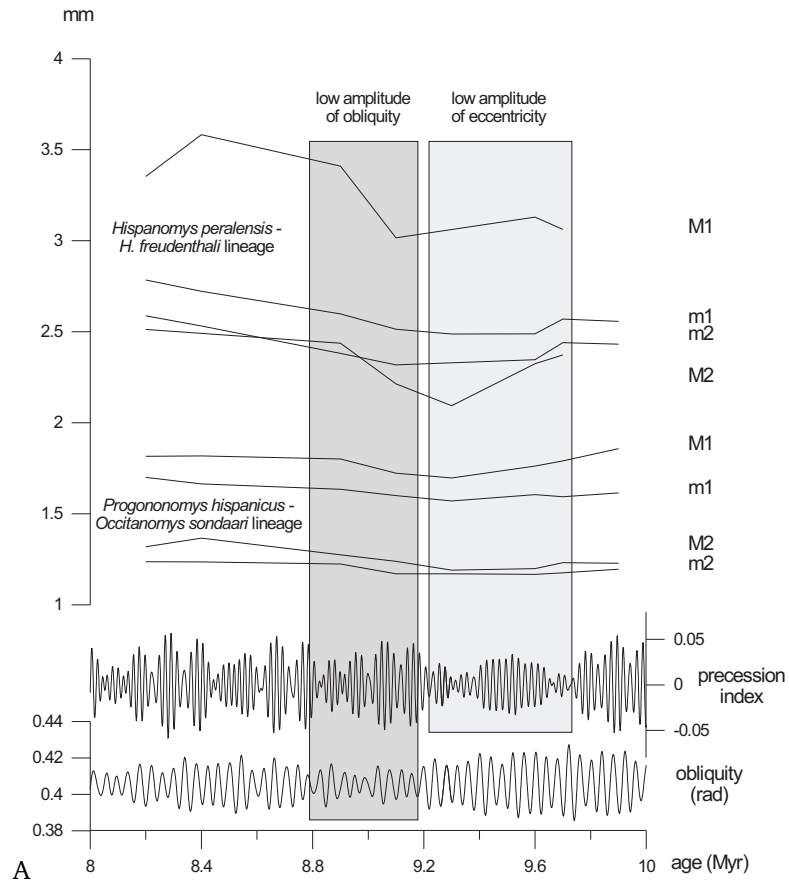


in times of need. In contrast, in DEB theory the energy reserves are given a much more central role and are more closely linked to other physiological processes such as growth and reproduction. Assimilates derived from food are added to the reserves, which then fuel all other processes including maintenance, growth and reproduction. As a result, growth and reproduction do not depend directly on the available food resources, but on the reserves. This gives the reserves a broader interpretation than is generally the case: reserve material is not only set aside for later use (such as fat storages), but it consists of all material that is available for metabolic use, now or later. As a consequence of their central role, the reserves and their dynamics are fully embedded in the model. The assumptions underlying these reserve dynamics also lead to various body size scaling-relationships. One of these is the scaling of storage capacity (maximum energy density [E_m]) with body size, which relationship is supported by empirical data [40, 51]. In the model of Shertzer and Ellner [53], however, the size of the energy storage is not physiologically limited, and energy capacity and body size evolve independently. The contrasting findings illustrate the great importance of a physiologically based model structure.

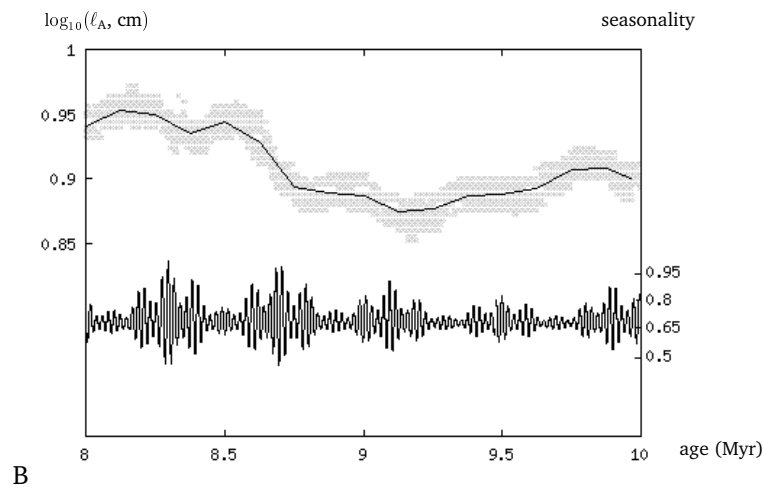
Of the studied cycle characteristics, period length has the largest impact on the evolutionary equilibrium of body size (Figure 6.3B). Though period lengths other than a year may not be relevant for most rodent species, they may be for other species, as both longer and shorter environmental periodicities exist (e.g. daily, tidal and El Niño cycles). Also the relative duration of the good and bad seasons is of importance (Figure 6.3C). Figure 6.3D shows that smaller environmental productivity leads to smaller body sizes, which is also found by Shertzer and Ellner [53]. This result may be explained by the lower maintenance and reproduction costs of small individuals, as well as by their higher relative food intake rate. Also, it may be related to the density dependence of the fitness measure, as increased mortality during the bad season reduces competition during the good season. Furthermore, the relative amplitude ϵ was found to have considerably more effect than the absolute amplitude ($\epsilon \bar{X}_{0,\text{in}}$), which can be seen when comparing Figures 6.2 and 6.3D. Finally, the cycle shape did not have much effect on the evolution of body size (Figure 6.3E), indicating that the organisms are not very sensitive to the low resource densities experienced during the transition periods between good and bad seasons.

Figures 6.2 and 6.3 also show that, for the used set of parameter values, the evolutionary equilibrium of body size is always smaller than the adequate body size. This indicates that it is costly to be large, and it is better to break down structural biomass for paying maintenance in times of need. Of course, this only holds when breaking down biomass is not costly itself. If it would be more costly, the evolutionary equilibrium would shift in the direction of the (larger) adequate body size. This would, however, not lead to qualitatively different conclusions, as the curves of adequate body sizes follow those of the evolutionary equilibrium, though at a higher value. Yet, the population would become less sensitive to small amplitudes, and an evolutionary equilibrium would still exist at lower seasonalities.

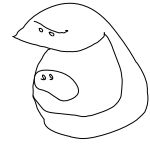
Temporal changes in seasonality and the body size response over time were



A



B



studied by means of two simulations. The pattern resulting from the first simulation (Figure 6.4) resembles very well the one observed in the fossil record of bushy-tailed woodrats from the Great Basin and Colorado Plateau, as studied by Smith et al. [54]. This body size response was attributed to (astronomically-triggered) climatic change (temperature) since the Last Glacial maximum [54]. Our results illustrate that these evolutionary patterns may as well be explained by changes in seasonality. We realize, however, that the forced change in seasonality used in the simulation, though based on [34], may be different from the actual seasonality as was experienced by the woodrats, as large local differences exist in seasonality patterns in the Great Basin and Colorado area [27]. Moreover, the influence of the retreating glacial sheet may not be neglected and does suggest a large role for temperature changes as well.

The Late Miocene simulation results (Figure 6.5) also fit the empirical observations of the rodent fossil record well. During the interval 9.6-9.2 million years ago, which is characterized by intermediate levels of seasonality without extreme winters or summers, body sizes attain lower values, as is shown by the decrease in tooth size. The continuation of smaller body sizes between 8.9-8.6 million years ago, shown in the empirical data, could be attributed to lower absolute levels of food due to smaller amplitudes of obliquity (Figure 6.5), as small obliquity values could have favoured high-latitude glaciation [56] and an overall more arid climate. This decrease is not shown in the simulated body size response, because changes in obliquity were not considered. Lower average temperature related to glaciation might also have contributed to a lower mean body size in this period.

As we expected on basis of the widespread recognition of climate cycles in sediments, cyclical patterns in body size are empirically observed indeed, e.g. in the fossil record of Miocene rodents (Figure 6.4a), in the fossil record of the woodrats mentioned above [54], and in the fossil records of Late Pleistocene and Holocene fossil rodents [24]. Our simulation results show that these cyclical patterns may be attributed to periodic changes in seasonality. However, the simulations also show that the peaks (largest and smallest values) of body size are not by definition reached at seasonality maxima and minima. On closer inspection, Figure 6.4 shows that seasonality does not correlate with the resulting body size, but rather with the *direction* of evolution. This is because

- ◁ Figure 6.5: A: Fossil teeth sizes of *Progonomys-Occitanomys* and *Hispantomys* lineages collected from fluvial and lacustrine sediments in Central Spain. Tooth size is a good estimator of body size. M1=first upper molar, M2=second, m1=first lower molar, m2=second lower molar. Data after [12]. B: Average body size (upper continuous curve) from 10 to 8 Myr ago, resulting from a simulation in which the seasonality (lower continuous curve) is varied according to the changes in precession in that period. The gray areas around the average size indicate the range of body sizes that are present simultaneously in the system.

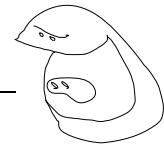
the organisms do not reach the predicted evolutionary end point immediately. Instead, they need time to evolve towards this equilibrium, and the direction of evolution has changed before they have reached it. This type of body size response, which is out of phase with seasonality, may be obtained only when the body size value at the evolutionary equilibrium increases sufficiently steeply with seasonality, such as is found here close at the tangent bifurcation point.

If the evolutionary equilibrium body size values increases less steeply with seasonality, evolution will be able to keep up with the changes in seasonality, and variations in body size and in seasonality will be in phase. When seasonality varies symmetrically around the bifurcation point, the body size response may be perfectly cyclical, and body size may be exactly the same at the beginning and end of each cycle. This is for instance the case in Figure 6.4, where the amplitude ϵ of the seasonal cycle was given the exact value of the bifurcation point. In case seasonality varies asymmetrically around the tangent bifurcation, body size response will also get a directional component. This is the case, for example, in Figure 6.5, where the organisms have a larger size at the end than at the beginning of the simulation. In this case, body size will only return at its start value when the system is reset, for example due to a mass extinction in which all larger organisms go extinct.

Please note that in this study we deliberately left out complex behaviors and adaptations such as hoarding and torpor to single out the effects of seasonality on body size. We realize, however, that these factors may affect the starvation rate considerably, and thus the evolutionary outcomes. Hence, it would be very interesting to extend our current model to include these factors and study their combined effects on the evolution of body size. This also holds for the adaptive change of allocation patterns [48, 50], which may lead to counter-intuitive results, such as why in some cases body size is not related to starvation time [28]. Other important factors include thermo-regulation, predation ability and vulnerability. These factors may, for example, lead to an evolutionary equilibrium of body size that exists also at small seasonalities.

References

- [1] Abdul Aziz, H., van Dam, J. A., Hilgen, F. J. and Krijgsman, W. (2004). Astronomical forcing in Upper Miocene continental sequences: implications for the Geomagnetic Polarity Time Scale. *Earth and Planetary Science Letters*, 222:243–258.
- [2] Adhton, K. G. (2001). Body size variation among mainland populations of the western rattlesnake (*Crotalus viridis*). *Evolution*, 55(12):2523–2533.
- [3] Bennett, K. D. (1997). *Evolution and ecology: the pace of life* Cambridge.
- [4] Benton (2002). *Encyclopedia of evolution*, chapter on Cope's rule, pages 209–210. Oxford University Press, Oxford, U.K.



- [5] Bergmann, C. (1847). Über die Verhältnisse der Wärmeökonomie der Thiere zu ihre Grösse. *Göttinger Studien*, 3:595–708.
- [6] Boyce, M. S. (1978). Climatic variability and body size variation in the muskrats (*Ondatra zibethicus*) of north america. *Oecologia*, 36:1–19.
- [7] Boyce, M. S. (1979). Seasonality and patterns of natural selection for life histories. *The American Naturalist*, 114(4):569–583.
- [8] Chown, S. L. and Klok, C. J. (2003). Altitudinal body size clines: latitudinal effects associated with changing seasonality. *Ecography*, 26(4):445–455.
- [9] Cohen, D. and Parnas, H. (1976). An optimal policy for the metabolism of storage materials in unicellular algae. *J. theor. Biol.*, 56:1–18.
- [10] Cope, E. D. (1896). *The primary factors of organic evolution*. The Open Court Publishing Company, Chigago.
- [11] Daams, R., Alcal, L., de los Angeles Sierra, M., Azanza, B., van Dam, J. A., van der Meulen, A. J., Morales, J., Nieto, M., Pelez- Campomanes, P and Soria, D. (1998). A stratigraphical framework for Miocene (MN4MN13) continental sediments of central Spain. *Comptes Rendus de l'Academie des Sciences Serie II A Sciences de la Terre et des Planetes*, 327:625–631.
- [12] van Dam, J. A. (1997) The small mammals from the upper Miocene of the Teruel-Alfambra region (Spain): paleobiology and paleoclimatic reconstructions. *Geologica Ultraiectina*, 156:1–204. PhD thesis.
- [13] van Dam, J. A., Alcal, L., Alonso Zarza, A., Calvo, J. P., Garcs, M. and Krijgsman, W. (2001). The upper Miocene mammal record from the Teruel-Alfambra region (Spain): the MN system and continental stage/age concepts discussed. *Journal of Vertebrate Paleontology*, 21:367–385.
- [14] van Dam, J. A. (2006). Geographic and temporal patterns in the late Neogene (12-3 Ma) aridification of Europe. The use of small mammals as paleoprecipitation proxies. *Palaeogeography, Palaeoclimatology, Palaeoecology* (in press).
- [15] Dickman, C. R., Mahon, P. S., Masters, P., and Gibson, D. F. (1999). Long-term dynamics of rodent populations in arid australia: the influence of rainfall. *Wildlife Research*, 26(4):389–403.
- [16] Dieckmann, U. (1997). Can adaptive dynamics invade? *Trends in Ecology and Evolution*, 12:128–131.
- [17] Dieckmann, U. and Law, R. (1996). The mathematical theory of coevolution: a derivation from stochastic processes. *J. Math. Biol.*, 34:579–612.
- [18] Dunsbrack, R. L. and Ramsay, M. A. (1993). The allometry of mammalian adaptations to seasonal environments - a critique of the fasting endurance hypothesis. *OIKOS*, 66(2):336–342.

- [19] Ferguson, S. H. (2002). The effects of productivity and seasonality on life history: comparing age at maturity among moose (alces alces) populations. *Global Ecology and Biogeography*, 11(4):303–312.
- [20] French, N. R., Stoddart, and Bobek, D. M. (1975). Patterns of demography in small mammal populations. In Golley, F. B., Petruszewicz, K., and Ryszkowski, L., editors, *Small mammals: their productivity and population dynamics*, pages 73–102. Cambridge University Press, Cambridge.
- [21] Geritz, S. A. H., Kisdi, E., Meszéna, G., and Metz, J. A. J. (1998). Evolutionarily singular strategies and the adaptive growth and branching of the evolutionary tree. *Evolutionary Ecology*, 12:35–57.
- [22] Geritz, S. A. H., van der Meijden, E. and Metz, J. A. J. (1999). Evolutionary dynamics of seed size and seedling competitive ability. *Theoretical Population Biology*, 55:324–343.
- [23] Geritz, S. A. H., Metz, J. A. J., Kisdi, É., and Meszéna, G. (1997). Dynamics of adaptation and evolutionary branching. *Physical Review Letters*, 78:2024–2027.
- [24] Hadly, E. A. (1997). Evolutionary and ecological response of pocket gophers (*Thomomys talpoides*) to late-Holocene climatic change. *Biological Journal of the Linnean Society*, 60: 277–296.
- [25] Hays, J. D., Imbrie, J. and Shackleton, N. J. (1976) Variations in the earth's orbit: Pacemaker of the ice ages. *Science*, 194, 1121–1132.
- [26] Hilgen, F. J. et al. (2000). Extending the astronomical (polarity) time scale into the Miocene. *Earth Planet. Sci. Lett.*, 136:495.
- [27] Hostetler, S., Giorgi, F., Bates, G. and Bartlein, P. (1994b). Lake-atmosphere feedbacks associated with paleolakes bonneville and lahontan. *Science*, 665-668.
- [28] Kirk, K. L. (1997). Life-history responses to variable environments: starvation and reproduction in planctonic rotifers. *Ecology*, 78(2):434–441.
- [29] Kooi, B. W. and Kooijman, S. A. L. M. (1999). Discrete event versus continuous approach to reproduction in structured population dynamics. *Theoretical Population Biology*, 56(1):91–105.
- [30] Kooi, B. W. and Kooijman, S. A. L. M. (1997). Population dynamics of rotifers in chemostats. *Nonlinear Analysis, Theory, Methods & Applications*, 30(3):1687–1698.
- [31] Kooi, B. W. and Troost, T. A. (2005). Advantages of storage in a fluctuating environment. Submitted to *Journal of Theoretical Population Biology*.
- [32] Kooijman, S. A. L. M. (1986). Energy budgets can explain body size relations. *Journal of Theoretical Biology*, 121:269–282.



- [33] Kooijman, S. A. L. M. (2000). *Dynamic Energy and Mass Budgets in Biological Systems*. Cambridge University Press.
- [34] Laskar, J., Robutel, P., Joutel, F., Gastineau, M., Correia, A. C. M. and Levrard B. (2004). A long-term numerical solution for the insolation quantities of the Earth. *Astronomy & Astrophysics*, 428:261–285.
- [35] van Leeuwen, I. M. M., Kelpin, F. D. L., and Kooijman, S. A. L. M. (2002). A mathematical model that accounts for the effects of caloric restriction on body weight and longevity. *Biogerontology*, 3(6):373–381.
- [36] Legendre, S. (1989). Les communautés de mammifères du Paleogene (Eocene supérieur et Oligocene) d'Europe occidentale: structures, milieux et évolution. *Munchner geowissenschaftliche Abhandlungen, (A)*, 16: 1–110.
- [37] Lehman, S. M., Mayor, M., and Wright, P. C. (2005). Ecogeographic size variations in sifakas: A test of the resource seasonality and resource quality hypotheses. *American Journal of Physical Anthropology*, 126(3):318–328.
- [38] Lima, M., Keymer, J. E., and Jaksic, F. M. (1999). El nino-southern oscillation-driven rainfall variability and delayed density dependence cause rodent outbreaks in western south america: linking demography and population dynamics. *The American Naturalist*, 153(5):476–491.
- [39] Lindsey, C. C. (1966). Body sizes of poikilotherm vertebrates at different latitudes. *Evolution*, 20:456–465.
- [40] Lindstedt, S. L. and Boyce, M. S. (1985). Seasonality, fasting endurance, and body size in mammals. *American Naturalist*, 125:873–878.
- [41] Madson, T. and Shine, R. (1999). Rainfall and rats: climatically-driven dynamics of a tropical rodent population. *Australian journal of ecology*, 24(1):80–89.
- [42] Mayr, E. (1956). Geographical charactergradients and climatic adaptation. *Evolution*, 10:105–108.
- [43] Mayr, E. (1963). *Animal species and evolution*. Harvard University Press, Cambridge, Mass.
- [44] Meiri, S., Dayan, T., and Simberloff, D. (2005). Biogeographical patterns in the western palearctic: the fasting-endurance hypothesis and the status of murphy's rule. *Journal of Biogeography*, 32:369–375.
- [45] Metz, J. A. J, Geritz, S. A. H. and Meszéna, G. and Jacobs, F. J. A and van Heerwaarden, J. S. Adaptive Dynamics, a geometrical study of the consequences of nearly faithful reproduction. In: van Strien, S. J. and Verduyn Lunel, S. M. (Eds.). *Stochastic and Spatial structures of dynamical systems*. KNAW Verhandelingen, Amsterdam, 1996 pp. 183–231.

- [46] Metz, J. A. J. and Geritz, S. A. H. and Nisbet, R. M. (1992). How should we define 'fitness' for general ecological scenarios? *Trends in Ecol. Evol.*, 7:198–202.
- [47] Milankovitch, M. (1941). Kanon der Erdbestrahlungen und seine Anwendung auf das Eiszeitenproblem. *Royal Serbian Academy, Spec. Publ.*, 133: 1–633.
- [48] Muller, E. B. and Nisbet, R. M. (2000). Survival and production in variable resource environments. *Bulletin of Mathematical Biology*, 62:1163–1189.
- [49] Olsen, P. E. and Kent, D. V. (1999). Long-period Milankovitch cycles from the Late Triassic and Early Jurassic of eastern North America and their implications for the calibration of the early Mesozoic time scale and the long-term behavior of the planets. *Phil. Trans. R. Soc. Lond. (A)*, 357, 1761–1784.
- [50] Parnas, H. and Cohen, D. (1976). The optimal strategy for the metabolism of reserve materials in micro-organisms. *J. theor. Biol.*, 56:19–55.
- [51] Peters, R. H. (1983). *The Ecological Implications of Body Size*. Cambridge University Press, New York.
- [52] Predavec, M. (1994). Population-dynamics and environmental changes during natural irruptions of Australian desert rodents. *Wildlife Research*, 21(5):569–582.
- [53] Shertzer, K. W. and Ellner, S. P. (2002). Energy storage and the evolution of population dynamics. *J. theor. Biol.*, 215:183–200.
- [54] Smith, F. A., Betancourt, J. L., and Brown, J. H. (1995). Evolution of body size in the woodrat over the past 25,000 years of climate change. *Science*, 270:2012–2014.
- [55] Tuenter, E. (2004). *Modeling Orbital induced variations in circum-Mediterranean climate*. PhD thesis.
- [56] Westerhold, T., Bickert, U., and Rohl, U. (2005). Middle to late Miocene oxygen isotope stratigraphy of ODP site 1085 (SE Atlantic): new constraints on Miocene climate variability and sea-level fluctuations. *Palaeogeogr., Palaeoclim., Palaeoecol.*, 217: 205–222.
- [57] Wigginton, J. D. and Dobson, F. S. (1999). Environmental influences on geographic variation in body size of western bobcats. *Canadian Journal of Zoology*, 77(5):802–813.



7

General Discussion

In this thesis, the evolution of community metabolism was studied by application of AD theory [1, 2, 4, 8] to models based on DEB theory [6, 7, 9]. In Chapters 2 to 4 a model was used that deals with a population of mixotrophic organisms, which could specialize into different trophic functions (autotrophic or heterotrophic assimilation). In Chapters 5 and 6 a model was used that deals with a size-structured population of which the (purely heterotrophic) organisms could evolve towards different body sizes. Variations were made on both the mixotrophy model and the size-structured model by including two, instead of one, adaptive traits (Chapter 2 and 5) and by considering a heterogeneous instead of a homogeneous environment (Chapters 4 and 6).

In this final chapter, the differences between these two models and model variations are discussed, and the implications of these differences to the modeling of realistic evolutionary communities. First the differences with respect to the approach to specialization are discussed, as well as how these differences affect the possibilities to define realistic trade-offs (Section 7.1). Then, differences in system structure and scope are discussed, and how these differences relate to the difference in approach to specialization (Section 7.2). In Section 7.3, differences in the considered number of adaptive traits and in the shape of the trade-offs are discussed, and the consequences for the resulting community structure. Finally, in Section 7.4, results are summarized, and possibilities for improving evolutionary community models are discussed.

7.1 Specialization into and within functional groups

One of the essential differences between the population in the mixotrophy model (used in Chapters 2 to 4) and that in the size-structured model (used in Chapters 5 to 6) is their potential for specialization. The mixotrophic organisms are capable of specialization *into* trophic functions, which will lead to various functional groups (autotrophs and heterotrophs). In contrast, the size-structured population is capable of specialization *within* a trophic func-

tion, which will lead to diversity within a functional group (heterotrophs of different body sizes).

A problem in evolutionary community models is that all physiological functions, traits and trade-offs need to be defined beforehand. Therefore, the organisms cannot acquire any new trophic functions during the evolutionary process; all potential material pathways and the maximum number of pure species (species that are fully specialized on one trophic function) are already known from the start. This sets boundaries to the system's development, especially when focusing on specialization into different trophic functions: new pure populations or species will only arise as long as their trophic pathways allow for it; though new substrates or (waste) products of the existing populations may be added to the system, these cannot be utilized unless the required function was defined already in the primary population or species. This is illustrated by Figure 7.1, which shows a diagram of the begin stage and a possible end stage of the mixotrophy model system.

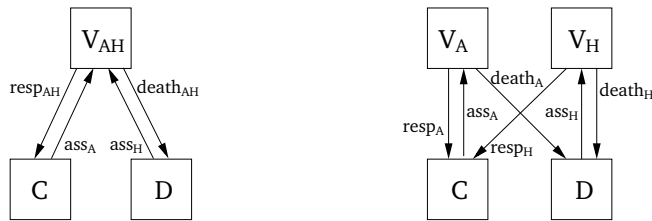


Figure 7.1: Schematic representation of the mixotrophy model at the beginning (left) and end of its development (right). The mixotrophy model consists of two substitutable carbon substrates, DIC (C) and detritus (D); the mixotrophic population (V_{AH}) is capable of both assimilatory pathways, while the specialized populations (V_A and V_H) are capable of either of these.

In the size-structured model, that focuses on specialization *within* a functional group, again various substrates are available, but now all are used by the same metabolic function, in this case heterotrophic assimilation. The modeling advantage of this approach is that only one physiological mechanism (or set of mechanisms) is involved in the evolutionary process. As a result, new populations or species may arise as long as new substrates become available, for which no additional physiology, traits, or trade-offs are required. Figure 7.2 shows the possible development of a size structured system with three substrates. This system is a schematic representation of the model system studied in Chapter 5, where prey with a range of sizes were available as substrate.

This approach allows for even more flexibility in community development when the organisms themselves act as a substrate to other organisms, resulting

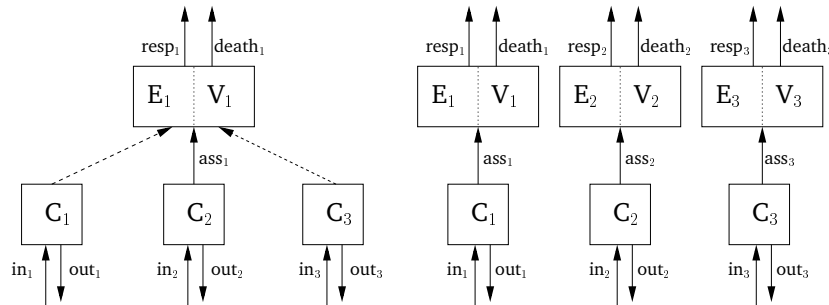


Figure 7.2: Schematic representation of a size-structured model at the beginning (left) and end of its development (right). In this model, three substrates of different sizes C_i are present; the organisms in each population have a different size, and consist of an energy reserve (E_i) and structural biomass (V_i). Dashed arrows indicate weak or non-existing links.

in predation among predators. In this case, each new population will form a new substrate and, in theory, the system may endlessly develop more populations and more trophic levels. A diagram of such a development is shown in Figure 7.3. Predation among predators was briefly studied in Section 5.5.3.

Another difficulty of specialization into trophic functions is the formulation of the trade-offs. This is because the involved physiological mechanisms involved with these functions do not directly interfere with the other, such that they may operate in parallel. Therefore, interactions between trophic functions are mainly indirect and often far from clear. This results in trade-off functions that are either based on unknown mechanisms, or not based on mechanisms at all. In either case, a more or less arbitrary trade-off will result. Yet, these trade-off functions are very important, as they largely determine the outcome of the evolutionary process (see Section 7.3). The often used rationale behind simple trade-off functions, stating that energy can only be spent once, does not hold for trade-offs between trophic functions, because trophic functions yield, rather than cost, energy. The large number of symbionts illustrates that in some cases a trade-off may not even exist, and it suggests that the separation of functions between species may sometimes have a phylogenetical or environmental origin rather than one related to physiological or morphological trade-offs.

In contrast, when studying specialization within a trophic function, the trade-off lies within one trophic function and can be derived on basis of more specific and concrete mechanisms. For example, when the involved machinery can process only one resource item at a time and parallel handling is thus impossible, a trade-off arises automatically due to differences in handling times and energy yields of the various prey items that lead to differences in their prof-

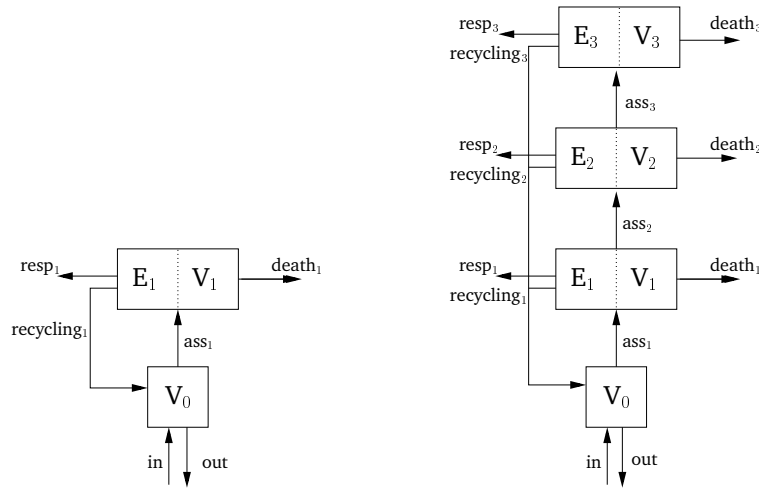


Figure 7.3: This size-structured model considers predation among predators, i.e. the predators themselves can act as prey; at death, the energy reserves (E_i) are recycled into the basal substrate (V_0).

itability. Though a trade-off within a trophic function is thus more easily found, an often encountered problem is that, in many of the studied systems, the most obvious trade-off is a linear one. This will not lead to interesting results like intermediate trait values or multiple coexisting populations (see Section 7.3).

7.2 System structure

The approach to specialization discussed above is closely related to the system scope and structure. This applies in particular to the system boundaries, which can be open or closed. The mixotrophy system, for example, includes both autotrophic and heterotrophic functions that enable a full carbon recycling (see Figure 7.1). In nature, fluxes involved in the carbon recycling take place over large spatial (maybe even global) scales and large (evolutionary) time scales. Considering the mixotrophy system closed for mass is in correspondence with these large scales and the complete material cycling. Note that the system is still open for energy (light), which is necessary to keep it from its thermodynamic equilibrium. The size-structured system, in contrast, considers specialization only within the scope of heterotrophic assimilation. Hence, the system can represent only part of an ecosystem and relies on other subsystems to perform complementary functions like autotrophic assimilation. Though recycling processes may be taken into account (see Figure 7.3), these are not expected to result in full material recycling. Hence, considering the size-structured system



to be open for mass is required by its smaller scope and incomplete recycling.

It was found that opening a system for mass affects its evolutionary outcomes. In Chapter 2 it was shown that, in a closed system, the evolutionary outcomes are determined only by parameter values that are intrinsic to the organisms, such as physiological constants; system properties such as the total nitrogen content or incoming light intensity do not have any effect. This is changed when the system is opened for mass; in that case the trait values at the singular strategies come to depend on boundary fluxes as well.

Another system property that was found to affect evolution, is environmental heterogeneity. As was shown in Chapter 4, a spatial gradient facilitates evolutionary branching by creating locally different environments (habitats). Obviously, different habitats allow for niche differentiation, which is an important source of biodiversity. Spatial heterogeneity of the environment was also found to affect the role of other system properties, such as mixing intensity and total nitrogen content. These properties could acquire effect on the evolutionary outcomes through their effect on the spatial gradient. Besides spatial heterogeneity, also temporal heterogeneity may exist. The evolutionary analysis of temporal heterogeneity, however, requires very different techniques (Floquet theory) and was studied in Chapter 6.

Environmental heterogeneity not only affects the evolutionary outcomes, but also the *process* of evolution. It facilitates evolutionary branching by locally increasing the density dependence [3]. A similar argument probably holds for closing the system for mass. In a closed system, the effects of density dependence are not diluted (literally) by the in- or outflux of material. Therefore, closing the system for mass is also expected to facilitate evolutionary branching.

7.3 Adaptive traits and trade-offs

Two other factors that were found to play important roles in the evolutionary outcomes of the community models, are the number of adaptive traits and the precise shape of the trade-off function. The number of adaptive traits determines the dimensionality of the trait space, and therefore the ‘potential’ of the resulting community in terms of network structure. In case of a one-dimensional trait space, the community structure will at best evolve to a food *chain*. With a two- or more dimensional trait space it may evolve to a more complex and realistic food *web*. Food chains are characterized by a linear hierarchy, in which the ranking of the organisms can be expressed by a single value; food chains only have integer trophic levels. In contrast, in food webs the notion of ‘trophic level’ is replaced by ‘trophic position’ which may take any value and form a continuum [11]. Also, the hierarchy in food webs is often ambiguous, because species are characterized by two or more traits, and different rankings result when based on either of these.

Note that the dimensionality of the trait space is determined only by the ‘effective’ number of adaptive traits, for which only the number of independent

traits counts. Independent traits are not coupled or traded off with other traits, directly nor indirectly. An *indirect trade-off* is used in the mixotrophy model in Chapter 2, where the adaptive trait values for autotrophic and heterotrophic affinity are traded off through a cost function. An example of a *direct trade-off* is used in the mixotrophy system in Chapters 3 and 4, in which the two affinities for autotrophic and heterotrophic assimilation were assumed to add up to unity, such that they could be represented by a single trait value. An example of an *indirect coupling* is present in the size-structured system used in Chapter 5, where the organisms are characterized by their prey-size preference and their body size; these two traits are indirectly coupled by the functional response. A *direct coupling* between two traits exists when their mutation distributions are covariant. An example of complete covariance is present in for instance the model of Loeuille and Loreau [10], in which the prey-size preference of the predator is determined directly by its size, such that the predator-prey size ratio is fixed.

Indirect or direct trait dependencies decrease the dimensionality of the system. They may reduce the system structure from a true food web into a set of overlapping food chains and, in case of complete dependency, into a true food chain. An example of a model that considers two totally independent traits is that of Ito and Ikegami [5], which results in rather complex community structures indeed. However, the two traits that they considered are related to the organism's ability and vulnerability to predation, and the assumption that the two traits are totally independent is not very realistic.

While the number of traits determines the potential of the resulting network structure, the shape of the trade-off functions largely determine the number of populations to which the system may actually evolve. For a linear trade-off function, in most cases only one population will result with a trait value at one of the boundaries or extremes of the trait space. For a non-linear trade-off function, the result is determined by the precise shape of this function. Concavely curved trade-off functions will often lead to one population at an intermediate trait value, while convexly curved trade-off functions may lead to two populations each at one of the extremes of the trait space. More complexly curved trade-off functions may lead to more than two populations, which trade-offs may arise from functions with multiple peaks, such as polynomials of higher degrees. Also, more complexly curved shaped trade-off curves may arise from a bounded trait space, or from an indirect trade-off. In these cases, however, the requirements for evolutionary branching may become more complicated as well (Chapter 2).

7.4 Conclusions

In this thesis, the evolution of community metabolism was studied. Many factors were found to influence the evolutionary process and outcomes of model communities. One of the most important was found to be the choice for specialization into functional groups (as in the mixotrophy model) or within a func-



tional group (as in the size-structured model). Focusing on different trophic functions may lead to complete ecosystems that include various functional groups, but such models are limited in the flexibility of their development. In contrast, models focusing on specialization within a functional group have a smaller scope, but are more flexible in their development. Also, the trade-off between trophic functions is often indirect or may not even exist, which leads to complex requirements for, or intrinsic disadvantages to specialization, while within a trophic function, more concrete and direct trade-offs may exist.

Environmental heterogeneity was found to overrule intrinsic disadvantages to specialization by creating locally different environments. This suggests that environmental heterogeneity is an important cause of specialization, especially in case of specialization into trophic functions. Heterogeneity also leads to an advantage for having energy reserves, which has large implications for body size as well. Other important factors were found to be the number of adaptive traits and the shape of the trade-off functions. The number of traits determines the network potential, while the shape of the involved trade-off functions largely determine the number of populations that will actually result. Opening the system for mass will provide the boundary fluxes with influence on the evolutionary outcomes; in closed systems only intrinsic properties will be of importance.

Unsurprisingly, including more realism in evolutionary community models considerably complicates the evolutionary analysis. Because DEB models consist of two state-variables for each population and an explicitly formulated environment, analytical solutions are often not available. Introducing, on top of that, an indirect and physiologically-based trade-off, a two-dimensional trait space, or heterogeneities in the environment made the analysis even more difficult. The models had to be simplified in various ways (Sections 1.2.1 and 1.3.2), and bifurcation techniques had to be applied to analyze the models (Chapter 3). Fortunately, DEB models are well suitable for analysis by bifurcation techniques, because unrealistic switches are avoided, for example by using synthesizing units (instead of Liebig's law) to model simultaneous substrate limitation, which avoids switches hampering the application of bifurcation techniques (see Section 3.2.1).

Despite of all the realistic features that were studied, the resulting communities remained unrealistically simple. Even at the end of their development, most model systems consisted of only two or three populations, while in natural systems the number of populations is enormous. Though some comparisons with real data could be made, this discrepancy hampered a large-scale testing of the evolutionary outcomes resulting from the models with the community structure and functioning of real world (eco)systems. Although experiments allow for isolation of simple (sub)systems, the studied evolutionary outcomes are not suitable for testing in experimental set ups either. Not only would the evolutionary time scale require extremely long experimental duration, also would it be difficult to induce evolution specifically in the traits under investigation.

The models should thus be improved in order to lead to larger number of

populations with a more complex network structures, such that a better comparison with real ecosystems could be made. This could be done by considering multiple adaptive traits that are totally independent, or by defining well-chosen convexly curved trade-offs between these traits, both almost certainly leading to (a series of) evolutionary branching events, and thus to an increased biodiversity and complex network structures. However, the resulting models can hardly be considered realistic, even though some of their parts may be process-based, if such important parts like the trade-offs are not.

Alternatively, more realistic and complex ecosystem structures could evolve from models in which various realistic features are combined. These models should then allow for specialization both into and within trophic functions, include both temporal and spatial heterogeneities, and they should, besides evolutionary processes, also include processes that allow for qualitative changes of community structure on ecological time scales, such as migration and phenotypic plasticity. Even with all these realistic features, evolutionary branching events are not guaranteed. Apart from the fact that realistic process-based trade-offs between trophic functions are difficult to find, the resulting trade-offs will often be indirect and complexly shaped, such that evolutionary branching will occur only under very specific conditions or parameter values. On the other hand, linear trade-offs will not lead to evolutionary branching either. Even when seemingly realistic food web structures would result, these models would be very difficult to analyze, because of their very complexity.

A solution to this problem, as was also employed in the second part of this thesis (Chapters 5 and 6), is to focus first on *subsystems*, and thus on specialization within a trophic function (producers, consumers, detritivores, etc). Though the resulting models systems have a smaller scope and are not capable of a full material recycling, the underlying dynamics and trade-off functions can be fully based on physiological mechanisms. Of course, combining these various subsystems into a full ecosystem model will not be easy either. Therefore, modeling the community metabolism of complete and evolutionary ecosystems still remains a challenge.

References

- [1] Dieckmann, U. (1997). Can adaptive dynamics invade? *Trends in Ecology and Evolution*, 12:128–131.
- [2] Dieckmann, U. and Law, R. (1996). The dynamical theory of coevolution: a derivation from stochastic ecological processes. *Journal of Mathematical Biology*, 34:579–612.
- [3] Doebeli, M. and Dieckmann, U. (2003). Speciation along environmental gradients. *Nature*, 421:259–264.



- [4] Geritz, S. A. H., Metz, J. A. J., Kisdi, É., and Meszéna, G. (1997). Dynamics of adaptation and evolutionary branching. *Physical Review Letters*, 78:2024–2027.
- [5] Ito, H. C. and Ikegami, T. (2006). Food-web formation with recursive evolutionary branching. *Journal of theoretical Biology*, 238:1–10.
- [6] Kooijman, S. A. L. M. (2000). *Dynamic Energy and Mass Budgets in Biological Systems*. Cambridge University Press.
- [7] Kooijman, S. A. L. M. (2001). Quantitative aspects of metabolic organization; a discussion of concepts. *Phil. Trans. R. Soc. B*, 356: 331 - 349.
- [8] Metz, J. A. J. and Geritz, S. A. H. and Meszéna, G. and Jacobs, F. J. A. and van Heerwaarden, J. S. Adaptive Dynamics, a geometrical study of the consequences of nearly faithful reproduction. In: van Strien, S. J. and Verduyn Lunel, S. M. (Eds.). *Stochastic and Spatial structures of dynamical systems*. KNAW Verhandelingen, Amsterdam, 1996 pp. 183–231.
- [9] Nisbet, R. M. and Muller, E. B., and Lika, K. and Kooijman, S. A. L. M. (2000). From molecules to ecosystems through dynamic energy budget models. *J. Anim. Ecol*, 69: 913 - 926.
- [10] Loeuille, N. and Loreau, M. (2005). Evolutionary emergence of size-structured food webs. *PNAS*, 102(16):5761–5766.
- [11] Pahl-Wostl, C. (1997). Dynamic structure of a food web model: comparison with a food chain model. *Ecological Modelling*, 100:103–123.



Summary

The aim of this thesis was to include more realism in evolutionary community models. This was done by combining Adaptive Dynamics theory with models based on Dynamic Energy Budget theory, and by including various realistic features, such as multiple adaptive traits, and inhomogeneities in time and space.

At first, specialization into different trophic functions was studied. The process of specialization into different trophic functions may correspond to the development of a simple (single-species) community into a more complex (multiple-species) community. To study this process, a model of a population of mixotrophic organisms was used. Mixotrophs are capable of both autotrophy and heterotrophy, i.e., they can use both inorganic and organic carbon as a material and energy source. The mixotrophs were considered to have two adaptive traits, representing the organism's affinities for the autotrophic and heterotrophic assimilatory pathway. Evolution in these two traits enabled the organisms to specialize in autotrophic and heterotrophic assimilation. It was then studied under which conditions the population would split into two populations, an autotrophic one in which the organisms have lost their abilities for heterotrophy, and an heterotrophic one in which the organisms have lost their abilities for autotrophy. This specialization process is referred to as 'evolutionary branching', and provides the system with a means for autonomously increasing its biodiversity.

It was found that the occurrence of evolutionary branching was largely determined by the way the two adaptive traits are traded off. In many evolutionary modeling studies, simple, direct, and convex-shaped trade-offs are assumed that will guarantee evolutionary branching. However, simple and direct trade-offs do not always exist, especially between two different trophic functions. Therefore, in the mixotrophy model, an indirect and physiologically-based trade-off function was used. This trade-off function was based on costs and benefits that are involved with having a high affinity for either or both autotrophy and heterotrophy. It was found that such an indirect trade-off function complicates the requirements for evolutionary branching considerably. Also, the shape of the trade-off curve was greatly affected by the constraints on the trait values. As a result, only at intermediate cost levels and when an explicit advantage to pure strategies existed, would evolutionary branching occur. These results suggest that specialization of mixotrophs into separate autotrophs and

heterotrophs in particular, and specialization into different trophic functions in general, is not a common event.

Initially, the mixotrophy system was assumed to be homogeneous and closed for mass. As a result, environmental properties such as the total nutrient content did not have any effect on evolution. In order to study more closely the role of environmental factors on the evolutionary outcomes, the mixotrophs were placed in a spatially heterogeneous environment, a mixed water column with a light-intensity gradient. It was found that a spatial heterogeneity facilitated the process of ecological specialization by providing locally different environments (habitats). Furthermore, it was found that environmental properties could also acquire influence on evolution, through their effect on the spatial gradient. As such, the organism's intrinsic disadvantage to specialization could be overcome at intermediate mixing and high nutrient contents. This makes environmental heterogeneity a very important factor for inducing specialization, especially in case of specialization into different trophic functions, where indirect or non-existing trade-offs create complex requirements or intrinsic disadvantages to evolutionary branching. Furthermore, the model provided a new explanation for why mixotrophs are often more dominant in oligotrophic waters, while specialist strategies are associated with eutrophic systems.

In the second part of the thesis, (Chapters 5 and 6) focus was shifted from specialization *into* trophic functions, to specialization *within* a trophic function. In this case, evolution allowed the organisms to specialize, not by increasing or decreasing the ability or affinity for a certain metabolic pathway, but by increasing the affinity of a given pathway for one or another substrate. The advantage of this approach is that the system's development is much more flexible, and that a mechanistic and realistic trade-off is more easily derived.

For studying specialization within a function, I focused on body size as the main adaptive trait. Body size is an obvious and important morphological property with many functional and physiological implications. Differences in body size are associated with differences in scale of time and space in which the organisms live, and they reflect differences in physiological processes and life histories. From the basic assumptions of DEB theory various body-size scaling relationships can be derived and understood, which makes this modeling framework very suitable for studying body-size related processes.

For studying evolution of body size, a predator-prey model was used in which the predators had an adaptive body size. Predator body size, together with its prey-size preference, determine which predator-prey size combinations are established, and thus largely define the structure of a community. Therefore, we studied the joint evolution of these two traits. The resulting model could explain various empirical observations, such as the triangular distribution of predator-prey size combinations, the island rule, and the difference in predator-prey size ratios between filter feeders and raptorial feeders. The model also revealed key factors for the evolution of predator-prey size ratios. Capture mechanisms turned out to have a large effect on this ratio, while prey-size availability and competition for resources only help explain variation in



predator size, not variation in predator-prey size ratio. Furthermore, predation among predators was identified as an important factor. Together, these factors explained a wide range of predator-prey size ratios, and thus provided insight in the complex community structures found in nature.

As the environment was again considered to be homogeneous in space and time, the energy reserves formed a burden rather than a profit to the organisms involved, slowing down their reproduction rates. This, of course, does not do justice to the important role of reserves in the real world. Therefore, a temporal fluctuation was introduced in the incoming resource densities, and the effects on the evolution of body size were studied. It was found that the evolutionary body size increases with increasing variability of the environment. As such, it is the first model to support the 'seasonality hypothesis'. This hypothesis states that variable climates, characterized by large annual cycles, select for large body sizes. This result emphasizes the importance of basing model dynamics on physiological processes. Simulations across geological time scales illustrated that evolutionary patterns in body size may be a response to temporal variability in seasonality related to the Milankovitch cycles.

In summary, the results presented in this thesis show the impact of various realistic factors on the evolution of community metabolism. In the last chapter it is argued that these factors are all linked to each other, and to the choice for studying specialization into or within a trophic function. It is concluded that, to result in the complex community structures as are observed in nature, one should probably combine various of these factors into one model. This, however, will be very difficult, and it is suggested that we better focus first on small subsystems. Of course, combining several of these subsystems into a full ecosystem model will not be easy either. Therefore, modeling the community metabolism of complete and evolutionary ecosystems still remains a challenge.



Samenvatting

De natuur bestaat niet uit een verzameling van losse soorten, maar uit groepen soorten die elkaar helpen, tegenwerken of opeten. Deze groepen soorten vormen dus levensgemeenschappen. De opbouw of 'structuur' van zo'n gemeenschap wordt grotendeels bepaald door het aantal soorten en het type interacties dat zij onderling aangaan. Deze structuur is belangrijk voor het functioneren van de gemeenschap als geheel. Het bepaalt bijvoorbeeld of een gemeenschap met veranderingen of verstoringen kan omgaan.

De structuur van de levensgemeenschap staat niet vast, maar kan veranderen. Soorten kunnen bijvoorbeeld veranderen, maar er kunnen ook soorten bijkomen of juist uitsterven. Een belangrijk proces dat bij dergelijke veranderingen een rol speelt is evolutie. Evolutie kan namelijk leiden tot de aanpassing van soorten, maar soms ook tot het ontstaan van totaal nieuwe soorten.

Evolutionaire processen zijn over het algemeen erg langzaam en vinden dus plaats over lange tijdschalen. Daardoor lijkt het soms of er helemaal niets verandert en lijkt ook de structuur van levensgemeenschappen vaak constant. Mede hierdoor wordt ook in veel van de wiskundige modellen, die van biologische levensgemeenschappen gemaakt worden, de structuur van de gemeenschap vaak als onveranderlijk beschouwd. In de praktijk betekent dit dat er van te voren wordt vastgelegd hoeveel soorten er aanwezig zijn in het modelstelsel, en welke eigenschappen deze soorten precies hebben. Toch kunnen de veranderingen in de gemeenschapsstructuur juist erg belangrijk zijn. Dit is met name het geval als er sprake is van langdurige processen, zoals bijvoorbeeld bij klimaatsveranderingen, bij het nemen van maatregelen voor natuurbeheer of bij het duurzaam exploiteren van natuurlijke bronnen.

In dit proefschrift staan de veranderingen van levensgemeenschappen centraal. Deze veranderingen worden bestudeerd met behulp van wiskundige modellen, waarin evolutionaire processen worden nagebootst. Er bestaan al wel andere modelstudies over de evolutie van biologische gemeenschappen, maar daarin wordt over het algemeen gebruik gemaakt van erg eenvoudige modellen die de complexe biologische en fysiologische processen in de natuur niet goed omvatten. Zulke eenvoudige modellen kunnen daardoor leiden tot onrealistische resultaten. Vaak wordt er in deze modellen ook slechts rekening gehouden met een enkele eigenschap of strategie die kan evolueren, terwijl in werkelijkheid vele eigenschappen tegelijkertijd kunnen evolueren. Tevens wordt er meestal een eenvoudig verband verondersteld tussen de kosten en

baten van een strategie of eigenschap. In het echt is dit verband vaak veel ingewikkelder. Ten slotte wordt er over het algemeen van uitgegaan dat de model-organismen leven in een sterk vereenvoudigde omgeving. Zo'n leefomgeving is overal hetzelfde (homogeen), terwijl in de natuur de leefomgeving plaatselijk of tijdelijk juist heel erg kan verschillen (heterogeen).

In dit proefschrift wordt er meer realisme in de modellen gebracht, en wordt er bestudeerd wat het effect hiervan is op de evolutie van de levensgemeenschappen. Dit wordt onder andere gedaan door de modellen te baseren op de zogenaamde Dynamic Energy Budget (DEB) theorie. Dit is een modelleerraamwerk, waarmee de groei en voortplanting van vrijwel elke soort kan worden gemodelleerd. De theorie bestaat uit fysiologische regels voor voedsel opname en verwerking, die voortkomen uit een beperkt aantal aannames.

Naast de DEB theorie wordt gebruik gemaakt van de Adaptive Dynamics (AD) theorie. Deze theorie helpt bij het analyseren van evolutionaire processen. In tegenstelling tot andere methodes om evolutionaire processen te analyseren, houdt AD theorie rekening met een aantal realistische factoren, waaronder dichtheidsafhankelijkheid (de optimale strategie ligt niet vast, maar hangt af van wat soortgenoten doen) en de bereikbaarheid van de strategie (evolueert de soort wel naar de optimale strategie toe?).

Naast het combineren van DEB theorie en AD theorie, wordt er ook meer realisme in de levensgemeenschaps-modellen gebracht door meerdere eigenschappen tegelijkertijd te laten evolueren. Tevens zijn de kosten- en batenfuncties realistischer gemaakt, door deze te baseren op fysiologische processen. Ten slotte worden ook de effecten van een heterogene (en dus realistischere) leefomgeving bestudeerd.

In het eerste deel van het proefschrift ligt de focus op specialisatie tussen 'trofische functies'. Trofische functies zijn de ecosysteem processen die de organismen in het systeem uitvoeren, of de interactie die zij hebben met dergelijke processen. Voorbeelden van trofische functies zijn fotosynthese, respiratie of stikstofomzetting, maar in dit proefschrift bestudeer ik 'autotrofie' en 'heterotrofie'. Autotrofe organismen kunnen (zoals de meeste planten) zelf organisch materiaal aanmaken uit zonlicht; heterotrofe organismen (de meeste dieren) kunnen zelf geen organisch materiaal maken, maar moeten dat binnen halen door het eten van andere planten of dieren.

Het model wordt opgestart met één enkele soort van organismen die zowel autotroof als heterotroof zijn, ook wel 'mixotrofen' genaamd. Feitelijk kunnen deze organismen dus alles zelf (zowel het aanmaken van organisch materiaal als het omzetten ervan) en hebben ze dus geen andere soorten voor het vervullen van deze trofische functies. Mixotrofie komt vrij veel voor, met name in algen, ookal is dat niet algemeen bekend.

De mixotrofen in het model hebben twee evolutionaire eigenschappen, één die bepaalt hoe goed de organismen zijn in autotrofie en de andere die bepaalt hoe goed ze zijn in heterotrofie. Door middel van evolutie in deze twee eigenschappen kunnen de mixotrofen zich gaan specialiseren in één of in beide trofische functies. Zo kan er de speciale situatie ontstaan waarbij de mixotrofe soort zich opsplijt en er twee aparte soorten ontstaan, een die helemaal auto-



troof is en een die helemaal heterotroof is. Zo'n evolutionaire splitsing wordt in het Engels 'evolutionary branching' genoemd en geeft de levensgemeenschap de kans om het aantal soorten te vergroten en zo zijn structuur aan te passen.

Het al dan niet plaatsvinden van een dergelijke evolutionaire splitsing hangt grotendeels af van de precieze kosten en baten die zijn verbonden aan de evolutionaire eigenschappen. In het geval van de mixotrofen zijn deze kosten en baten gebaseerd op fysiologische processen, waardoor ze ingewikkelder uitpakken dan vaak het geval is in evolutionaire modellen. Het blijkt dat een evolutionaire splitsing hierdoor alleen onder zeer specifieke fysiologische omstandigheden voor kan komen, en alleen als het fysiologisch gezien voordelig is. Deze resultaten suggereren dus dat specialisatie van mixotrofen in aparte auto- en heterotrofen niet voor de hand ligt. In iets algemenere bewoordingen zou gesteld kunnen worden dat specialisatie tussen trofische functies niet vaak voor zal komen. Dit zou een verklaring kunnen vormen voor het feit dat er in de natuur zoveel mixotrofen voorkomen, maar bijvoorbeeld ook dat er zoveel symbionten bestaan. Symbionten zijn organismen van twee verschillende soorten die nauw met elkaar samenwerken, door beide een verschillende trofische functie uit te voeren. Deze symbionten zijn vaak zodanig met elkaar verbonden, dat zij feitelijk één organisme vormen. Bekende voorbeelden van symbionten zijn korstmossen en koralen.

In eerste instantie (en zoals in de meeste modellen) is uitgegaan van een eenvoudige, homogene omgeving. Daardoor hebben omgevingseigenschappen (zoals de totale hoeveelheid voedingsstoffen in het systeem) totaal geen effect op de evolutie van het systeem. Om het effect van een meer realistische, heterogene omgeving te bestuderen, zijn de mixotrofen vervolgens in een (virtuele) waterkolom geplaatst. In deze waterkolom dringt aan de oppervlakte veel licht door, maar wordt het naar beneden toe steeds donkerder. Het blijkt dat een dergelijke licht-gradiënt het evolutionaire proces in gang kan zetten. Dat komt omdat de leefomgeving op sommige plekken (nabij de oppervlakte) gunstiger is voor autotrofen, en op andere plekken (nabij de bodem) gunstiger is voor heterotrofen. Dankzij de heterogeniteit van de omgeving kan een evolutionaire splitsing dus ook plaatsvinden als er niet aan de bovengenoemde fysiologische voorwaarden wordt voldaan. Kortom, een heterogene leefomgeving speelt een erg belangrijke rol bij specialisatie. Dit is met name het geval bij specialisatie tussen verschillende trofische functies, waar vaak geen duidelijk fysiologisch voordeel, maar eerder een nadeel hangt aan het specialiseren in een van die functies. Tevens kan het model verklaren waarom mixotrofen veel voorkomen in voedsel-arme omgevingen, en minder in voedselrijke omgevingen.

In het tweede gedeelte van dit proefschrift is de focus verlegd van specialisatie *tussen* trofische functies naar specialisatie *binnen* trofische functies. Ik heb me hierbij niet meer gericht op mixotrofen die zich splitsen in auto- en heterotrofen, maar op heterotrofe organismen die zich specialiseren op verschillende prooien. Hierbij is lichaamsgrootte gekozen als de belangrijkste evolutionaire eigenschap. Lichaamsgrootte is een in het oog springende en belangrijke eigenschap, die gekoppeld is aan veel fysiologische processen. Grote diersoorten hebben bijvoorbeeld een langzamere hartslag, ze leven over het algemeen lan-

ger, hebben grotere territoria en ze hoeven minder frequent te eten. Lichaams-grootte speelt een belangrijke rol in de DEB theorie en de theorie verklaart veel van de waargenomen relaties tussen lichaamsgrootte en fysiologie. Dit maakt de theorie bij uitstek geschikt voor het modelleren van evolutionaire veranderingen in lichaamsgrootte.

Eerst is de relatie tussen de grootte van een predator (roofdier) en een prooi bestudeerd. Immers, de grootte van een predator en zijn voorkeur voor een bepaalde prooi-grootte bepalen grotendeels de structuur van een levensgemeenschap. Er wordt hiervoor een model gebruikt met prooien van verschillende (maar vaste) lichaamsgroottes, en met een predator waarvan de lichaamsgrootte kan evolueren. Het resulterende model kan verschillende fenomenen verklaren, zoals bijvoorbeeld waarom een predator meestal groter is dan zijn prooi (maar niet altijd) en het fenomeen dat op eilanden grote soorten kleiner worden (en kleine soorten juist groter). Het model laat ook zien dat er verschillende typen factoren bestaan, die allemaal een ander effect op predator-grootte en prooikeuze hebben. Samen kunnen deze factoren leiden tot de complexe levensgemeenschappen zoals die in de natuur voorkomen.

In deze predator-prooi studie is opnieuw uitgegaan van een homogene omgeving. In zo'n gelijkmatige omgeving zijn energie reserves vrijwel niet nodig, en vormen ze eerder een last dan een voordeel. Dat komt omdat er overal en altijd evenveel voedsel voorhanden is en het dus niet nodig is om een voorraad aan te leggen. Ook nu wordt er weer een heterogeniteit in het model ingebouwd. Dit keer niet een ruimtelijk verloop (zoals bij de licht-gradiënt), maar een fluctuatie in de tijd (verschillend voedselaanbod in de verschillende seizoenen). Het blijkt dat de hoeveelheid energie reserve en de daaraan verbonden lichaamsgrootte toenemen met de variabiliteit van de omgeving. Deze resultaten ondersteunen de zogenaamde 'seizoens-hypothese'. Deze hypothese stelt dat variabele klimaten (hete zomers en koude winters) selecteren op een toename in lichaamsgrootte. Hoewel de onderliggende verklaring al eerder werd bedacht, bestond er nog geen model die dit verschijnsel ook daadwerkelijk liet zien. Dit komt doordat de andere modellen teveel aan fysiologisch detail missen. Dankzij de DEB theorie, doet het model in deze studie dat wel. Dit resultaat benadrukt opnieuw het belang van het opnemen van voldoende mate van realisme in modellen van biologische levensgemeenschappen.

Kortom, dit proefschrift laat zien wat de impact is van een aantal realistische factoren op de evolutie van levensgemeenschappen. In het laatste hoofdstuk wordt bovendien besproken dat (en hoe) deze factoren samenhangen met elkaar en met de keuze voor het bestuderen van specialisatie tussen of binnen trofische functies. Een van de conclusies is dat, om de complexiteit van levensgemeenschappen in de natuur te benaderen, verschillende factoren moeten worden gecombineerd in één model. Dit levert echter grote praktische problemen op, en daarom kan het onderzoek beter eerst gericht worden op kleinere sub-systemen. Voor het bestuderen van het volledige system, moeten deze sub-systemen dus weer gecombineerd worden. Ook dat zal een lastige opgave zijn, en daarom blijft het modelleren van evolutionaire levensgemeenschaps modellen voorlopig nog een uitdaging.



Dankwoord

Het boekje is af. Ik heb er veel van geleerd, en daarvoor ben ik veel mensen dankbaar. Ten eerste natuurlijk Bas, voor zijn visie en de vele ideeën. En Bob, voor de goede samenwerking, en voor de wiskundige hulp bij ongelukken.

Ook wil ik alle andere mensen van de afdeling Theoretische Biologie bedanken voor hun gezelligheid, goede tips en flauwe grappen, dit alles met name op de maandagmorgen. Door de tijd heen waren dit Lothar, Matthijs, Bernd, Tjalling, Cor, Fleur, Ingeborg, Karin, Jorn, Annewillem, George, Daniel, en Jan.

Verder wil ik graag mijn vrienden bedanken, voor de nodige afleiding en feestjes. Ik hoop jullie vanaf nu allemaal weer veel vaker te zien: (ook weer op chronologische volgorde) Alma, Nathalie, Bart P, Michiel, JanWillem, Coen, MaartenJay, Roland, Marleen, Joost, Edwin, Lex, Paul, Marja, Johan, Marieke, Eduard, Wouter, Leonie, Josien, Bart S., Ruben en Hermijn. En natuurlijk het hele voetbalteam.

En dan een apart bedankje voor mijn paranimfen, Tessa en Liesbeth. Goed teamwork, toch? Nog één keertje doen dan?

En ten slotte, maar zeker niet op de laatste plaats, wil ik bedanken mijn ouders, Paul en Jos, mijn zussen, Els en Maartje, en in het bijzonder mijn tweelingzusje Monique. Laten we zeggen voor de goede aanloop. Wat de goede afloop betreft, die is grotendeels te danken aan Joris. Zonder jou was het zeker nog niet “in tha pocket”! Bedankt!

Tineke